Etablissement des nouveaux réseaux multi-observations géodésiques et gravimétriques et détermination du géoïde en Iran

Yaghoub Hatam

Géosciences Montpellier

ÉTABLISSEMENT des NOUVEAUX RÉSEAUX MULTI-OBSERVATIONS GÉODÉSIQUES et GRAVIMÉTRIQUES & DÉTERMINATION DU GÉOÏDE EN IRAN

~

Yaghoub HATAM CHAVARI

décembre 2010

UNIVERSITE MONTPELLIER II
SCIENCES ET TECHNIQUES DU LANGUEDOC

THESE

Pour obtenir le grade de

DOCTEUR DE L'UNIVERSITE MONTPELLIER II

Discipline : Sciences de la Terre et de l'Univers-Géodésie

Ecole Doctorale : SIBAGHE

Présenté et soutenue publiquement par

Yaghoub Hatam Chavari

Le 08 décembre 2010

Etablissement des nouveaux réseaux multi-observations géodésiques et gravimétriques et détermination du géoïde en Iran

JURY

Roger Bayer	GM	Directeur de Thése
Sylvain Bonvalot	BGI	Rapporteur
Marc Daignières	GM	Examinateur
Michel Diament	Paris VII	Rapporteur
Yahya Djamour	NCC, Iran	Invité
Isabelle Panet	LAREG – IGN	Examinateur
Jérôme Verdun	ENSG-LAREG – IGN	Examinateur

RESUME

L'Iran couvre une grande superficie en longitude entre les méridiens 44°E et 64°E et en latitude entre les parallèles 25°N et 40°N. la cartographie de champ de pesanteur sur l'Iran est de premiére importance pour des considérations d'ordre géodésique, géophysique et geodynamique. Dans cette thèse, les mesures de pesanteur sont utilisées pour déterminer le géoïde gravimétrique sur l'Iran. Ce géoïde est couplé à la mesure de hauteur GPS et d'altitude (nivellement) pour réaliser une surface verticale opérationnelle sur le territoire Iranien. La contribution aux principaux travaux géodésiques et gravimétriques réalisés ces dernières années porte sur l'établissement: 1) du réseau national de gravimétrique absolu de l'Iran (NAGNI09), 2) de la ligne nationale d'étalonnage de gravimétrique de l'Iran (NGCLI10), 3) du réseau multi- observations géodésiques et gravimétriques de l'Iran (MPGGNI10).

Le réseau gravimétrique absolu, comporte 24 stations où la mesure de la pesanteur a été réalisée à l'aide de gravimètres FG5, avec une précision meilleure que 5 μGal. La répétition des observations sur deux sites entre 2000 et 2007 met en évidence des variations inter-annuelles de la pesanteur en relation avec l'évolution du contenu en eau du sous-sol et (ou) la déformation tectonique.

Le réseau a servi de point d'appui pour la réalisation du réseau géodésique et gravimétrique MPGGNI10 de maille 55 km sur lequel a été mesuré la pesanteur à l'aide des gravimètres relatifs CG5 et CG-3/M, la hauteur de GPS et l'altitude avec une précision respectivement de 0.010 mGal, 0.03 m et $3mm\sqrt{km}$. La technique de retrait- restoration couplée à la méthode de condensation de Helmert a permis de calculer un nouveau modèle de géoïde gravimétrique, IRGeoid10, avec une précision absolue et relatif respectivement de l'ordre de 0.26 m et 2.8 ppm. Ce géoïde est ajusté aux points GPS nivelés pour définir un nouveau referentiel des altitudes sur l'Iran.

TITLE : Establishment of multi-observations geodetic and gravimetric networks, and determination of geoid in Iran

ABSTRACT

Iran covers a large area limited in longitude by the meridians 44°E and 64°E and in latitude by the parallels 25°N and 40°N. Mapping a new gravity field over Iran is the first important data for geodetic, geophysical and geodynamical considerations. In this thesis, the gravity measurements are used to determine the gravimetric geoid over Iran. This geoid is coupled with the GPS height and altitude (levelling) to realize an operational vertical surface at the territory of Iran. The contribution of the principal geodetic and gravimetric works realized in recent years are the establishment of: 1) the national absolute gravity network of Iran (NAGNI09), 2) the national gravity calibration line of Iran (NGCLI10) and 3) the multi-observations geodetic and gravimetric network of Iran (MPGGNI10).

The absolute gravity network consists in 24 stations where the gravity measurement has been realized with the help of gravimeters FG5, with a precision better than 5 μGal. The repetition of the observations at two stations between 2000 and 2007 makes obvious the inter-annual variations of gravity in relation of the amount of underground water changes and (or) tectonic deformation.

The absolute gravity network has served the base stations for the realization of the MPGGNI10 geodetic and gravimetric network with a mesh of 55 km, at which the gravity is measured with the help of relative gravimeters CG-5 and CG-3/M, the GPS height and the altitude with a precision of 0.010 mGal, 0.03 m, and $3mm\sqrt{km}$ respectively. The remove-restore technique coupled with the Helmert's condensation method is chousen to compute a new gravimetric geoid model, IRGeoid10, with a absolute and relative precision of the order of 0.26 m and 2.8 ppm respectively. The gravimetric geoid is adjusted at the GPS/levelling points to define new vertical reference surface over Iran

DISCIPLINE: Sciences de la Terre et de l'Univers- Géodésie

MOTS-CLES:
Gravimétrie, étalonnage, géoïde, GPS, Nivellement, géodésie, Iran
Gravimetry, calibration, geoid, GPS, levelling, geodesy, Iran

Laboratoire Géosciences Montpellier, UMR CNRS/UM2 5243, CC 60, Université Montpellier 2, Place E. Bataillon 34095 Montpellier cedex 5, France

A ma mère

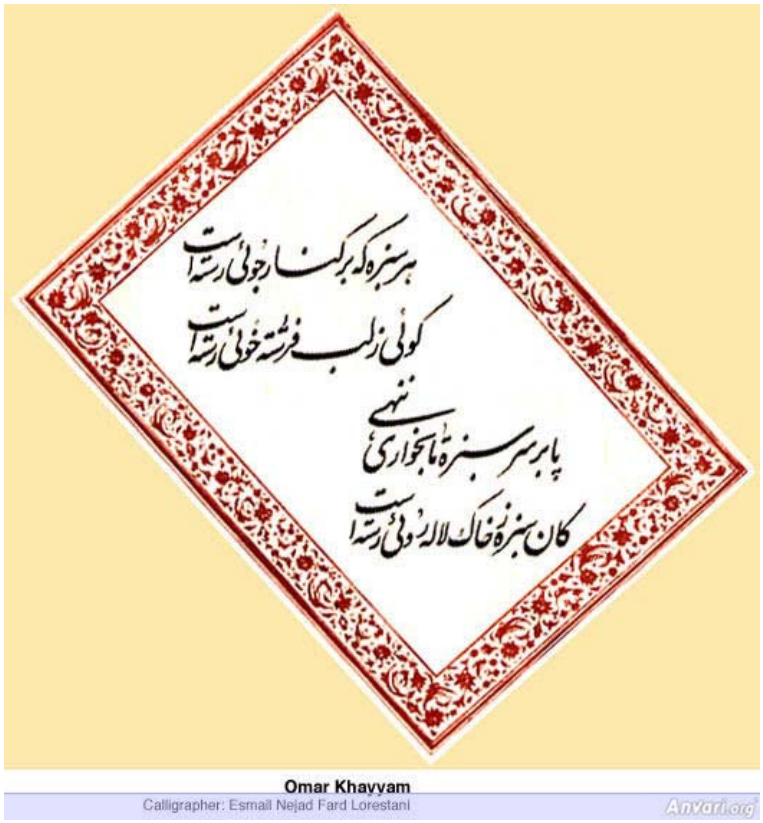

L'amour et la jeunesse, le vin de clair rubis,
Les concerts d'amitié,
Les rivaux fraternels, le circuit de la coupe;
Charmants enfants aux lèvres distillant le miel,
Musiciens inspirés,
Compagnons au cœur noble, amis à l'âme pure;
D'adorables objets dont les grâces offensent,
La source de jouvence,
Dont l'éclat sans second rend jalouse la lune;
Convives bienveillants et serviteurs civils,
Combats de courtoisie,
Confrères initiés aux mystères ultimes;
Vin ardent et léger empruntant à la rose,
Sa teinte et son parfum,
Dont des lèvres de sucre effacent l'amertume;
Belles dont les appas s'élancent glaive nu,
à l'assaut des raisons,
Et dont les boucles sont aux cœurs autant de pièges;

(Hâfez de Chirâz,
Traduit du persan
Par Gilbert Lazard, 2010)

Remerciements

Cette thèse a été réalisée dans le cadre du programme de recherche franco-iranien entre le Laboratoire Geosciences Montpellier de l'Université Montpellier II (Montpellier, France) et le National Cartographique Centre (Téhéran, Iran).

En premier lieu, Je voudrais remercier sincèrement Roger Bayer qui a dirigé ma thèse et m'a aidé toujours avec patience non seulement sur le plan scientifique mais aussi pour l'apprentissage du français lors de longues discussions au cours des missions en Iran ou au laboratoire en France. Merci Roger.

Je voudrais aussi remercier sincèrement les membres du jury : S. Bonvalot, M. Diament (rapporteurs), M. Daignières, J. Verdun, I. Panet (examinateurs) et Y. Djamour (invité) qui ont accepté la responsabilité de juger ce travail. Je remercie aussi J. Chery pour avoir participé au comité de thèse et jugé l'avancée du travail de thèse. Mes remerciements vont aussi à P. Vanicek dont le support dans le domaine de la géodésie physique a été précieux pendant le déroulement de la thèse.

Pendant ces quelques années de thèse, j'ai eu l'opportunité d'accompagner les équipes gravimétriques absolues de Montpellier (R. Bayer et N. Le Moigne) et de Strasbourg (J. Hinderer et B. Luck) sur le terrain me permettant ainsi d'acquérir une bonne expérience dans le domaine de la métrologie gravimétrique. Merci aux collègues français qui ont consacré du temps pour m'apprendre toute la finesse de la mesure absolue en gravimétrie.

J'exprime ma gratitude aux personnes du NCC qui m'ont donné la responsabilité de ce travail et qui m'ont aidé à le réaliser. Merci aux (nouveaux et anciens) responsables du NCC, M. Ilkan, M. Madad, Y. Mahmood zadeh, Y. Djamour, H. Vaaezi, M. Sarpoulaki, A. Shariatmadar, M. emtiaz, F. Tavakoli, A. Soltanpour et M. Sedighi.

Je tiens à exprimer ma gratitude la plus sincère à mes amis, les techniciens et les ingénieurs du NCC des départements et des services gravimétrie, GPS et Nivellement, notamment H. Cheraghi, R. Saadat, A. Poursharifi, N. Azizian, B. Sharifat, S. Rafiey, M. Ayazian, S. Arabi, A. Montazerin, A. Charkhzarrin, Gharakhani, H. Nankali, Z. Moosavi, Asadpour, Rahimi, H. Asghari, A. Bahrampour, H. Meygooni, K. Nazari, K. Sayyar, M. Akbari, G. Ebrahimi, Salimi, H. Khoshbayan, H. Hanifeh Zadeh, Taghikhani, Samani, Farahani, M. Alali, Khorrami, Chenari, Babaee.

Je n'oublierais pas dans mes remerciements S. Lallemand, directeur du laboratoire Géosciences Montpellier qui m'a accueilli dans ce laboratoire et les collègues et compagnons que j'ai croisés quotidiennement et qui m'ont apporter souvent du réconfort, J-E. Hurtrez, N. Le Moigne, B. Smith, J. Malavieille, D. Arcay, A. Delplanque, E. Doerflinger, J-F. Ritz, C. Champollion, M. Peyret, P. Collard, S. Dominiguez, F. Boudin, M-F. Roch, E. Ball, T. Jacob, S. Deville, M. Rizza, T. Theunissen, R. Soliva, J. Tack, F. Grosbeau, J. Losq, R. Cattin, N. Mouly, S. Raynaud, C. Fabregat, P. Steer, V. Soustille. Merci aussi à J-P Boy, V. Corchete et P. Valty.

Je n'oublierais pas mes amis, mes collègues et mes professeurs de l'Université , A. Abolghasem, Y. Djamour, M. Mohammadkarim, M. Nadjafi, M. Zolfaghari, A. Azizi, H. Nazari, M. Abbasi, B. Vosoughi, J. Asgari, S. Soleymani, R. Salamati, A. Amiri Simkooee, K. Ghazavi, M. Mashhadi, A. Ardalan, M.A. Sharifi, A. Safari, B. Tajfirooz, M. Motagh, M. Nikkhou, M. Naeimi, M. karpychev, F.G. Lemoine avec qui la collaboration scientifique a été fructueuse.

Le CROUS du Montpellier et les services scientifiques de l'ambassade de France à Téhéran m'ont soutenu financièrement pendant ces 3 années. Qu'ils recoivent ici mes remerciements.

Merci à mes parents et mes sœurs qui m'ont soutenu.

Tables des matières

1. Introduction - Problématique

La Géodésie est l'étude mathématique de la forme et des dimensions de la terre, et l'étude de son champ de pesanteur. L'étude pratique se traduit notamment par l'établissement des réseaux géodésiques et gravimétriques et la détermination du géoïde. La connaissance du champ de pesanteur a servi depuis bien longtemps de support à la détermination du géoïde. L'évolution de techniques, aussi bien spatiales, aéroportées qu'au sol a permis des avancées considérables sur cette surface de reference tant en résolution qu'en précision. Depuis 2000 on a assisté à de nouvelles générations des satellites (CHAMP, GRACE, GOCE) ayant comme objectif de décrire globalement de la pesanteur terrestre avec une résolution atteignait aujourd'hui environ 100 km pour GOCE. De plus, la multiplication des mesures absolues de la pesanteur, avec une précision de quelques μGal a permis d'uniformiser les systèmes observations. Les gravimètres relatifs de nouvelle génération, de type Scintrex CG-3M et CG-5, ont contribué au développement rapide des réseaux gravimétriques de grande précision. Enfin, la gravimétrie aéroportée s'est avérée dans certains cas un outil indispensable pour couvrir des vastes régions sou vert inaccessibles d'un point de vue climatique ou géographique.

L'objectif premier du NCC (Teheran, Iran) était la constitution d'un réseau national gravimétrique absolu, comportant des stations distribuées régulièrement sur le territoire iranien. Ce projet aboutissant à la constitution du réseau appelé NAGNI09, stipulait que la pesanteur devait être mesurée à mieux que 5 μGal. Il posait ainsi la question fondamentale de la représentativité des observations absolues acquises en quelques années, vis-à-vis des variations annuelles et interannuelles probablement en relation avec l'évaluation de contenu en eau du sous sol iranien, de l'évolution du niveau moyen des mers [mer Caspienne, golfe Persique, mer d'Oman] et de la déformation tectonique. Cette question devait être abordée sur des sites tests mesurés régulièrement avec un gravimétrique absolu. En parallèle la densification de la couverture gravimétrique constituait un objectif important par l'intermédiaire des nouveaux réseaux du 1^{ére}, 2^{éme} et 3^{éme} ordres à partir de 2005 [Ardalan et al, 2004].

Enfin, le calcul précis du géoïde sur l'Iran justifiait la réalisation d'un réseau multi- observations géodésiques et gravimétriques. Le réseau triangulaire, nommé MPGGNI10, devait être constitué des stations réparties tous les 55 km aux nœuds duquel les mesures de gravité relative, de positionnement GPS et de

nivellement étaient réalisées avec une précision attendue respectivement de 10 μGal, 1-3 cm sur la hauteur GPS et 3mm $\sqrt{km}$ pour le nivellement.

La précision requise sur les données gravimétriques nécessitait d'établir une ligne d'étalonnage des gravimètres relatifs disposant d'une amplitude de variation de la pesanteur la plus grande possible et d'un accès rapide des sites. Il a donc été décidé de mettre en place une ligne d'étalonnage nommé NGCLI10 en région montagneuse [montagne de l'Alborz] caractérisée potentiellement par une variation théorique de plus de 1 Gal.

Enfin, l'ensemble des observations de pesanteur devait être transformé en hauteur de géoïde. Dans cette thèse, nous avons choisi la technique de retrait – restoration en incluant la méthode de condensation de Helmert pour calculer le nouveau géoïde en Iran, IRGeoid10. La réalisation du réseau MPGGNI10 offrait une bonne opportunité pour 1) comparer ce géoïde gravimétrique au géoïde déterminé ponctuellement par mesures GPS et de nivellement 2) proposer un nouveau référentiel des altitudes sur l'Iran. Le manuscrit est structuré en 6 chapitres. Après cette brève introduction (chapitre 1) et quelques rappels sur les techniques gravimétriques et géodésiques (chapitre 2), nous présentons les nouvelles données, gravimétriques acquises ces 10 dernières années et servant de base à la détermination du géoïde gravimétrique(chapitre 3). La méthode de Stokes – Helmert est ensuite présentée (chapitre 4). Enfin, le géoïde est calculé en utilisant le logiciel GRAVSOFT [Forsberg et Tcsherning, 2008]. Nous concluons cette thèse en proposant quelques perspectives à ce travail (chapitre 6).

2. Gravimétrie, GPS et Nivellement

1. Gravimétrie terrestre

La pesanteur sur la Terre est de l'ordre de 9,81 m s^{-2} (ou 981 Gal), que nous appelons $\overline{g}$ .Les variations en latitude (du pôle à l'équateur) et en altitude (des montagnes les plus élevées aux fosses océaniques) sont au maximum de 5.10^{-3} $\overline{g}$. Les masses perturbatrices localisées dans la lithosphère induisent des anomalies de l'ordre de 5.10^{-5} $\overline{g}$. Les effets dus aux forces de marée atteignent 5.10^{-7} $\overline{g}$.

La mesure de la pesanteur a pour base la loi fondamentale de la dynamique : un corps de masse m placé dans un champ gravitationnel $\vec{g}$ subit une force $\vec{F}$ qui lui est proportionnelle :

$$\vec{F} = m\vec{g} \qquad (2.1)$$

Tout instrument capable de mesurer l'effet que produit la pesanteur sur une masse connue, c'est-à-dire une force, peut être qualifié de gravimètre. La mesure de la pesanteur en tant qu'accélération est intimement liée à une mesure de longueur et de temps. La gravimétrie s'intéresse surtout au module de l'accélération de la pesanteur, g.

Deux grandes familles d'instruments permettent d'appréhender la pesanteur sur terre : les gravimètres absolus et les gravimètres relatifs. Les gravimètres absolus mesurent g en utilisant des standards S.I. de longueur et temps. Les premiers gravimètres absolus étaient des pendules simples: dans un cas idéal, la valeur de g est en effet reliée à la période d'oscillation, à la longueur du fil pendulaire et à la période d'oscillation. Les améliorations apportées avec le pendule réversible permirent d'obtenir une valeur de g à 5.10^{-7} près, soit une valeur connue à 0.1 mGal (Fig. 2.1). Depuis le milieu du siècle dernier, les gravimètres absolus à chute libre ou balistiques ont pris le pas sur les gravimètres pendulaires. Le principe de ces instruments est de déterminer g à partir de la trajectoire d'un objet (sa position en fonction du temps), les distances et les temps étant reliés à des étalons S.I. De tels instruments permettent aujourd'hui de connaître g à 5.10^{-9} près, soit au μGal près (Fig. 2.1).

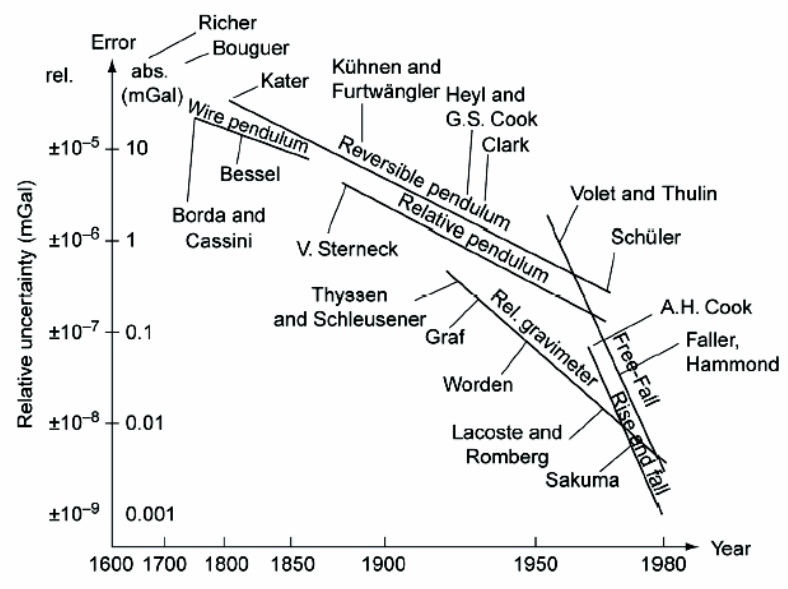

Fig. 2.1. Précision relative et absolue des gravimètres depuis le 17ème siècle, d'après Torge (1989) et Niebauer (1995)

Les gravimètres relatifs ne donnent pas directement une lecture de la valeur de g car ils ne sont pas reliés à des standards de distance et de temps. De tels instruments mesurent la variation d'une grandeur qui elle peut être étalonnée à l'aide de mesures réalisées avec un gravimètre absolu. Ainsi, les gravimètres relatifs permettent la mesure des différences de g entre points ainsi que les variations de g dans le temps, sans permettre d'accéder à la valeur absolue de g.

Si des gravimètres relatifs pendulaires ont existé par le passé, aujourd'hui, les gravimètres relatifs actuels de terrain sont des gravimètres à ressort: les variations de force de gravité agissant sur une masse donnée sont compensées par une force de réaction mesurable. L'évolution de cette force de réaction traduit l'évolution de g. Ces gravimètres relatifs, comme le Lacoste et Romberg model D ou les Scintrex CG3 et CG5, permettant d'effectuer des levés gravimétriques avec une précision < 0.01 mGal, et se distinguent des gravimètres relatifs d'observatoire comme le gravimètre supraconducteur commercialisé par GWR (www.gwrinstruments.com) et le gravimètre à ressort G-Phone commercialisé par Microg-Lacoste (www.microglacoste.com). Ces derniers enregistrent de manière quasi continue les variations de la pesanteur avec une grande précision à des fins géodynamiques comme l'étude des marées terrestres. Dans ce travail, nous avons utilisé le gravimètre absolu FG5 produit par Microg-Lacoste (Niebauer et al., 1995) ainsi que des gravimètres relatifs CG5 produit par Scintrex (www.scintrexltd.com).

1.1 Le gravimètre absolu FG5

Le gravimètre absolu FG5 permet de déterminer la valeur de g avec une précision de l'ordre de 1-2 μGal (Niebauer et al., 1995). La trajectoire d'un objet en chute libre est déterminée à l'aide d'un interféromètre laser de type Mach-Zender. Les étalons de longueur et de temps sont respectivement donnés par la longueur d'onde du laser généralement Helium-Néon stabilisé par l'iode (laser WEO model 100), et par une horloge atomique à Rubidium, assisté parfois par une fréquenceGPS. Le FG5, comme d'autres gravimètres absolus, est construit autour de trois principes ou entités :

- une chambre de chute ;
- un système de mesure du temps et de la distance ;
- une isolation sismique.

De façon simplifiée, un FG5 n'est autre qu'un interféromètre de type Mach-Zender modifié (voir figure 2.2a). Le faisceau issu du laser est scindé en deux par un miroir semi- réfléchissant générant le faisceau 'test' et le faisceau de référence. Le faisceau 'test' va d'abord se réfléchir sur un coin de cube en chute libre puis passe par le coin de cube de référence inertiel, isolé des vibrations ambiantes par le système 'superspring', qui est un ressort asservi (figure 2.2a). Les faisceaux test et de référence sont alors recombinés par un second miroir semi- réfléchissant, et une photodiode détecte les franges d'interférences issues de ces deux faisceaux. La longueur du chemin optique du faisceau de référence est fixe alors que celle du faisceau test varie avec la chute de l'objet. Soit λ la longueur d'onde du laser. Des interférences constructives et destructives ont lieu quand la différence des chemins optiques est un multiple de λ, c'est-à-dire lorsque le coin de cube chute de $\lambda/2$ (figure 2.2b). Ainsi, les variations interférométriques de l'intensité lumineuse (appelées franges) sont détectées par la photodiode (figure 2.2c). Lors d'une chute du coin de cube qui dure ~ 0.2 s sur ~ 0.2 m, plus de 600000 franges se forment, avec une fréquence d'autant plus rapide que l'objet est accéléré par la pesanteur. L'horloge atomique sert à précisément déterminer le temps de formation de ces franges, dont ~ environ 700 sur 600000 sont analysées. Finalement, environ 700 couples temps-distance selon la chute servent à obtenir la valeur de g en inversant par moindres carrés le système :

$$x_i = x_0 + v_0\tilde{t}_i + \frac{g_0\tilde{t}_i^2}{2} + \frac{\gamma x_0\tilde{t}_i^2}{2} + \frac{1}{6}\gamma v_0\tilde{t}_i^3 + \frac{1}{24}\gamma g_0\tilde{t}_i^4 \ , \qquad \tilde{t} = t_i - \frac{(x_i - x_0)}{c}. \tag{2.2}$$

Avec x_i la position au temps $\tilde{t}_i$, temps qui prend en considération la nature finie de la vitesse de la lumière c : une frange est en effet détectée après que l'objet soit en position (eq. 2.2). x_0, v_0 et t_0 les positions, vitesses et accélérations initiales de l'objet, et γ le gradient vertical de la pesanteur, considéré proche de ~3 μGal/cm, ou mesuré par un gravimètre relatif. La valeur de g est estimée pour chaque chute. Les résidus de l'ajustement par moindres carrés de la trajectoire sont de l'ordre du nm (10^{-9} m), ce qui rend compte de la précision du système.

L'obtention d'une valeur de g précise à 10^{-9} près nécessite une multitude d'attentions particulières. L'objet soumis à des chutes libres dans la chambre de chute est un coin de cube, qui a les propriétés optiques suivantes :

- la distance du chemin optique réfléchi par le cube est indépendante d'éventuelles translations horizontales ou de rotation de celui-ci,
- le faisceau réfléchi est toujours parallèle au faisceau incident.

Ces propriétés sont importantes car, en pratique, l'objet a toujours une composante non nulle en rotation et translation lors d'une chute. Ainsi, seul l'effet de la chute libre influe sur la longueur du chemin optique. De plus, la chambre de chute doit être sous vide pour que l'objet ne soit pas freiné par les particules de l'air: une pression de 10^{-4} Pa est maintenue en son sein.

Le rôle du 'superspring' est primordial dans la qualité de la mesure : il isole le référentiel des vibrations pour la mesure de la position. En effet, le 'superspring' est un sismomètre actif longue période (~ 60 s) qui atténue les vibrations terrestres, pour une période fondamentale de ~ 6 s, soit le même ordre de grandeur que la répétition normale des chutes (~ 10s). Pour donner une idée de l'importance de ce dispositif, l'écart type sur 100 chutes sans le 'superspring' est plus de 10 fois supérieur à celui obtenu avec le « superspring ». Le laser et l'horloge à rubidium sont régulièrement étalonnés car leur bon fonctionnement est un élément clé de la mesure. Finalement, la qualité de la mesure dépend aussi de la bonne installation et des bons réglages de l'instrument (verticalité, alignement des faisceaux…), ce qui induit un facteur 'humain' et produit une erreur communément appelée « setup error ».

Une mesure type avec un FG5 consiste en un ensemble de 'sets' ou de séries horaires, généralement plus de 12, chaque série comportant 100 chutes effectuées typiquement à 10 s d'intervalle. Selon la qualité des sites

et l'intensité du bruit micro sismique ambiant, l'écart type sur une série (ou 100 chutes) varie entre 5 et 15 μGals.

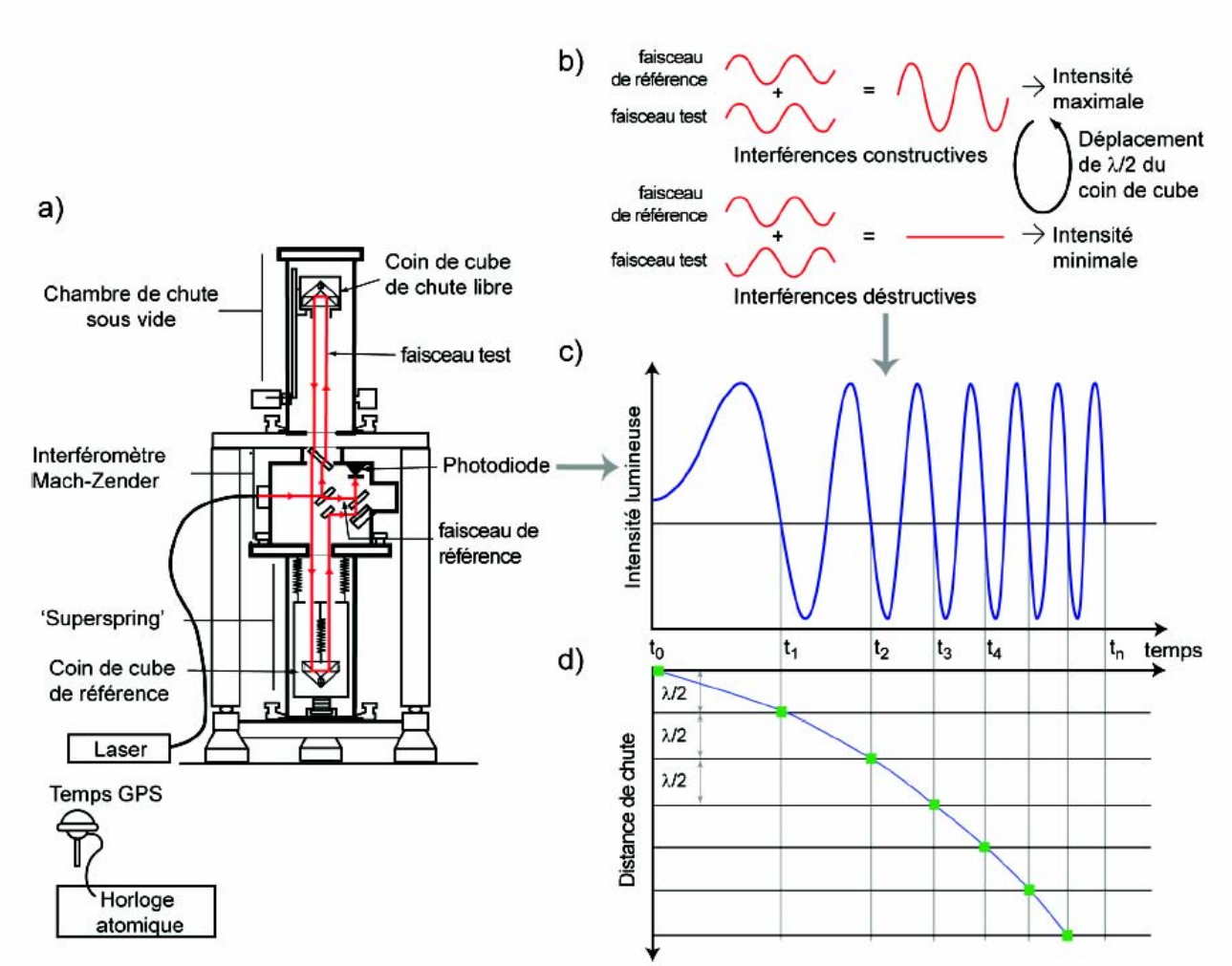

Fig. 2.2. a) Schéma de fonctionnement du FG5, b) principes de base d'interférométrie de deux faisceaux de lumière cohérente, c) Franges d'interférences lors d'une chute de l'objet mesurée par la photodiode, d) Couples positions- temps de l'objet en chute libre permettant d'obtenir la valeur de g, d'après Niebauer et al. (1995), modifié par Jacob (2010).

Une valeur de g est donnée par la moyenne pondérée des séries de 100 chutes, préalablement corrigées des effets dynamiques de la gravité : marée terrestre, surcharge océanique associée, effets atmosphériques, effets relativistes et effets du mouvement du pôle. Le fait de moyenner les séries sur des périodes multiples de 12 h permet d'atténuer les éventuelles erreurs sur les corrections de marées ou de surcharges océaniques dont les effets principaux sont diurnes et semi diurnes.

L'incertitude sur une mesure absolue est donnée par la formule suivante :

$$\delta_{tot} = \sqrt{\delta_{sys}^2 + \delta_{stat}^2 + \delta_{setup}^2} \quad (2.3)$$

Où δ_{instr} est une incertitude liée aux corrections apportées (marées terrestres, surcharge océanique, effets atmosphériques, mouvement du pôle) ainsi qu'aux erreurs instrumentales intrinsèques systématiques : laser, horloge atomique. La valeur de g est donnée en haut de la chute, à une hauteur de ~1.3 m. Si la valeur de g est projetée avec un gradient vertical, par exemple au sol, l'erreur associée à cette projection est ajoutée quadratiquement à δ_{instr} . Le terme δ_{instr} est alors dominé par l'erreur due au gradient (typiquement 3 μGal/m pour un gradient vertical de ~ 300 μGal/m), et sera d'autant plus élevé que la distance de projection est grande.

Pour des mesures répétées dans le temps, la projection au sol n'est pas nécessaire et l'on s'affranchit alors de cette erreur, conduisait à sur une valeur de δ_{instr} de ~1 μGal, déterminée (Niebauer et al, 1995). L'erreur statistique est définie par :

$$\delta_{stat} = \sigma_{set} / \sqrt{N_{set}} \quad (2.4)$$

avec σ_{set} l'écart type sur les sets, et N_{set} le nombre de sets. Comme σ_{set} vaut typiquement entre 0.5 et 2 μGal pour 24 sets, δ_{stat} est ainsi compris entre 0.1 et 0.4 μGal selon les sites de mesures. Cette erreur statistique suppose que le bruit sur une durée d'une mesure (> 12 h) soit 'blanc', c'est-à-dire que le bruit soit indépendant de la fréquence et que chaque série horaire soit indépendante. Ceci a en effet été vérifié par Van Camp et al. (2005) , qui montrent que le spectre de puissance spectrale pour le FG5 est plat pour des périodes inférieures au jour. Le bruit blanc du FG5 est estimé entre 30 et 50 μGal Hz$^{-0.5}$ (Van Camp et al., 2005) sur les sites de mesures utilisés (15 μGal $Hz^{-0.5}$ selon le constructeur pour un site à bas bruit) pour les périodes inférieures à 24 heures. Ainsi, pour un bruit de 50 μGal $Hz^{-0.5}$ et une période de mesure d'un jour (86400 s), on retrouve une erreur de $50/(86400)^{0.5}$ = 0.17 μGal, compatible avec celle calculée avec les écarts types sur les séries de 100 chutes.

De plus, en comparant les chroniques faites avec un FG5 et un gravimètre supraconducteur, dont le bruit blanc instrumental est estimé à 0.1-0.3 μGal $Hz^{-0.5}$, Van Camp et al. (2005) ont déterminé l'erreur liée à l'installation de l'instrument δ_{instal} , soit l'erreur 'humaine', à 1.6 μGal.

Lorsque l'on ne projette pas la valeur de g, l'erreur totale sur la valeur peut être estimée à ~ 2 μ Gal. Cette valeur sera retenue pour la suite.

1.2 Le gravimètre relatif Scintrex CG5

La description et le principe de mesure des Scintrex CG-3M et CG-5 sont détaillés dans Jousset et al (1995) ; Budetta and Carbon (1997) ; Bonvalot et al (1998), Jousset et al (2000) ; Gabalda et al (2003); Scintrex (2006); Ukawa et al (2010). Nous renvoyons à ces références pour plus d'informations.

Le gravimètre relatif Scintrex Autograv CG5 a été utilisé dans ce travail. Le capteur utilisé dans cet instrument relève du secret industriel, mais quelques informations sont disponibles. Celui-ci est constitué d'un ressort en silice amorphe auquel une masse d'épreuve est suspendue. L'utilisation d'un capteur en silice est justifiée par les éléments suivants :

- La silice a un coefficient de dilatation thermique α de ~3-5 $10^{-4}\, cm^{-1}K^{-1}$, un ordre de grandeur inférieur à ceux des métaux usuels, elle est donc moins sensible aux variations de température ;

- La silice est un matériel résistant, au module d'élasticité élevé (10^{11} Pa) ;

- La silice est facile à travailler et le ressort peut être fabriqué en une seule fusion, de façon monolithique. La position de la masse d'épreuve est à l'équilibre sous l'effet des poids de la masse de la réaction d'une force électrostatique. Si l'équilibre est perturbé par un changement de pesanteur, la force induite sur la masse est détectée, et une contre-réaction électrostatique maintient la masse à une position fixe. La tension de contre-réaction donne une mesure indirecte de la variation de pesanteur. Cet asservissement est effectué avec des plaques capacitives, qui ont un double rôle de positionnement extrêmement précis de la masse ainsi qu'un rôle de transducteur de force en maintenant la masse fixe. La technique est décrite par Vaillant (1986), et permet un positionnement avec un bruit de 1 nm $Hz^{-1/2}$, ce qui entraîne une précision instrumentale meilleure que 10 μ Gal (Scintrex limited, 2006). De plus, cet instrument peut faire des mesures sur une gamme de 8000 mGal ($8\,10^{-2}\, m.s^{-2}$).

Par contre, une caractéristique intrinsèque du capteur du CG5 consiste en une dérive continue due au fluage du quartz. Cette dérive peut-être considérée comme linéaire sur des périodes inférieures au jour, un polynôme de degré supérieur la décrivant sur des périodes plus longues (Bonvalot et al., 1998). L'estimation

de cette dérive est primordiale pour obtenir des différences temporelles (et donc spatiales) de la pesanteur précises.

Le capteur du CG5 est inclus dans une enceinte thermostatée afin de limiter la dilatation thermique du ressort. Un capteur de température y est aussi présent afin d'enregistrer les variations thermiques de l'ordre du mK° pour ensuite pouvoir corriger l'impact de ces effets sur la gravité mesurée (constante Tempco, Fig. 2.3). L'enceinte est aussi maintenue à pression constante et isolée afin de limiter les effets de variation de pression atmosphérique sur le capteur.

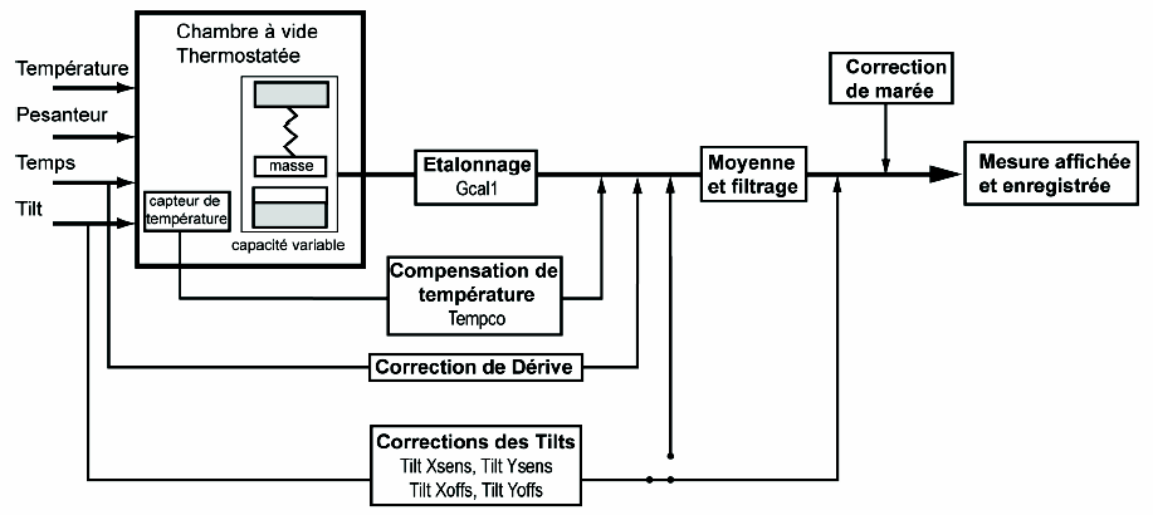

Fig. 2.3 Fonctionnement interne du Scintrex CG5 montrant les corrections appliquées et les constantes associées.

Le bon nivellement de l'instrument assure une bonne mesure, à condition que les paramètres de corrections de l'inclination soient régulièrement étalonnés.

Le passage d'une tension mesurée entre les éléments capacitifs du capteur à une grandeur qui s'apparente à la pesanteur est une étape importante : la constante d'étalonnage des gravimétrie (Fig. 2.3). Cette constante est déterminée sur une ligne d'étalonnage, ou de fortes variations de g connues grâce à des mesures absolues sont comparées aux variations de g données par le CG5. La constante Gcal1 évolue dans le temps et doit être réévaluée régulièrement, avec une évolution d'autant plus rapide que l'instrument est récent. La ligne de calibration Tochal7-Astara à été utilisée à plusieurs reprises pour la calibration des gravimètres relatifs ($\Delta g \sim$ 1152 mgal).

Le gravimètre CG5 échantillonne le signal à une fréquence de 6 Hz, moyenné toutes les secondes, sur une session de mesure dont le temps définie par l'utilisateur. En sortie, une valeur moyenne, dont les données à la seconde s'écartant de plus ou moins 3 fois l'écart type de la moyenne sont rejetées, est fournie. Les mesures

sont corrigées des effets de marées terrestres (algorithme de Longman (1959)) ainsi que d'une dérive selon le choix de l'utilisateur. Un bruit blanc est supposé dominer la mesure (chaque seconde de mesure est supposée indépendante l'une de l'autre), et l'erreur est ainsi définie comme le rapport de l'écart type sur la racine du nombre de données à la seconde non rejetées.

Pour une utilisation en levé gravimétrique, plusieurs sessions de mesures sont effectuées à chaque station, typiquement plus de trois. La détermination du temps de mesure de chaque série passe par la considération suivante : à partir de quelle durée l'effet du bruit micro sismique est-il minimisé ? Merlet et al. (2008) ont calculé la variance d'Allan sur une série CG5 brute et ont montré qu'une période de 85 s minimise l'influence du bruit sismique (pour le site du LNE à Trappes) sur les données non corrigées de la marée (Fig. 2.4). Au-delà de 85 s, la variance augmente car l'influence des marées terrestres se fait ressentir.

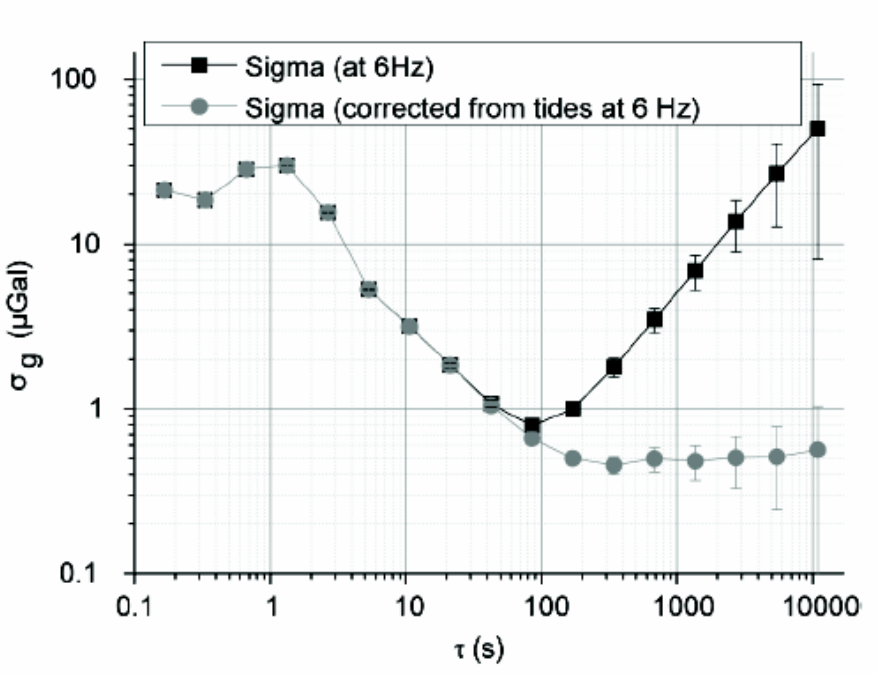

Fig. 2.4 Ecart-type d'Allan en fonction du temps considéré pour des données brutes de CG5 corrigées ou non des marées terrestres, d'après Merlet et al (2008)

2. Gravimètrie Satellitaire

2.1 CHAMP

CHAMP (CHAllenging Minisatellite Payload for geoscience and application, Fig. 2.5) a été lancée le 15 juillet 2000 par l'Agence Spatiale Allemande (DLR, Deutsches Zentrum für Luftund Raumfahrt) sur proposition du centre de recherche de Potsdam (GFZ, Geo-ForschungsZentrum). Placé sur une orbite polaire à 400 km d'altitude, le satellite CHAMP est constamment positionné par les satellites de la constellation GPS.

L'analyse des perturbations d'orbite de CHAMP permet de reconstituer les ondulations du géoïde avec une précision de 10 cm pour 485 km de résolution spatiale. De telles performances ont pu être atteintes grâce à des mesures fines des forces de surface appliquées au satellite (amplitude de $10^{-9}\, m/s^2$) obtenues par le micro-accéléromètre STAR conçu par l'ONERA (Office National d'Études et de Recherches Aérospatiales) en collaboration avec le CNES (Centre National d'Études Spatiales) (http://www-app2.gfz-potsdam.de/pb1/op/champ//; de Saint-Jean, 2008).

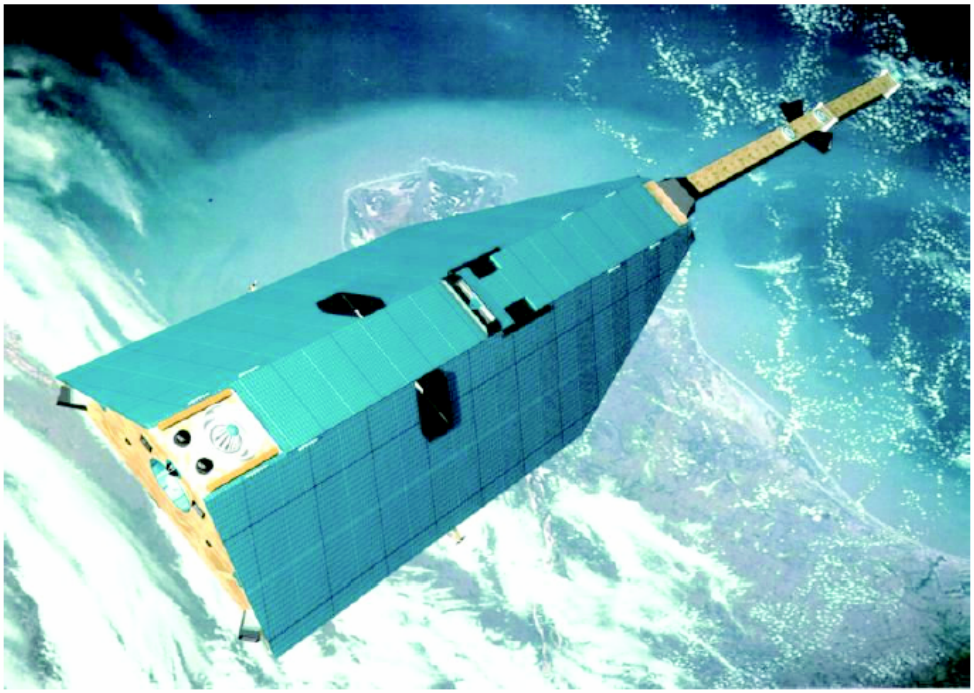

Fig. 2.5 Vue du satellite CHAMP, GFZ-Potsdam, Germany.

Après seulement 12 mois d'observation, les données du satellite CHAMP ont permis de déterminer un premier modèle du champ européen dénommé EIGEN (European Improved Gravity model of the Earth by New techniques) donné sous forme d'un développement en harmoniques sphériques jusqu'au degré 120 soit à 150 km de résolution spatiale.

2.2 GRACE

GRACE (Gravity Recovery and Climate Experiment) a été lancée le 16 mars 2002 pour une durée de cinq ans extensible. Fruit d'une collaboration entre la NASA et la DLR, cette mission a pour objectif la cartographie du géoïde mondial, à un rythme mensuel ou décadaire, avec une résolution spatiale d'environ 300-400 km et une précision centimétrique. Les applications principales de cette mission concernent le suivi de l'évolution des masses d'eau, de neige ou de glace mal connue à l'échelle mondiale, voire l'étude des déformations consécutives aux grands séismes tel le tremblement de terre de Sumatra en décembre 2004.

Le principe de la mesure repose sur l'utilisation de deux satellites jumeaux GRACE-A et GRACE-B (Fig. 2.6) placés à une distance de 200 km sur des orbites polaires quasi-circulaires à 480 km d'altitude. Les deux satellites mesurent constamment la distance qui les sépare, dont sont déduites les perturbations relatives des orbites au micromètre près. Le premier modèle de champ mondial obtenu à partir des données de la mission GRACE a été publié à la fin de l'année 2003 par la NASA et le GFZ sous le nom de GGM02S (Tapley et al. 2005). Il consiste en un développement en harmoniques sphériques jusqu'au degré 160, soit 125 km de résolution spatiale ((http://www.csr.utexas.edu/grace/; Sharifi et al, 2008).

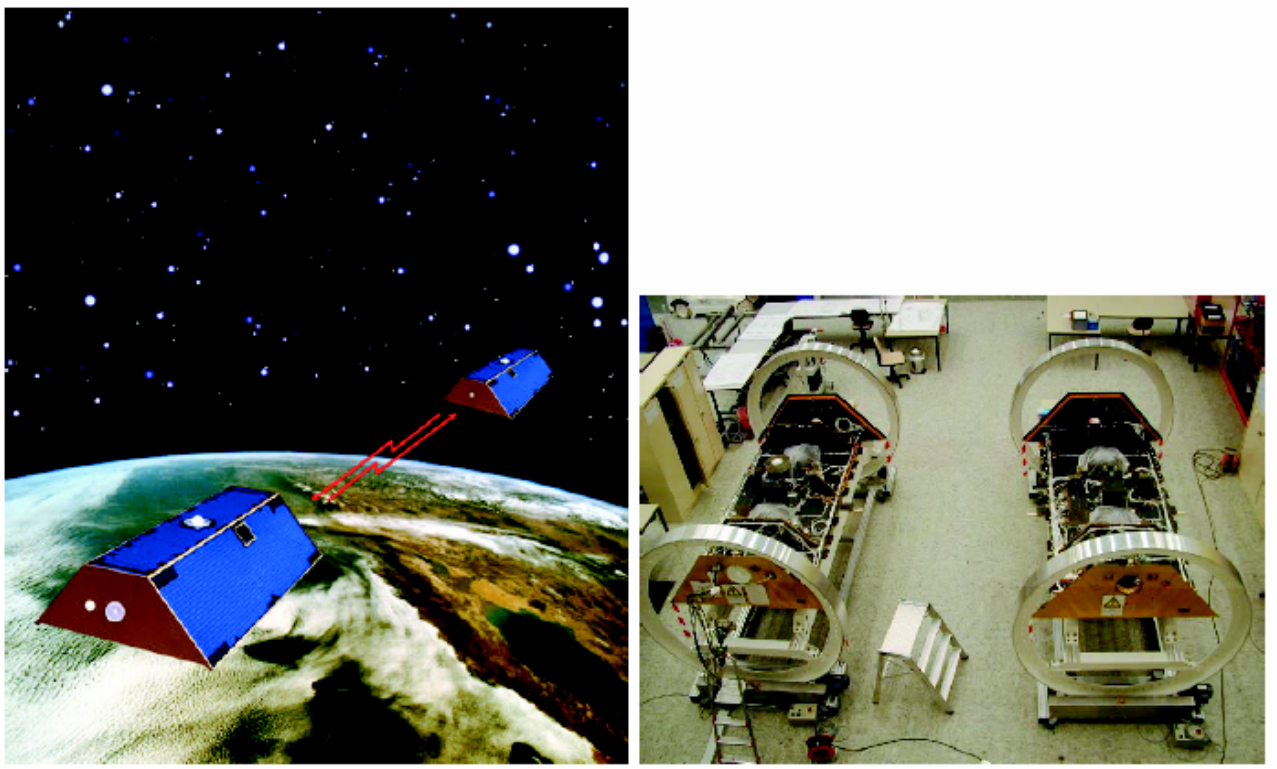

Fig. 2.6 Vues des satellites GRACE : GRACE-A et GRACE-B, NASA's Jet Propulsion Laboratory (JPL), USA et GFZ-Potsdam, Germany.

Le CNES publie également ses propres déterminations du champ de gravité mondial et les ondulations du géoïde à un rythme mensuel, mises à disposition sur le site du Bureau Gravimétrique International (BGI).

2.3 GOCE

GOCE (Gravity field and steady state Ocean Circulation Explorer mission, Fig. 2.7) a été lancée le 17 mars 2009 par l'Agence Spatiale Européenne (ESA). Cette mission utilise un satellite placé sur une orbite héliosynchrone à 250 km d'altitude, qui embarque un gradiomètre. Cet instrument enregistre les accélérations à partir de six accéléromètres placés à 50 cm de distance les uns des autres. La détermination des différences de l'accélération (amplitude de $10^{-12}\ m/s^2$) permet de reconstituer le tenseur des gradients de gravité constitué de neuf termes dont seuls six sont indépendants (http://www.esa.int/SPECIALS/GOCE).

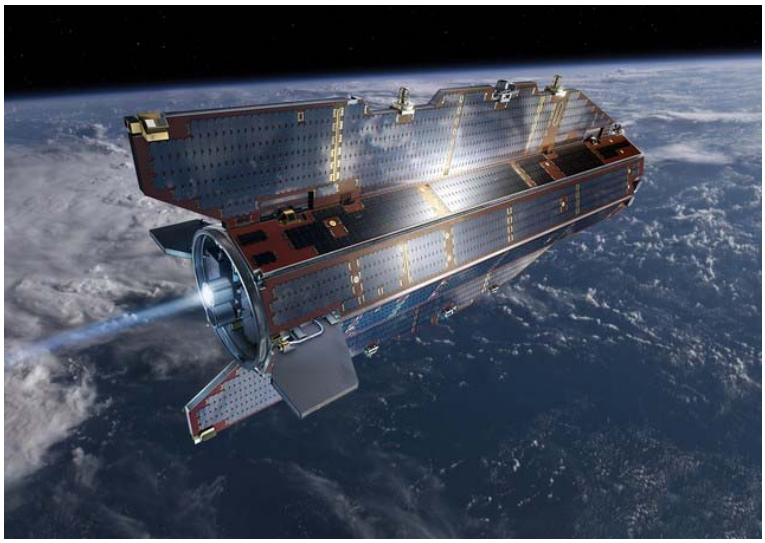

Fig. 2.7 Vue du satellite GOCE, ESA.

Les objectifs de cette mission sont plus ambitieux que ceux de GRACE : cartographier le géoïde au centimètre près avec une résolution spatiale de 100 km.

La contribution de différente technique spatiale et terrestre pour découvrir le champ de pesanteur est montrée dans figure 2.8. Différentes Résolutions et précisions en gravimétrie nécessaires pour différentes études sont montré dans figure 2.9.

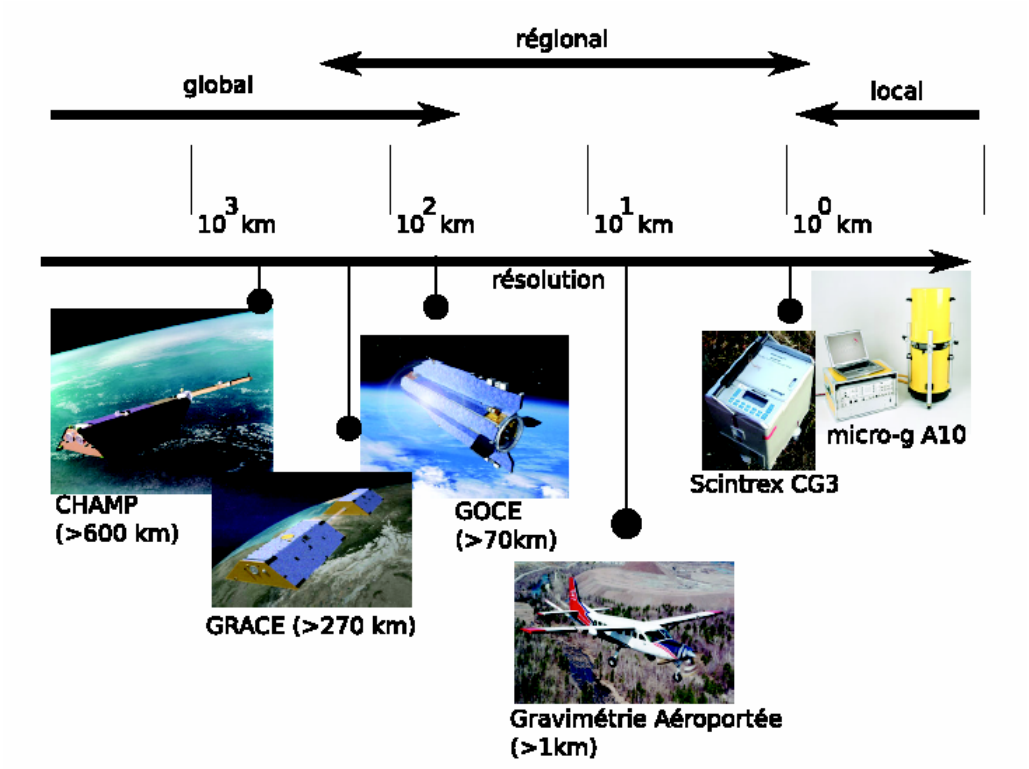

Fig. 2.8 Résolutions spatiales et applications des différents systèmes gravimétriques actuels (Kreye et al. 2006).

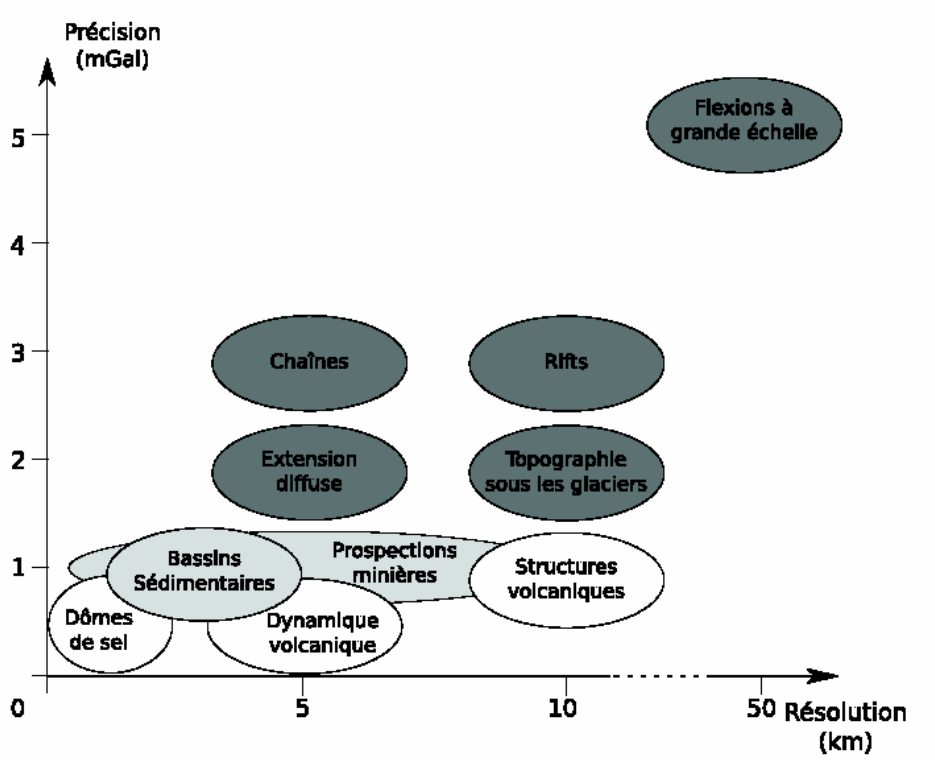

Fig. 2.9 Résolutions et précisions en gravimétrie nécessaires pour différentes études structurales (Hein 1995).

4. La technique GPS

Développé dans les années 80 par le Département de la Défense américain, le système GPS (Global Positioning System) est un système descendant. Chaque satellite possède plusieurs horloges atomiques et génère deux ondes porteuses (à 1575,42 MHz et 1227,60 Mhz), modulées par des codes pseudo-aléatoires, qu'ils émettent vers la Terre. Les antennes au sol reçoivent ces signaux et le calcul de la position en découle (Fig. 2.10). La précision de ce positionnement varie suivant le traitement adopté. Ainsi, les récepteurs GPS "grand public" permettent un positionnement métrique. En géodésie, on atteint une précision de quelques millimètres. En raison du faible coût des récepteurs GPS, il existe un très grand nombre de sites internationaux hébergeant des récepteurs GPS permanents. Cette technique spatiale est celle fournissant la meilleure qualité de positionnement. Il faut toutefois souligner que celle-ci est hétérogène.

Fig. 2.10 Un satellite et une antenne GPS, d'après site de IGN

En effet, la qualité du positionnement altimétrique (5 mm environ) est moindre par rapport à celle du positionnement planimétrique (2 mm environ), principalement en raison de la mauvaise connaissance du contenu en vapeur d'eau de l'atmosphère.

5. Nivellement de précision

Le nivellement de haute précision est actuellement l'une des techniques les plus efficaces pour mesurer l'altitude et sa variation. Cette technique consiste en la mesure de la différence de hauteur entre deux points (repères) sur une ligne de visée horizontale à la surface de la terre. La somme des différences de

hauteurs mesurées le long d'une ligne de nivellement donne la hauteur d'un repère par rapport au repère initial (Fig. 2.11). Une ligne est définie par des sections entre deux repères. La précision attendue sur la hauteur dépend du matériel utilisé, du mode opératoire sur le terrain et des traitements opérés sur les mesures brutes. Le nivellement se pratique à pied ou motorisé (Fig. 2.11, Fig. 2.12). Le procédé est identique et la seule différence est que dans le nivellement a pied on déplace les deux mires et le niveau a pied, alors que dans le nivellement motorisé on les déplace par 3 véhicules.

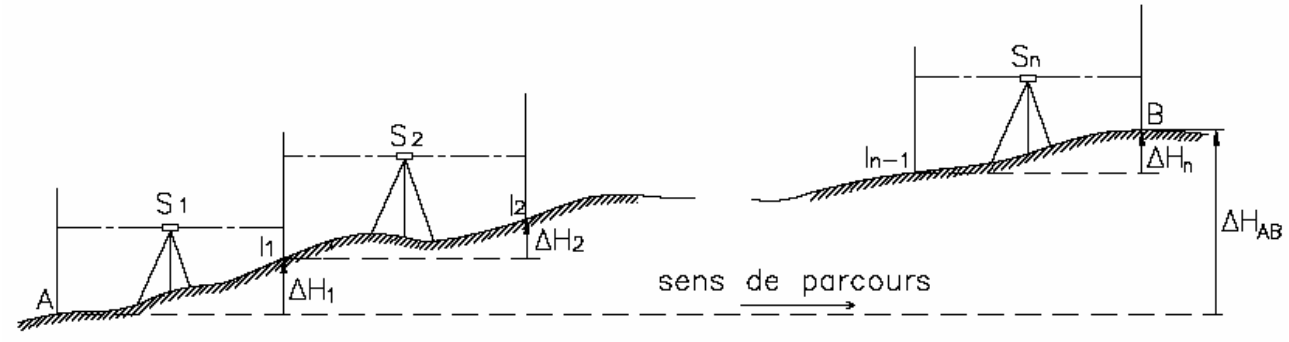

Fig. 2.11 Principe traditionnel du nivellement géodésique

Fig. 2.12 Le systéme Nivellement motorisé en Iran (Poursharifi et al., 2008)

La différence de hauteur brute ΔH_{AB} entre 2 points A et B (Fig. 2.11) est obtenue par

$$\Delta H_{AB} = \sum_{i=1}^{N} \Delta H_i = \sum_{i=1}^{N} b_i - \sum_{i=1}^{N} f_i = \sum_{i=1}^{N} (b_i - f_i) \quad (2.5)$$

Où N est nombre de mise en station, ΔH_i différence de hauteur de la $i^{éme}$ mise en station, b_i relevé arrière, f_i relevé avant.

Pour réaliser un nivellement de haute précision, les sections d'une ligne sont mesurées deux fois selon un aller ($A \rightarrow B$) et retour ($B \rightarrow A$). Chaque section est alors caractérisée par 2 mesures qui sont comparées (analyse de la qualité du nivellement) puis moyennées.

Bien que simple dans sa mise en œuvre, cette méthode nécessite de corriger les valeurs brutes d'effets physiques afin de minimiser les sources d'erreurs propres aux conditions de terrain.

3. Les observations gravimétriques et géodésiques en Iran

1. Motivation

Dans ce chapitre, nous réalisons un ‘’état des lieux’’ des réseaux gravimétriques et géodésiques en Iran résultant des travaux géodésiques et gravimétriques antérieurs à cette thèse. Ce bilan montre la nécessité de construire de nouveaux réseaux précis et détaillés en particulier pour la pesanteur aux points positionnés précisément par les techniques GPS et nivellement condition au calcul précis d’un géoïde sur l’Iran.

Les observations gravimétriques

En Iran, les premières mesures de la pesanteur débutent en 1905 par l’utilisation d’un gravimètre de Torsion Balance-Eotvos pour l’exploration géophysique (Afshar et Zomorrodian, 1970). Depuis 1958, la gravimétrie académique, la mesure et la cartographie des anomalies de pesanteur sont initiées en collaboration avec le Worldwide Gravity Survey (ibid). Pendant l’époque 1960-1968, le réseau gravimétrique du 1er ordre de l’Iran est établi et mesuré à l’aide d’un gravimètre Askania Graf, réseau rattaché au système référentiel de pesanteur de Potsdam, avec une précision relative de 0.1 mGal (ibid). La station fondamentale se situe à l’aéroport Mehrabad (Tehran), et est liée à d’autres stations internationales dans le système de Potsdam. La mauvaise qualité de ce réseau nécessite alors la réalisation d’un nouveau réseau du 1er ordre en 1970 composé de 23 stations implantées dans les aéroports ou dans les gares ferroviaires. La station de Mehrabad et le réseau du 1er ordre sont mesurés par l’Organisation Géographique Iranienne en coopération avec L’US Army Topography Command (Défense Mapping Agency, 1979). Afshar et Zomorrodian (1970) estime un écart type de 0.004 mGal/km pour les valeurs de pesanteur de ce réseau. A la même époque le réseau du 2ème ordre composé de 27 stations dans la région de Azerbaidjan complète le réseau du 1er ordre (Zomorrodian, 1971). Ce travail est accompagné en 1970 par l’implantation d’une ligne d’étalonnage dans un projet associant l’IGTU et le Centre Cartographique National de l’Iran (NCC) ligne modifiée ultérieurement (Zomorrodian, 1985). La période 1960-79 se caractérise par la réalisation des levés gravimétriques par l’IGTU et d’autres organismes en coopération avec la Défense Mapping Agency soit 12000 nouveaux points. Ces données sont attachées aux réseaux gravimétriques de 1er et 2ème ordres et finalement sont référencées au réseau IGSN 71 (Dehghani et Makris, 1984; Zomorrodian, 1987). Signalons enfin que, depuis 1979, la

pesanteur et mesuré sur le réseau de nivellement de 1er ordre par l'IGTU et le NCC. L'ensemble de ces observations est reporté sur la figure 3.1. Ces travaux de terrestre ont permis d'établir une carte d'anomalie de Bouguer sur l'Iran publié par Dehghani et Makris (1984) (voir figure 3.2) à partir des données incluses dans la Banque des Données au BGI. Depuis 2000, un programme de coopération a été établi entre le NCC (Iran), le laboratoire Geosciences Montpellier (Université Montpellier 2, France) et l'EOST (Université de Strasbourg, France) visant à la réalisation d'un réseau fondamentale gravimétrique, d'une ligne d'étalonnage et d'un réseau multi-observations géodésiques et gravimétriques afin d'établir une nouvelle carte d'anomalie de pesanteur et de calculer un modèle du géoïde sur l'Iran. L'ensemble de ces travaux gravimétriques est décrit en détail dans ce chapitre sous la forme de trois d'articles.

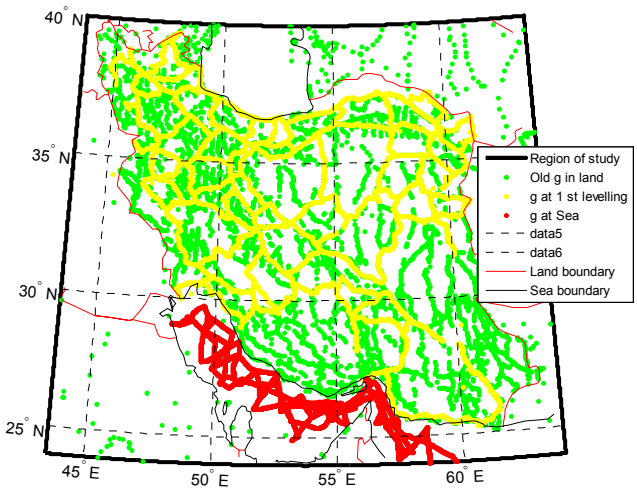

Fig. 3.1 Distribution les données pesanteur sur l'Iran

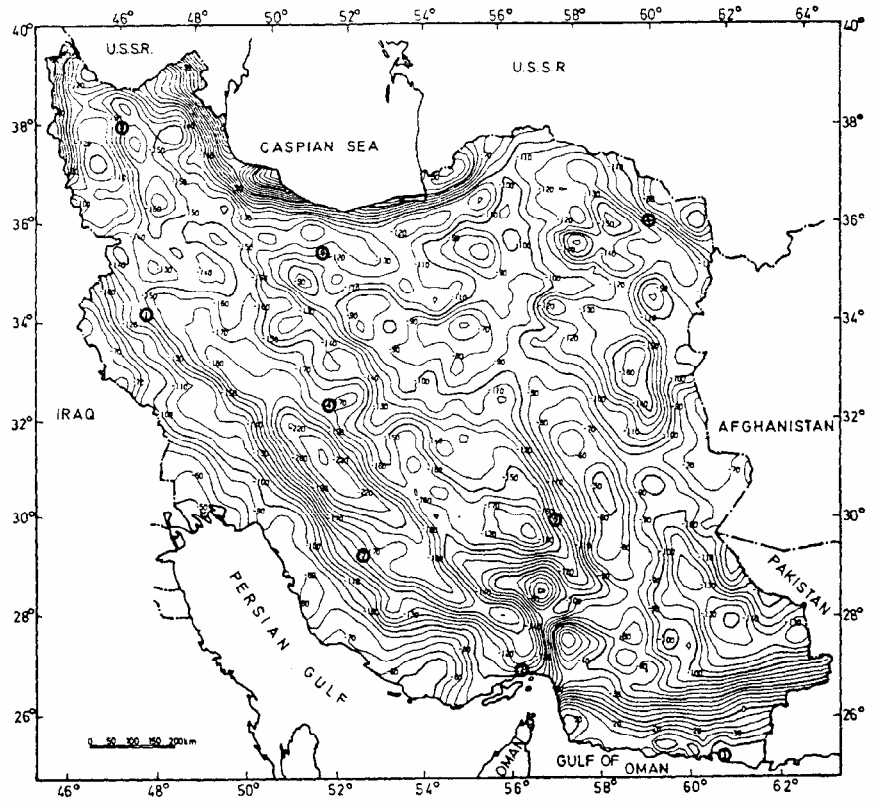

Fig. 3.2 Carte d'anomalie de Bouguer complete de l'Iran d'après Dehghani et Makris (1984)

Les Réseaux GPS sur l'Iran

L'établissement de réseaux GPS précis en Iran présente un double intérêt. D'une part, nous verrons ulterieurement que, de la hauteur GPS, il est possible de déterminer ponctuellement la hauteur du géoïde, via la connaissance de la hauteur orthométrique. D'autre part, les reseaux GPS permettent la localisation précise des points gravimétriques.

Le réseau géodésique GPS du 1er ordre a été établi et mesuré pendant 1988-1990 sur le territoire Iranien (Djamour et Nankali, 2009). Ce réseau comporte 242 stations avec une maille 110 km (Fig. 3.3). Le réseau géodésique GPS du 2eme ordre a été implanté et mesuré avec une maille de 20 – 25 km, soit 7 stations dans chaque triangle du 1er ordre (Fig. 3.3). Ultérieurement, le réseau géodésique GPS du 3ème ordre a été réalisé avec une maille de 8 – 15 km. Nous allons donc décrire rapidement les réseaux GPS iraniens en montrant la nécessité d'établir un nouveau réseau multi-observation géodésiques et gravimétriques.

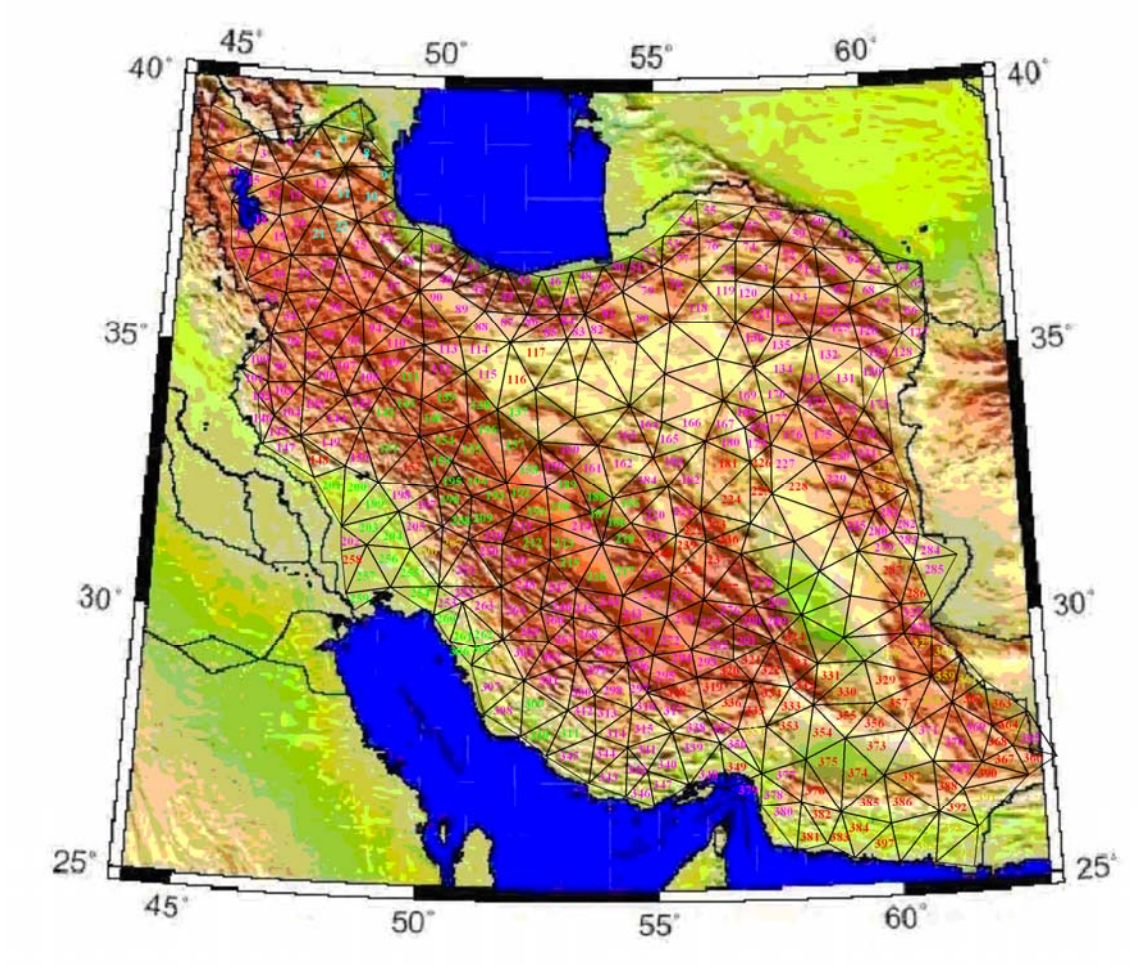

Fig. 3.3 Réseau géodésique satellitaire (GPS) du 1er ordre de l'Iran avec 242 stations. Les réseaux du 2ème et du 3ème ordre correspondent spectivement à 2607 et 6700 stations

Depuis 1999, les réseaux GPS à vocation géodynamique se sont multipliés associant plusieurs organismes, le NCC, l'International Institut of Earthquake Engineering and Seismology IEES (Iran), l'Université Montpellier 2 (France) et l'Université Joseph Fourier (France) (Fig. 3.4). Enfin, un réseau GPS permanent a été construit entre 2003 et 2004 (Fig. 3.5). Compte tenu du cahier des charges concernant la réalisation des réseaux GPS du 1er, 2ème et 3ème ordre (www.ncc.org.ir), ces réseaux ne pouvaient pas servir de base pour la réalisation d'un réseau multi-observations géodésiques et gravimétriques. Le NCC a donc décidé de réaliser un nouveau réseau sur lequel les mesures gravimétriques sont colocalisées aux mesures de positionnement GPS (Hatam et Djamour, 2004). L'existence du réseau GPS permanent en Iran offrait aussi l'opportunité de positionner avec précision l'ensemble de points des mesures colocalisées dans le système ITRF 2005. Le nouveau réseau, nommé MPGGNI10, de maille 55 km est présenté dans le 3ème article de ce chapitre.

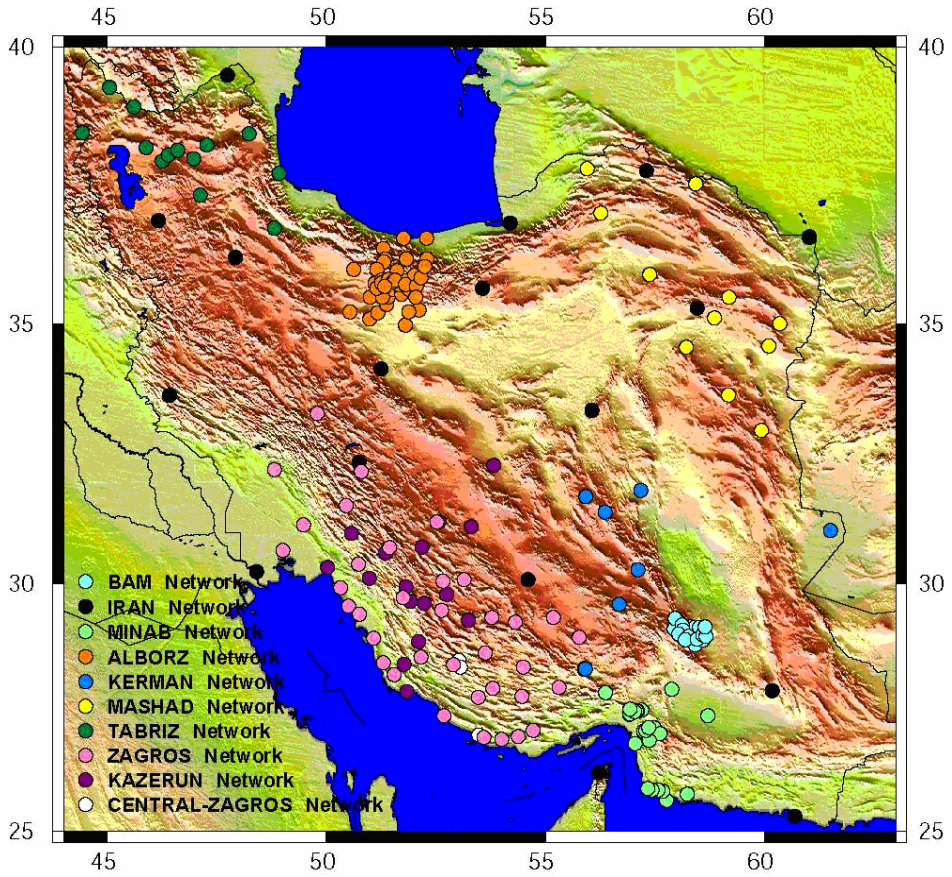

Fig. 3.4 Réseaux GPS locaux à vocation géodynamique

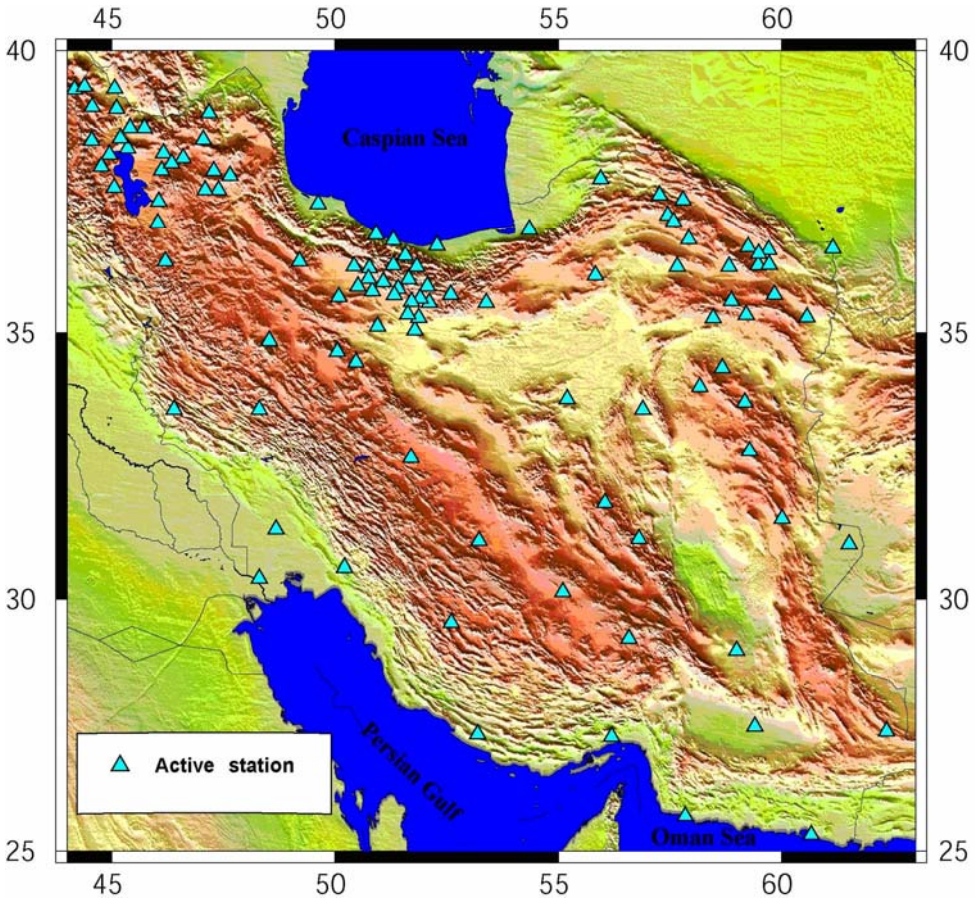

Fig. 3.5 Réseau GPS permanent

Les réseaux de nivellement en Iran

Dans l'objectif de mesurer la hauteur orthométrique des sites du réseau MPGGNI10, il etait important de rattacher les mesures de nivellement aux réseaux de nivellement existants. La figure 3.5 représente les réseaux de nivellement du 1er, 2ème et 3ème ordre en Iran établis depuis 1979 [Meamarzadeh, 1998; Poursharifi, 2008]. Les erreurs sur les réseaux du 1er, 2ème et 3ème ordre sont respectivement de $\pm 3mm\sqrt{km}$, $\pm 8mm\sqrt{km}$ et $\pm 12mm\sqrt{km}$ (Meamarzadeh, 1998). Depuis 2008, le nivellement est motorisé améliorant ainsi la vitesse d'acquisition des mesures (Poursharifi et al, 2008).

Fig. 3.6 Les réseaux nationaux de nivellement du 1er (en rouge), 2ème (en vert) et 3ème (en violet) ordre en Iran

Ainsi, nous pouvions espérer niveler les points du réseau MPGGNI09 avec une précision de $\pm 3mm\sqrt{km}$ préconisée dans ce projet.

2. Etablissement du réseau nationale gravimétrique absolue de l'Iran

Establishment of National Absolute Gravity Network of Iran: An opportunity to detect long-term and seasonal gravity changes, and their relation to crustal deformation and hydrology

To be submitted to Newton's Bulletin

Y. Hatam(1,2), R. Bayer(1), J. Hinderer(4), Y. Djamour(3), K. Ghazavi(2), M. Sedighi(2), B. Luck (4), N. Le Moigne(1), P. Vanicek(5), H. Cheraghi(2), R. Saadat(2), A. Bahrampour(2), H. Asghari(2), H. Meygooni (2), S. Rafiey(2), F. Tavakoli(2), A. Soltanpour(2), N. Azizian(2), M. M. Hossaniali (6), J. P. Boy (7)

(1) Geosciences Montpellier cc60,Universite Montpellier 2–CNRS, Pl. E. Bataillon, 34095 Montpellier Cedex05, France. Email: yaghoub.hatam@gm.univ-montp2.fr , roger.bayer@gm.univ-montp2.fr

(2,3) [(2) Physical Geodesy Department, Geodesy and Land Surveying Management + (3)Geomatics College], National Cartographic Centre (NCC), PO Box 13185-1684, Meraj Ave, Tehran, Iran. Email: yaghoubhatam@yahoo.com, djamour@ncc.org.ir

(4) Ecole et Observatoire des Sciences de la Terre, Institut de Physique du Globe de Strasbourg, CNRS-ULP UMR 7516, 5, rue Des cartes, 67084 Strasbourg Cedex, France. Email: jacques.hinderer@eost.u-strasbg.fr

(5) University of New Brunswick, Fredericton, Canada. Email: vanicek@unb.ca

(6) Faculty of Geodesy and Geomatics Engineering, KN. Toosi University of Technology, Tehran, Iran. Email: hossainali@kntu.ac.ir

(7) NVI, Inc./NASA Goddard Space Flight Center, Greenbelt, Maryland, MD 20771 USA: jpboy@eost.u-strasbg.fr

Abstract

The National Absolute Gravity Network of Iran is established during 2000-2007 and consists in 24 stations implemented close to the airports with an average spacing of 300 km. It was measured during the period 2000-2007 with 2 absolute gravimeters FG5 from Microg/Lacoste Inc. The gravity field at each station was recorded at least half a day depending on the environmental noise. All the data sets are processed identically using the processing software g version 7.0 from Micro-g Solutions Inc, and corrected for solid earth tides, tidal oceanic, atmospheric pressure loading and polar motion effects. Precision of the absolute gravity values varies between 2 and 5μGals. From the analysis of the time series recorded at National Cartographic Center (Tehran) and at Abali (Alborz mountains) gravity stations during the same epoch, we point out the dependency of the gravity values with time as a factor limiting the precision of the gravity data collected at different epochs with relative spring gravimeters and tied to the absolute network. We show that active tectonics and continental water storage in Iran may be at the origin for seasonal and inter-annual gravity variations.

Key words: Absolute gravity, national network, tectonic, field experiments, processing, NAGNI2009.

1. Introduction

Iran covers a large area limited in longitude by the meridians 44°E and 64°E and in latitude by the parallels 25°N and 40°N. Mapping a new gravity field over Iran is at present a great challenge for geodesic and geodynamic considerations: gravity anomaly maps are precious geophysical tools to understand the structure of the earth. From geodetic point of view, coupling precise leveling, gravity surveys and GPS measurements is required to determine accurately altitude and a geoid model over the Iranian territory. Numerous gravity surveys were carried out in Iran before the years 70 (see for example Zomorrodian (1971) and Dehghani and Makris (1984); see also http://www.geodesie.ird.fr/bgi/). The gravity value at the old fundamental Tehran Airport site was firstly determined by relative measurements linked to stations in the Potsdam reference network, and finally transferred in IGSN71 system (Zomorrodian (1987)). It was decided by the National Cartographic Center of Iran (Nadjafi et al., 1998; Nadjafi et al., 2006) to build a new national gravity network of Iran (NGNI) with a final mesh of 5'x 5' (after densification in several steps) and a precision of the order of 10 μGals. The NGNI will consist in 0 to 3th order linked networks. These gravity data will be combined with precise levelings, GPS-obtained heights and global earth gravity models to compute a national geoïd with an expected precision of a few cm. First, we return to a historical background of the gravity surveys in Iran. Then, we present the design of the new fundamental absolute network, named National Absolute Gravity Network of Iran 2009 (NAGNI2009) and detail the metrological specifications and the process of the data. From reiteration of the absolute measurements at two sites during the 2000-2007 epoch, we show that the secular variation must be taken into account to update the NAGNI2009 gravity values which needs regular reiteration of the network.

2. Historical background of the gravimetric surveys in Iran

In Iran, first gravity measurements are initiated in 1905 and collected by using a Torsion Balance-Eotvos gravimeter for geophysical exploration (Afshar and Zomorodian, 1970). During the 1910's years, gravity measurements are carried out for petroleum exploration in Khouzestan province using a Thyssen gravimeter (ibid). Since 1958, academic gravimetry, surveying and mapping the gravity anomalies are initiated by the Institute Geophysics of Tehran University (IGTU) in collaboration with Worldwide Gravity Survey (ibid).

During the epoch 1960-1968, the 1st order gravity network of Iran is implemented and measured with an Askania Graf gravimeter and the obtained values were referred to the Gravity Postdam System, with a relative precision of 0.1 mGal (ibid). The low precision of this network requires the realization in 1970 of a new 1st order gravity network, consisting of 23 stations localized in airports or in the railway stations (**Fig. 3.7**) (Afshar and Zomorrodian, 1970). This network is preceded by the measurement of the fundamental gravity reference station in Mehrabad airport (Tehran), by linking this station to other stations where g is given in the Potsdam Gravity Reference System. The Mehrabad airport and the first order network are measured by the Iranian Geographic Organization in cooperation with the US Army Topographic Command (Defense Mapping Agency, 1979). Because there is no gravity calibration line in Iran at that time, the calibration tables in the gravimeter booklet are used to calibrate the instruments. Afshar and Zomorrodian (1970) estimate to ±0.004 mGal/km the standard deviation of the gravity values for this network. At the same epoch, a 2nd order network made of 27 stations in Azarbaydjan province completes the 1st order network (Zomorrodian, 1971). This survey is also accompanied in 1970 by the implantation of a calibration line in a frame of a collaborative project between the IGTU and the National Cartographic Center of Iran (NCC). The mentioned calibration line is modified once more after several years (Zomorrodian, 1985). Since 1960, about 12000 gravity data are collected on the Iranian territory by IGTU and other organisms in cooperation with the Defense Mapping Agency. These data are tied to the 1st and 2nd order networks already mentioned and finally referenced to the International Gravity Standardization Net IGSN 71 (Zomorrodian, 1987). After 1979, the 1st order leveling sites are measured with Lacoste and Romberg, and Scintrex relative meters by IGTU and NCC. At present day, a multi-purpose physical geodesy and geodynamic network of Iran is carried out by NCC which calls for the realization of the very precise NAGNI2009 network.

3. The NAGNI2009 network

The first objective of NCC is to establish the NAGNI2009 network and measure the absolute gravity (AG) with an accuracy of 2-5 μGals at sites.

3.1 Design of the network

The absolute gravity sites of the NAGNI2009 network are implemented successively during the 1998-2002 and 2005-2007 periods. The stations are distributed homogeneously on the Iranian territory with a mean spacing of 300 km. During the first epoch, stations are located in airports and correspond to concrete

monuments. The recent stations are built in general at about 20-30 km from airports, out of cities and on the bedrocks in order to attenuate the anthropic noise. The **figure 3.8** indicates the location of the sites over Iran.

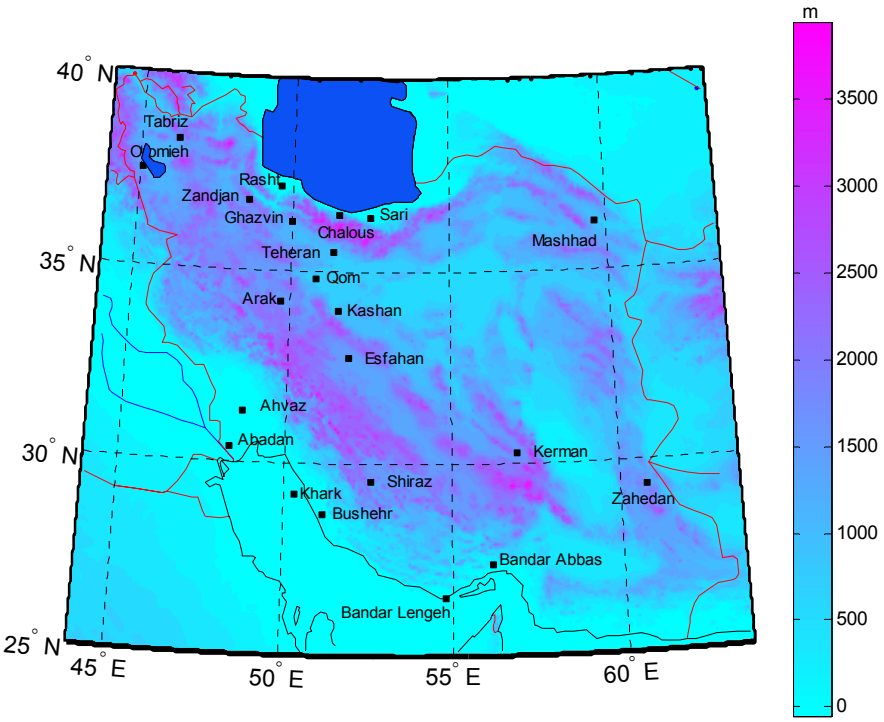

Fig. 3.7 Ancient first order gravity network of Iran (destroyed) (Afshar and Zomorrodian (1970))

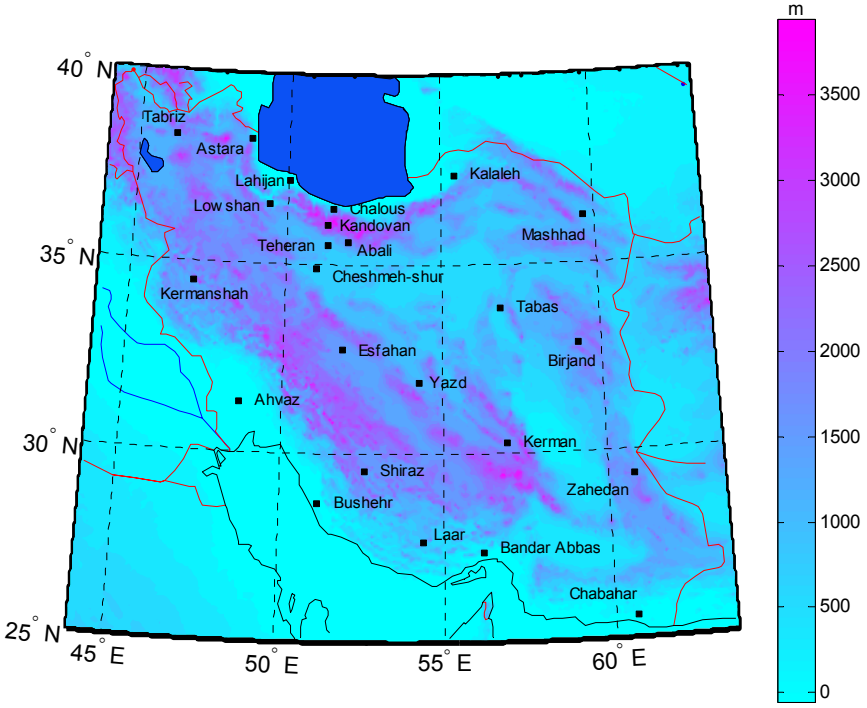

Fig. 3.8 Stations of the National Absolute Gravity network of Iran NAGNI2009

3.2 Survey setup campaigns and measurement protocol

The AG sites are occupied during 2000-2007. The absolute measurements are realized with the two French national FG5 206 and 228 ballistic meters manufactured by Micro-g Lacoste Inc. and belonging to the DT/INSU of CNRS (France).

The AG measurements start in October 2000. AG measurement campaigns take place in September-October epoch, in order to minimize the variation of the annual gravity component with respect to long term fluctuations. The measurements during 2000-2004 were realized on heavy concret pillar and inside a tent. Such installation was not efficient in bad meteorological conditions (high daily variations of temperature and windy conditions) and sometimes deteriorates the accuracy of measurements. High level of noise was also observed in some places near urbanized zones and when pillars are implanted in unconsolidated sediments. Thus, it was decided since 2005 to install the meters in an insulated mobile home (**photo 1**) to decrease the environmental noise. Moreover, the measurements are carried out on a concrete pillar fixed to bedrock to increase the stability of the sites. Duration of the campaigns is optimized by transporting the FG5 meter between distant stations by the NCC aircraft (**photo 2**). Since 2000, some stations, like NCC and Abali, are measured several times (**Fig. 3.13 and Fig. 3.16**). Measurements are repeated at these stations to monitor possible inter-annual variations of gravity related to continental water storage change or (and) to present-day tectonic vertical deformation (Djamour et al., 2010).

The FG5 gravimeter measures the acceleration of a free-falling corner-cube in a vacuum (a "drop") using an iodine-stabilised laser interferometer and a Rubidium atomic clock (Niebauer et al., 1995) (**Fig. 3.9**). Basically, a test mass is dropped and the earth gravity g_0 is determined by fitting the distance-time couples (x_i,t_i) to the theoretical relationship (Niebauer et al. 1995):

$$x_i = x_0 + v_0\tilde{t}_i + \frac{g_0\tilde{t}_i^2}{2} + \frac{\gamma x_0\tilde{t}_i^2}{2} + \frac{1}{6}\gamma v_0\tilde{t}_i^3 + \frac{1}{24}\gamma g_0\tilde{t}_i^4 \quad , \qquad \tilde{t} = t_i - \frac{(x_i - x_0)}{c}. \quad , \qquad \text{(eq. 1)}$$

where γ is the vertical gravity gradient, (x_0,v_0) represent the initial values of position and speed of the dropping object inside the vacuum chamber and (x_i, t_i) are for the time t_i. The mechanics of the dropping system are such that it can not return exactly to the same height for every drop. However, x_0 is one of the free parameters in the equation of motion. Inaccuracies in the gradient γ estimation bring further uncertainty to the gravity value g_0. In order to minimize these uncertainties, the reference gravity value g_{ref} independent of the gravity gradient at height h_{ref} is determined (**Fig. 3.9**). Several authors have worked on the determination

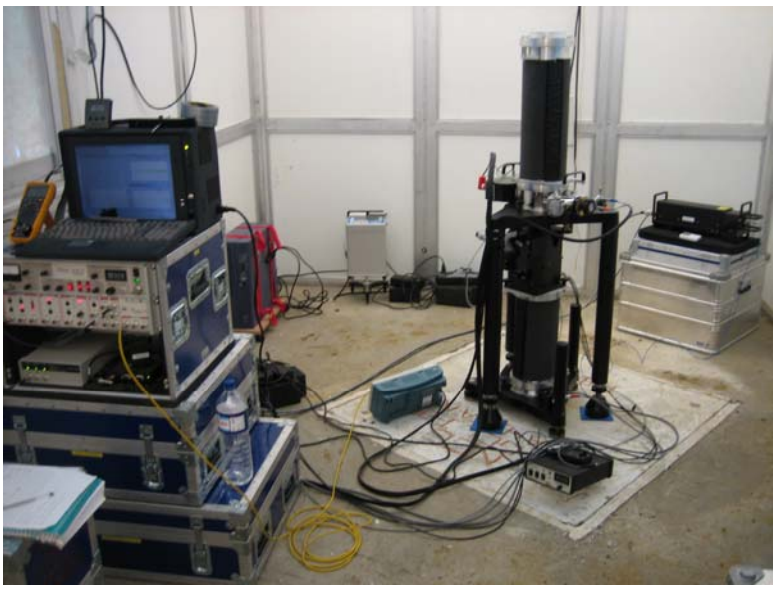

Photo 1. Absolute Gravity experiment using FG5 206 in a mobile home at Lahijan (South Caspian border)

Photo 2. Airway transportation of FG5 using the NCC Dornier 228 between stations of the NAGNI2009 network

of h_{ref}, which, as a rule-of-thumb, is located approximately one third of the way down the drop (Niebauer, 1989; Timmen, 2003; Zumberge, 1981). Height h_{ref} depends on instrument dimensions and instrument setup. The mean value of g_0 is estimated from a series of 100 or 120 drops per hour and referred to a "set" (**Fig. 3.10)**. At the end, the AG value is estimated by averaging several hourly sets (in general ≥ 12) (**Fig. 3.11)**.

3.3 Data processing and results

All the data sets are processed identically using the new processing software g-version 7.0 from Micro-g Lacoste Inc. The value for each drop is rejected if its difference with the hourly value exceeds 3σ.

Various corrections are applied in order to obtain the gravity value:

1. Gravity values are corrected for solid earth tides using successively ETGTAB software (Wenzel, 1996) with the Tamura tidal potential development (Tamura, 1987), Berger model (Microg, 2007) and tidal oceanic loading effects from Schwiderski's (1980), FES2004 (Lyard et al., 2006) and CSR different models (Micro-g, 2007). Typically, Gravimetric Earth Tides may reach peak-to-peak amplitudes of 110 μgals, while ocean tide loading effects in Iran depend on the proximity to the ocean and may reach peak-to-peak amplitudes of tens of microgals. Correction values estimated from the combination of the various models are close (<1 μGal). Therefore, ETGTAB and FES2004 are adopted for the corrections.

2. Atmospheric pressure loading (mass and deformation effects) are corrected using the classical empirical admittance value of -0.3 μGal/ hPa.

3. Polar motion effects due to changes in the centrifugal potential which are caused by changes in the Earth's rotation are also removed according to the International Earth Rotation Service (IERS-www.iers.org).

AG recordings during the Iranian campaigns are often performed in low seismic noise conditions as it is proved by the drop to drop noise ranging from 7 to 12 μGal (see example in **Fig. 3.10**).

The error on the AG values (δ_{tot}) is considered as the sum of an instrumental high frequency noise (δ_{stat}), a setup error (δ_{setup}) and the systematic instrumental uncertainty (δ_{sys}), i.e. $\delta_{tot} = \sqrt{\delta_{sys}^2 + \delta_{stat}^2 + \delta_{setup}^2}$. The instrumental noise δ_{stat} is usually obtained by the formula $\delta_{stat} = \sigma_{set} / \sqrt{N_{set}}$ where σ_{set} and N_{set} are respectively the set scatter and the number of sets. The set scatters observed during the campaigns (**Fig. 3.12**) suggest an evidence for a measurement precision lower than 0.4 μGal for at least 12 hours of measurements.

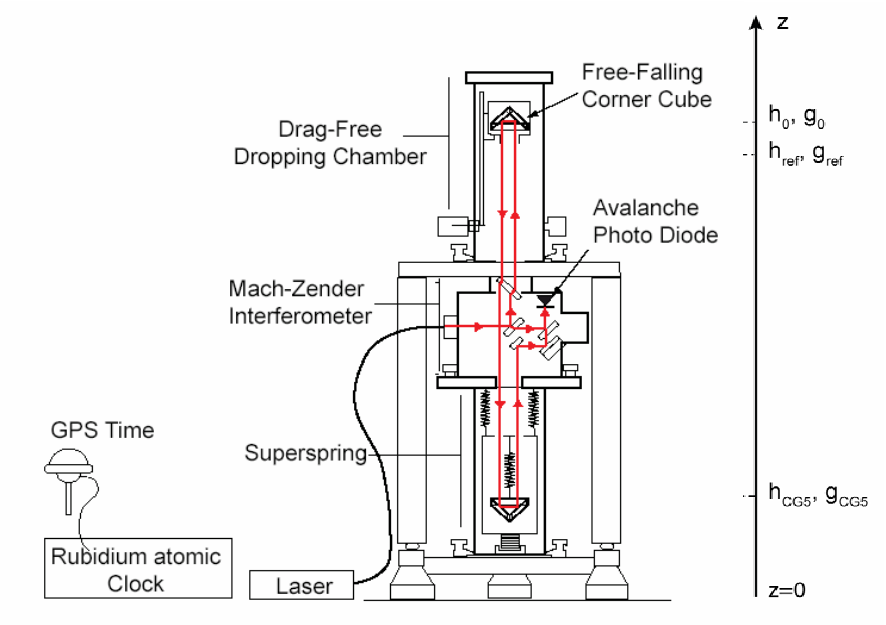

Fig. 3.9 The FG5 Absolute gravimeter (from Niebauer et al. (1995) and modified by Jacob et al. (2010))

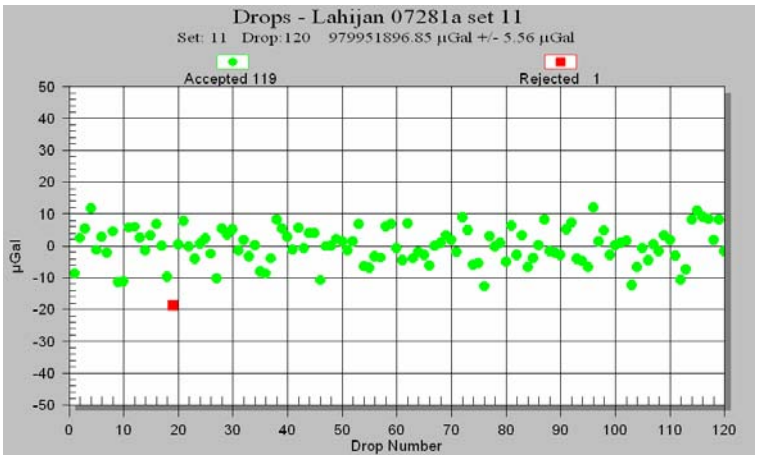

Fig. 3.10 Exemple of time series of AG values recorded during one set of 1 hour at Lahijan (South Caspian coast, see location on Fig.3.8)

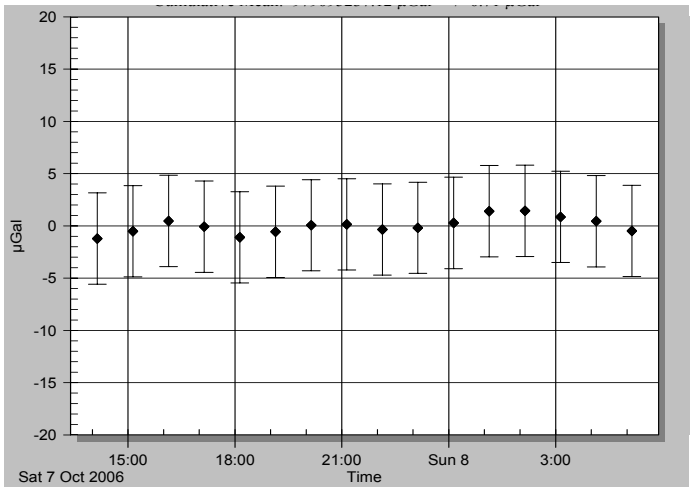

Fig. 3.11: A time series of 16 hourly AG measurements recorded at Kandovan (Central Alborz, see location in Fig. 3.8); the set scatter σ_{sc} is $\pm 0.71\mu Gal$.

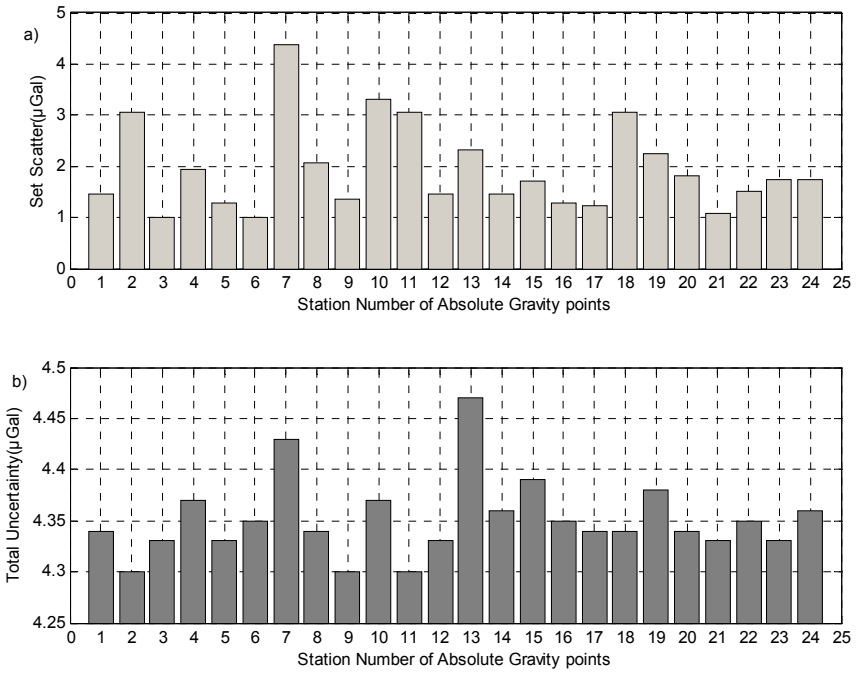

Fig. 3.12: Set Scatter σ_{sc} (a) and Total Uncertainty σ_t (b) on the AG values at bases of the NAGNI2009 network; . The weak environmental noise at the stations is attested by the values of the set scatter lower than 2 μGal for 75 % of the sites.

Station names: 1- Abali, 2- Ahvaz, 3- Astara, 4- Bandar Abbas, 5- Birjand, 6- Bushehr, 7- Chabahar, 8- Chalous, 9- Cheshmeh-shur, 10- Esfahan, 11- Kalaleh, 12- Kandovan, 13- Kerman, 14- kermanshah, 15- Laar, 16- Lahijan, 17- Lowshan, 18- Mashhad, 19- Shiraz, 20- Tabas, 21- Tabriz, 22- Tehran, 23- Yazd, 24- Zahedan.

Such a precision is perfectly consistent with our drop to drop noise level. The uncertainties on the g values for the 2005-2007 epoch is lower than the one for the first epoch 2000-2004 (**table 1**), confirming the best quality of the stations built on the bedrock and the ability of the mobile home to damp the wind and temperature effects on the measurements.

The systematic instrumental uncertainty δ_{sys} includes errors of modeling (earth tides factor, ocean loading factor, barometric and polar motion), error of system (laser, clock and system model) and environmental error (unmodeled tide swell water table effect). An error budget of 1.1 μGal is proposed by Niebauer et al. (1995) for the systematic instrumental uncertainty. From the analysis of superconducting gravimeter and AG measurements (FG5-202) at Membach station (Belgium), Van Camp et al. (2005) observe a setup instrumental white noise process at low frequency (< 1cycle/day) with a standard deviation of 1.6 μGal. Periodically inter-comparing the French FG5-206 and FG5-228 meters shows that the systematic

instrumental error of the two FG5 gravimeters is similar and the AG value given by the two instruments differs by less than 1 μGal (unpublished results).

Recent 2007 inter-comparisons between 20 absolute meters including the FG5-206 and FG5-228 at Walferdange (Luxemburg) (Francis et al., 2010) show an agreement between the meters with a standard deviation of 2 μGal. At end, The total instrumental uncertainty is estimated to ~1.9 μGals.

The 2002 and 2004 campaign is characterized by a failure of the iodine–stabilized laser of the FG5-206 meter which is the standard equipment of the FG5 (Niebauer et al., 1995). The measurements are performed for 7 stations (table 1, showed by *) with a spare polarization-stabilised He-Ne laser which uses two frequencies and is less stable especially versus temperature changes (Mäkinen & Stahlberg, 1998). As a consequence, the uncertainty on the 2002-04 values is larger roughly by a factor 2 (see **table 1**). Measurements at J9 observatory (Strasbourg) leads to a shift of 3.5 μgal between the mean values obtained from instrument equipped with a iodine–stabilized laser and a polarization-stabilised He-Ne laser. The corrected values are reported on **table 1** by **.

From a practical point of view, absolute gravity values measured by the FG5 gravimeters need to be transferred to the benchmark altitude of the pillar. We have shown previously that The FG5 absolute gravimeter yields the gravity value from the adjustment of the trajectory of a free-falling corner cube to the equation of motion (see **equation 1**) accounting for the vertical gravity gradient at the measurement site of motion. Furthermore, the vertical gradient is also used to downward continue the gravity value g_{ref} from x_{ref} to a user-defined height h which correspond to the altitude of the benchmark. The vertical gravity gradient is determined by measuring gravity ties with CG3-M or CG5 Scintrex relative gravimeters between different heights. The gradient was measured with a special tripod consisting in 3 plates at height of 0, 0.6 and 1.2 m above pillar. Gravity gradient is estimated from measurements along an “up and down” loop and by computing the gravity difference between the three different levels.

Inaccuracies in the gradient estimate bring further uncertainty to the gravity value g_0, but they mostly affect the uncertainty of all transferred gravity values. The AG value g_{ref} is defined at a height x_{ref} and the typical height differences between the x_{ref} and the bench marks range between 1.283 and 1.288 m for the FG5-228 and between 1.295 and 1.310 for the FG5-206. g_{ben} is determined at the bench marks by means of a least squares adjustment accounting for the instrumental drift of relative gravimeters. Results are given in **table 1**.

Station	Latitude (Deg.)	Longitude (Deg.)	Height (m)	Date yy.mm.dd	Gradient (µgal/m)	Gravity (µgal)	σ_{sc} (µgal)	σ_t (µgal)	Instrument
Abali	35.792	51.987	3177	2007.10.04	-409.0	979032640.5	± 2.0	± 4.3	Fg5#206
Ahvaz	31.339	48.684	13	2004.10.13	-320.0	979358518.5	± 3.1	± 4.3	Fg5#206*
Astara	38.289	48.853	25	2006.10.13	-360.8	980047305.5	± 1.0	± 4.3	Fg5#206
BandarAbas	27.372	56.163	791	2007.10.19	-324.0	978850979.1	± 2.0	± 4.4	Fg5#206
Birjand	32.892	59.291	1512	2004.10.06	-319.7	979086532.4	± 1.3	± 4.3	Fg5#206
Bushehr	28.681	51.164	251	2007.10.20	-333.0	979085455.1	± 1.0	± 4.4	Fg5#206
Chabahar	25.293	60.650	25	2000.10.22	-309.0	979011322.5	± 3.0	± 4.4	Fg5#206
Chalous	36.685	51.310	-10	2007.10.07	-304.0	979828784.2	± 2.1	± 4.3	Fg5#206
CheshmehShur	35.091	50.991	971	2005.10.23	-342.3	979467470.6	± 1.4	± 4.3	Fg5#228
Esfahan	32.746	51.877	1557	2002.10.20	-310.0	979081411.4	± 3.3	± 4.4	Fg5#206*,**
Kalaleh	37.381	55.458	126	2004.10.16	-319.2	979862718.8	± 3.1	± 4.3	Fg5#206*
Kandovan	36.151	51.316	3058	2007.10.06	-378.0	979095242.3	± 1.5	± 4.3	Fg5#206
Kerman	30.257	56.958	1761	2004.10.07	-313.3	978830164.9	± 2.4	± 4.5	Fg5#206
Kermanshah	34.497	47.045	1355	2007.10.22	-352.0	979279131.2	± 1.5	± 4.4	Fg5#206
Laar	27.670	54.385	795	2004.10.11	-304.0	978909511.3	± 1.7	± 4.4	Fg5#206*
Lahijan	37.198	50.024	127	2006.10.11	-399.0	979951899.2	± 1.3	± 4.4	Fg5#206
Lowshan	35.579	49.402	800	2006.10.15	-343.0	979612278.7	± 1.2	± 4.3	Fg5#206
Mashhad	36.230	52.591	988	2002.10.11	-314.9	979530233.5	± 3.1	± 4.3	Fg5#206*,**
Shiraz	29.547	51.310	1531	2002.10.17	-304.5	978838987.1	± 2.2	± 4.4	Fg5#206*,**
Tabas	33.837	56.859	964	2007.10.15	-305.8	979348444.1	± 1.8	± 4.3	Fg5#206
Tabriz	38.117	46.233	1360	2000.10.17	-302.7	979588943.9	± 1.1	± 4.3	Fg5#206
Tehran	35.697	51.331	1181	2007.10.03	-317.0	979430704.8	± 1.2	± 4.3	Fg5#206
Yazd	31.904	54.289	1265	2002.10.14	-319.9	979069822.1	± 1.7	± 4.3	Fg5#206*,**
Zahedan	29.341	60.794	1543	2007.10.17	-360.0	978836219.7	± 1.7	± 4.4	Fg5#206

Table. 1. Stations of the National Absolute Gravity network of Iran NAGNI09

* bi-color (red and blue) laser used

** corrected g values from the inter-comparisons of FG5-206 and FG5-228 (3.5 µgals)

σ_{sc} set scatter and σ_t total uncertainty

The range of gravity gradient values is from -409 to -302.7μGal/m. The difference with the classical -300 μGal/m free-air gravity gradient is explained by the topographic mass effect at stations in mountainous environment. Independent uncertainties on g_{ref} and vertical gradient are summed to estimate the error on g_{ben}. The accuracy on the vertical gradient is typically from 2 to 3μGal/m and error analysis yields a total uncertainty of 4 to 5 μGal for the g_{ben} values (**Fig. 3.12b**). The final g_{ben} values and their uncertainties are presented in **table 1**. The results satisfy the initial specifications of the NAGNI2009.

3.4 Seasonal to secular gravity changes and stability of the NAGNI2009 gravity field

As the rule, absolute gravity network is designed in order to measure gravity at undisturbed locations characterized by geological and hydrogeological stability and little microseismicity (Torge, 1989). No time change in g value was classically considered for such a network, assuming that temporal variations are lower than the uncertainty on the measured g, around 4-5 μGal for this work. At present day, we know that gravity changes are observed at permanent gravity stations: for instance, a 1-3 μGal annual varying gravity are evidenced in Europe at ground-based superconducting gravimeter stations within the Global Geodynamics Project (GGP) and are related to continental hydrology (Crossley et al., 2005). Hydrological signature is clearly identified on gravity field observed by the Gravity Recovery and Climate Experiment (GRACE) for annual variations (Wahr et al., 2004; Tapley et al., 2004; Ramillien et al., 2004) and inter-annual change (Andersen and Hinderer, 2005; Ramillien et al. 2006). Nowadays, Iran territory is characterized by tectonic deformations and a high seismic activity as a consequence of the shortening between Eurasia and Arabian plates. Active vertical motions are evidenced in numerous mountain belts, for example in Alborz and Zagros belts and may induce gravity change.

We illustrate the hydrological and tectonic dependencies on AG values of the NAGNI2009 network by analyzing the AG time series of the NCC-Tehran and Abali sites located respectively at the immediate southern foothills and in the Central part of Alborz Mountains (**Fig. 3.8**).

During the epoch 2000-2007, AG values at NCC show an inter-annual variation with the amplitude of ~23 μGal and a steep decrease in 2000-2002 (**Fig. 3.13a**). The time series gives an inter-annual decrease of ~0.75μGal/yr. No significant vertical inter-annual change is observed from analysis of the GPS observations at NCC-Tehran at the same period (slope of 1mm/yr) (**Fig. 3.14**). Thus, it is tempting to explain the gravity variation at NCC by the Newtonian effect of groundwater mass change.

As discussed by Llubes et al. (2004) the gravity variations due to hydrology can be separated into two major scales: local and regional. First, it is tempting to compare NCC-Tehran time series with the soil moisture gravity effect deduced from global hydrological models. Therefore, the gravity changes derived from two global water storage models are computed using convolution formalism (Farrell, 1972; Neumeyer et al., 2006). This is done by convolving surface mass distribution associated to soil moisture with the Green functions associated to Newtonian and flexure effects. The Global Land Data Assimilation System (GLDAS) (Rodell et al., 2004) describes soil moisture, snow and canopy water content variations and has a 0.25 degree grid and daily temporal sampling. The European Center for Medium Range Weather Forecasts (ECMWF, www.ecmwf.int) model quantifies soil moisture and snow cover variations with a resolution of about 0.2 degree and 6 hours solutions (Viterbo and Beljaars, 1995). Aquifer storage variations are not included in both these models. These models are not expected to perfectly account for measured gravity variations given their grid size but are useful for the estimation of hydrological regional gravity. **Figure 3.13b** shows the simulated gravity variations from GLDAS and ECMWF soil moisture distribution. The gravity calculated using ECMWF and GLDAS models are in-phase with a similar inter-annual decrease of ~-0.4 μGal/yr. Annual variations on the order of 6-8 μGal (ECMWF) or 4-5 μGal (GLDAS) peak to peak are observed over the Tehran zone. This regional effect may be considered as an "environmental noise" and must be known from global hydrogeological models to reduce the gravity value at each site of the NAGNI2009 network at a standard given epoch (for instance, the middle of year). Fortunately, repeating the AG campaigns at the same epoch for NCC site introduces only a slight variation (±1 μGal for 5 years) due to the non-exactly annual hydrological component. Moreover, we will suppose that the inter-annual variations at NCC-Tehran may be approximated by linear trend of the GLDAS and ECMWF curves. The GLDAS and ECMWF models do not include aquifer storage variations. Local aquifer can induce gravity effect which must be also cancelled. It is illustrated at NCC-Tehran site by the variation in depth of the water table measured in 2 boreholes near NCC-Tehran (distance ~3 km) (unpublished data, Water Research Center of Tehran) (**Fig. 3.13c**). The 2001-2002 decrease of ~20 μGal is correlated with a deepening of the water table while the ~10 μGal increasing in 2003-2005 is associated with a rising of the water table. In 2000-2002, the water table was deepening beneath Tehran due to heavy pumping in dry climatic condition. The hydrological data indicate a decrease of h of 7 m at depth of ~ 50m followed by an increase of 5.5m in 2003-2005.

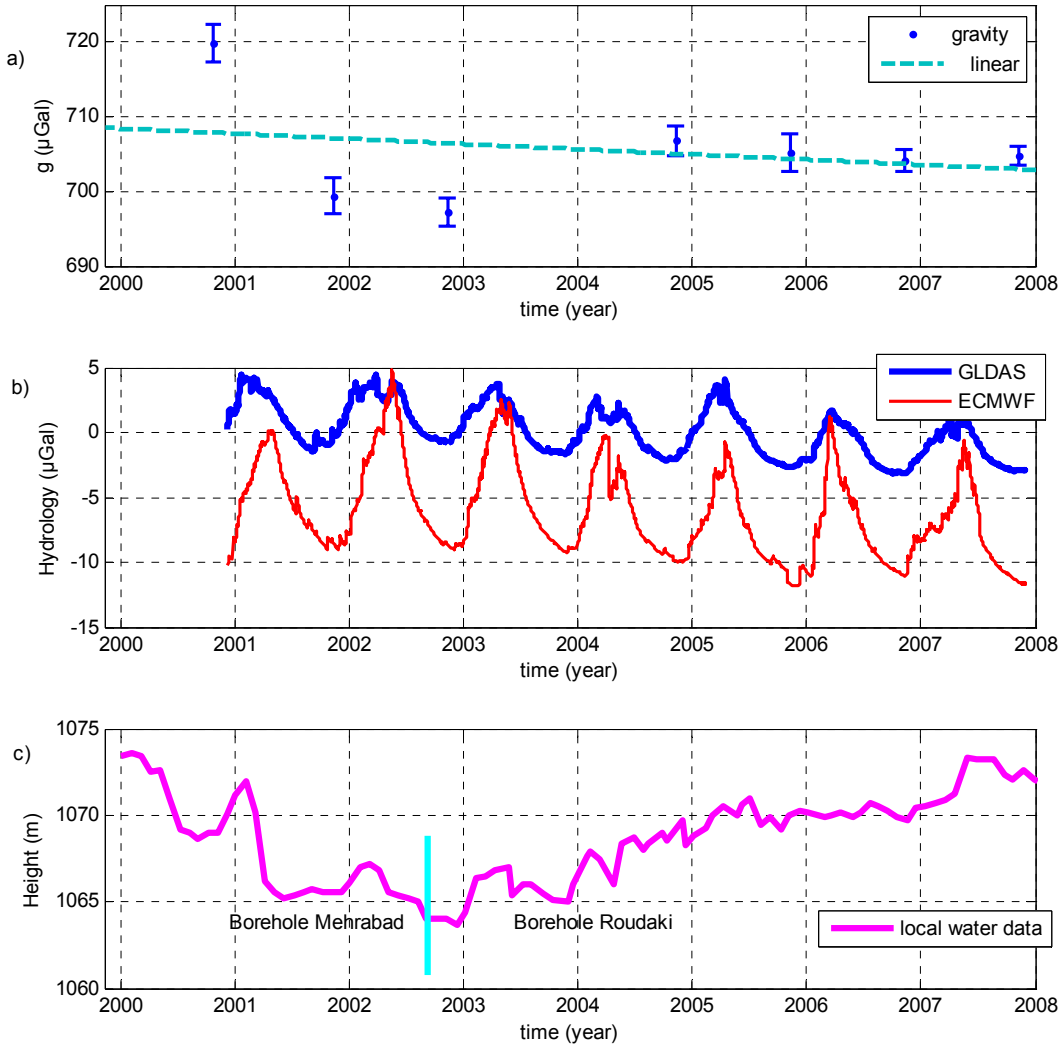

Fig. 3.13: a) AG measurements at NCC-Tehran site during the 2000-2007 period; b) the gravity changes derived from the global water storage models ECMWF and GLDAS for the same period; c) Heights of the groundwater table measured within 2 boreholes located at Mehrabad and Roudaki at a distance less than 3 km from the NCC-Tehran site(unpublished data, Water Research Center, Tehran). Measurements stopped at Mehrabad in 2002 and are tied to Roudaki data at this date .

We conjecture that the gravity variation is induced by the evolution of the water storage in saturated zone. Assuming an homogeneous water storage, the relation between absolute gravity variation δg during the 2000-2007 time interval and the corresponding water slab thickness variation δh is given by the Bouguer's formula:

$$\delta g = 2\pi G \rho \Phi \delta h, \qquad \text{(eq. 2)}$$

where ρ the density of water and Φ the porosity. The AG values are plotted versus the water table height after removing the inter-annual trend given by ECMWF curve (**Fig. 3.15**). Using (eq. 2), it is easily proved that δg and δh data are consistent for porosity ranging from 2 % and 12%. Pumping tests operated within the free-aquifers in the shallow elastic formations of Tehran provide a porosity of ~10% (Engalenc, 1968) compatible with the "gravity porosity".

In the central part of Alborz mountains, the gravity change at Abali is estimated to ~ - 6 µGal for the 2000-2007 period **(Fig. 3.16a)**. As for NCC-Tehran site, the time variation involve annual to inter-annual hydrological components of regional scale. The gravity calculated using ECMWF and GLDAS shows similar annual cycles with the amplitude of 5-8 µGal peak to peak (**Fig. 3.16b**). As for NCC-Tehran site, the annual amplitude of GLDAS model is ~3 µGal lower than the ECMWF one. Moreover, the inter-annual trend for the 2000-2007 is 0.28 µGal/yr for GLDAS and -0.35 µGal/yr for ECMWF model. Such a "secular"regional change cannot explain the -0.76 ± 32 µGal/yr (1 σ level) observed during the same epoch (**Fig. 3.16a**). We conjecture that any local hydrological gravity change at Abali is attenuated because of the geomorphological conditions of the site located at 3100 m on the summit of a steep mountain. It is tempting

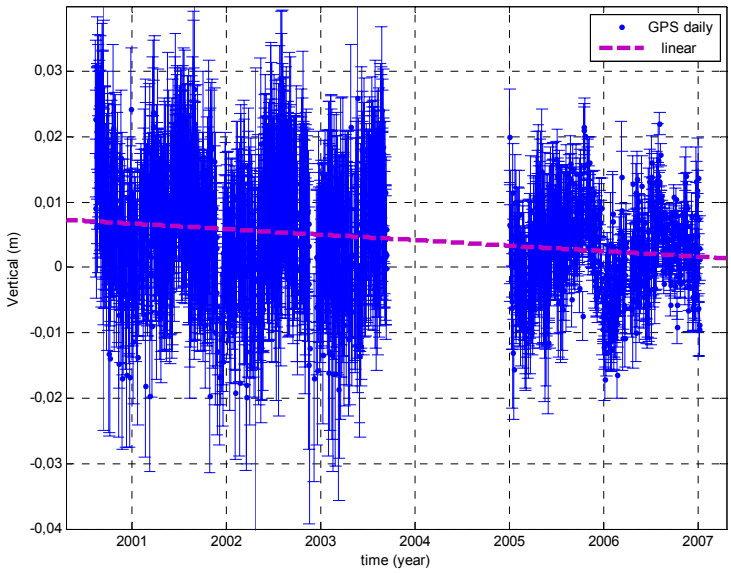

*Fig 3.14: Time series of daily solutions of the GPS vertical component at NCC-Tehran (*see *//www.ncc.org.ir/. Recording was stopped in 2003 due to a failure of the GPS receiver. A new GPS receiver was installed in 2005 on another place at NCC-Tehran. The 2 time series are tied by estimating the shift constant which minimize the rms when computing the regression line. The 1mm/yr slope is not significant.*

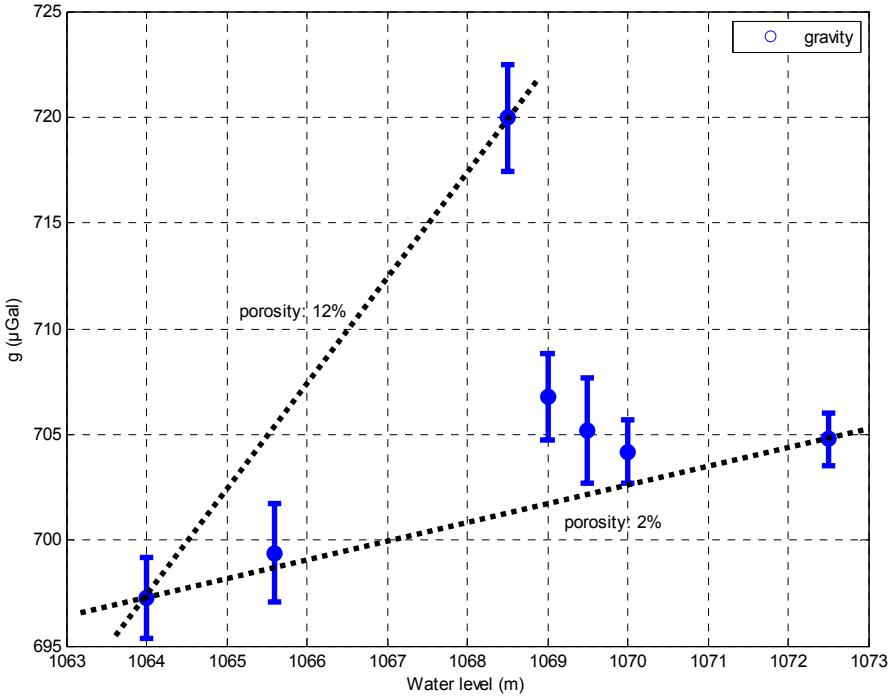

Fig 3.15: AG values are plotted versus heights of groundwater table at NCC-Tehran. These data are consistent with porosity ranging from 2 to 12 %

to consider the inter-annual AG changes at Abali as markers of the vertical tectonic deformation in Alborz Mountains (Djamour et al., submitted).

The AG values are corrected from the ECMWF and GLDAS gravity models at time of measurements (**Fig. 3.16c**). The linear trend of the residues are respectively -0.3 ± 0.38 µGal/yr (1σ level; ECMWF correction) and -0.99 ± 0.31 µGal/ yr (1σ level; GLDAS correction) which reveals a weak uplift at Abali in the internal part of the belt. We assume an admittance function between gravity and elevation changes of -0.30 µGal/ mm (free air gradient) to -0.19 µGal /mm (uncompensated isostatic model) (Djamour et al., submitted). Using ECMWF model, we estimate the rate of uplift respectively to 1 ± 1.26 mm/yr and 1.6 ±2.00 mm/yr. The GLDAS assumption leads to greater uplifts of 3.3 ± 1.03 mm/yr (free air assumption) and 5.2 ± 1.63 mm/yr (uncompensated isostatic model). This result is consistent with the uplift rate of ~2 mm/yr that can be deduced from the drainage incision in northern Alborz (Antoine et al., 2006; Djamour et al. 2010). This rate is also in agreement with 5 mm/yr of NS shortening on the active Khazar thrust fault bounding the range to the north and dipping to the south (Djamour et al., submitted).

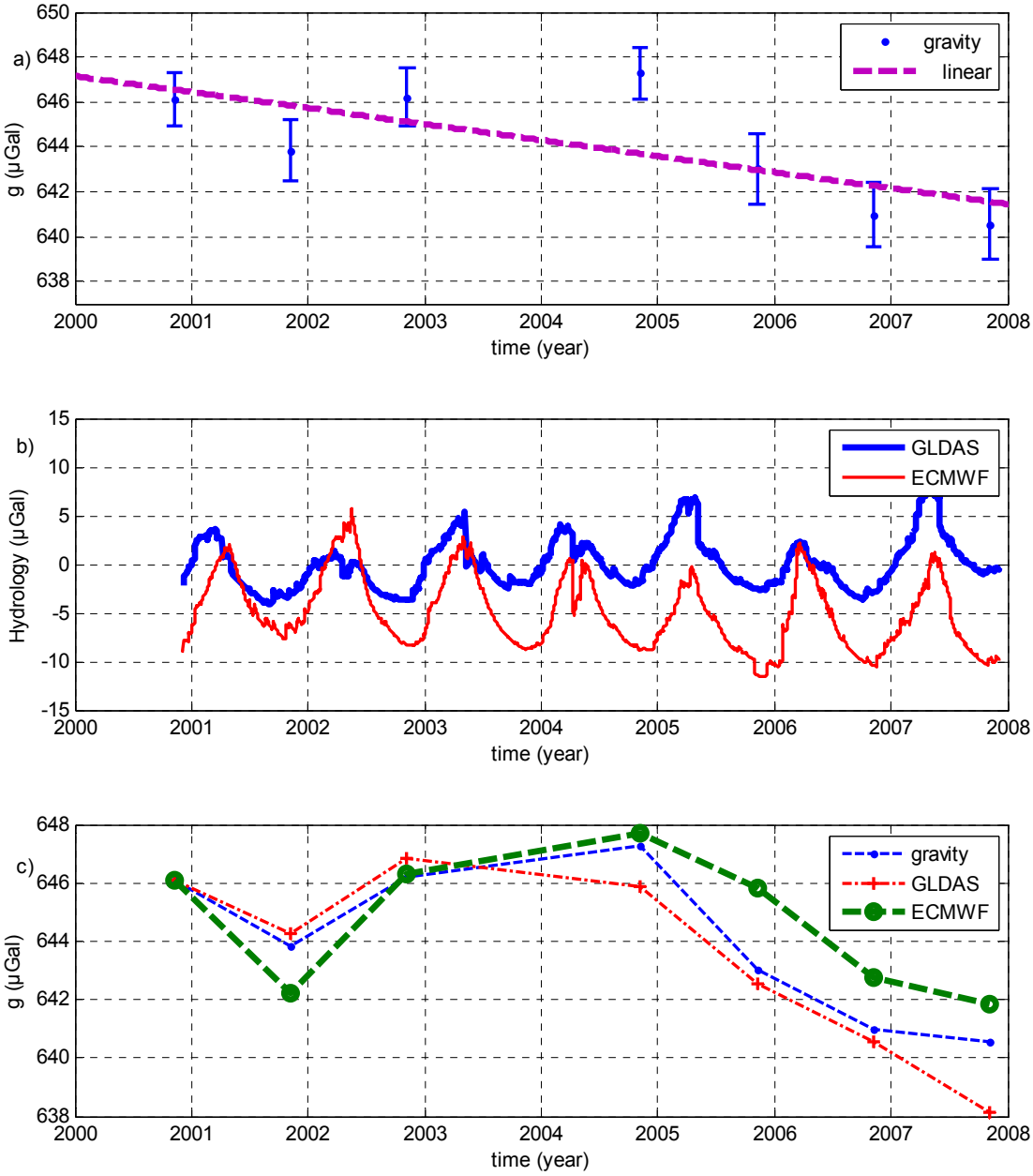

Fig. 3.16: a) AG measurements at Abali site during the 2000-2007 period; the gravity decrease at Abali with a slope of -0.70 ± 0.32 µGal/yr; b) the gravity changes derived from the global water storage models ECMWF and GLDAS for the same period; c) The AG measurements are corrected from gravity response of the ECMWF and GLDAS models. The computed slopes are respectively -0.99 ± 0.31 µGal/yr(GLDAS correction) and -0.30 ± 0.38 µGal/yr(ECMWF correction).

5. Conclusions

In this paper, two main aims are presented for the absolute gravity networks: 1- as a reference frame for the densification of lower order gravity networks, 2-for geodynamical studies by repeating gravity measurements at different time epochs. The national absolute gravity network of Iran (NAGNI2009) has been realized by meeting the initial specifications in terms of geographical distribution, maximum of dynamics in g variations over the Iranian territory and acceptable uncertainty (< 5μGal).

The studied time series at NCC-Tehran and Abali evidence for temporal variations with an amplitude of 1-20 μGal/ yr due to mass transfer (groundwater or rocks deformed by tectonic activity) and vertical displacement (crustal tectonic loading and isostatic response of the lithosphere for Abali site). Whatever is the hydrological or tectonic environment, these results point out the necessity to choose carefully the implantation of sites for establishment of fundamental absolute gravity network. Taking into account the uncertainties of the absolute gravity measurements and the observed inter-annual variations at the 2 sites, we recommend a reiteration of the measurements every 5 years. This interval is necessary to accurately estimate the secular variation of the gravity filed in Iran and to better understand its geodynamical origin. Moreover, long term GPS observations and water table depth measurements in borehole are needed for numerous stations to constrain 1) vertical deformation and induced free air gravity change and 2) variation of ground water storage

Acknowledgements: this work was realized in the frame of a co-operative research agreement between National Cartographic center (NCC, Tehran), University of Montpellier 2 and Strasbourg university. This work was funded by the Institut National des Sciences de l'Univers (INSU/CNRS), and by the Agence Nationale à la Recherche (ANR), under the program CATNAT.We thank the all teams who went out in the field to collect the data. The FG5 absolute gravimeters 228 and 206 were provided for by the INSU.

References

Afshar, H.K., Zomorrodian, H., 1970. The measurement and adjustment of the first order gravity network of Iran. Pub No 48, Institute of Geophysics, Tehran University, Tehran, Iran.

Andersen, O.B., Hinderer, J., 2005. Global inter-annual gravity changes from GRACE: early results, Geophysical Research Letters 32 (1), 4.

Antoine, P., Bahain, J.-J., Berillon, G., Asgari Khaneghah, A., 2006. Tuf calcaire et se'quence alluvial en contexte tectonique actif : La formation de Baliran(province du Mazandaran,Iran), Quaternaire, 17 (4), 321-331.

Crossley, D., Hinderer, J., Boy, J.P., 2005.Time variation of the European gravity field from superconducting gravimeters. Geophys. J. Int., 161: 257-264.

Djamour, Y., Vernant, P., Bayer, R., Nankali, H., Ritz, J.F., Hinderer, J., Hatam, Y., Luck, B., Le Moigne,N.,Sedighi, M., Khorrami, F., 2010. GPS and gravity constraints on continental deformation in the Alborz mountain range, Iran, Geophys. J. Int., submitted.

Defense Mapping Agency, 1979. Gravity stations data in the area 25-40 degree north and 43-65 degree east [4], Aerospace center, St. Louis air force stations.

Dehghani, G. A., Makris, J., 1984.The gravity field and crustal structure of Iran. Neues Jahrbuch Fuer geologie und Palaeontologie, Abhandlungen 168, 215-229.

Engalenc, M., 1968. Contribution à la Géologie, Géomorphologie, Hydrogéologie de la région de Teheran (Iran), Ph.D. thesis, 365 pp., Univ. of Montpellier II, Montpellier, France.

Farrell, W.E., 1972. Deformations of the Earth by surface loads. Reviews of Geophysics and Space physics 10 (3), 761-797.

Francis, O., van Dam, T., Germak, A., et al., 2010. Results of the European Comparison of Absolute Gravimeters in Walferdange (Luxembourg) of November 2007, IAG International Symposium on Gravity, Geoid and Earth Observation 2008, Crete, June 2008 (in press).

Jacob, T., Bayer, R., Chery, J, and Le Moigne, N., 2010. Time lapse microgravity surveys reveal water storage heterogeneity of a karst aquifer, J. Geophys. Res. , 115, B06402, doi:10.1029/2009JB006616.

Llubes, M., Florsch, N., Hinderer, J., Longuevergne, L., Amalvict, M., 2004. Local hydrology, the Global Geodynamics Project and CHAMP/GRACE perspective: some case studies. J. Geodyn., 38 (58): 355-374.

Lyard F., Lefevre, F., Letellier, T., Francis, O., 2006. Modelling the global ocean tides: modern insights from FES2004. Ocean Dynamics, 56(5-6): 394-415.

Mäkinen, J., Stahlberg, B., 1998. Long- term frequency stability and temperature response of a polarization-stabilized He–Ne laser, Measurements, 24, pp. 179–185.

Microg, 2007. ‘g’ 7.00 absolute gravity data acquisition and processing. In: M.-g. Solutions (Editor). Micro-g Solutions, Lafayette, Colorado,USA.

Nadjafi, M., Mashhadi, M., Hatam, Y., Tavakoli, F., 1998. Design of a gravity base network for Iran, Technical report, NCC, Iran. 51 pp.

Nadjafi, M., Mashhadi, M., Hatam, Y., Tavakoli, F., 2006. Design of a gravity base network, Journal of Allgemeine Vermessungs – Nachrichten (AVN), 11-12, 374-382,
http://imperia.mi-verlag.de/imperia/md/upload/article/374_382_alamdari.pdf

Neumeyer, J., Barthelmes, F., Dierks, O., Flechtner, F., Harnisch, M., Harnisch, G., Hinderer, J., Imanishi, Y., Kroner, C., Meurers, B., Petrovic, S., Reigber, Ch., Schmidt, R., Schwintzer, P., Sun, H.-P., Virtanen, H.,

, 2006. Combination of temporal gravity variations resulting from Superconducting Gravimeter recordings, GRACE satellite observations and global hydrology models. J Geod 79(10-11): 573-585, doi: 10.1007/S00190-005-0014-8

Niebauer, T.M., Sasagawa, G.S., Faller, J.E., Hilt, R., Klopping, F., 1995. A new generation of absolute gravimeters. Metrologia, 32, 159-180.

Niebauer, T.M., 1989. The effective measurement height of free-fall absolute gravimeters. Metrologia, 26,: 115-118.
Ramillien, G., Cazenave A., Brunau, O., 2004. Global time variations of hydrological signals from GRACE satellite gravimetry, Geophys. J. Int., 158, 3, 813-826.

Ramillien, G., Lombard, A., Cazenave, A., Ivins, E. R., Llubes, M., Remy, F. Biancale, R. 2006. Interannual variations of the mass balance of the Antarctica and Greenland ice sheets from GRACE. *Global and Planetary Change,* 53, 198-208.

Rodell, M., P. R. Houser, U. Jambor, J. Gottschalck, K. Mitchell, C.-J. Meng, K. Arsenault, B.Cosgrove, J. Radakovich, M. Bosilovich, J. K. Entin, J. P. Walker, D. Lohmann, and D. Toll, 2004. The Global Land Data Assimilation System, Bull. Amer. Meteor. Soc., 85 (3), 381–394.

Schwiderski, E. W., 1980. Ocean tides, II: a hydrological interpolation model, Marine Geodesy 3, 219-255.

Tamura Y., 1987.A harmonic development of the tide-generating potential. Bull. d'Inf. Marées Terrestres, 99, 6813-6855.
Tapley, B.D., Bettadpur, S., Ries, J.C., Thompson, P.F., Watkins, M.M., 2004. GRACE Measurements of mass variability in the earth system. *Science* 23 July 2004, 305, 5683, 503-505.

Torge, G., 1989. Gravimetry, Walter de Gruyter & Co., Berlin, 465 pp.

Timmen, L., 2003. Precise definition of the effective height of free- fall absolute gravimeters. Metrologia, 40, 62, doi: 10.1088/0026-1394/40/2/310

Van Camp, M., S. D. P. Williams, O. Francis (2005). Uncertainty of absolute gravity measurements, J. Geophys. Res., 110, B05406, doi: 10.1029/2004JB003497
Viterbo, P., Beljaars, A.C.M, 1995. An improved land surface parameterization scheme in the ECMWF model and its validation, J. Climate, 8, 2716-2748.

Wahr, J., Swenson, S., Zlotnicki V., Velicogna, I., 2004. Time-variable gravity from GRACE: first results, Geophys. Res. Lett., 31**,** L11501*,* doi:10.1029/2004GL019779.

Wenzel H.G., 1996. The Nanogal software: earth tide data processing package ETERNA 3.30. Bull. Inf. Marées Terrestres , 124, 9425-9439.

Zomorrodian, H., 1971. The measurements and adjustments of the second order gravity network in Iran, Pub. No. 53, IGTU, Tehran.

Zomorrodian, H., 1985.The Iranian National Calibration Line 1985. Technical Report of the Institute of Geophysics, Tehran University

Zomorrodian, H., 1987.The establishment of the Iranian Gravity Datum, Bureau Gravimetrique International, Bul. Information, 60.
Zumberge, M. A., 1981.A portable apparatus for absolute measurement of the earth's gravity, PhD Thesis, University of Colorado at Boulder.

3. Etablissement de la ligne nationale calibration de l'Iran

Establishment of National (Tele Cabin/ Land) Gravity Calibration Line of Iran (NGCLI10) and calibrating six Scintrex relative micro-gravimeters

Y. Hatam(1,2), R. Bayer(1), Y. Djamour(3), J. Hinderer(4), P. Vanicek(5), M. Mohammad Karim(6), N. Le Moigne(1), B. Luck (4), M. Karpychev(7), N. Azizian(2), H. Cheraghi(2), R. Saadat(2), A. Bahrampour(2), H. Asghari(2), H. Meygooni (2)

(1) Geosciences Montpellier cc60,Universite Montpellier 2–CNRS, Pl. E. Bataillon, 34095 Montpellier Cedex05, France. Email: yaghoub.hatam@gm.univ-montp2.fr , roger.bayer@gm.univ-montp2.fr

(2,3) [(2) Physical Geodesy Department, Geodesy and Land Surveying Management + (3)Geomatics College], National Cartographic Centre (NCC), PO Box 13185-1684, Meraj Ave, Tehran, Iran. Email: yaghoubhatam@yahoo.com, djamour@ncc.org.ir

(4) Ecole et Observatoire des Sciences de la Terre, Institut de Physique du Globe de Strasbourg, CNRS-ULP UMR 7516, 5, rue Des cartes, 67084 Strasbourg Cedex, France. Email: jacques.hinderer@eost.u-strasbg.fr

(5) University of New Brunswick, Fredericton, Canada. Email: vanicek@unb.ca

(6) Faculty of Geodesy and Geomatics Engineering, KN. Toosi University of Technology, Tehran, Iran.

(7) Centre Littoral de Geophysique, Université de La Rochelle, La Rochelle, France

Abstract

Gravity calibration line is needed for the accurate calibration of relative gravimeters before they are taken into the field. The existing calibration line in Iran, used to calibrate gravimeters recently, contain a selection of stations from the National Absolute Gravity Network of Iran. This calibration line run north-south along the whole country, and the points are widely spaced; it is thus quite expensive to use them because it is necessary to employ an aircraft to transport the gravimeter from point to point.

Hence, we started looking into the establishment of an alternative calibration line by avoiding the mentioned problem. Two parts of a line were considered: one part connecting TehranNCC with tochal summit of Tochal Mountain in north of Tehran, and second part on the northern slopes of Elburz Mountain from TehranNCC to Astara. It turns out that a combination of these two lines: Tochal7-TehranNCC (537 mGal) and TehranNCC-Astara (617 mGal), located at the southern shore of Caspian Sea, has a very large gravity difference of 1154 mGal. This difference in gravity is larger than the previous gravity calibration line (851 mGal) and covers mostly all the gravity values encountered in Iran, as well as in the neighboring countries.

The NGCLI10 stations are measured using 2 absolute gravimeters FG5 from Microg/Lacoste Inc. Six Scintrex relative micro gravimeters are calibrated at the new established calibration line. The experiences allow determining the calibration coefficients with a precision of 10^{-4} and the non linearity of the calibration parameter is clearly determined depending on the gravity value variation through the Iranian territory.

Keywords: Absolute and Relative gravimeters, Gravity calibration line, NGCLI10, Calibration error, Tele Cabin, Absolute Gravity (AG), Plane, Helicopter

1. Introduction

In 2004, the National Cartographic Center (NCC, Iran) decided to perform a new gravity network of the Iranian territory (Hatam and Djamour, 2004) in order to map in detail and accurately the gravity field and the geoid by combining gravity anomaly, levelling and GPS data.

The first step is dedicated to the realization of a fundamental absolute gravity network (Hatam et al., to be submitted, see sec. 3.1). This network consists in 24 sites approximately equally distributed over the Iranian territory where the absolute gravity field was measured with two FG5 ballistic meters (Niebauer et al., 1995; see photo 1) with an accuracy of 2-5 μGal. In a second step, it was proposed to perform a first, second and third order networks, resulting in density of one station per 100 km², and a required precision of the order of 10 μGals. This challenge needed to measure gravity field with high sensitive relative spring meter such as CG-3/M or CG-5 micro-gravimeters (Seigel, 1995; Scintrex, 2006). Quality of measurements will depends on the precision of the coefficient of calibration of such instruments for 2 reasons: 1) the furthest distance in latitude is ~2500 km and making large loops in measuring the first order gravity network could propagate an error associated with a poor resolved coefficient of calibration; 2) this is also the case for loops carried out in highly mountains areas. In fact, the precise determination of the calibration coefficients (scale factor) for relative gravimeters is always an important and unavoidable job in gravimetry (Torge, 1989; Budetta and Carbone, 1997; Bonvalot et al., 1998; Dias and Escobar, 2001; Jacob, et al., 2010; Ukawa et al. 2010).

For all the above mentioned gravity activities, we need to calibrate the relative gravimeters regularly before any field work. The systematical error in calibration may easily reach more than 1 mGal over Iran (Ardalan et al., 2004), whereas the error is required to be smaller than 10 μGal.

There are several important points that should be mentioned here. First, the gravity along the calibration line must be at least as large as the gravity variations in the field. Thus for a national calibration line, the gravity difference should be as large as the range encountered in the whole of Iran. Second, the relative gravity measurements between each two neighbor calibration stations must be measurable, as quickly as possible, to keep the time dependent drift error as small as possible. Third, the calibration coefficient is not linear and a series of stations making up the calibration line is needed to evaluate these non-linear terms. Fourth, the gravimeters should preferably be calibrated at the same gravity difference that is expected in the field.

The gravity differences necessary for the calibration can be realized in horizontal or vertical calibration lines. Horizontal gravity calibration line utilizes the change of gravity with latitude. A latitude difference of 12 degrees between Chabahar and Kalaleh results in a gravity difference of 851 mGals, i.e. ~71 mGal per one degree of latitude change (**Fig. 3.17**). A disadvantage is the larger transportation distance required for the calibration, necessary to use a plane as a high cost solution (**Photo 2**). Vertical calibration line is based on the change of gravity with altitude. A height difference of 3800 m between Alborz mountains and border of Caspian sea and latitude difference of 2.5°, resulting a vertical gradient of 0.30 mGal/m.

To overcome the problem of the transportation along the proposed calibration line, it is decided to add a short calibration line between Tehran and the Tochal summit, located north of the Tehran city. This line is caracterizd by a differene of height of 2600 m, i.e. a theoretical difference of -537 mGal [Fig.3.18]. The tele cabin connection between Velenjak (Tochal1) at the bottom, and the Tochal7, contains 2 intermediate stations, and it thus offers an interesting solution to the reduction of the cost accrued by transportation of gravimeters. The 537 mGal magnitude of the gravity difference between TehranNCC and Tochal7 is larger than the difference between TehranNCC and Chabahar, the southernmost end of the existing calibration line. Therefore, the TehranNCC-Tochal7 line, made of 5 absolute gravity stations, is considered more efficient to replace the southern branch (TehranNCC-Chabahar) of the existing calibration line.

The gravity difference from TehranNCC to Astara, located at the southern shore of Caspian Sea (**Fig. 3.18**) is larger than the gravity difference between Tehran and Kalaleh (~432 mGals) or Tehran and Tabriz (~158 mGal), the northernmost point of the existing calibration line. The relatively short distance between Tehran and Astara, and the existence of 3 intermediate gravity stations between them, make possible to densify the measurements and to transfer the gravimeter between the stations in a short time. These

intermediate stations are Kandovan, Chalous and Lahijan by Chalous road, and Lowshan and Lahijan by Lowshan road (**Fig. 3.18**).

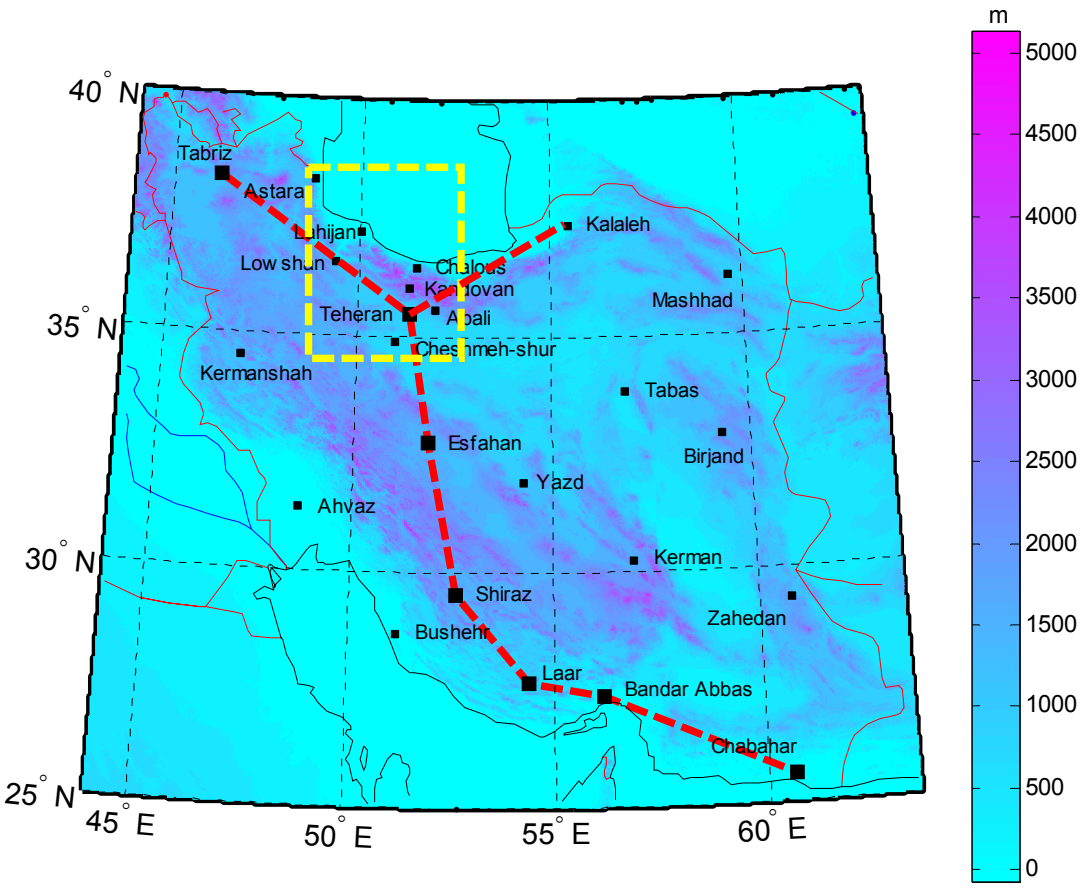

Fig. 3.17. A selection of 8 absolute gravity stations of National Absolute Gravity Network of Iran as the horizontal Gravity calibration line of Iran (between Kalaleh (or Tabriz) and Chabahar, red dashed line, 851 mGal gravity difference) and the region of new vertical gravity calibration line of Iran NGCLI10 (yellow dashed rectangle, 1154 mGal gravity difference), see ***Figure 3.18****.*

The new combined Gravity Calibration Line, Tochal7 - TehranNCC – Astara (**Fig. 3.18**) contains 10 gravity stations and covers a gravity difference of 1154 mGals, which is larger than any difference encountered in the whole of Iran, except for several high mountainous regions like the Damavand summit in the Tehran area. This line is completed by 2 absolute gravity stations, i.e. Abali and CheshmehShur (435 mGal gravity difference, equivalent approximately with the gravity difference between Tochal5 and TehranNCC), which are frequently occupied for calibration purpose before the establishment of NGCLI10. All stations of the new calibration line, except NCC station, anchored in insulated bedrock.

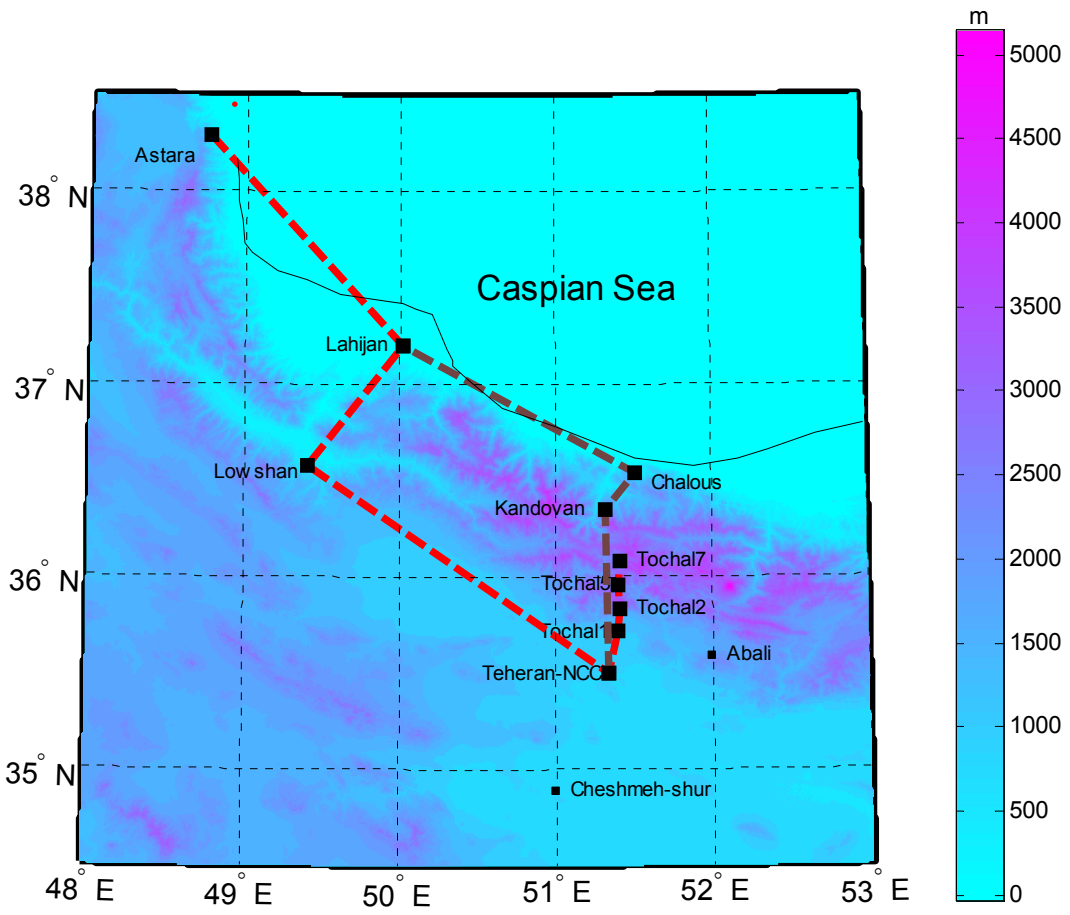

Fig. 3.18 Stations of the National (Tele Cabin/ Land) Gravity Calibration Line of Iran NGCLI10. The gravity difference between the first and the last stations (Tochal7 and Astara) is 1157mGals. For all stations between Tochal7 and Tochal2 (397mGal) there is a Tele cabin facility (as a replacement for high cost NCC Dornier 228 used in before calibration line), important to transport relative gravimeters frequently for calibration in a short time duration and with a low cost. Between Tehran-NCC and Lahijan stations (521 mGal) there are two possibilities: Lowshan road and Chalous roud. The Abali and CheshmehShur stations (with the gravities inside NGCLI10) were mostly used for calibration by using car and helicopter to transport relative gravimeters before estblishing the NGCLI10.

Up to now, two gravity calibration lines were established in Iran (Zomorrodian, 1987; Ghazavi et al, 2003; Najafi et al, 1998). The first one consisted in finally 89 NS oriented gravity sites which were used to estimate the coefficients of calibration by adjusting the gravity changes observed for various relative meters (Zomorrodian, 1987), and then modified and completed by reconstruction of the destroyed stations, re-measurement of it with 3 CG-3/Ms, and applying 4 absolute gravity stations to adjust it (Ghazavi et al,

2003). The second one was defined by selecting 8 absolute gravity stations, with a north-south distribution; belong to the National Absolute Gravity Network of Iran (**Fig. 3.17**; Nadjafi et al., 1998). Large distances between each two neighboring stations (~300-500 km) lead to great consuming time during the car displacements or expensive surveys by plane. Also, in a local scale, 3 absolute gravity stations, i.e. TehranNCC, CheshmehShur and Abali were used to calibrate the relative gravimeters, and, the transportation were done either by car or by helicopter in winter (**Photo 4**).

2. The NGCLI10 gravity calibration line

The main objective of establishing NGCLI10 is to frequently calibrate different relative gravimeters in nationwide by avoiding the high cost transportation of plane or helicopter. The absolute gravity stations of NGCLI10 gravity calibration line are implemented during the 2004-2005 with a local distribution, but with a gravity range that mostly cover all gravity coverage of Iran. The facility of Tele Cabin in Velenjak-Tochal mountainous region in north of Tehran has a important role to transport the gravimeters during calibration procedure in a relatively short time and without high cost. Effectively, the Tele Cabin is replaced for plane and helicopter in the new calibration line to transport the relative gravimeters in calibration procedure without cost limitation.

3.1 Design of the NGCLI10

The NGCLI10 is a vertical gravity calibration line, i.e. its gravity difference is based on the change of altitude. All stations are built at bedrocks to have a good stability for AG measurements, except NCC station. At all stations, except Tochal7, a mobile house is implemented AG measurements. At Tochal7, a permanent cellar is built for wind and to damp cold temperature effects.

3.2 Survey setup campaigns and measurement protocol

The AG sites of NGCLI10 are occupied during 2005-2007. The absolute measurements are realized with the two French national FG5 206 and 228 ballistic meters manufactured by Micro-g Lacoste Inc. and belonging to the DT/INSU of CNRS (France).

The AG measurements start in October 2005. The measurement campaigns take place in September-October epoch, in order: 1) to measure the gravity in good weather condition and 2) to

minimize the variation of the annual gravity component with respect to long term fluctuations. The measurements were realized on a concrete pillar fixed to bedrock to increase the stability of the sites, and inside an insulated mobile home (**Photo1**) to decrease the environmental noise. The measurements at several stations of NGCLI10, i.e. Tochal5, Kandovan, Chalous, Lahijan, were repeated each year during 2005-2007 to study the needed stability of the stations for calibration line (**Table1**) and to monitor possible inter-annual variations of gravity related to continental water storage or (and) to present-day tectonic vertical deformation (Djamour et al., 2010; Hatam et al., to be submitted; see sec. 3.2).

The FG5 gravimeter measures the acceleration of a free-falling corner-cube in a vacuum (a "drop") using an iodine-stabilised laser interferometer and a Rubidium atomic clock (Niebauer et al., 1995) (**Fig. 3.19**). Basically, a test mass is dropped and the earth gravity g_0 is determined by fitting the distance-time couples (x_i,t_i) to the theoretical relationship (Niebauer et al. 1995):

$$x_i = x_0 + v_0\tilde{t}_i + \frac{g_0\tilde{t}_i^2}{2} + \frac{\gamma x_0\tilde{t}_i^2}{2} + \frac{1}{6}\gamma v_0\tilde{t}_i^3 + \frac{1}{24}\gamma g_0\tilde{t}_i^4 \quad , \qquad \tilde{t} = t_i - \frac{(x_i - x_0)}{c}. \quad , \qquad \text{(eq. 1)}$$

where γ is the vertical gravity gradient, (x_0,v_0) represent the initial values of position and speed of the dropping object inside the vacuum chamber and (x_i, t_i) are for the time t_i. The mechanics of the dropping system are such that it can not return exactly to the same height for every drop. However, x_0 is one of the free parameters in the equation of motion. Inaccuracies in the gradient γ estimation bring further uncertainty to the gravity value g_0. In order to minimize these uncertainties, the reference gravity value g_{ref} independent of the gravity gradient at height h_{ref} is determined (**Fig. 3.19**). Several authors have worked on the determination of h_{ref}, which, as a rule-of-thumb, is located approximately one third of the way down the drop (Niebauer, 1989; Timmen, 2003; Zumberge, 1981). Height h_{ref} depends on instrument dimensions and instrument setup.

The mean value of g_0 is estimated from a series of 100 or 120 drops per hour and referred to a "set" (**Fig. 3.20)**. At the end, the AG value is estimated by averaging several hourly sets (in general ≥ 12) (**Fig. 3.21)**.

3.3 Data processing and results

All the data sets are processed identically using the new processing software g-version 7.0 from Micro-g Lacoste Inc. The value for each drop is rejected if its difference with the hourly value exceeds 3σ.

Various corrections are applied in order to obtain the gravity value:

1. Gravity values are corrected for solid earth tides using successively ETGTAB software (Wenzel, 1996) with the Tamura tidal potential development (Tamura, 1987), Berger model (Microg, 2007) and tidal oceanic loading effects from Schwiderski's (1980), FES2004 (Lyard et al., 2006) and CSR different models (Micro-g, 2007). Typically, Gravimetric Earth Tides may reach peak-to-peak amplitudes of 110 µGals, while ocean tide loading effects in Iran depend on the proximity to the ocean and may reach peak-to-peak amplitudes of tens of µGals. Correction values estimated from the combination of the various models are close (<1 µGal). Therefore, ETGTAB and FES2004 are adopted for the corrections.

2. Atmospheric pressure loading (mass and deformation effects) are corrected using the classical empirical admittance value of -0.3 µGal/ hPa.

3. Polar motion effects due to changes in the centrifugal potential which are caused by changes in the Earth's rotation are also removed according to the International Earth Rotation Service (IERS-www.iers.org).

AG recordings during the Iranian campaigns are often performed in low seismic noise conditions as it is proved by the drop to drop noise ranging from 7 to 12 µGal (see example in **Fig. 3.20**).

The error on the AG values (δ_{tot}) is considered as the sum of an instrumental high frequency noise (δ_{stat}), a setup error (δ_{setup}) and the systematic instrumental uncertainty (δ_{sys}), i.e. $\delta_{tot} = \sqrt{\delta_{sys}^2 + \delta_{stat}^2 + \delta_{setup}^2}$. The

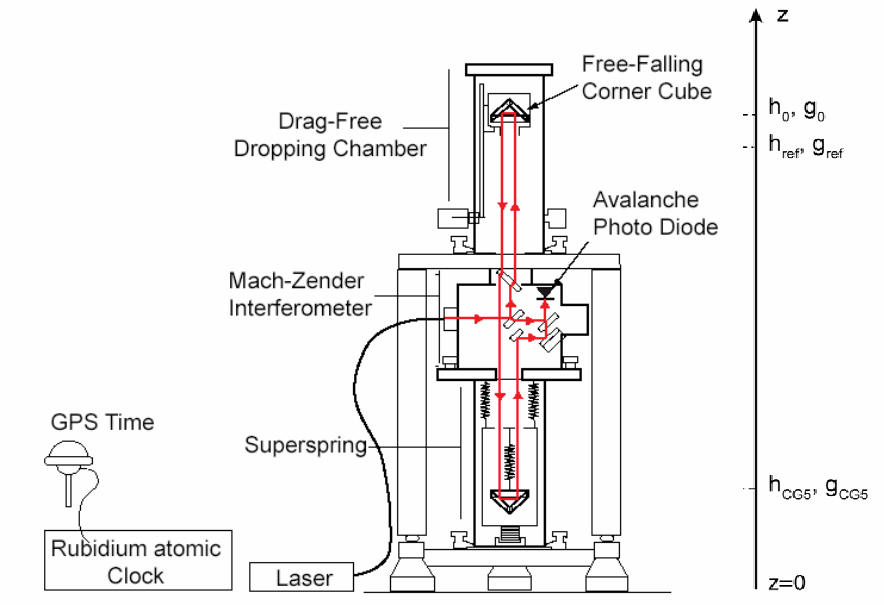

Fig. 3.19. The FG5 Absolute gravimeter (from Niebauer et al. (1995) and modified by Jacob et al. (2010))

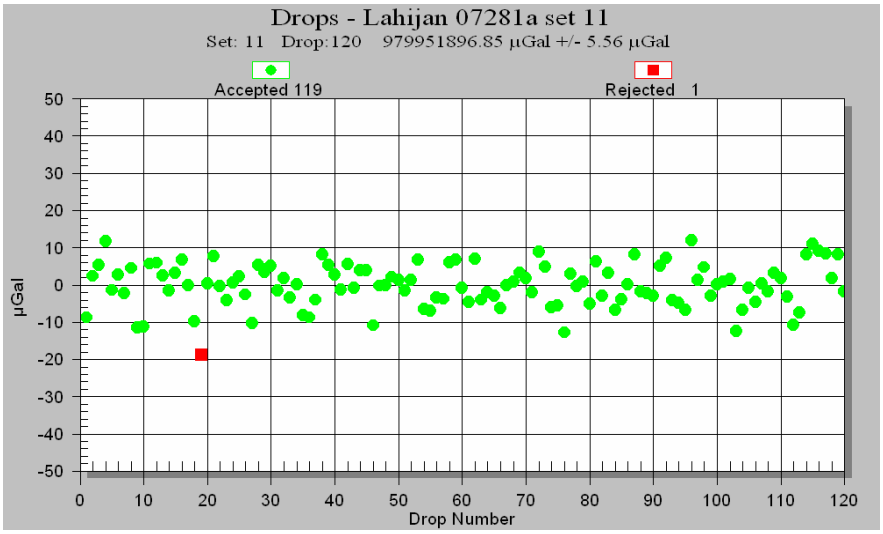

Fig. 3.20. Exemple of time series of AG values recorded during one set of 1 hour at Lahijan (South Caspian coast, see location on Fig.3.17)

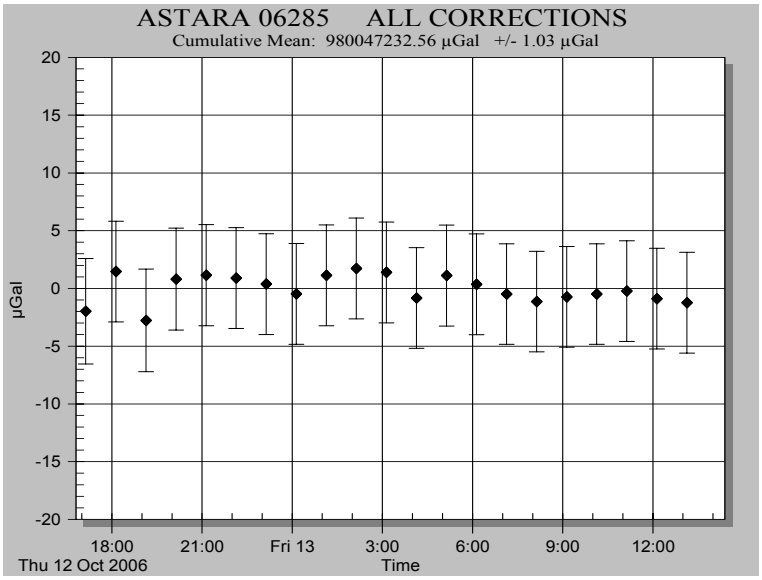

Fig. 3.21 A time series of 16 hourly AG measurements recorded at Astara (Central Alborz, see location in Fig. 3.17); the set scatter σ_{sc} is ± 1.03µGal.

instrumental noise δ_{stat} is usually obtained by the formula $\delta_{stat} = \sigma_{set} / \sqrt{N_{set}}$ where σ_{set} and N_{set} are respectively the set scatter and the number of sets. The set scatters observed during the campaigns (**Fig. 3.22**) suggest an evidence for a measurement precision lower than 0.4 µGal for at least 12 hours of measurements. Such a precision is perfectly consistent with our drop to drop noise level.

The systematic instrumental uncertainty δ_{sys} includes errors of modeling (earth tides factor, ocean loading factor, barometric and polar motion), error of system (laser, clock and system model) and environmental error (unmodeled tide swell water table effect). An error budget of 1.1 μGal is proposed by Niebauer et al. (1995) for the systematic instrumental uncertainty. From the analysis of superconducting gravimeter and AG measurements (FG5-202) at Membach station (Belgium), Van Camp et al. (2005) observe a setup instrumental white noise process at low frequency (< 1cycle/day) with a standard deviation of 1.6 μGal. Periodically inter-comparing the French FG5-206 and FG5-228 meters shows that the systematic instrumental error of the two FG5 gravimeters is similar and the AG value given by the two instruments differs by less than 1 μGal (unpublished results).

Recent 2007 inter-comparisons between 20 absolute meters including the FG5-206 and FG5-228 at Walferdange (Luxemburg) (Francis et al., 2010) show an agreement between the meters with a standard deviation of 2 μGal. At end, The total instrumental uncertainty is estimated to ~1.9 μGals.

From a practical point of view, absolute gravity values measured by the FG5 gravimeters need to be transferred to the benchmark altitude of the pillar. We have shown previously that the FG5 absolute gravimeter yields the gravity value from the adjustment of the trajectory of a free-falling corner cube to the equation of motion (see **equation 1**) accounting for the vertical gravity gradient at the measurement site of motion. Furthermore, the vertical gradient is also used to downward continue the gravity value g_{ref} from x_{ref} to a user-defined height h which corresponds to the altitude of the benchmark. The vertical gravity gradient is determined by measuring gravity ties with CG3-M or CG5 Scintrex relative gravimeters between different heights. The gradient was measured with a special tripod consisting in 3 plates at height of 0, 0.6 and 1.2 m above pillar. Gravity gradient is estimated from measurements along an “up and down” loop and by computing the gravity difference between the three different levels.

The AG value g_{ref} is defined at a height x_{ref} and the typical height differences between the x_{ref} and the bench marks range between 1.283 and 1.288 m for the FG5-228 and between 1.295 and 1.310 for the FG5-206. g_{ben} is determined at the bench marks by means of a least squares adjustment accounting for the instrumental drift of relative gravimeters. Results are given in table 1. The range of gravity gradient values is from -409 to -279.0μGal/m.

Station	Latitude (Deg.)	Longitude (Deg.)	Height (m)	Date yy.mm.dd	Gradient (µgal/m)	Gravity (µgal)	σ_{sc} (µgal)	σ_t (µgal)	Instrument
Tochal7	35.883	51.411	3795	2005.10.08	-356.0	978893055.7	±3.9	±4.4	Fg5 #228
Tochal5	35.859	51.101	3004	2005.10.09	-401.0	979070374.9	±1.2	±4.3	Fg5#228
				2006.10.17		979070377.3	±1.1	±4.4	Fg5#206
				2007.10.11		979070372.8	±1.3	±4.4	Fg5#206
Tochal2	35.833	51.411	2414	2005.10.10	-375.0	979183538.8	±1.4	±4.3	Fg5#228
Tochal1	35.814	51.397	1888	2005.10.11	-279.0	979290277.9	±1.3	±4.3	Fg5#228
Tehran-NCC	35.697	51.331	1181	2000.10.05	-317.0	979430721.5	±2.2	±4.4	Fg5#206
				2001.09.11		979430699.4	±2.4	±4.4	Fg5#206
				2002.10.03		979430697.2	±1.9	±4.4	Fg5#206
				2004.09.30		979430706.8	±2.1	±4.4	Fg5#206
				2005.10.06		979430705.1	±2.5	±4.3	Fg5#228
				2006.10.04		979430704.2	±1.5	±4.4	Fg5#206
				2007.10.03		979430704.7	±1.3	±4.3	Fg5#206
Kandovan	36.151	51.316	3058	2005.10.16	-378.0	979095240.0	±1.4	±4.3	Fg5#228
				2006.10.07		979095237.1	±0.7	±4.3	Fg5#206
				2007.10.06		979095242.3	±1.5	±4.3	Fg5#206
Chalous	36.685	51.310	-10	2005.10.18	-304.0	979828787.0	±6.6	±4.5	Fg5#228
				2006.10.09		979828791.2	±1.9	±4.4	Fg5#206
				2007.10.07		979828784.2	±2.1	±4.3	Fg5#206
Lowshan	35.579	49.402	800	2006.10.15	-343.0	979612278.7	±1.2	±4.3	Fg5#206
Lahijan	37.198	50.024	127	2005.10.21	-399.0	979951898.5	±1.3	±4.3	Fg5#228
				2006.10.11		979951899.2	±1.3	±4.4	Fg5#206
				2007.10.09		979951895.4	±1.6	±4.3	Fg5#206
Astara	38.289	48.853	25	2006.10.13	-360.8	980047305.5	±1.0	±4.3	Fg5#206
Abali	35.792	51.987	3177	2000.10.12	-409.0	979032638.1	±1.2	±4.3	Fg5#206
				2001.09.13		979032640.8	±1.4	±4.4	Fg5#206
				2002.10.08		979032640.7	±1.3	±4.3	Fg5#206
				2004.10.03		979032647.3	±1.1	±4.3	Fg5#206
				2005.10.14		979032643.0	±2.1	±4.3	Fg5#228
				2006.10.06		979032641.0	±1.4	±4.3	Fg5#206
				2007.10.04		979032640.5	±2.0	±4.3	Fg5#206
CheshmehShur	35.091	50.991	971	2000.10.09	-342.3	979467463.0	±3.1	±4.4	Fg5#206
				2001.10.22		979467470.6	±1.0	±4.4	Fg5#206
				2002.10.22		979467467.8	±5.9	±4.4	Fg5#206
				2005.10.23		979467470.6	±1.4	±4.3	Fg5#228

Table. 3.2. Stations of the National (Tele Cabin/ Land) Gravity Calibration of Iran NGCLI10. After name of station, 3 dimensional position and date of measurements, vertical gravity gradients,computed absolute gravity and its set scatter and total uncertainty are presented in the table.

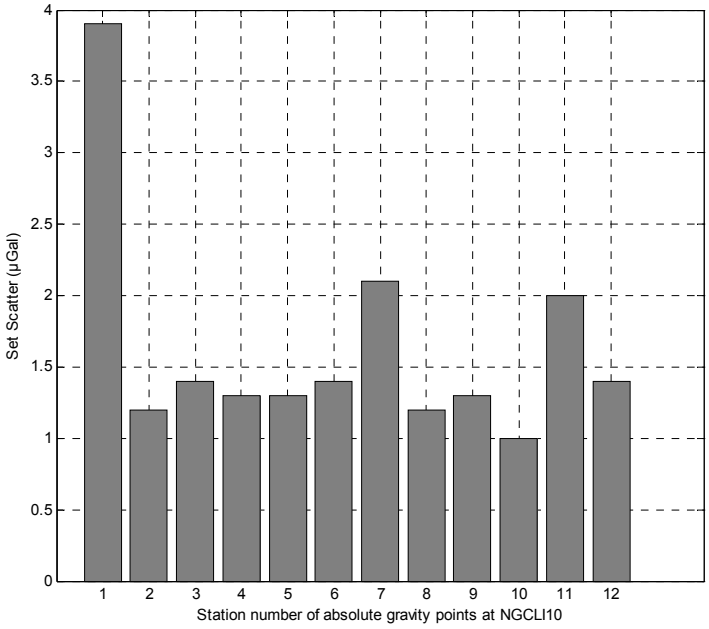

Fig. 3.22 Set Scatter σ_{sc} on the AG values at bases of the NGCLI10 gravity calibration line. The weak environmental noise at the stations is attested by the values of the set scatter lower than 2 µGal for 75 % of the sites.Station names: 1- Tochal7, 2- Tochal5, 3- Tochal2, 4- Tochal1, 5- Tehran-NCC, 6- Kandovan, 7- Chalous, 8- Lowshan, 9- Lahijan, 10- Astara, 11- Abali, 12- CheshmehShur

The difference with the classical -300 µGal/m free-air gravity gradient is explained by the topographic mass effect at stations in mountainous environment. Independent uncertainties on g_{ref} and vertical gradient are summed to estimate the error on g_{ben}. The accuracy on the vertical gradient is typically from 2 to 3µGal/m and error analysis yields a total uncertainty of 4.3 to 4.4 µGal for the g_{ben} values. The final g_{ben} values and their uncertainties are presented in **table 1**. The results satisfy the initial specifications of the NGCLI10.

4. Calibration of relative gravimeters at NGCLI10

The stations of the NGCLI10 calibration line are used to calibrate 6 Scintrex micro-gravimeters (3 CG-3/M and 3 CG-5) (**Photo 3**) in different years during 2005-2008. Between two neighboring A and B gravity stations is measured with relative gravimeters in A-B-A manner, with 30 minutes duration measurements at each setup and automatic recording, and with a precision better than 10 µGal on the difference. The drift and scale factor are considered linear for each A-B-A relative measurement between two neighboring stations. After correcting the measurements for different effects, i.e. tide, atmospheric and instrumental height corrections, the linear instrumental drift and scale factor are evaluated by the eq. 2.

$$C_f\,(m_{S_j}^{t_j} - m_{S_i}^{t_i}) = g_j - g_i + D(t_j - t_i) \qquad (2)$$

where C_f is the calibration correction factor of the relative gravimeter, $m_{S_j}^{t_j}$ and $m_{S_i}^{t_i}$ are mean gravity readings at stations S_j and S_i and at times t_j and t_i respectively, g_j and g_i the gravity values at stations S_j and S_i to be adjusted, and D the instrumental drift parameter. Therefore, the calibration table is constructed with the computed C_f values for different gravimeters and for different gravity differences of the NGCLI10 calibration line, to correct the future equivalent gravity differences experiencing at field (**Annex 1**, **Fig. 3.23** and **Table 3.3**). It is important to emphasize that a low-order polynomial approximation to the calibration table will affect the gravimeter's precision specification. Also, the use of a high-order polynomial will introduce numerical instability. Hence, the optimum way for practical application is to use directly the coefficients of calibration tables for different equivalent gravity differences.

5. Conclusions

A gravity calibration line, NGCLI10, with a gravity difference of 1154 mGals and with a local distribution of stations is established, based on altitude change of gravity differences. A set scatter of about $\sigma_{sc} = \pm 1.5$ μGal and a total uncertainty of about ± 4.3 μGal are evaluated for the absolute gravity values at NGCLI10 stations (**Table 3.2** and **Fig. 3.22**). The main advantage of the NGCLI10 is that its stations are distributed locally, and by using the facility of Tele Cabin for the section Velenjak (Tochal1) - Tochal7 and, using car for the remained part of the calibration line to transport the relative gravimeters, it is a practical established calibration line. For the before calibration line, however, there existed always a limitation of expensive transportation by plane or helicopter.

Six scintrex relative gravimeters are calibrated at the NGCLI10 calibration line. The computed calibration factors for six relative gravimeters range from 0.99874 to 1.0008 (**Annex 1** and **Fig. 3.23**). A precision of the order of 0.5×10^{-4} is estimated for the calibration factors. The values of the coefficients with respect to gravity and time is demonstrated in **figure 3.23**. The linear calibration factors are also computed for each survey (see **table 3.3**). The evolution of the scale factors with respect to time, of the order of several parts in a 10000 over a few year periods are estimated and presented in **figure 3.24**

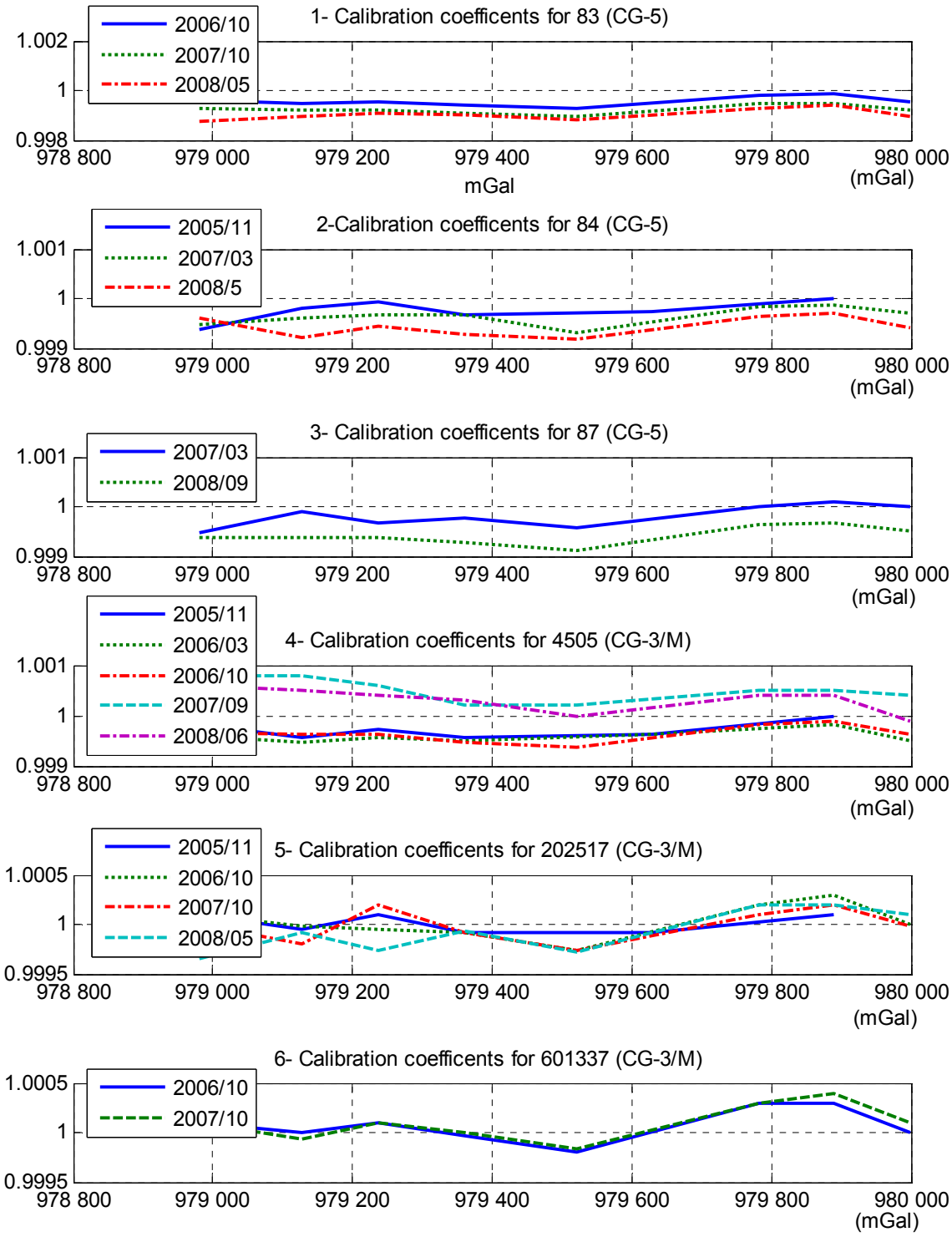

Fig. 3.23. Calibration coefficients for six Scintrex relative gravimeters (3 CG-5s and 3 CG-3/Ms) with an accuracy of 0.5×10^{-4}

Calibration time	Calibration factors for 6 relative gravimeters					
	CG-5 (83)	CG-5 (84)	CG-5 (87)	CG-3M (4505)	CG-3M (202517)	CG-3M (601337)
2005/11		0.99964 ± 0.00018		0.99962 ± 0.00010	0.99988 ± 0.00006	
2006/03				0.99967 ± 0.00007		
2006/10	0.99988 ± 0.00013			0.99984 ± 0.00014	1.00020 ± 0.00012	1.00040 ± 0.00013
2007/03		0.99984 ± 0.00015	1.00010 ± 0.00019			
2007/10	0.99938 ± 0.00019			1.0005 ± 0.00022	1.00000 ± 0.00016	1.00041 ± 0.00015
2008/05	0.99918 ± 0.00024	0.99966 ± 0.00019		1.00040 ± 0.00024	1.00010 ± 0.00023	
2008/10			0.99954 ± 0.00021			

Table 3.3 Calibration factors for six Scintrex gravimeters combuted by each calibration survey

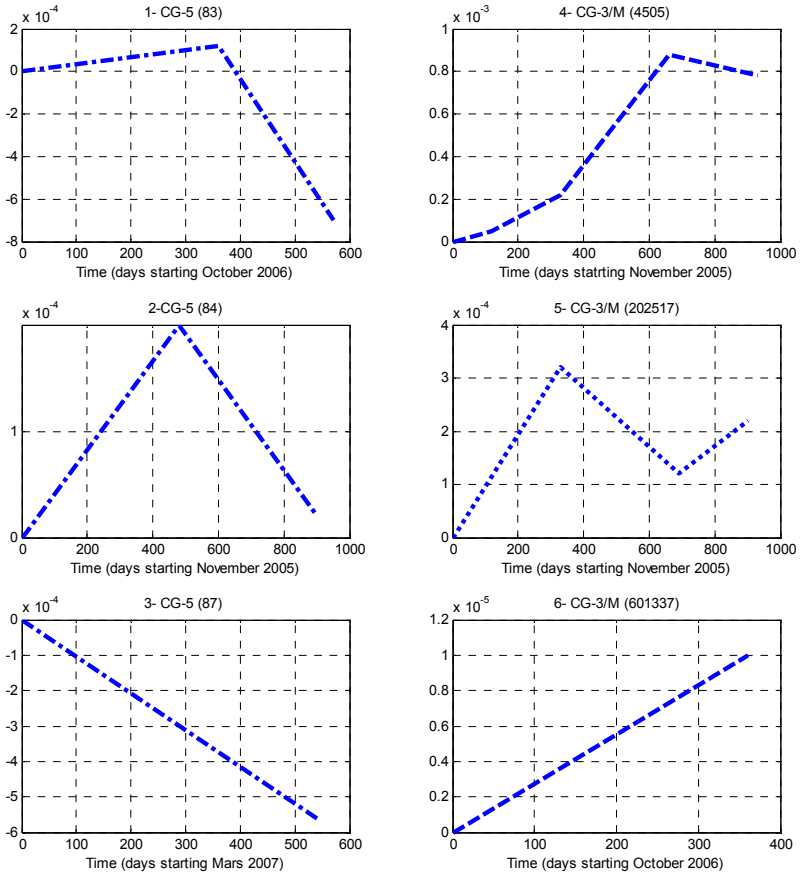

Fig. 3.24. The evolution of calibration factors for six Scintrex gravimeters as a function of time (see table 3.3).

Station1	Station2	R_j-R_i (mGal)	SD (mGal)	Ins	g_j - g_i (mGal)	C_f	Date	Drift	dT(h)
1002	1003	177,35546	0,00472	4505	177.3232	0.99982	14/11/2005	-4,78	3,32
1003	1004	113,21027	0,00462	4505	113.1607	0.99956	09/11/2005	-6,2	2,85
1004	1005	106,7731342	0,00497	4505	106.7423	0.99971	09/11/2005	-3,49	6,02
1005	9002	140,48604	0,00383	4505	140.4263	0.99957	10/11/2005	0,26	9,49
9002	1008	398,22277	0,00668	4505	398.0800	0.99964	15/11/2005	1,26	12,36
1008	1009	123,11626	0,00584	4505	123.1143	0.99998	17/11/2005	-0,06	7,5
1002	1003	177,43142	0,00214	84	177.3232	0.99939	2005/11/14	-2,27	3,31
1003	1004	113,18338	0,0015	84	113.1607	0.9998	2005/11/16	-1,15	2,64
1004	1005	106,75135	0,00156	84	106.7423	0.99992	2005/11/16	3,06	5,5
1005	9002	140,47378	0,00181	84	140.4263	0.99966	2005/11/11	0,92	8,36
9002	1008	398,18761	0,00712	84	398.0800	0.99973	2005/11/15	-0,25	12,35
1008	1009	123,11213	0,00458	84	123.1143	1	2005/11/17	-0,5	7,43
1002	1003	177,31369	0,00335	202517	177.3232	1.0001	14/11/2005	-1,5	3,31
1003	1004	113,16658	0,00294	202517	113.1607	0.99995	12/11/2005	-5,23	2,26
1004	1005	106,73557	0,00253	202517	106.7423	1.0001	12/11/2005	-2,89	4,68
1005	9002	140,43862	0,00275	202517	140.4263	0.99991	16/11/2005	0,14	8,46
9002	1008	398,11289	0,00602	202517	398.0800	0.99992	15/11/2005	0,18	12,38
1008	1009	123,09613	0,00574	202517	123.1143	1.0001	17/11/2005	-0,29	7,47
1002	1003	177,39157	0,00364	4505	177.3232	0.99961	14/03/2006	-1,37	2,5
1003	1004	113,22222	0,00322	4505	113.1607	0.99946	02/03/2006	-3,13	2,56
1004	1005	-106,7886827	0,0027	4505	106.7423	0.99957	02/03/2006	-0,1	5,22
1005	9002	-140,4967499	0,00296	4505	140.4263	0.9995	06/03/2006	-3,06	9,6
9002	1008	398,22277	0,00668	4505	398.0800	0.99964	15/11/2005	1,26	12,36
1008	1009	123,13626	0,00351	4505	123.1143	0.99982	09/03/2006	3,28	8,03
1009	1010	95,45538	0,00256	4505	95.4070	0.99949	08/03/2006	2,16	9,75
1002	1003	-177,29685	0,0027	601337	177.3232	-1.0001	03/10/2006	-4,64	5,48
1003	1004	113,1568	0,00237	601337	113.1607	1	02/10/2006	-2,89	3,14
1004	1005	106,7315253	0,00223	601337	106.7423	1.0001	02/10/2006	-2,91	6,1
1005	9002	140,43018	0,00333	601337	140.4263	0.99997	01/10/2006	-4,57	3,38
9002	1011	181,6091	0,00377	601337	181.5745	0.99981	09/10/2006	-1,68	8,93
1011	1008	339,52371	0,00313	601337	339.6198	1.0003	07/10/2006	-0,25	7,6
1008	1009	123,07331	0,05279	601337	123.1143	1.0003	05/10/2006	-0,38	8,45
1009	1010	95,40686	0,00389	601337	95.4070	1	06/10/2006	-0,62	10,67
1002	1003	177,38907	0,00166	83	177.3232	0.99963	2006/9/25	0,34	5,04
1003	1004	113,21811	0,00139	83	113.1607	0.99949	2006/9/24	1,82	2,62
1004	1005	106,7944215	0,00127	83	106.7423	0.99951	2006/9/24	0,71	5,28
1005	9002	140,5043088	0,00185	83	140.4263	0.99944	2006/9/24	0,43	9,08
9002	1011	181,70168	0,00249	83	181.5745	0.9993	2006/9/28	0,93	8,47
1011	1008	339,69214	0,00231	83	339.6198	0.99979	2006/10/2	-0,23	6,56
1008	1009	123,13313	0,05491	83	123.1143	0.99985	2006/10/1	1,02	7,51
1009	1010	95,45112	0,00187	83	95.4070	0.99954	2006/09/30	0,58	10,08
1002	1003	177,30986	0,00258	202517	177.3232	1.0001	28/09/2006	-0,21	2,91
1003	1004	113,1616	0,003	202517	113.1607	0.99999	01/10/2006	-1,1	2,52
1004	1005	106,7473555	0,00453	202517	106.7423	0.99995	28/09/2006	-1,7	8,24
1005	9002	140,43945	0,00289	202517	140.4263	0.99991	26/09/2006	-1,07	3,41
9002	1011	181,62125	0,00246	202517	181.5745	0.99974	02/10/2006	-0,45	9,98
1011	1008	339,56168	0,00273	202517	339.6198	1.0002	07/10/2006	0,84	7,58
1008	1009	123,07689	0,05205	202517	123.1143	1.0003	05/10/2006	-0,56	8,45
1009	1010	95,40706	0,00327	202517	95.4070	1	06/10/2006	0,67	10,69
1002	1003	177,381031	0,00306	4505	177.3232	0.99967	12/10/2006	-5,83	3,85
1003	1004	113,2024308	0,00258	4505	113.1607	0.99963	12/10/2006	-4,45	6,2
1004	1005	106,7828408	0,00256	4505	106.7423	0.99962	12/10/2006	-3,86	8,38
1005	9002	140,50023	0,00445	4505	140.4263	0.99947	11/10/2006	-6,43	2,9
9002	1011	181,68728	0,00254	4505	181.5745	0.99938	30/09/2006	-0,71	9,3
1011	1008	339,68589	0,00406	4505	339.6198	0.99981	05/10/2006	2,64	6,15
1008	1009	123,12605	0,01094	4505	123.1143	0.9999	07/10/2006	1,45	6,33

1009	1010	95,44294	0,00332	4505	95.4070	0.99962	06/10/2006	1,2	8,99
1002	1003	177,4172	0,0013	87	177.3232	0.99947	07/10/2008	-0,8	4,16
1003	1004	113,17312	0,00153	87	113.1607	0.99989	2007/3/15	-2,31	3,08
1004	1005	106,7764389	0,00156	87	106.7423	0.99968	2007/3/15	-1,25	6,24
1005	9002	140,46035	0,00386	87	140.4263	0.99976	2007/3/7	-1,86	3,55
9002	1011	181,65109	0,00274	87	181.5745	0.99958	2007/3/8	1,46	9,37
1011	1008	339,6077	0,00165	87	339.6198	1	2007/3/13	0,83	6,83
1008	1009	123,10719	0,00734	87	123.1143	1.0001	2007/3/13	-0,12	7,37
1009	1010	95,40641	0,00181	87	95.4070	1	2007/3/12	0,87	10,4
1002	1003	177,41705	0,0015	84	177.3232	0.99947	14/03/2007	-0,23	4,09
1003	1004	113,20418	0,00151	84	113.1607	0.99962	2007/3/15	-1,35	3,1
1004	1005	106,7777101	0,00147	84	106.7423	0.99967	2007/3/15	-1,23	6,23
1005	9002	140,47343	0,00364	84	140.4263	0.99966	2007/3/7	14,83	3,56
9002	1011	181,69821	0,00283	84	181.5745	0.99932	2007/3/8	-0,91	9,37
1011	1008	339,67915	0,00172	84	339.6198	0.99983	2007/3/13	-4,03	6,84
1008	1009	123,13185	0,00682	84	123.1143	0.99986	2007/3/13	-0,51	7,36
1009	1010	95,435	0,00175	84	95.4070	0.99971	2007/3/12	-3,15	10,42
1002	1003	177,30327	0,00327	601337	177.3232	1.0001	02/10/2007	0,59	2,92
1003	1004	113,16727	0,00277	601337	113.1607	0.99994	02/10/2007	-6	3
1004	1005	106,73127	0,00286	601337	106.7423	1.0001	06/10/2007	-4,36	3,17
1005	9002	140,42652	0,00305	601337	140.4263	1	01/10/2007	-2,1	3,2
9002	1011	181,60286	0,00312	601337	181.5745	0.99984	04/10/2007	-2,72	9,1
1011	1008	339.5159	0,00431	601337	339.6198	1.0003	11/10/2007	0,74	12,67
1008	1009	123,06525	0,00554	601337	123.1143	1.0004	12/10/2007	-2,47	8
1009	1010	95,39601	0,00295	601337	95.4070	1.0001	12/10/2007	1,55	10,7
1002	1003	177,44718	0,0013	83	177.3232	0.9993	2007/10/2	-1,09	2,92
1003	1004	113,25193	0,00132	83	113.1607	0.99919	2007/10/2	-1,69	2,95
1004	1005	106,82389	0,00133	83	106.7423	0.99924	2007/10/1	2,26	2,88
1005	9002	140,552	0,00205	83	140.4263	0.99911	2007/10/1	-0,86	3,61
9002	1011	181,75994	0,00206	83	181.5745	0.99898	2007/10/11	0,01	8,17
1011	1008	339.8001	0,03802	83	339.6198	0.99947	2007/10/16	-0,31	11,71
1008	1009	123,17668	0,04411	83	123.1143	0.99949	2007/10/17	-0,83	7,18
1009	1010	95,47925	0,0025	83	95.4070	0.99924	2007/10/18	-1,89	10,78
1002	1003	177,31472	0,00265	202517	177.3232	1	26/09/2007	0,69	3,18
1003	1004	113,18262	0,00331	202517	113.1607	0.99981	26/09/2007	0,43	3,34
1004	1005	106,72495	0,00298	202517	106.7423	1.0002	27/09/2007	-3,53	2,95
1005	9002	140,43873	0,01164	202517	140.4263	0.99991	30/09/2007	2,47	3,14
9002	1011	181,62213	0,00517	202517	181.5745	0.99974	28/09/2007	1,14	9,99
1011	1008	339.5991	0,022	202517	339.6198	1.0001	03/10/2007	1,52	10,83
1008	1009	123,09097	0,00745	202517	123.1143	1.0002	02/10/2007	1,08	8,38
1009	1010	95,40806	0,00204	202517	95.4070	0.99999	01/10/2007	0,45	9,97
1002	1003	177,17415	0,00266	4505	177.3232	1.0008	26/09/2007	-0,74	3,18
1003	1004	113,06561	0,00339	4505	113.1607	1.0008	26/09/2007	-2,91	3,33
1004	1005	106,67925	0,00299	4505	106.7423	1.0006	27/09/2007	-2,48	2,95
1005	9002	140,40397	0,00288	4505	140.4263	1.0002	01/10/2007	-13,85	3,81
9002	1011	181,53279	0,00316	4505	181.5745	1.0002	06/10/2007	-2,05	8,44
1011	1008	339.4476	0,00625	4505	339.6198	1.0005	09/10/2007	-5,09	10,69
1008	1009	123,05699	0,00416	4505	123.1143	1.0005	11/10/2007	-6,48	6,68
1009	1010	95,36688	0,00255	4505	95.4070	1.0004	10/10/2007	2,91	9,02
1002	1003	177,39111	0,00277	84	177.3232	0.99962	2008/04/29	0,26	4,72
1003	1004	113,24897	0,00147	84	113.1607	0.99922	2008/04/26	-9,18	3,39
1004	1005	106,802	0,00142	84	106.7423	0.99944	2008/04/28	-14,77	3,55
1005	9002	140,52756	0,00212	84	140.4263	0.99928	2008/04/27	-6,34	3,48
9002	1011	181,72206	0,00214	84	181.5745	0.99919	2008/04/25	-5,34	11,72
1011	1008	339.7404	0,02121	84	339.6198	0.99965	2008/05/01	-2,7	12,9
1008	1009	123,14933	0,03513	84	123.1143	0.99972	2008/05/02	-0,69	8,26
1009	1010	95,46302	0,00158	84	95.4070	0.99941	2008/05/03	-0,05	10,49
1002	1003	177,54653	0,00204	83	177.3232	0.99874	2008/05/06	-1,85	2,92
1003	1004	113,27603	0,00155	83	113.1607	0.99898	2008/04/26	2,68	4,29
1004	1005	106,8438	0,00158	83	106.7423	0.99905	2008/05/07	6,02	3,16
1005	9002	140,56813	0,00188	83	140.4263	0.99899	2008/04/25	-0,83	3,28
9002	1011	181,79207	0,00228	83	181.5745	0.9988	2008/04/24	1,25	9,88

1011	1008	339.8546	0,01568	83	339.6198	0.99931	2008/04/29	0,33	12,42
1008	1009	123,19034	0,0066	83	123.1143	0.99938	2008/04/28	-1,27	7,67
1009	1010	95,50544	0,00127	83	95.4070	0.99897	2008/04/30	-0,84	10,57
1002	1003	177,38362	0,00273	202517	177.3232	0.99966	06/05/2008	0,91	2,95
1003	1004	113,16974	0,00244	202517	113.1607	0.99992	26/04/2008	0,43	4,28
1004	1005	106,77022	0,0027	202517	106.7423	0.99974	07/05/2008	-1,15	3,15
1005	9002	140,43436	0,00279	202517	140.4263	0.99994	25/04/2008	0,41	3,15
9002	1011	181,62526	0,00307	202517	181.5745	0.99972	24/04/2008	2,39	9,76
1011	1008	339.5553	0,01413	202517	339.6198	1.0002	29/04/2008	1,45	12,23
1008	1009	123,09281	0,0051	202517	123.1143	1.0002	28/04/2008	2,96	7,6
1009	1010	95,39622	0,00189	202517	95.4070	1.0001	30/04/2008	1,18	10,48
1002	1003	177,2191	0,003	4505	177.3232	1.0006	17/06/2008	1,48	4,86
1003	1004	113,106	0,002	4505	113.1607	1.0005	16/06/2008	1,67	4,56
1004	1005	106,70198	0,002	4505	106.7423	1.0004	15/06/2008	-6,76	4,35
1005	9002	140,38398	0,003	4505	140.4263	1.0003	14/06/2008	-5,51	3,94
9002	1011	181,57134	0,003	4505	181.5745	1	21/06/2008	-5,8	11,61
1011	1008	339.4864	0,022	4505	339.6198	1.0004	24/06/2008	-5,97	13,47
1008	1009	123,06903	0,021	4505	123.1143	1.0004	23/06/2008	-3,97	8,89
1009	1010	95,41678	0,002	4505	95.4070	0.9999	25/06/2008	-2,76	11,52
1002	1003	177,4172	0,0013	87	177.3232	0.99947	07/10/2008	-0,8	4,16
1003	1004	113,2307	0,0015	87	113.1607	0.99938	05/10/2008	-1,57	3,98
1004	1005	106,8085	0,0019	87	106.7423	0.99938	30/09/2008	-2,26	2,87
1005	9002	140,5256258	0,0026	87	140.4263	0.99929	30/09/2008	-1,67	7,1
9002	1011	181,7337	0,0021	87	181.5745	0.99912	04/10/2008	0,6	10,7
1011	1008	339.7405	0,0226	87	339.6198	0.99964	13/10/2008	0,09	13,07
1008	1009	123,1537	0,0055	87	123.1143	0.99968	14/10/2008	1,87	7,75
1009	1010	95,4545	0,0013	87	95.4070	0.9995	15/10/2008	-0,54	10,16

Annex 1. Gravity calibration coefficients (scalefactor) C_f for 3 CG-5s and 3 CG-3/Ms relative gravimeters, computed by using relative gravity measurements (R_j-R_i) and absolute gravity differences (g_j - g_i) at the NGCLI10 calibration line.The station names: 1002- Tochal7, 1003- Tochal5, 1004- Tochal2, 1005- Tochal1, 9002- TehranNCC, 1008- Chalous, 1009- Lahijan, 1010- Astara, 1011- Lowshan, 2000- Abali, 2001- CheshmehShur

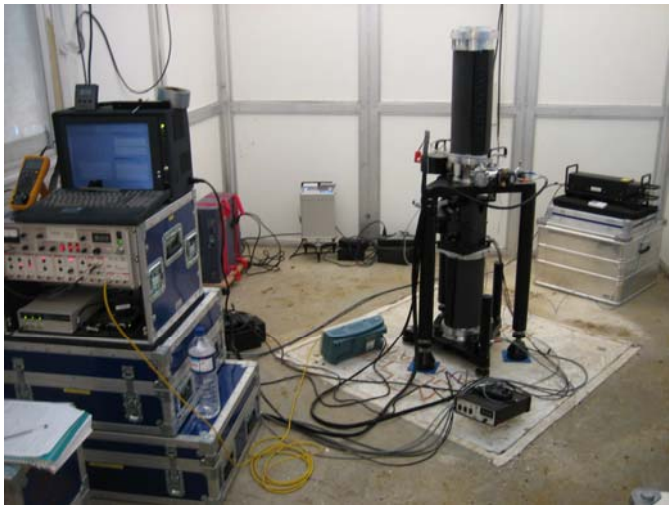

Photo 1. Absolute Gravity experiment using FG5 206 in a mobile home at Lahijan (South Caspian border)

Photo. 2. Calibration of relative gravimeters (2004). Measurement at Kalaleh absolute gravity station (inside tent), belong to horizontal gravity calibration line of Iran (see Fig. 3.17, dashed red line). Transportation of gravimeters is done by NCC Dornier 228.

Photo. 3. Six Scintrex relative micro-gravimeters, 3 CG-5 (left) and 3 CG-3/M (right), used for calibration at NGCLI10 calibration line

Photo. 4. Calibration of relative gravimeters at CheshmehShur station, transportation was done by Helicopter

Photo. 5. Tele Cabin facility between Tochal1 and Tochal7 and two other intermediate absolute gravity stations (see Fig. 3.18) in north of Tehran with a gravity difference of 397 mGal and height difference 1907 m. It is the replacement for before high cost plane and helicopter to transport the gravimeters for calibration.

Acknowledgements: this work was realized in the frame of a co-operative research agreement between National Cartographic center (NCC, Tehran), University of Montpellier 2 and Strasbourg university. This work was funded by the Institut National des Sciences de l'Univers (INSU/CNRS), and by the Agence Nationale à la Recherche (ANR), under the program CATNAT.We thank the all teams who went out in the field to collect the data. The FG5 absolute gravimeters 228 and 206 were provided for by the INSU. The six Scintrex micro-gravimeters 83, 84, 87, 4505, 202517 and 601337 were provided by NCC of Iran.

References

Ardalan, A.A., Hatam, Y., Ghazavi, K., Ghavamian, S., 2004. Standard and specifications for gravimetry. NCC, Iran.

Bonvalot, S., Diament, M., Gabalda, G., 1998. Continuous gravity recording with Scintrex CG-3M meters: a promising tool for monitoring active zones. Geophys. J. Int., 135: 470-494.

Budetta, G., Carbone, D., 1997. Potential of application of the Scintrex CG-3M gravimeter for monitoring volcanic activity: results of field trials on Mt. Etna, Sicily. J. Volcanol. Geotherm. Res., 76: 199-214.

Djamour, Y., Vernant, P., Bayer, R., Nankali, H., Ritz, J.F., Hinderer, J., Hatam, Y., Luck, B., Le Moigne,N.,Sedighi, M., Khorrami, F., 2010. GPS and gravity constraints on continental deformation in the Alborz mountain range, Iran, Geophys. J. Int., submitted.

Dias, F.J.S.S., Escobar, I.P., 2001.A model for adjustment of differential gravity measurements with simultaneous gravimeter calibration. J Geod 75: 151-156.

Francis, O., van Dam, T., Germak, A., et al., 2010. Results of the European Comparison of Absolute Gravimeters in Walferdange (Luxembourg) of November 2007, IAG International Symposium on Gravity, Geoid and Earth Observation 2008, Crete, June 2008 (in press).

Ghazavi, K., tavakoli, F., 2003.National Gravity Calibration Line of Iran. Technical report, NCC.

Hatam, Y., Djamour, Y., 2004. Multi-purpose Physical Geodesy and Geodynamics Network of Iran. Technical report, NCC, Iran, 28 pp.

Hatam, Y., Bayer, R., Djamour, Y., Hinderer, J., Vanicek, P., Mohammad Karim, M., Le Moigne, N., Luck, B., Karpychev, M., Azizian, N., Cheraghi, H., Saadat, R., Bahrampour, A., Asghari, H., Meygooni, H. Establishment of National Absolute Gravity Network of Iran: An opportunity to detect long-term and seasonal gravity changes, and their relation to crustal deformation and hydrology. Submitted to Newton's Bulletin.

Jacob, T., Bayer, R., Chery, J, and Le Moigne, N., 2010. Time lapse microgravity surveys reveal water storage heterogeneity of a karst aquifer, J. Geophys. Res. , 115, B06402, doi:10.1029/2009JB006616.

Lyard F., Lefevre, F., Letellier, T., Francis, O., 2006. Modelling the global ocean tides: modern insights from FES2004. Ocean Dynamics, 56(5-6): 394-415.

Mäkinen, J., Stahlberg, B., 1998. Long- term frequency stability and temperature response of a polarization-stabilized He–Ne laser, Measurements, 24, pp. 179–185.

Microg, 2007. 'g' 7.00 absolute gravity data acquisition and processing. In: M.-g. Solutions (Editor). Micro-g Solutions, Lafayette, Colorado,USA.

Nadjafi, M., Mashhadi, M., Hatam, Y., Tavakoli, F., 1998. Design of a gravity base network for Iran, Technical report, NCC, Iran. 51 pp.

Nadjafi, M., Mashhadi, M., Hatam, Y., Tavakoli, F., 2006. Design of a gravity base network, Journal of Allgemeine Vermessungs – Nachrichten (AVN), 11-12, 374-382,
http://imperia.mi-verlag.de/imperia/md/upload/article/374_382_alamdari.pdf

Niebauer, T.M., Sasagawa, G.S., Faller, J.E., Hilt, R., Klopping, F., 1995. A new generation of absolute gravimeters. Metrologia, 32, 159-180.

Niebauer, T.M., 1989. The effective measurement height of free-fall absolute gravimeters. Metrologia, 26,: 115-118.

Schwiderski, E. W., 1980. Ocean tides, II: a hydrological interpolation model, Marine Geodesy 3, 219-255.

Scintrex limited, 2006.CG-5 Scintrex Autograv System Operation Manual. Scintrex Limited, Concord, Ontarion.

Seigel, H.O., (1995). A guide to high precision land gravimeter surveys. Scintrex L.T.D, Concord, Ontraio, Canada.

Tamura Y., 1987.A harmonic development of the tide-generating potential. Bull. d'Inf. Marées Terrestres, 99, 6813-6855.
Tapley, B.D., Bettadpur, S., Ries, J.C., Thompson, P.F., Watkins, M.M., 2004. GRACE Measurements of mass variability in the earth system. *Science* 23 July 2004, 305, 5683, 503-505.

Torge, G., 1989. Gravimetry, Walter de Gruyter & Co., Berlin, 465 pp.

Timmen, L., 2003. Precise definition of the effective height of free- fall absolute gravimeters. Metrologia, 40, 62, doi: 10.1088/0026-1394/40/2/310

Ukawa, M., Nozaki, K., Ueda, H., Fujita, E., 2010. Calibration shifts in Scintrex CG-3M gravimeters with an application to detection of microgravity changes at Iwo-tou caldera, Japan. Geophysical Prospecting, 47: 73-83

Van Camp, M., S. D. P. Williams, O. Francis (2005). Uncertainty of absolute gravity measurements, J. Geophys. Res., 110, B05406, doi: 10.1029/2004JB003497

Zomorrodian, H., 1985.The Iranian National Calibration Line 1985. Technical Report of the Institute of Geophysics, Tehran University

Zomorrodian, H., 1987.The establishment of the Iranian Gravity Datum, Bureau Gravimetrique International, Bul. Information, 60.

Zumberge, M. A., 1981.A portable apparatus for absolute measurement of the earth's gravity, PhD Thesis, University of Colorado at Boulder.

4. Etablissement du réseau ''multi-observations'' en Iran à objectifs géodésiques et géodynamiques

Designing and Implementation of the Multi-purpose Physical Geodesy and Geodynamics Network of Iran (MPGGNI2010)

Y. Hatam(1,2), Y. Djamour(3), R. Bayer(2), P. Vanicek(4), A. M. Abolghasem(5,6),H. Cheraghi(2), R. Saadat(2), N. Azizian(2), S. Rafiey(2), S. Arabi(2), Z. Moosavi(2), A. Soltanpour(2), F. Tavakoli(2), M. Mohammad Karim(6), M. Najafi Alamdari(6)

(1) Geosciences Montpellier cc60,Universite Montpellier 2–CNRS, Pl. E. Bataillon, 34095 Montpellier Cedex05, France. Email: yaghoub.hatam@gm.univ-montp2.fr , roger.bayer@gm.univ-montp2.fr

(2,3) [(2) Physical Geodesy Department, Geodesy and Land Surveying Management + (3)Geomatics College], National Cartographic Centre (NCC), PO Box 13185-1684, Meraj Ave, Tehran, Iran. Email: yaghoubhatam@yahoo.com, djamour@ncc.org.ir

(4) University of New Brunswick, Fredericton, Canada. Email: vanicek@unb.ca

(5) Dept of Geo- and Environmental Sciences, Ludwig-Maximilian University, Munich, Germany

(6) Faculty of Geodesy and Geomatics Engineering, KN. Toosi University of Technology, Tehran, Iran.

Abstract

The Multi-purpose Physical Geodesy and Geodynamics Network of Iran (MPGGNI05) is established during 2005-2010 and consists about 600 stations with an average spacing of 55 km. Three types of observations, i.e. relative gravity, GPS and precise levelling, were measured at the MPGGNI05 stations in co-localized manner. The relative gravities between the neighbour stations are measured in A-B-A line method with 6 relative gravimeters (3 CG-5 and 3 CG-3/M) from Scintrex Ltd. The stations are tied to the absolute gravity network stations. After correcting for different systematical effects, i.e. earth tide, instrumental drift, levelling effect, pressure effect and calibration effect , an adjustment is made by weighted least squares method. A precision about 10-20 μGal is obtained for the network. The precise geometrical 3D positions of the network stations is determined by measuring them with 6 dual frequency Trimble GPS receivers of Trimble Ltd in campaign mode, for a duration of 24 hours. The observed GPS data are merged to the data of 20 permanent IGS stations and processed with GAMIT software. The precision of 2 mm is obtained for the horizontal components, and 1-3 cm for vertical components. It is proposed to gather precise levelling measurments between stations of the 55 km network and the nearest bench mark of the first or second order

national precise levelling network of Iran, using Wild N3 and Ziess Dini11 precise levels. The expected precisions is $3mm\sqrt{km}$. Nowadays, 118 stations of the network are levelled.

Keywords: relative gravity, GPS, precise levelling, multi-purpose network, MPGGNI10

1. Introduction

Iran covers a large area limited in longitude by the meridians 44°E and 64°E and in latitude by the parallels 25°N and 40°N. Mapping a new gravity field over Iran is at present a great challenge for geodesic and geodynamic considerations: gravity anomaly maps are precious geophysical tools to understand the structure of the earth. From geodetic point of view, coupling precise leveling, gravity surveys and GPS measurements is required to determine accurately altitude and a geoid model over the Iranian territory. The national absolute gravity network (Hatam et al, to be submitted, see section 3.2) and national gravity calibration line of Iran have been recently established in Iran (Hatam et al ; to be submitted; see section 3.3). It is decided by the National Cartographic Centre of Iran (Hatam and Djamour, 2004) to establish a geodetic network in nation-wide with co-locallized multi-observations; i.e. gravity-GPS-precise levelling with a mesh of 55 km and with a precision of the order of 10 μGals for gravity, 1-3 cm for GPS height and $3mm\sqrt{km}$ for precise levelling.

2. Gravity at MPGGNI10 network

2.1 The CG-5 Scintrex autograv system

The sensing element of the Autograv is based on a fused quartz elastic system, details presented in figure 3.25 (Scintrex, 2006). The gravitational force on the proof mass is balanced by a spring and a relatively small electrostatic restoring force. The position of the mass, which is sensed by a capacitive displacement transducer, is altered by a change in gravity. An automatic feedback circuit applies DC voltage to the capacitor plates producing an electrostatic force on the mass which brings it back to a null position. The feedback voltage, which is a measure of the relative value of gravity at the reading site, is converted to a digital signal and then transmitted to the instrument's data acquisition system for processing, display and storage. The inherent strength and excellent elastic properties of fused quartz together with limit stops around the proof mass permit the instrument to be operated without clamping. Further protection is provided

by a durable shock mount system which attaches the sensor to the housing. The parameters of the gravity sensor and its electronic circuits are chosen so that the feedback voltage covers a range of over 8000 mGals without resetting.The use of a low-noise electronic design, together with a highly accurate auto-calibrating analog to digital converter, results in a resolution of 0.001 mGal, equipping the gravity meter for both detailed field investigations and large scale regional or geodetic surveys. The instrument's tilt sensors are also electronic, with a resolution of 1 arc second. The outputs from the sensors are displayed on the instrument's front panel and also transmitted to the data acquisition system where they are displayed and stored. If the instrument is operated on an unstable base, real-time corrections for tilt errors can be automatically made over a range of ±200 arc seconds. Protection from ambient temperature changes is provided by locating the quartz elastic system, the analog to digital converter, sensitive electronic components and the tilt sensors inside a high-stability, two stage, thermostatically controlled environment. There is no mechanical temperature compensation. External temperature changes are reduced by a factor of 10^{-5} and small residual effects are corrected in software using the output of a sensor located in close thermal contact with the main spring. The operating range of the thermostat in the standard instrument is -40°C to +45°C. However, since there is no critical operating point for the sensor, the upper operating temperature can be set at a lower or higher value (optional -45°C). The entire gravity sensing mechanism is enclosed in a vacuum chamber. Since there are no mechanical feed-throughs, excellent isolation from variations in atmospheric pressure is obtained. This extremely stable operating environment for the quartz elastic system allows the long-term drift of the sensor to be accurately predicted, and real-time software correction reduces it to less than 0.2 mGals/day. The sensor design is mechanically very simple. The fine balancing required to obtain astatisation is not needed, as the displacement transducer has sufficient resolution (0.02nm) to detect the beam position of a non-astatised system, and electronic filtering reduces the effect of seismic noise. The mechanisms, micrometer screws, gearboxes and mechanical feed-throughs associated with mechanical feedback systems have been replaced by a voltage applied to the same plates which form the displacement transducer. The temperature control is also accurate enough for the sensor to operate without mechanical compensation.

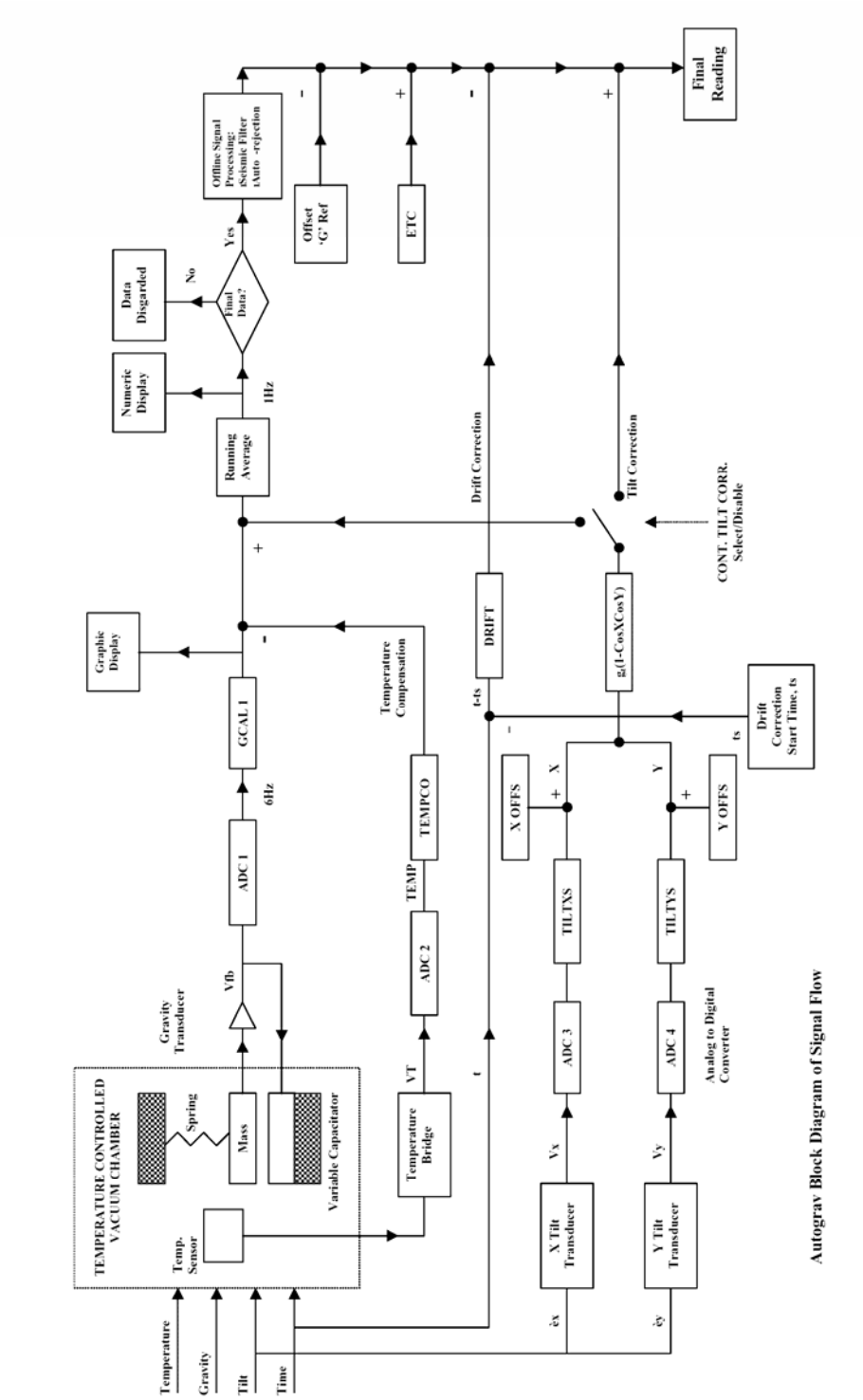

Figure 3.25 The acquisition scheme for the Scintrex relative gravimeter CG-5 (Scintrex, 2006). ETC is the Earth tide correction based on the Longman (1959) algorithm. The parameters TILT X S and TILT YS are the tilt sensor sensitivities adjusted by the operator. TEMPCO is the temperature correction factor determined by the manufacturer. GCALl and GCAL2 are the first- and second-order calibration factors of the gravity signal. DRIFT is the correction factor used for the instrumental linear drift correction.

2.2 Gravity observation and computation

The relative gravity measurements are gathered at MPGGNI10 network by using 6 relative gravimeters (3 CG-3/M and 3 CG-5) and by line method (A-B-A), with 30 minutes measurements at each setup, and with triangular loop coverage over Iran (**Fig. 3.25**). Additional measurements are made to tie the network to the Absolute gravity network of Iran, four ties from four nearest points to each absolute gravity station. Several corrections for different systematical effects, i.e. earth tide, levelling effect, pressure effect are automatically made by the gravimeter by entering the needed initiate infromation. After instrumental drift and calibration error correcting, both by linear approximation, the gravity difference and its precision is computed for each measured line between two neighboring points. The gravity misclosure error for each measured triangular loop is computed by its 3 corrected gravity differences (**Fig. 3.26**). The relative gravity differences and the absolute gravity values are adjusted by weighted least squares method to obtain the gravity values of MPGGNI10 network stations and their precisions. The following procedure is used.

For a go-returned relative gravity measurement between stations S_j and S_i we can write

$$C_f\,(m_{S_j}^{t_j} - m_{S_i}^{t_i}) + V_{S_i}^{S_j} = g_j - g_i + D(t_j - t_i) \qquad (1)$$

where C_f is the calibration correction factor of the relative gravimeter, $m_{S_j}^{t_j}$ and $m_{S_i}^{t_i}$ are mean gravity readings at stations S_j and S_i and at times t_j and t_i respectively, $V_{S_i}^{S_j}$ the residual of $(m_{S_j}^{t_j} - m_{S_i}^{t_i})$, g_j and g_i the gravity values at stations S_j and S_i to be adjusted, and D the instrumental drift parameter.

An absolute gravity measurement $g_{S_i}^{abs}$ is linked to the gravity value g_i to be adjusted by:

$$g_{S_i}^{abs} + V_{S_i}^{abs} = g_i \qquad (2)$$

The matrix representation of the observation equations for n gravity stations and m go-returned relative measurements is:

$$L + V = AX \qquad (3)$$

where L is the n vector of relative and absolute gravity readings with $n \times n$ weight matrix P given by the inverse of the variance of the gravity readings, V is the vector of residuals, A is the $n \times (m+s)$ design matrix and X is the m+s vector of unknowns to be inverted, i.e., m gravity values (one for each station) and s linear drift (one for each go-returned relative measurement). The least-squares adjustment for X is:

$$X = (A^T PA)^{-1}(A^T PL) \quad (4)$$

and the residuals are:

$$V = AX - L \quad (5)$$

The a posteriori variance of unit weight is computed as:

$$\sigma_0^2 = \frac{V^T PV}{n-(m+s)} \quad (6)$$

where $n-(m+s)$ is the degree of freedom of the least-squares fit. The a posteriori covariance matrix of X is

$$\Sigma = \sigma_0^2 (A^T PA)^{-1} \quad (7)$$

In the adjustment, 1598 gravity differences with 24 absolute graviy values are used to compute the gravity values of 593 points at MPGGNI10. The histograms of residual values (eq. 5) and precision of the adjusted gravity values (eq. 7) are presented in **figures 3.27** and **3.28** respectively.

The precision on g values is distributed around 12 μGal which is close to the expected value of 10 μGal initially declared in the project.

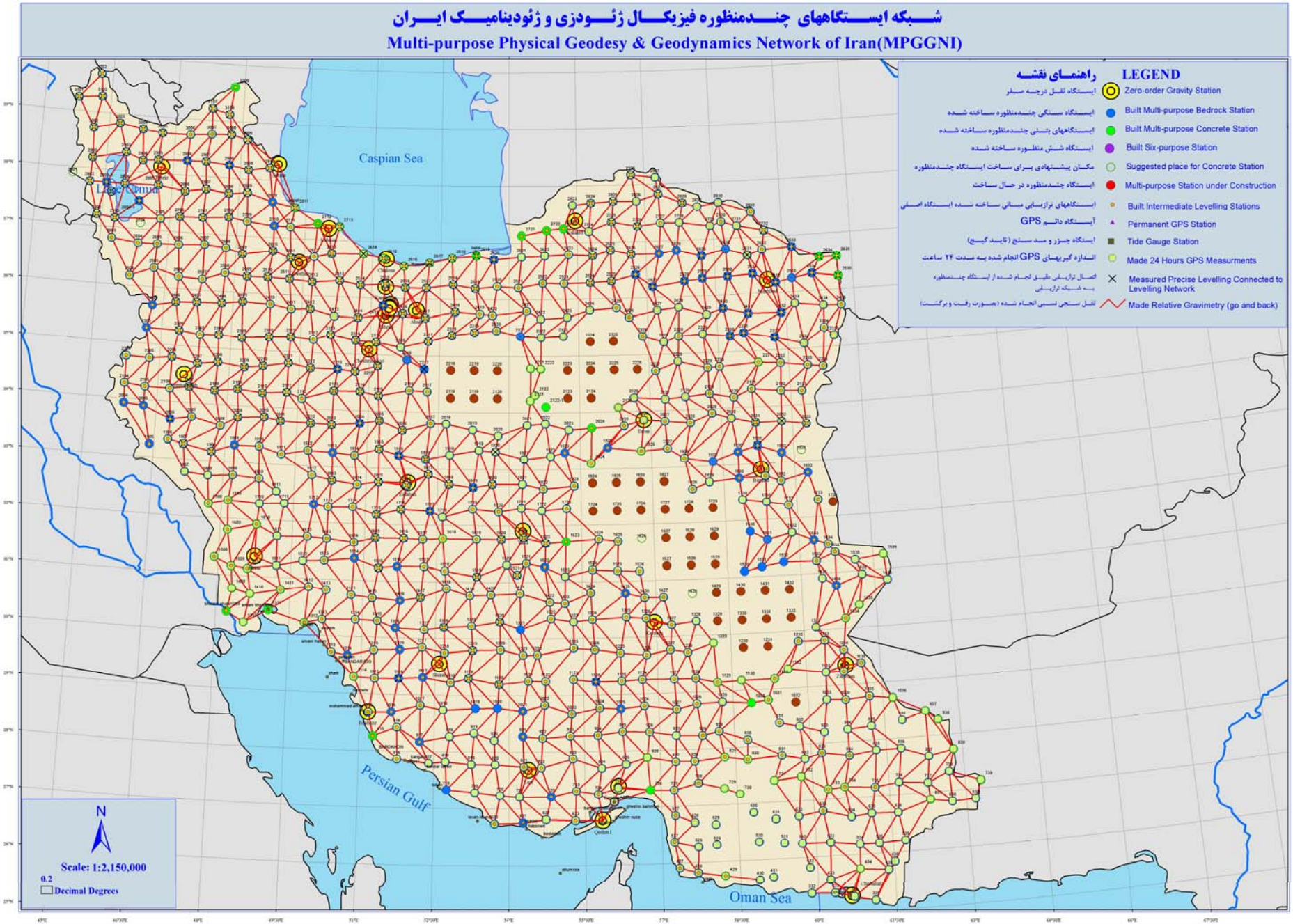

Fig. 3.25 Multi-purpose (Gravity, GPS and precise leveling) Physical Geodesy and Geodynamics Network of Iran (MPGGNI110).

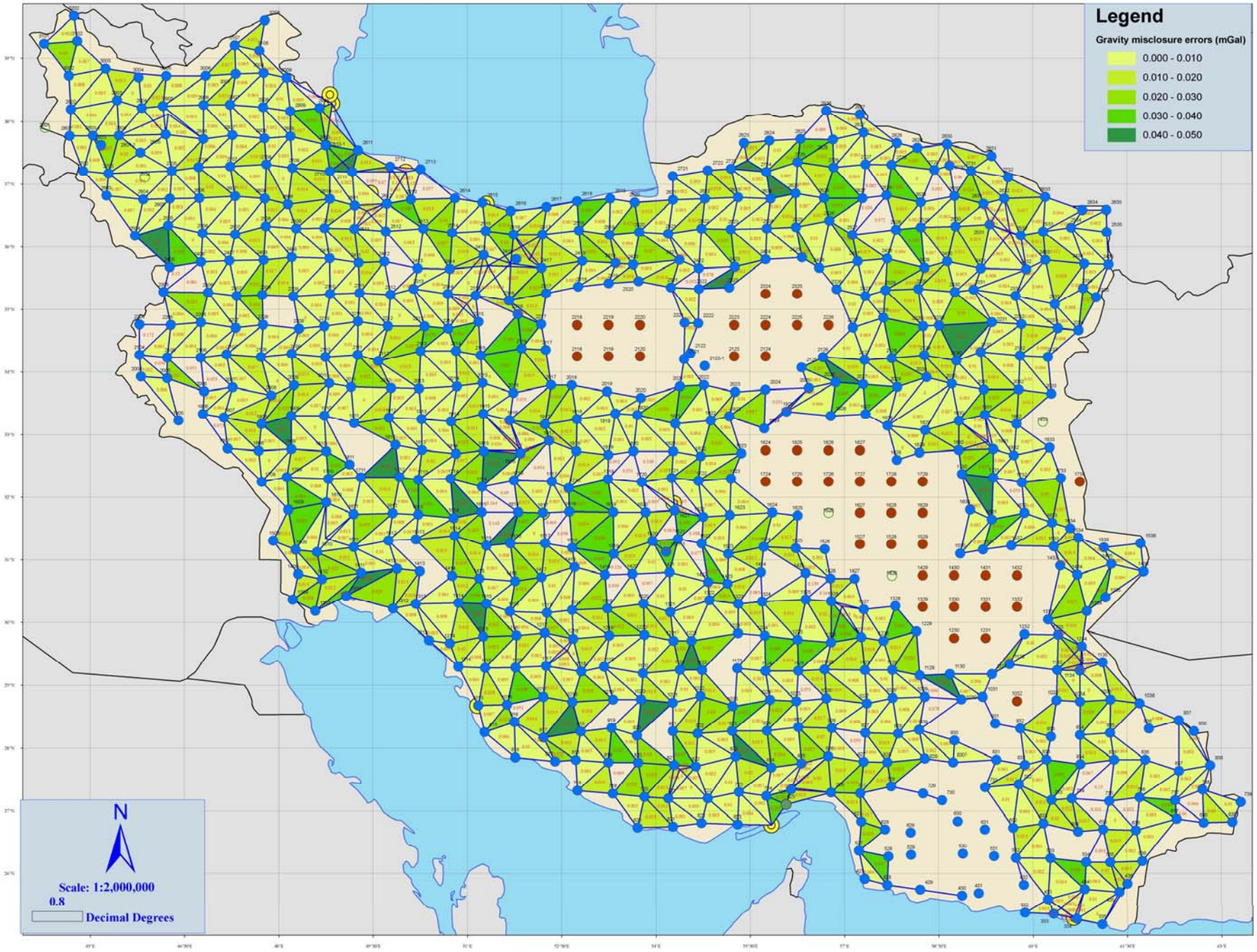

Fig. 3.26 Triangular gravity loop misclosure errors of MPGGNI10 network after drift and calibration corrections

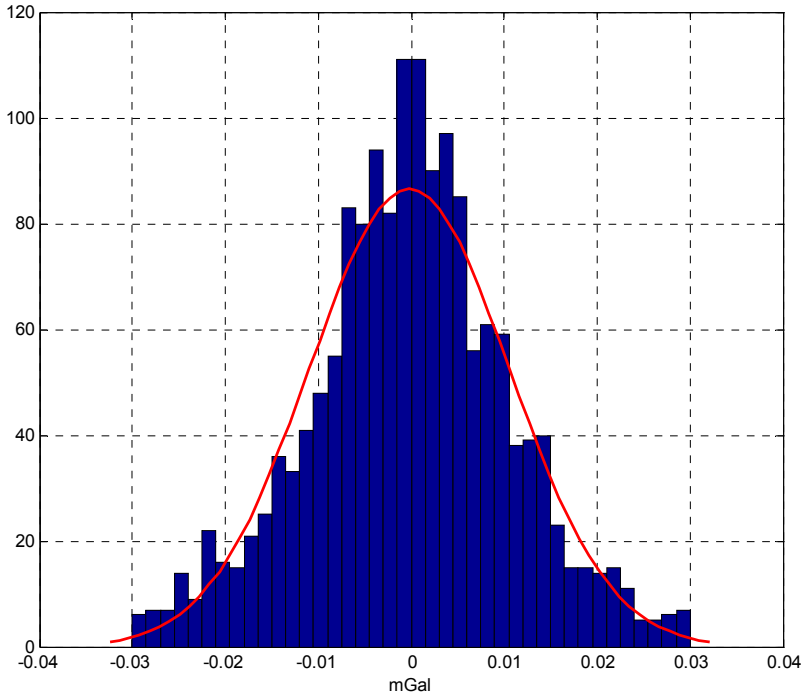

Fig. 3.27 Histogram of residual values of relative gravities at MPGGNI10

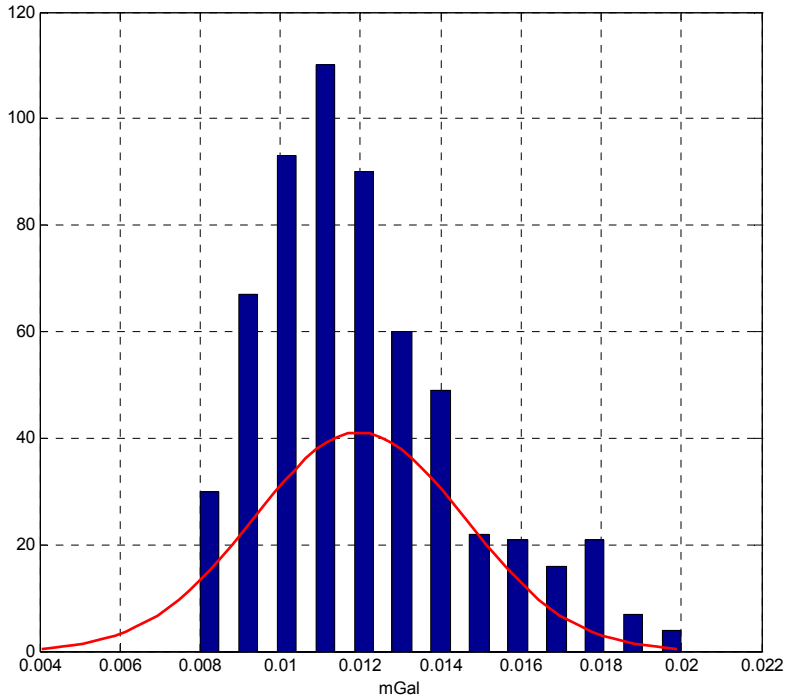

Fig. 3.28. Histogram of gravity precisions at MPGGNI10

3. GPS measurements at MPGGNI05 network

Precise GPS positioning are planned in the frame of the MPGGNI10 project. Localisation of the 55 km noeds of the MPGGNI10 is realized using 6 double frequency Trimble GPS receivers. The duration of the observations is fixed to 24 h in order to localize the height of the noeds with a precision of ~0.01 - ~0.3 m.

3.1. GPS data processing

In order to strengthen the reference frame and constrain the orbital parameters, data of 20 IGS stations: ANKR, ARTU, BAHR, BOR1, GLSV, GOPE, GRAZ, IISC, IRKT, JOZE, KIT3, LAMA, LHAS, NICO, PENC, POL2, POTS, RAMO, ZECK, ZIMM (Beutler et al ., 1993) are merged to Tehran network data. The GPS data are analyzed using GAMIT software from Massachusetts Institute of Technology (King and Bock, 2002) in a well known procedure of three steps (see for example Feigl et al, 1993; Bock et al., 1986; Dong et al., 1998; McClusky et al., 2000; Oral, 1994). Starting from weak constraints on the parameters, doubly differenced GPS phase observations are used to estimate daily stations coordinates, one tropospheric parameter every 2 hours and orbital and earth parameters (EOP). The solutions are used to compute independently the daily baseline components. The repeatability of the daily solutions characterizes the precision of coordinates for a short interval of time (i.e. duration of a campaign). Repeatabilities are of 0.002 mm for horizontal components and 0.005 mm for vertical component. In the 2nd step, a consistent set of coordinates and velocities is obtained by means of GLOBK software based on Kalman Filter (Herring, 2002) using quasi-observations the loosely constrained daily stations coordinates, orbits and EOP, and their covariance as quasi-observations. The local quasi-observations are combined with the global quasi-observations during the 2000-2008 epochs at >150 globally distributed IGS stations, solutions computed by the Scripps Orbit and Permanent Array Center (SOPAC) (Bock et al, 1997). The daily SOPAC solutions which are not belong to survey epochs, are transformed in monthly average solutions. Finally, the quasi-observations from all GPS surveys realized in Iran are added to the Tehran quasi-observations. In the 3rd step, solution is estimated from generalized constraints including offsets and rotations of the reference frame, EOP and orbits as parameters of the adjustment. In order to estimate 3D positions relative to the International Terrestrial Reference Frame, we considered 21 IGS stations to be enough fixed to the ITRF2000 (Altamami et al, 2002). By this way a stable reference frame with a precision of 1.4 mm for the position is obtained.

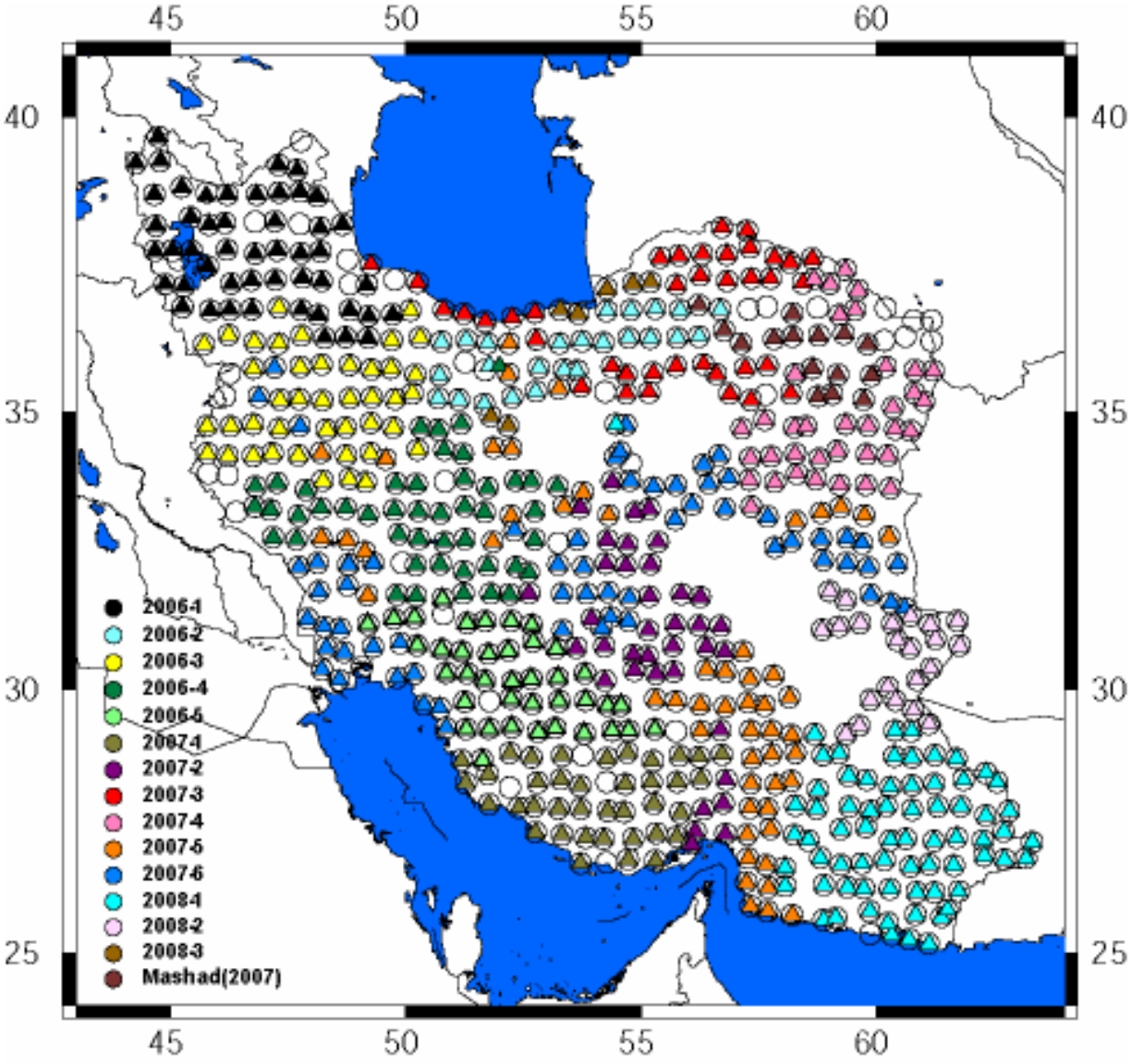

Fig. 3.29. The schedule of GPS campaign measurements at MPGGNI10 network.

4. Precise leveling measurements at MPGGNI05 network

It is planned to tie each station of MPGGNI10 to the national precise leveling network (1-st or 2-nd order) with the two- way precise leveling measurements and with a precision criteria of $3mm\sqrt{km}$. Till now, a number of 118 stations are measured. We will assume that the mesure for the MPGGNI10 is of the order of the mesure of the 1-st order levelling network, as to the experimented protocole is identical for the 2-nd order network (Hatam et Djamour, 2004).

References

Altamimi Z., P. Sillard, and C. Boucher, 2002, ITRF2000: A new release of the International Terrestrial Reference Frame for earth sciences applications, *J. Geophys. Res.*, *107* (B10), NIL_119-NIL_137.

Bock Y., S. A. Gourevitch, C. C. Counselman, R. W. King, and R. I, 1986. Abbot, Interferometric analysis of GPS phase observations, *Manuscripta Geodaetica*, *11*, 282-288

Bock Y., J. Behr, P. Fang, J. Dean, and R. Leigh, 1997. Scripps Orbit and Permanent Array Center (SOPAC) and Southern Californian Permanent GPS Geodetic Array (PGGA), in *The Global Positioning System for the Geosciences*, pp. 55-61, Nat. Acad. Press, Washington, D.C.

Feigl K. L., D. C. Agnew, Y. Bock, D. Dong, A. Donnellan, B. H. Hager, T. A. Herring, D. D. Jackson, T. H. Jordan, R. W. King, S. Larsen, K. M. Larson, M. H. Murray, Z. Shen, and F. H. Webb, 1993. Space geodetic measurement of crustal deformation in central and southern California, *J. Geophys. Res.*, *98*, 21677-21712

Hatam, Y., Djamour, Y., 2004. Multi-purpose Physical Geodesy and Geodynamics Network of Iran. Technical report, NCC, Iran, 28 pp.

Herring T. A., 2002. *GLOBK: Global Kalman filter VLBI and GPS analysis program, version 10.0*, Mass. Inst. of Technol., Cambridge

Longman, I. M., 1959. "Formulas for computing the tidal accelerations due to the Moon and the Sun," J. Geophys. Res., 64, 2351-2356.

McClusky S., S. Balassanian, A. Barka, C. Demir, S. Ergintav, I. Georgiev, O. Gurkan, M. Hamburger, K. Hurst, H. Kahle, K. Kasten, G. Kekelidze, R. W. King, V. Kotzev, O. Lenk, S. Mahmoud, A. Mishin, M. Nadariya, A. Ouzoumis, D. Paradissis, Y. Peter, M. Prilepin, R. Reilinger, I. Sanli, H. Seeger, A. Tealeb, M. N. Toksöz, and G. Veis, 2000. GPS constraints on plate motions and deformations in eastern Mediterranean and Caucasus, *J. Geophys. Res.*, *105*, 5695-5719

Oral B., 1994. Global Positioning System (GPS) measurements in Turkey (1988-1992): Kinematics of the Africa-Arabia-Eurasia Plate collision zone, Cambrige, 344 pp. p., thesis

Scintrex limited, 2006.CG-5 Scintrex Autograv System Operation Manual. Scintrex Limited, Concord, Ontarion.

5. Calcul des anomalies de pesanteur – Cartographie des anomalies à l'Air Libre et de Bouguer

Au cours du chapitre 3, nous avons présenté l'ensemble des données de pesanteur intégrant la base des données du Bureau Gravimétrique International et celles nouvellement acquises par le NCC et présentées dans ce travail de Thèse, soit un total de 22300 données disponibles sur l'Iran (Fig. 3.30).

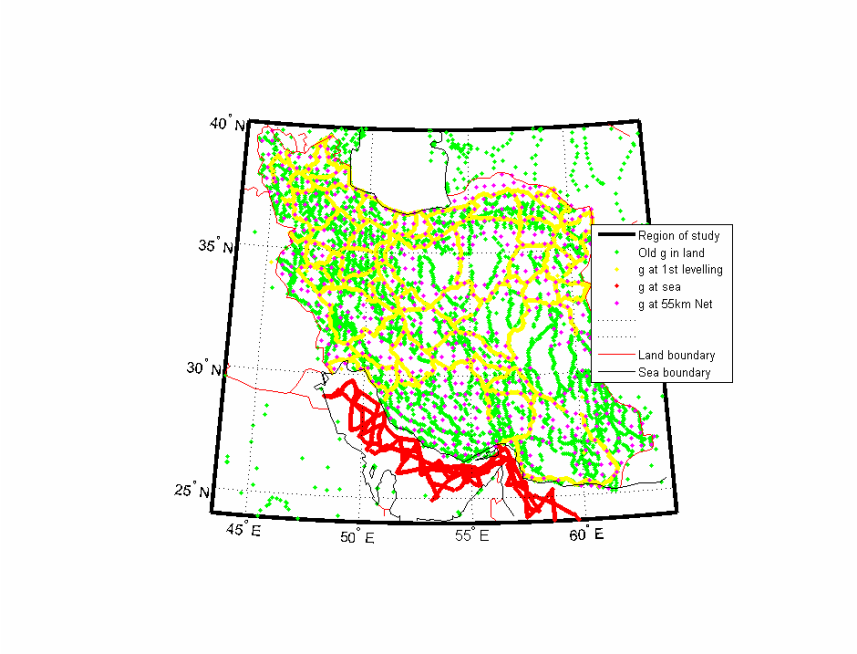

Fig. 3. 30 Distribution des données gravimétriques en Iran

L'anomalie a l'air libre a été calculée pour l'ensemble des points en adoptant pour la pesanteur normale la formule internationale définie en 1980 (IAG, 1980) corrigée de l'effet d'air libre $\delta g = -0.3806h$, où δg est donnée en mGal et h est la hauteur orthométrique donnée en m. Compte tenu de l'incertitude sur la valeur de g et sur la hauteur h, la précision sur l'anomalie à l'air libre est estimée entre 0.1 et 3.1 mGal respectivement pour les nouvelles et anciennes données (voir $\oint$ 1 du chapitre 3). L'anomalie à l'air libre est interpolée sur une grille $3' \times 3'$ en utilisant la méthode du krigeage, et présentée sur la figure 3.31.

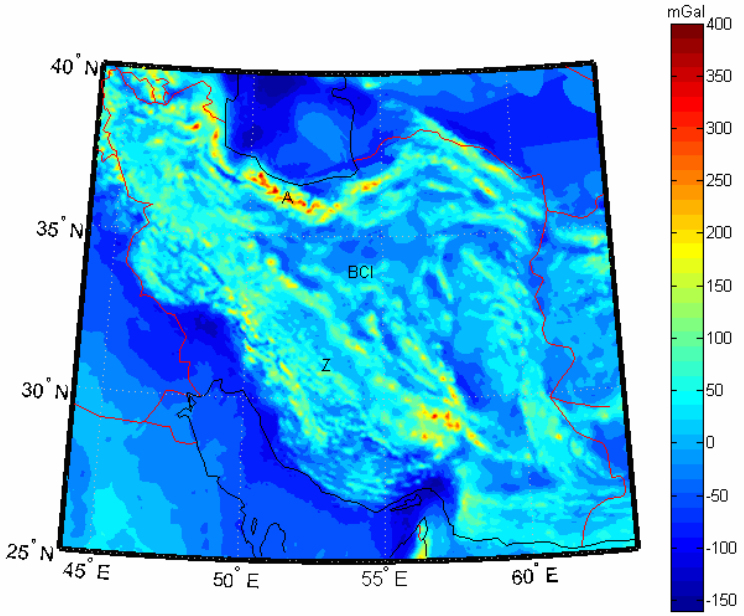

Fig. 3.31 Carte d'anomalie à l'air libre de l'Iran avec la maille $3' \times 3'$. *BCI : Bloc Central Iranien, A : Chaîne de l'Alborz, Z : Chaîne du Zagros*

Les anomalies de pesanteur ainsi calculées se serviront des données de base pour le calcul du géoïde gravimétrique. L'anomalie à l'air libre est proche de zéro sur l'Iran, en particulier sur le Bloc Central Iranien (moyenne de 4 mGal) excepté sur certaines zones de l'Iran comme les chaînes de Montagne de l'Alborz et du Zagros où les hauts reliefs sont associés à des fortes anomalies ($\succ 150\, mGal$). Il est probable que la faible amplitude des anomalies à l'air libre de grande longueur d'onde sur l'Iran Central d'altitude moyenne de 1000 m, soit la conséquence de la compensation isostatique des reliefs à grande longueur d'onde soit par un mécanisme d'épaississement crustal [Dehghani et Makris, 1984; Snyder et Barzaghi, 1986; Paul et al., 2006] soit par la présence d'un manteau supérieur anormal de faible densité [Kaviani et al, 2007].

L'anomalie de Bouguer est déterminée par retrait de l'effet du relief. La densité moyenne adoptée des reliefs est de 2670 kg/m^3. La correction de relief est opérée en utilisant le Modèle Numérique de Terrain SRTM (Shattle Radar Topographic Mission, voire http: //www2. jpl.nasa.gov/srtm/) de maille $18'' \times 18''$ soit environ 500 m (Fig. 3.32).

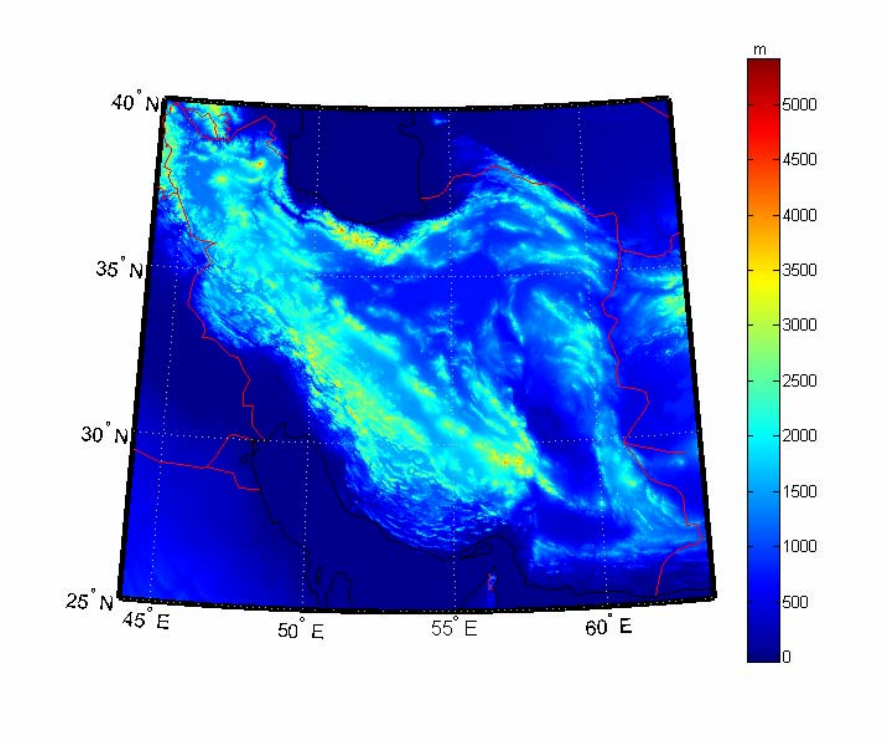

Fig. 3.32 Carte de la topographie de l'Iran (SRTM) avec la maille $18'' \times 18''$

L'effet de terrain proche n'est pas pris en compte, ce qui introduit vraisemblablement des erreurs pouvant atteindre plusieurs mGal dans les chaines de Montagnes. Le rayon d'intégration des effets topographiques est fixé à 1 degré. Par ailleurs, l'effet des océans n'est pas corrigé. La carte d'anomalie de Bouguer [Fig. 3.33] révèle des variations de courtes longueurs d'onde qui n'étaient pas visibles sur la dernière carte publiée par Dehghani et Makris [1984] (chapitre 3, Fig. 3.2).

Une analyse rapide de ce document indique une forte anomalie négative sur la Chaîne du Zagros ($\prec -200\,mGal$).Paul et al. [2006 et 2010] ont réalisé une analyse des fonctions récepteurs issues de l'enregistrement de téléséismes sur deux profils traversant le Zagros, le Bloc Central Iranien et l'Alborz pour le profil le plus au nord ouest (*Fig.3.34*). Ils mentionnent que le Moho atteint une profondeur maximum de 69 km sous le Zagros Central et de 56 km sous le Nord Zagros au niveau du chevauchement majeur du Zagros (MZRF, *fig 3.34 et 3.35*) en relation avec le chevauchement de la croûte de marge arabe par la croûte du Bloc Iran Central. Un modèle d'échelle crustal a été proposé avec succès par Paul et al. [2006] permettant de réconcilier les modèles sismiques issus des fonctions récepteurs et les anomalies de Bouguer sur le profil Zagros Central.

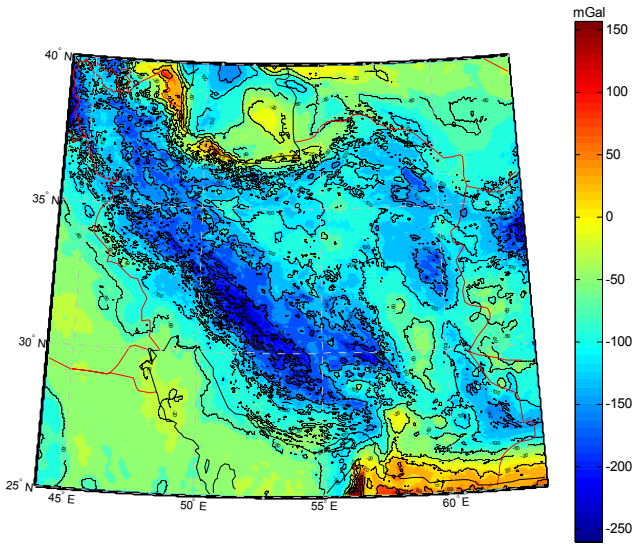

Fig. 3.33 Carte d'anomalie de Bouguer de l'Iran. Densité de correction 2670 kg/m^3. La correction de terrain est réalisé à l'aide du Modèle Numérique de Terrain SRTM 18'', par intégration des effets topographiques sur une distance au point de mesure n'excèdent pas 1 degré.

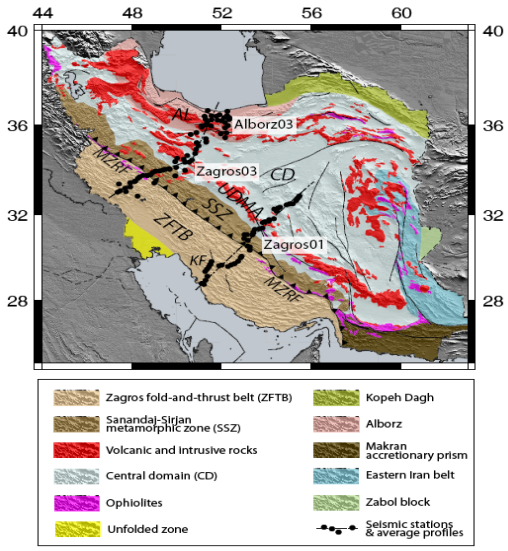

. Fig. 3.34 localisation des expériences télésismiques réalisées par Paul et al. [2010]

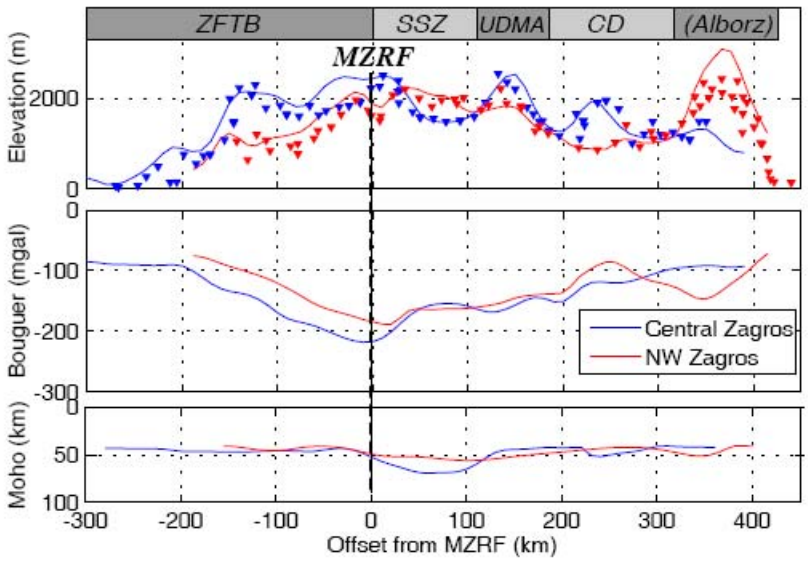

Fig. 3.35 Profils topographies (en haut), de l'anomalie de Bouguer (au centre), et de profondeur du Moho (en bas) recoupant le Zagros Central (bleu) et Zagros NW (rouge), [Paul et al, 2010]

Si à l'évidence le relief de l'alborz semble anti-correlé avec la profondeur du Moho, traduisant ainsi le mécanisme de compensation isostatique qui reste à mieux définir avec ces nouvelles données sismiques et gravimétriques récentes, en revanche le déphasage entre le relief (>2000 m)et l'anomalie de Bouguer négative et l'absence d'approfondissement du Moho sous l'Alborz reste énigmatique (*fig. 3.35*). Nous suggérons que la chaîne de l'Alborz s'est récemment construite sur une marge amincie. Ainsi la profondeur actuelle du Moho sous cette chaine, proche de celle du Bloc Central Iranien, résulterait principalement du chevauchement vers le sud du bloc Alborz sur le Bloc Iran Central le long de grands chevauchements émergeant sur le front sud de la chaîne (Chevauchement Nord Téhéran,….). L'anomalie de Bouguer négative de -50 mGal centrée en limite sud de l'Alborz reflèterait alors l'effet d'un prisme d'accrétion d'épaisseur à déterminer. Un modèle mécanique ou isostatique de cette chaîne reste à réaliser prenant en compte en particulier les propriétés élastiques de la lithosphère.

Le Bloc Iran Central est caracterisé par une anomalie négative de -50 à -100 mGal qui ne peut pas être exclusivement expliqué par la forme du Moho.

Au niveau du manteau supérieur, l'analyse des ondes de surface et la tomographie en ondes P réalisées sur le profil Zagros Central a révélé un fort contraste de vitesse entre des vitesses élevées

sous la marge du continent arabe et des vitesses faibles sous le Bloc Iran Central [Kaviani et al., 2007 ; Paul et al. 2010] (*fig. 3.36*)

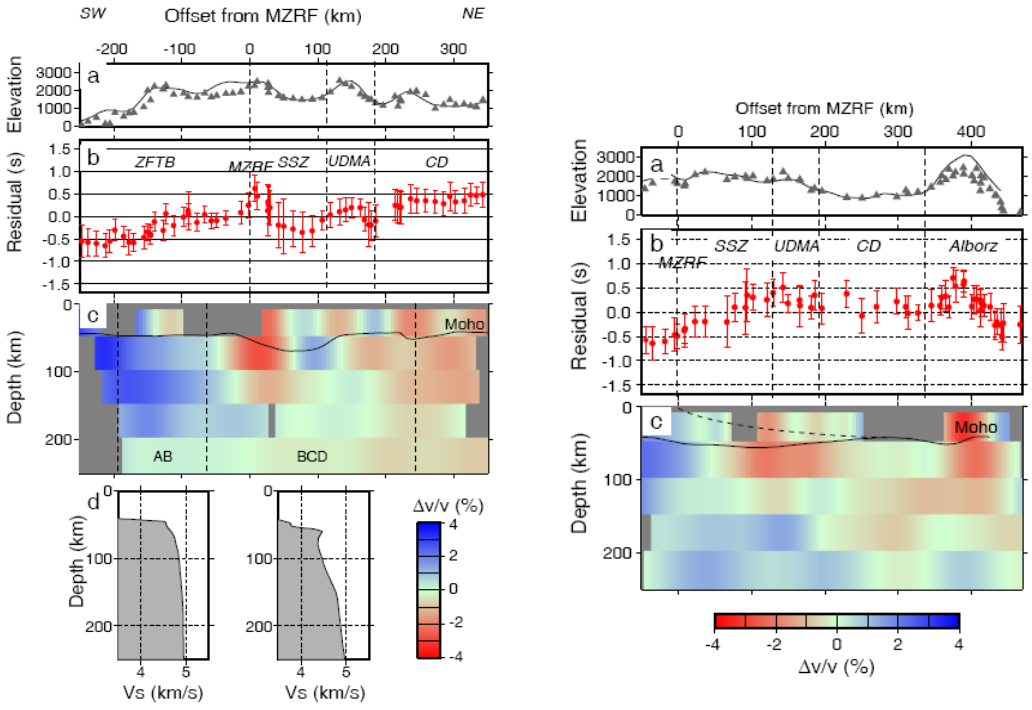

a) b)

Fig. 3.36 : a) Tomographie en onde P-et modèles « locaux » de vitesse en onde S issus de l'analyse des ondes de surface le long du profil Zagros Central (Zagros01, fig. 3.34) ; b) Tomographie en onde P et modèle de variation de vitesse en onde P le long du profil Zagros NW (Zagros03) [Kaviani et al., 2007 ; Paul et al., 2010].

Paul et al. [2010] suggérent que le modèle de vitesse en ondes S obtenu pour la marge arabe est proche de ceux observés habituellement sur les boucliers alors que les faibles vitesses dans le manteau supérieur seraient associées à des températures plus élevées. Ainsi, il serait nécessaire de prendre en compte ces hétérogénéités mantelliques pour modéliser à grande échelle la lithosphère en couplant les observations sismiques et gravimétriques. Ce travail reste à faire.

Enfin, signalons la présence d'anomalies fortement positives sur le pourtour sud et ouest de la mer Caspienne. Compte tenu de l'épaisseur importante de sédiments récents accumulés dans le bassin Sud Caspien, il est probable que cette signature gravimétrique relève de la présence d'une croûte continentale amincie, voir même océanique comme cela a déjà été suggéré par plusieurs auteurs sous la mer Caspienne (voir Berberian, 1983 ; Jackson et al, 2002 ; Allen et al, 2002). Selon le signal gravimétrique, cette croûte amincie ou océanique pourrait s'étendre à l'ouest sous le bassin de Kura.

4. Méthodologie de la détermination du Géoïde

1. Méthode de Stokes-Helmert

Dans cette partie nous présentons un bref aperçu théorique de la méthode de Stokes-Helmert utilisée ultérieurement pour la détermination précise du géoïde gravimétrique. Nous renvoyons à Ellmann and Vanicek (2007) et Ellmann and Vanicek (2009) pour plus de détail.

1.1 Introduction

Le calcul du géoïde par la méthode de Stokes consiste à déterminer la solution d'un problème aux valeurs limites, le géoïde étant la surface frontière, à partir des observations de pesanteur sur la surface topographique de la terre. Ainsi satisfaire la condition aux limites nécessite de prolonger l'anomalie de pesanteur vers le bas sur le géoïde (solution du problème inverse de Dirichlet). La condition d'harmonicité du potentiel de pesanteur ou de ses dérivées devant être respectée lors du prolongement vers le bas, il y a lieu d'effectuer plusieurs corrections sur l'observation de pesanteur relative aux masses atmosphérique et topographique. Il s'agit là d'un enjeu majeur car l'estimation de ces effets conditionne la précision du modèle de géoïde.

Une manière d'accéder aux effets des masses topographiques consiste à utiliser la stratégie dite ''deuxième méthode de condensation de Helmert'' dans laquelle les masses topographiques sont réduites à une couche mince sur le géoïde (Heiskanen and Moritz, 1987 ; Vanicek and Martinec, 1994). Ainsi, nous transformons les quantités réelles (masses du relief) en quantités nouvelles (masses surfaciques) dans l'espace du modèle appelé ici « Espace de Helmert ». Le nouveau champ d'anomalie peut être ensuite décomposé en ses parties haute et basse fréquence. L'information basse fréquence du géoïde est décrite avec précision par les modèles de potentiel globaux tandis que les composantes à haute fréquence seront calculées localement par la résolution de l'intégrale de Stokes par le noyau sphéroïdal de Stokes modifié (Vanicek and Kleusberg, 1987). Ce schéma de résolution atténue l'erreur associée à la contribution du champ des zones

éloignées présentes sur la zone d'étude même si cette contribution est rigoureusement évaluée à partir des modèles géopotentiels globaux.

L'anomalie de gravité résiduelle haute fréquence est ainsi introduite dans l'intégrale de Stokes afin de calculer le co-géoïde résiduel de Helmert. Enfin, au cours de l'étape ultime, le géoïde est calculé dans l'espace réel en retirant l'effet indirect de la topographie et de l'atmosphère des hauteurs du co-géoïde de Helmert.

Le principe de la méthode de Stokes-Helmert est illustré sur la figure 4.1:

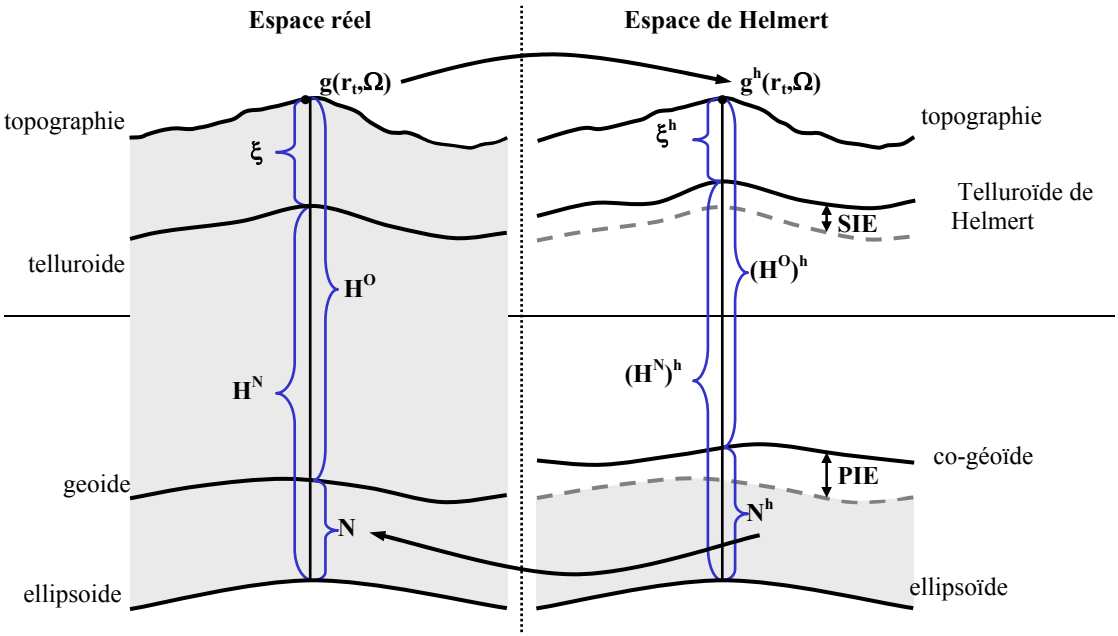

Fig. 4.1 Définition des quantités physiques dans l'espace réel et l'espace de Helmert ;SIE ;PIE. Notez que la condensation de Helmert a comme conséquence de modifier la distribution du potentiel et conduit à la notion de co-géoïde et de telluroïde de Helmert dans l'espace de Helmert (Ellmann et Vanicek, 2007)

1.2 Formule fondamentale de la géodésie physique

1.2.1 Espace réel

Suivant la définition de Gauss (1828) et de Gauss et Listing (1873), le géoïde est construit comme la surface équipotentielle de valeur W_o qui intercepte la pesanteur à angle droit et qui se confond avec le niveau moyen des mers.

Le géoïde est estimé en référence à un champ (champ normal) généré par un ellipsoïde de référence. Le potentiel normal est choisi identique au potentiel sur le géoïde.

L'anomalie de potentiel de pesanteur $T(r_t,\Omega)$, est définie à la surface de la terre par la différence entre le potentiel de pesanteur $W(r_t,\Omega)$ et le potentiel de la pesanteur normale $U(r_t,\Omega)$ du modèle de terre de référence géocentrique et ellipsoïdal (les paramètres physiques du modèle sont U_o, ω_o,et GM_o pour une terre réelle de paramètres W_o, ω, et GM ; où GM est la constante géocentrique gravitationnelle, ω est la vitesse de rotation angulaire moyenne de la terre, $W_o \equiv W(r_g,\Omega)$ est le potentiel de pesanteur sur le géoïde $\forall \Omega \in \Omega_o : r_g(\Omega)$, et $U_o \equiv U(r_o,\phi)$ est le potentiel de pesanteur normale sur la surface de l'ellipsoïde $\forall \Omega \in \Omega_o : r_o(\phi)$, tel que

$$T(r,\Omega) = W(r,\Omega) - U(r,\Omega). \tag{4.1}$$

La position géocentrique du point (r,Ω) est définie par le rayon géocentrique r et la direction géocentrique $\Omega = (\phi,\lambda)$, où ϕ et λ sont les coordonnées géocentriques sphériques, et Ω_o représente l'angle solide total géocentrique $\left[\phi \in \langle -\pi/2, \pi/2\rangle, \lambda \in \langle 0, 2\pi\rangle\right]$. Le rayon géocentrique à la surface terrestre $r_t(\Omega)$ est donné par la somme du rayon géocentrique de la surface géoïdale $r_g(\Omega)$, et de la hauteur orthométrique $H^O(\Omega)$, i.e. $r_t(\Omega) \cong r_g(\Omega) + H^O(\Omega)$

En absence des effets gravimétriques de la topographie et de l'atmosphère, T est harmonique au dessus du géoïde et satisfait à l'équation de Laplace :

$$\nabla^2 T(r,\Omega) = 0 \qquad\qquad r \geq r_g. \tag{4.2}$$

Pour T connu sur le géoïde, La hauteur du géoïde par rapport à l'ellipsoïde de référence est donnée par la formule de Bruns (Bruns, 1878)

$$N(\Omega) = \frac{T(r_g,\Omega)}{\gamma_o(\Omega)}, \tag{4.3}$$

où γ_o est la pesanteur normale sur l'ellipsoïde de référence. Il s'agit maintenant de déterminer T sur et à l'extérieur du géoïde.

Déterminer $T(r,\Omega)$ à l'extérieur du géoïde, nécessite de résoudre le problème aux valeurs limites de 3ème Espèce. Les valeurs de pesanteur sur le géoïde servent alors de valeurs limites.

Afin d'établir une relation entre l'anomalie de potentiel et l'anomalie de pesanteur, on introduit la relation différentielle suivante:

$$\frac{\partial T(r,\Omega)}{\partial r} = \frac{\partial W(r,\Omega)}{\partial r} - \frac{\partial U(r,\Omega)}{\partial r}. \tag{4.4}$$

Cette expression peut être approximée par (Vanicek et al, 1999) :

$$\left.\frac{\partial T(r,\Omega)}{\partial r}\right|_{r=r_t} \cong -g(r_t,\Omega) + \gamma(r_t,\Omega) + \varepsilon_{\delta g}(r_t,\Omega) = -\delta g(r_t,\Omega) + \varepsilon_{\delta g}(r_t,\Omega), \tag{4.5}$$

où $\delta g(r_t,\Omega)$, la perturbation de pesanteur, est la différence entre la pesanteur $g(r_t,\Omega)$ et la pesanteur normale $\gamma(r_t,\Omega)$ et $\varepsilon_{\delta g}(r_t,\Omega)$ est un terme correctif associé au modèle ellipsoïdal.

Au lieu d'utiliser la notion de perturbation de pesanteur, nous transformons cette notion en anomalie de pesanteur, qui recouvre des quantités mesurables. L'anomalie de pesanteur $\Delta g(r_t,\Omega)$:

$$\Delta g(r_t,\Omega) = g(r_t,\Omega) - \gamma\left[r_o(\phi) + H^{\mathrm{N}}(\Omega)\right], \tag{4.6}$$

est reliée à la perturbation de pesanteur $\delta g(r,\Omega)$ par la relation suivante (Vaníček et al., 1999) :

$$\Delta g(r_t,\Omega) = \delta g(r_t,\Omega) + \gamma(r_t,\Omega) - \gamma\left[r_o(\phi) + H^{\mathrm{N}}(\Omega)\right], \tag{4.7}$$

où $H^{\mathrm{N}}(\Omega)$ est la hauteur normale (Molodensky, 1945).

La différence entre la pesanteur normale $\gamma(r_t,\Omega)$ à la surface terrestre et la pesanteur normale $\gamma\left[r_o(\phi) + H^{\mathrm{N}}(\Omega)\right]$ référencée sur le telluroïde $r_o(\phi) + H^{\mathrm{N}}(\Omega)$ peut être exprimée, via la formule de Bruns, par :

$$\gamma(r_t,\Omega) - \gamma\left[r_o(\phi) + H^{\mathrm{N}}(\Omega)\right] \cong \left.\frac{\partial\gamma(r,\phi)}{\partial \mathrm{n}}\right|_{r=r_t(\Omega)} \varsigma(\Omega) = \left.\frac{\partial\gamma(r,\phi)}{\partial \mathrm{n}}\right|_{r=r_t(\Omega)} \frac{T(r_t,\Omega)}{\gamma\left[r_o(\phi) + H^{\mathrm{N}}(\Omega)\right]}, \tag{4.8}$$

où $\varsigma(\Omega)$ est l'anomalie de hauteur (Molodensky et al. ,1960), et $\partial\gamma(r,\phi)/\partial \mathrm{n}$ est le gradient de la pesanteur normale.

Utilisant l'approximation sphérique, l'équation (4.8) devient (Vanicek et Martinec, 1994) :

$$\left.\frac{\partial\gamma\left(r,\phi\right)}{\partial\,\mathrm{n}}\right|_{r=r_t(\Omega)}\frac{T\left(r_t,\Omega\right)}{\gamma\left[r_o\left(\phi\right)+H^{\mathrm{N}}\left(\Omega\right)\right]}=-\frac{2}{r_t\left(\Omega\right)}T\left(r_t,\Omega\right)-\varepsilon_{\mathrm{n}}\left(r_t,\Omega\right), \tag{4.9}$$

$\varepsilon_{\mathrm{n}}\left(r_t,\Omega\right)$ est le terme de correction ellipsoïdale, conséquence de l'approximation sphérique.

Introduisant les équations (4.5) et (4.9) dans l'équation (4.7), l'équation fondamentale de la géodésie physique prend la forme suivante (Vaníček et al.,1999) :

$$\Delta g\left(r_t,\Omega\right)=-\left.\frac{\partial\,T(r,\Omega)}{\partial\,r}\right|_{r=r_t(\Omega)}+\varepsilon_{\delta g}\left(r_t,\Omega\right)-\frac{2}{r_t\left(\Omega\right)}T\left(r_t,\Omega\right)-\varepsilon_{\mathrm{n}}\left(r_t,\Omega\right). \tag{4.10}$$

1.2.2 L'espace de Helmert

On remarque que T dans l'équation (4.1) ne satisfait pas à l'équation de Laplace lorsque le géoïde est situé à l'intérieur des masses topographiques. Etablir des propriétés d'harmonicité pour le potentiel perturbateur nécessite de "supprimer ou déplacer mathématiquement" les masses atmosphérique et topographique. Cette opération peut être réalisée par la deuxième méthode de condensation de Helmert.

Celle-ci permet la condensation des masses sur le géoïde, provoquant ainsi une légère modification du champ de pesanteur. L'espace ainsi obtenu est appelé « espace de Helmert » dont les quantités physiques seront dénotées par l'indice h .

Le potentiel de pesanteur de Helmert est alors donné par:

$$W^h\left(r,\Omega\right)=W\left(r,\Omega\right)-\delta V^t\left(r,\Omega\right)-\delta V^a\left(r,\Omega\right), \tag{4.11}$$

où $\delta V^t\left(r,\Omega\right)$ est le potentiel résiduel topographique, différence entre le potentiel des masses topographiques et le potentiel de la couche condensée

$$\delta V^t\left(r,\Omega\right)=V^t\left(r,\Omega\right)-V^c\left(r,\Omega\right). \tag{4.12}$$

De même, le potentiel résiduel atmosphérique $\delta V^a\left(r,\Omega\right)$ est calculé en ôtant le potentiel de la couche condensée atmosphérique au potentiel des masses atmosphériques, soit :

$$\delta V^a\left(r,\Omega\right)=V^a\left(r,\Omega\right)-V^{ca}\left(r,\Omega\right). \tag{4.13}$$

Ainsi, la perturbation de potentiel devient:

$$T^h\left(r,\Omega\right)=W^h\left(r,\Omega\right)-U\left(r,\Omega\right)=T\left(r,\Omega\right)-\delta V^t\left(r,\Omega\right)-\delta V^a\left(r,\Omega\right). \tag{4.14}$$

Vanicek et Martinec (1994) ont montré que la perturbation de potentiel de Helmert est harmonique en tout point à l'extérieur du géoïde; soit:

$$\nabla^2 T^h\left(r,\Omega\right)=0 \qquad\qquad r\geq r_g \tag{4.15}$$

De plus, la pesanteur de Helmert $g^h\left(r_t,\Omega\right)$ est obtenue à la surface de la terre à partir de la pesanteur observée g au même endroit, en ajoutant deux termes dits « effets topographique (ETD) et atmosphérique directs (EAD) », respectivement $\delta A^t\left(r_t,\Omega\right)$ et $\delta A^a\left(r_t,\Omega\right)$:

$$g^h\left(r_t,\Omega\right)=g\left(r_t,\Omega\right)+\delta A^t\left(r_t,\Omega\right)+\delta A^a\left(r_t,\Omega\right). \tag{4.16}$$

Les termes ETD et EAD sont des quantités résiduelles exprimant en surface la différence entre l'effet de gravité des masses topographique et atmosphérique et l'effet des masses condensées. ETD et EAD sont exprimés par les dérivées radiales des potentiels, soit:

$$\delta A^t\left(r_t,\Omega\right)=\frac{\partial \delta V^t\left(r_t,\Omega\right)}{\partial r}=\frac{\partial V^t\left(r_t,\Omega\right)}{\partial r}-\frac{\partial V^c\left(r_t,\Omega\right)}{\partial r}=A^t\left(r_t,\Omega\right)-A^c\left(r_t,\Omega\right), \tag{4.17a}$$

$$\delta A^a\left(r_t,\Omega\right)=\frac{\partial \delta V^a\left(r_t,\Omega\right)}{\partial r}=\frac{\partial V^a\left(r_t,\Omega\right)}{\partial r}-\frac{\partial V^{ca}\left(r_t,\Omega\right)}{\partial r}=A^a\left(r_t,\Omega\right)-A^{ca}\left(r_t,\Omega\right). \tag{4.17b}$$

Nous reviendrons ultérieurement en détail sur les estimations de $\delta A^t\left(r_t,\Omega\right)$ et $\delta A^a\left(r_t,\Omega\right)$.

Par analogie avec l'équation (4.5) la perturbation de gravité de Helmert est définie comme le gradient négatif du potentiel perturbateur de Helmert auquel on ajoute la correction ellipsoïdale, soit:

$$\delta g^h\left(r_t,\Omega\right)=-\frac{\partial T^h\left(r_t,\Omega\right)}{\partial r}+\varepsilon_{\delta g}\left(r_t,\Omega\right)=g\left(r_t,\Omega\right)-\gamma\left(r_t,\Omega\right)+\varepsilon_{\delta g}\left(r_t,\Omega\right)+\delta A^t\left(r_t,\Omega\right)+\delta A^a\left(r_t,\Omega\right) \tag{4.18}$$

A partir de l'équation (4.10), l'anomalie de pesanteur de Helmert $\Delta g^h\left(r_t,\Omega\right)$ peut être exprimée par :

$$\Delta g^h\left(r_t,\Omega\right)=-\left.\frac{\partial\, T^h(r,\Omega)}{\partial\, r}\right|_{r=r_t(\Omega)}+\varepsilon_{\delta g}\left(r_t,\Omega\right)+\left.\frac{\partial\gamma(r,\Omega)}{r_t\left(\Omega\right)}\right|_{r=r_t(\Omega)}\frac{T^h\left(r_t,\Omega\right)}{\gamma(r+H^o,\Omega)} \tag{4.19}$$

Prenant en compte les équations (4.8), (4.14) et (4.18) on aboutit à la relation suivante (cf. Vanicek et al 1999, Eq. 37) :

$$\begin{aligned}
&\Delta g^h(r_t,\Omega)=\delta g^h(r_t,\Omega)+\gamma(r_t,\Omega)-\gamma\left[r_o(\phi)+H^{\mathrm{N}}(\Omega)\right]-\left.\frac{\partial\gamma(r,\phi)}{\partial \mathrm{n}}\right|_{r=r_t(\Omega)}\frac{T(r_t,\Omega)}{\gamma\left[r_o(\phi)+H^{\mathrm{N}}(\Omega)\right]}+\\
&+\left.\frac{\partial\gamma(r,\phi)}{\partial \mathrm{n}}\right|_{r=r_t(\Omega)}\frac{T^h(r_t,\Omega)}{\gamma\left[r_o(\phi)+H^{\mathrm{N}}(\Omega)\right]}=\\
&=\delta g^h(r_t,\Omega)+\gamma(r_t,\Omega)-\gamma\left[r_o(\phi)+H^{\mathrm{N}}(\Omega)\right]-\left.\frac{\partial\gamma(r,\phi)}{\partial \mathrm{n}}\right|_{r=r_t(\Omega)}\frac{\left[\delta V^t(r_t,\Omega)+\delta V^a(r_t,\Omega)\right]}{\gamma\left[r_o(\phi)+H^{\mathrm{N}}(\Omega)\right]}=\\
&=g(r_t,\Omega)+\varepsilon_{\delta g}(r_t,\Omega)+\delta A^t(r_t,\Omega)+\delta A^a(r_t,\Omega)-\gamma\left[r_o(\phi)+H^{\mathrm{N}}(\Omega)\right]-\left.\frac{\partial\gamma(r,\phi)}{\partial \mathrm{n}}\right|_{r=r_t(\Omega)}\frac{\left[\delta V^t(r_t,\Omega)+\delta V^a(r_t,\Omega)\right]}{\gamma\left[r_o(\phi)+H^{\mathrm{N}}(\Omega)\right]}
\end{aligned} \tag{4.20}$$

L'anomalie de Helmert est exprimée habituellement via l'anomalie à l'air libre $\Delta g^{FA}(r_t,\Omega)$ (voir Heiskanen et Moritz, 1967), tel que:

$$\Delta g^{FA}(r,\Omega)=g(r,\Omega)-\gamma(r_o,\phi)-\frac{\partial\gamma(r,\Omega)}{\partial n}H^{\mathrm{o}}(\Omega)\approx g(r,\Omega)-\gamma(r_o,\phi)-0.3086H^{\mathrm{o}}(\Omega) \tag{4.21}$$

Dans le cas de l'approximation sphérique, on a alors :

$$\Delta g^h(r_t,\Omega)=\Delta g^{FA}(r_t,\Omega)+\delta A^t(r_t,\Omega)+\delta A^a(r_t,\Omega)+\varepsilon_{\delta g}(r_t,\Omega)+\frac{2}{r_t}\delta V^t(r_t,\Omega)+\frac{2}{r_t}\delta V^a(r_t,\Omega)-\varepsilon_n(r_t,\Omega) \tag{4.22}$$

D'un point de vue pratique, l'effet indirect atmosphérique (6ème terme) est négligé.

1.2.3 La correction Géoïde/quasi-Géoïde

L'utilisation des hauteurs orthométriques de Helmert dans l'équation (4.21) au lieu des hauteurs normales nécessite l'application d'une correction géoïde/quasi-géoïde aux conditions aux limites établies dans l'espace de Helmert (Vanicek et al, 1999). Cette correction est décrite comme une fonction de l'anomalie de Bouguer simple $\Delta g^B(r_t,\Omega)$. En effet Heiskanen et Moritz (1967) ont montré que

$$H^{\mathrm{N}}(\Omega)-H^{\mathrm{O}}(\Omega)\cong H^{\mathrm{O}}(\Omega)\frac{\Delta g^{\mathrm{SB}}(r_t(\Omega))}{\gamma_o(\phi)}, \tag{4.23}$$

où $\gamma_o(\phi)$ est la pesanteur normale sur la surface ellipsoïdale et $\Delta g^{\mathrm{SB}}(r_t(\Omega))$ l'anomalie de Bouguer simple définie par (Heilmann et Moritz, 1967)

$$\Delta g^{\mathrm{SB}}(r_t(\Omega))=g(r_t(\Omega))-\gamma\left[r_o(\phi)+H^{\mathrm{O}}(\Omega)\right]-2\pi\mathrm{G}\rho_{\mathrm{o}}H^{\mathrm{O}}(\Omega), \tag{4.24}$$

Le troisième terme décrit l'effet de gravité du plateau infini de Bouguer de masse volumique ρ_o et d'épaisseur $H^{O}(\Omega)$.

Ainsi, la correction de géoïde/quasi-géoïde s'exprime par la fonction

$$\chi(r_t(\Omega)) \cong -\frac{1}{\gamma_o(\Omega)} \frac{\partial \gamma(r,\Omega)}{\partial \, \mathrm{n}}\bigg|_{r=r_o(\Omega)} H^{O}(\Omega)\, \Delta g^{SB}(r_t(\Omega)) \approx \frac{2}{r_t(\Omega)} H^{O}(\Omega)\, \Delta g^{SB}(r_t(\Omega)) \tag{4.25}$$

Munie de cette correction et de l'équation (4.22), l'anomalie de pesanteur de Helmert est définie par :

$$\Delta g^{h}(r_t,\Omega) = \Delta g^{FA}(r_t,\Omega) + \delta A^{t}(r_t,\Omega) + \delta A^{a}(r_t,\Omega) + \varepsilon_{\delta g} + \frac{2}{r_t}\delta V^{t}(r_t,\Omega) + \frac{2}{r_t}\delta V^{a}(r_t,\Omega) - \varepsilon_n + \chi(r_t,\Omega) \tag{4.26}$$

La résolution ultérieure de l'équation intégrale de Stokes nécessite le prolongement vers le bas de l'anomalie de pesanteur de Helmert sur le géoïde. Le champ de pesanteur externe doit être harmonique. Vanicek et Martinec (1994) ont montré que le produit $\Delta g^{h} \cdot r$ est harmonique dans l'espace de Helmert.

Par ailleurs, Wong (2001) a démontré que les corrections ellipsoïdales sont aussi harmoniques. De plus, si la forme ellipsoïdale est une fonction harmonique alors il en va de même pour la forme sphéroïdale et le prolongement vers le bas peut être réalisé avec l'anomalie de Helmert sphéroïdale sans considérer les corrections ellipsoïdales $\varepsilon_{\delta g}$ et ε_n.

1.3. Le traitement des effets atmosphériques

L'évaluation de l'anomalie de Helmert $\Delta g^{h}(r_t,\Omega)$ donnée par l'équation (4.22) nécessite de calculer les effets directs et indirects atmosphériques et topographiques à la surface de la terre.

Suivant l'équation (4.13) le potentiel gravitationnel résiduel $\delta V^{a}(r_t,\Omega)$ représente la différence du potentiel $V^{a}(r_t,\Omega)$ des masses atmosphériques et le potentiel $V^{ca}(r_t,\Omega)$ des masses atmosphériques condensées.

Considérant une distribution radiale de la densité atmosphérique $\rho^{a}(r)$ et pour une approximation sphérique du géoïde ($r_g(\Omega) \approx \mathrm{R}$, avec $\mathrm{R} = \sqrt[3]{\mathrm{a}^2\,\mathrm{b}}$ le rayon moyen de la terre (Bomford, 1971), le potentiel gravitationnel $V^{a}(r_t,\Omega)$ s'écrit:

$$V^{a}(r_t,\Omega) = \mathrm{G} \iint_{\Omega' \in \Omega_{\mathrm{O}}} \int_{r'=\mathrm{R}+H^{O}(\Omega')}^{r_{\mathrm{lim}}} \rho^{a}(r')\, l^{-1}\left[r_t(\Omega), \psi(\Omega,\Omega'), r'\right] r'^{2}\, \mathrm{d}r'\, \mathrm{d}\Omega' , \tag{4.27}$$

où r_{lim} est la limite supérieure de l'atmosphère, $l\left[r,\psi(\Omega,\Omega'),r'\right]$ représente la distance entre le point d'observation (r,Ω) et les points de l'atmosphère (r',Ω') avec

$$\forall\ \Omega,\Omega'\in\Omega_O,\ r,r'\in\Re^+:\qquad l\left[r,\psi(\Omega,\Omega'),r'\right]=\sqrt{r^2+r'^2-2r\,r'\cos\psi(\Omega,\Omega')}\,, \tag{4.28}$$

Sachant que la distance sphérique $\psi(\Omega,\Omega')$ est donnée par:

$$\forall\ \psi\in\langle 0,\pi\rangle:\qquad \cos\psi(\Omega,\Omega')=\sin\phi'\sin\phi+\cos\phi'\cos\phi\cos(\lambda'-\lambda)\,. \tag{4.29}$$

Formellement, les masses atmosphériques peuvent être séparées en deux enveloppes sphériques : la première entre la limite supérieure de la topographie

($\forall\ \Omega\in\Omega_O : R+H_{lim}\,;\, H_{lim}=\max H^O(\Omega)$), et la limite supérieure de l'atmosphère (~ 50 km) ; le deuxième terme est situé entre la topographie et la limite supérieure de la topographie.

Alors $V^a(r,\Omega)$ est exprimé par

$$V^a\left(r_t,\Omega\right)=G\iint_{\Omega'\in\Omega_O}\int_{r'=R+H^O(\Omega')}^{R+H_{lim}}\rho^a\left(r'\right)l^{-1}\left[r_t\left(\Omega\right),\psi\left(\Omega,\Omega'\right),r'\right]r'^2\ dr'\,d\Omega'$$

$$+G\iint_{\Omega'\in\Omega_O}\int_{r'=R+H_{lim}}^{r_{lim}}\rho^a\left(r'\right)l^{-1}\left[r_t\left(\Omega\right),\psi\left(\Omega,\Omega'\right),r'\right]r'^2\ dr'\,d\Omega'\,. \tag{4.30}$$

Le potentiel de gravité des masses atmosphériques condensées $V^{ca}\left(r_t,\Omega\right)$ à la surface de la terre s'exprime par

$$V^{ca}\left(r_t,\Omega\right)=G\,R^2\iint_{\Omega'\in\Omega_O}\sigma^a\left(\Omega'\right)l^{-1}\left[r_t,\psi\left(\Omega,\Omega'\right),R\right]d\Omega'\,, \tag{4.31}$$

où $\sigma^a(\Omega)$ est la densité surfacique des masses surfaciques condensées.

Suivant le principe de la conservation de la masse, la densité surfacique $\sigma^a(\Omega)$ peut être définie par

$$\sigma^a(\Omega)=\frac{1}{R^2}\int_{r=R+H^O(\Omega)}^{r_{lim}}\rho^a\left(r\right)r^2\ dr\,. \tag{4.32}$$

Introduisant (4.32) dans (4.31), le potentiel gravitationnel $V^{ca}\left(r_t,\Omega\right)$ s'écrit:

$$V^{ca}\left(r_t,\Omega\right)=G\iint_{\Omega'\in\Omega_O}\int_{r'=R+H^O(\Omega')}^{r_{lim}}\rho^a\left(r'\right)r'^2\ dr'\,l^{-1}\left[r_t,\psi\left(\Omega,\Omega'\right),R\right]d\Omega'\,. \tag{4.33}$$

En fait, la densité surfacique atmosphérique $\sigma^a(\Omega)$ est formulée différemment en introduisant le modèle à deux couches défini ci-dessus, soit :

$$\sigma^a(\Omega)=\frac{1}{\mathrm{R}^2}\int_{r=\mathrm{R}+H^{\mathrm{O}}(\Omega)}^{\mathrm{R}+\mathrm{H_{lim}}}\rho^a(r)\,r^2\,\mathrm{d}r+\frac{1}{\mathrm{R}^2}\int_{r=\mathrm{R}+\mathrm{H_{lim}}}^{r_{\mathrm{lim}}}\rho^a(r)\,r^2\,\mathrm{d}r\,, \tag{4.34}$$

Le potentiel de gravité $V^{ca}(\mathrm{R},\Omega)$ devient alors:

$$V^{ca}(r_t,\Omega)=\mathrm{G}\iint_{\Omega'\in\Omega_{\mathrm{O}}}\int_{r'=\mathrm{R}+H^{\mathrm{O}}(\Omega')}^{\mathrm{R}+\mathrm{H_{lim}}}\rho^a(r')\,r'^2\,\mathrm{d}r'\,l^{-1}\left[r,\psi(\Omega,\Omega'),\mathrm{R}\right]\mathrm{d}\Omega'$$

$$+\mathrm{G}\iint_{\Omega'\in\Omega_{\mathrm{O}}}\int_{r'=\mathrm{R}+\mathrm{H_{lim}}}^{r_{\mathrm{lim}}}\rho^a(r')\,r'^2\,\mathrm{d}r'\,l^{-1}\left[r,\psi(\Omega,\Omega'),\mathrm{R}\right]\mathrm{d}\Omega'\,. \tag{4.35}$$

La combinaison de (4.30) et (4.35) permet le calcul de l'effet atmosphérique secondaire $\frac{2}{r_t}\delta V^a(r_t,\Omega)$. Cependant, cet effet est d'amplitude faible et sera négligé dans les calculs.

L'attraction de l'enveloppe atmosphérique supérieure est nulle pour un point intérieur tel que $r<\mathrm{R}+\mathrm{H_{lim}}$ (Mac Millan, 1930)

$$\mathrm{G}\iint_{\Omega'\in\Omega_{\mathrm{O}}}\int_{r'=\mathrm{R}+\mathrm{H_{lim}}}^{r_{\mathrm{lim}}}\rho^a(r')\left.\frac{\partial\,l^{-1}\left[r,\psi(\Omega,\Omega'),r'\right]}{\partial\,r}\right|_{r<\mathrm{R}+\mathrm{H_{lim}}}r'^2\,\mathrm{d}r'\,\mathrm{d}\Omega'=0\,. \tag{4.36}$$

Ainsi, l'effet de gravité direct atmosphérique n'est rien d'autre que la dérivée radiale du potentiel de « l'enveloppe rugueuse » atmosphérique soit (Novák, 2000)

$$\left.\frac{\partial V^a(r,\Omega)}{\partial\,r}\right|_{r=r_t(\Omega)}=\mathrm{G}\iint_{\Omega'\in\Omega_{\mathrm{O}}}\int_{r'=\mathrm{R}+H^{\mathrm{O}}(\Omega')}^{\mathrm{R}+\mathrm{H_{lim}}}\rho^a(r')\left.\frac{\partial\,l^{-1}\left[r,\psi(\Omega,\Omega'),r'\right]}{\partial\,r}\right|_{r=r_t(\Omega)}r'^2\,\mathrm{d}r'\,\mathrm{d}\Omega' \tag{4.37}$$

avec la dérivée radiale de l^{-1} qui s'écrit (Martinec, 1998)

$$\left.\frac{\partial\,l^{-1}\left[r,\psi(\Omega,\Omega'),r'\right]}{\partial\,r}\right|_{r=r_t(\Omega)}=-\frac{r_t(\Omega)-r'\cos\psi(\Omega,\Omega')}{l^3\left[r_t(\Omega),\psi(\Omega,\Omega'),r'\right]}\,. \tag{4.38}$$

Il est aisé de formuler l'attraction créée par les masses atmosphériques condensées

$$-\left.\frac{\partial V^{ca}(r,\Omega)}{\partial\,r}\right|_{r=r_t}=-\mathrm{G}\iint_{\Omega'\in\Omega_{\mathrm{O}}}\int_{r'=\mathrm{R}+H^{\mathrm{O}}(\Omega')}^{\mathrm{R}+\mathrm{H_{lim}}}\rho^a(r')\,r'^2\,\mathrm{d}r'\left.\frac{\partial\,l^{-1}\left[r,\psi(\Omega,\Omega'),\mathrm{R}\right]}{\partial\,r}\right|_r\mathrm{d}\Omega'$$

$$-\mathrm{G}\iint_{\Omega'\in\Omega_{\mathrm{O}}}\int_{r'=\mathrm{R}+\mathrm{H_{lim}}}^{r_{\mathrm{lim}}}\rho^a(r')\,r'^2\,\mathrm{d}r'\left.\frac{\partial\,l^{-1}\left[r,\psi(\Omega,\Omega'),\mathrm{R}\right]}{\partial\,r}\right|_r\mathrm{d}\Omega'\,. \tag{4.39}$$

Considérant que l'effet de gravité de la couche sphérique condensée de densité $\sigma^a(\Omega)$ est constant pour un point au dessus de la couche (i.e. $r>R$) (Mac Millan, 1930), alors

$$\mathrm{G}\iint_{\Omega'\in\Omega_\mathrm{O}}\int_{r'=\mathrm{R}+\mathrm{H}_{\mathrm{lim}}}^{\mathrm{r}_{\mathrm{lim}}}\rho^a\left(r'\right)r'^2\,\mathrm{d}r'\left.\frac{\partial l^{-1}\left[r,\psi\left(\Omega,\Omega'\right),\mathrm{R}\right]}{\partial r}\right|_r\mathrm{d}\Omega'=-4\pi\frac{R^2}{r^2}\int_{r'=\mathrm{R}+\mathrm{H}_{\mathrm{lim}}}^{\mathrm{r}_{\mathrm{lim}}}\rho^a\left(r'\right)r'^2\,\mathrm{d}r' \tag{4.40}$$

L'expression finale de l'effet direct atmosphérique devient

$$\left.\frac{\partial\delta V^a\left(r,\Omega\right)}{\partial r}\right|_{r=r_t(\Omega)}=\mathrm{G}\iint_{\Omega'\in\Omega_\mathrm{O}}\int_{r'=\mathrm{R}+H^{\mathrm{O}}(\Omega')}^{\mathrm{R}+\mathrm{H}_{\mathrm{lim}}}\rho^a\left(r'\right)\left.\frac{\partial l^{-1}\left[r,\psi\left(\Omega,\Omega'\right),r'\right]}{\partial r}\right|_{r=r_t(\Omega)}r'^2\,\mathrm{d}r'\,\mathrm{d}\Omega'+$$

$$+4\pi\frac{R^2}{r^2}\int_{r'=\mathrm{R}+\mathrm{H}_{\mathrm{lim}}}^{\mathrm{r}_{\mathrm{lim}}}\rho^a\left(r'\right)r'^2\,\mathrm{d}r'-\mathrm{G}\iint_{\Omega'\in\Omega_\mathrm{O}}\int_{r'=\mathrm{R}+H^{\mathrm{O}}(\Omega')}^{\mathrm{R}+\mathrm{H}_{\mathrm{lim}}}\rho^a\left(r'\right)r'^2\,\mathrm{d}r'\left.\frac{\partial l^{-1}\left[r,\psi\left(\Omega,\Omega'\right),\mathrm{R}\right]}{\partial r}\right|_{rr=r_t(\Omega)}\mathrm{d}\Omega' \tag{4.41}.$$

Une approche alternative peut être développée pour le calcul de l'effet direct de l'atmosphère. L'Association Internationale de Géodésie (IAG) recommande de corriger directement l'effet des masses atmosphériques sur l'anomalie de gravité au point de mesure (Moritz 1992). Cette méthode considère exclusivement l'effet direct (soit +0.87 mGal au maximum au niveau de la mer).

1.3.1. Traitement des effets topographiques

Rappelons que le potentiel et l'attraction de gravité de la topographie condensée sont évalués sur la surface terrestre. Suivant l'intégration classique de Newton on peut écrire

$$V^t\left(r_t,\Omega\right)=\mathrm{G}\iint_{\Omega'\in\Omega_\mathrm{O}}\int_{r'=\mathrm{R}}^{\mathrm{R}+H^{\mathrm{O}}(\Omega')}\rho\left(\Omega'\right)l^{-1}\left[r_t\left(\Omega\right),\psi\left(\Omega,\Omega'\right),r'\right]r'^2\,\mathrm{d}r'\,\mathrm{d}\Omega' \tag{4.42}$$

L'intégrale selon r de $l^{-1}\left[r_t\left(\Omega\right),\psi\left(\Omega,\Omega'\right),r'\right]\mathrm{r}'^2$ peut être exprimée par la forme analytique suivante (Gradstein et Ryzhik, 1980, voir aussi Martinec 1993)

$$\int_{r'=R}^{R+H^o(\Omega')}l^{-1}\left[r\left(\Omega\right),\psi\left(\Omega,\Omega'\right),r'\right]r'^2dr'=\left|\frac{1}{2}\left[r'+3r\cos\psi\left(\Omega,\Omega'\right)\right]l\left[r\left(\Omega\right),\psi\left(\Omega,\Omega'\right),r'\right]+\right.$$

$$\left.\frac{r^2}{2}\left(3\cos^2\psi\left(\Omega,\Omega'\right)-1\right)\ln\left|r'-r\cos\psi\left(\Omega,\Omega'\right)+l\left[r\left(\Omega\right),\psi\left(\Omega,\Omega'\right),r'\right]\right|\right|_{r'=R}^{R+H^o(\Omega')} \tag{4.43}$$

Alternativement, on sait que l'effet des masses topographiques peut être décomposé en un terme d'enveloppe sphérique et un terme traduisant la « rugosité » de la surface terrestre. Cette approche est introduite pour éliminer les singularités au voisinage des points lors de l'intégration.

Le potentiel de gravité $V^t\left(r_t,\Omega\right)$ présent dans l'effet topographique indirect (5ème terme de l'équation 3.22) a pour expression (Martinec et Vaníček, 1994b; Martinec, 1998)

$$V^t\left(r_t,\Omega\right)=4\pi\,\mathrm{G}\,\rho_{\mathrm{o}}\,\frac{\mathrm{R}^2}{r_t\left(\Omega\right)}H^{\mathrm{O}}\left(\Omega\right)\left[1+\frac{H^{\mathrm{O}}\left(\Omega\right)}{\mathrm{R}}+\frac{1}{3}\left(\frac{H^{\mathrm{O}}\left(\Omega\right)}{\mathrm{R}}\right)^2\right]$$

$$+\mathrm{G}\,\rho_{\mathrm{o}}\iint\limits_{\Omega'\in\Omega_{\mathrm{O}}}\int_{r'=\mathrm{R}+H^{\mathrm{O}}(\Omega)}^{\mathrm{R}+H^{\mathrm{O}}(\Omega')}l^{-1}\left[r_t\left(\Omega\right),\psi\left(\Omega,\Omega'\right),r'\right]r'^2\,\mathrm{d}r'\,\mathrm{d}\Omega'$$

$$+\mathrm{G}\iint\limits_{\Omega'\in\Omega_{\mathrm{O}}}\delta\rho\left(\Omega'\right)\int_{r'=\mathrm{R}}^{\mathrm{R}+H^{\mathrm{O}}(\Omega')}l^{-1}\left[r_t\left(\Omega\right),\psi\left(\Omega,\Omega'\right),r'\right]r'^2\,\mathrm{d}r'\,\mathrm{d}\Omega'\,. \qquad (4.44)$$

résultant de la contribution 1) de l'enveloppe sphérique de densité moyenne ρ_{o} et d'épaisseur égale à la hauteur orthométrique $H^{\mathrm{O}}\left(\Omega\right)$ au point$\left(r,\Omega\right)$) calculé (voir Wichiencharoen, 1982) de la rugosité de la topographie et 2) des hétérogénéités de densité $\delta\rho\left(\Omega\right)$ dans le relief.

Ce formalisme est étendu à l'expression de l'effet de gravité de la topographie, soit (Martinec et Vaníček, 1994a; Martinec, 1998)

$$\left.\frac{\partial V^t\left(r,\Omega\right)}{\partial\, r}\right|_{r=r_t(\Omega)}=-4\pi\,\mathrm{G}\,\rho_{\mathrm{o}}\,\frac{\mathrm{R}^2}{r_t^2\left(\Omega\right)}H^{\mathrm{O}}\left(\Omega\right)\left[1+\frac{H^{\mathrm{O}}\left(\Omega\right)}{\mathrm{R}}+\frac{1}{3}\left(\frac{H^{\mathrm{O}}\left(\Omega\right)}{\mathrm{R}}\right)^2\right]$$

$$+\mathrm{G}\,\rho_{\mathrm{o}}\iint\limits_{\Omega'\in\Omega_{\mathrm{O}}}\int_{r'=\mathrm{R}+H^{\mathrm{O}}(\Omega)}^{\mathrm{R}+H^{\mathrm{O}}(\Omega')}\left.\frac{\partial\, l^{-1}\left[r,\psi\left(\Omega,\Omega'\right),r'\right]}{\partial\, r}\right|_{r=r_t(\Omega)}r'^2\,\mathrm{d}r'\,\mathrm{d}\Omega'$$

$$+\mathrm{G}\iint\limits_{\Omega'\in\Omega_{\mathrm{O}}}\delta\rho\left(\Omega'\right)\int_{r'=\mathrm{R}}^{\mathrm{R}+H^{\mathrm{O}}(\Omega')}\left.\frac{\partial\, l^{-1}\left[r,\psi\left(\Omega,\Omega'\right),r'\right]}{\partial\, r}\right|_{r=r_t(\Omega)}r'^2\,\mathrm{d}r'\,\mathrm{d}\Omega'\,. \qquad (4.45)$$

L'origine des termes est identique à celle des termes de l'équation (4.44) du potentiel.

La décomposition précédente est aussi appliquée au potentiel $V^{ct}\left(r_t,\Omega\right)$ des masses topographiques condensées.

Ce potentiel est donné par (Martinec, 1998)

$$V^{ct}\left(r_t,\Omega\right)=\mathrm{G}\,\mathrm{R}^2\iint\limits_{\Omega'\in\Omega_{\mathrm{O}}}\sigma\left(\Omega'\right)l^{-1}\left[r_t,\psi\left(\Omega,\Omega'\right),\mathrm{R}\right]\mathrm{d}\Omega'\,, \qquad (4.46)$$

où $\sigma\left(\Omega\right)$ est la densité surfacique avec

$$\sigma\left(\Omega\right)=\frac{\rho\left(\Omega\right)}{\mathrm{R}^2}\int_{r=\mathrm{R}}^{\mathrm{R}+H^{\mathrm{O}}(\Omega)}r^2\,\mathrm{d}r=\rho\left(\Omega\right)\frac{r_t^3\left(\Omega\right)-\mathrm{R}^3}{3\mathrm{R}^2}=$$

$$= \rho(\Omega) H^{O}(\Omega) \left[1 + \frac{H^{O}(\Omega)}{R} + \frac{1}{3} \left(\frac{H^{O}(\Omega)}{R} \right)^{2} \right]. \qquad (4.47)$$

Ainsi, $V^{ct}(R,\Omega)$ peut être exprimé par

$$V^{ct}(r_t,\Omega) = 4\pi G \rho_o \frac{R^2}{r_t(\Omega)} H^{0}(\Omega) + G\rho_o \iint_{\Omega' \in \Omega_O} \frac{r^3(\Omega') - r^3(\Omega)}{3} l^{-1}\left[r_t, \psi(\Omega,\Omega'), R \right] d\Omega' \qquad (4.48)$$

Les termes de droite représentant successivement les potentiels de gravité de l'enveloppe sphérique d'épaisseur $H^{0}(\Omega)$, de la partie rugueuse des masses topographiques et des anomalies de densité de la topographie condensée

L'attraction des masses topographiques condensées se déduit aisément des expressions précédentes. Partant de $V^{ct}(r,\Omega)$, on en déduit que

$$\left. \frac{\partial V^{ct}(r,\Omega)}{\partial r} \right|_{r=r_t} = G R^2 \iint_{\Omega' \in \Omega_O} \sigma(\Omega') \left. \frac{\partial l^{-1}\left[r, \psi(\Omega,\Omega'), R \right]}{\partial r} \right|_{r=r_t} d\Omega'. \qquad (4.49)$$

En utilisant l'équation (4.48) on a

$$\left. \frac{\partial V^{ct}(r,\Omega)}{\partial r} \right|_{r=r_t} = -4\pi G \sigma_o \frac{R^2}{r_t^2(\Omega)} H^{O}(\Omega) + G\rho_o \iint_{\Omega' \in \Omega_O} \frac{r^3(\Omega') - r^3(\Omega)}{3} \left. \frac{\partial l^{-1}\left[r, \psi(\Omega,\Omega'), R \right]}{\partial r +} \right|_{r=r_t} d\Omega' +$$

$$+ G \iint_{\Omega' \in \Omega_O} \delta\rho(\Omega') \frac{r^3(\Omega') - R^3}{3} \left. \frac{\partial l^{-1}\left[r, \psi(\Omega,\Omega'), R \right]}{\partial r} \right|_{r=r_t} d\Omega'. \qquad (4.50)$$

L'effet topographique secondaire indirect $\frac{2}{r_t} \delta V^{t}(r_t,\Omega)$ s'écrit

$$\frac{2}{r_t} \delta V^{t}(r_t,\Omega) = \frac{2}{r_t} \left[V^{t}(r_t,\Omega) - V^{ct}(r_t,\Omega) \right] = \frac{2}{r_t} G \iint_{\Omega' \in \Omega_O} \int_{r'=R}^{R+H^{O}(\Omega')} \rho(\Omega') l^{-1}\left[r_t(\Omega), \psi(\Omega,\Omega'), r' \right] r'^2 \, dr' \, d\Omega' -$$

$$- \frac{2}{r_t} G \iint_{\Omega' \in \Omega_O} \rho(\Omega') \frac{r_t^3(\Omega') - R^3}{3} l^{-1}\left[r_t(\Omega), \psi(\Omega,\Omega'), R \right] d\Omega' \qquad (4.51)$$

Ainsi, l'effet résiduel topographique direct dans l'espace de Helmert est obtenu en ôtant l'effet de la couche condensée à l'attraction des masses topographiques.

Notons que l'enveloppe sphérique de Bouguer intervient de la même façon dans les équations (4.45) et (4.50) et n'intervient pas dans l'effet résiduel direct. On en déduit que

$$\delta A\left(r_t,\Omega\right)=\frac{\partial\left\{V^t\left(r_t,\Omega\right)-V^a\left(r_t,\Omega\right)\right\}}{\partial r}=$$

$$=\mathrm{G}\rho_o\iint_{\Omega'\in\Omega_O}\frac{\partial l^{-1}\left[r,\psi\left(\Omega,\Omega'\right),r'\right]}{\partial r}r'^2\,\mathrm{d}r'\Bigg|_{R+H(\Omega')}^{R+H(\Omega)}\mathrm{d}\Omega'-\mathrm{G}\rho_o\iint_{\Omega'\in\Omega_O}\frac{r_t^3(\Omega)-r^3(\Omega')}{3}\frac{\partial l^{-1}\left[r,\psi\left(\Omega,\Omega'\right),R\right]}{\partial r}\Bigg|_{R+H(\Omega')}\mathrm{d}\Omega'+ \tag{4.52}$$

$$+\mathrm{G}\iint_{\Omega'\in\Omega_O}\delta\rho(\Omega')\frac{\partial l^{-1}\left[r,\psi\left(\Omega,\Omega'\right),r'\right]}{\partial r}r'^2\,\mathrm{d}r'\Bigg|_{R+H(\Omega')}^{R+H(\Omega)}\mathrm{d}\Omega'-\mathrm{G}\iint_{\Omega'\in\Omega_O}\delta\rho(\Omega')\frac{r_t^3(\Omega)-R^3}{3}\frac{\partial l^{-1}\left[r,\psi\left(\Omega,\Omega'\right),R\right]}{\partial r}\Bigg|_{R+H(\Omega')}\mathrm{d}\Omega'$$

Les deux premiers termes se rapportent à la correction sphérique de terrain pour une topographie successivement non condensée et condensée. Les 3ème et 4ème termes relatent aussi des corrections de terrain faisant uniquement intervenir les anomalies de densité non condensées et condensées

1.4. Le problème de Dirichlet's aux valeurs limites et le prolongement vers le bas

L'anomalie de Helmert évaluée sur la surface terrestre (voir les équations (4.22) ou (4.26) doit être prolongée vers le bas sur la surface du géoïde.

Le prolongement vers le bas est résolu par inversion de l'intégrale de Poisson dont la formule est (Kellogg, 1929)

$$\Delta g^{\mathrm{h}}\left(r_t,\Omega\right)=\frac{\mathrm{R}}{4\pi r_t\left(\Omega\right)}\iint_{\Omega'\in\Omega_{\mathrm{O}}}\mathrm{K}\left[r_t\left(\Omega\right),\psi\left(\Omega,\Omega'\right),\mathrm{R}\right]\Delta g^{\mathrm{h}}\left(\mathrm{R},\Omega'\right)\mathrm{d}\Omega', \tag{4.53}$$

où $\mathrm{K}\left[r_t\left(\Omega\right),\psi\left(\Omega,\Omega'\right),\mathrm{R}\right]$ est le noyau de l'intégrale de Poisson en coordonnées sphériques (Sun et Vaníček, 1998)

$$\mathrm{K}\left[r_t\left(\Omega\right),\psi\left(\Omega,\Omega'\right),\mathrm{R}\right]=\sum_{n=0}^{\infty}\left(2n+1\right)\left[\frac{\mathrm{R}}{r_t\left(\Omega\right)}\right]^{n+1}\mathrm{P}_{\mathrm{n}}\left(\cos\psi\left(\Omega,\Omega'\right)\right)=\mathrm{R}\frac{r_t^2\left(\Omega\right)-\mathrm{R}^2}{l^3\left[r_t\left(\Omega\right),\psi\left(\Omega,\Omega'\right),\mathrm{R}\right]} \tag{4.54}$$

et $\mathrm{P}_{\mathrm{n}}\left(\cos\psi\left(\Omega,\Omega'\right)\right)$ les polynômes de Legendre (Hobson, 1931).

La forme discrète de l'équation intégrale de Poisson, dont la forme générique est une équation intégrale de Fredholm de 1ère espèce, peut être exprimée par (Martinec, 1996; Huang, 2002)

$$\mathbf{\Delta g}^h\left(r_t\left(\Omega\right)\right)=\mathbf{K}\left[r_t\left(\Omega\right),\psi\left(\Omega,\Omega'\right),\mathrm{R}\right]\ \mathbf{\Delta g}^h\left(\mathrm{R},\Omega'\right), \tag{4.55}$$

où $\mathbf{\Delta g}^h\left(r_t,\Omega\right)$ est le vecteur "anomalie de gravité à la surface terrestre", $\mathbf{\Delta g}^h\left(\mathrm{R},\Omega'\right)$ est le vecteur "anomalie de gravité sur la surface du géoïde" (approximé par une sphère de référence de rayon R), et

$\mathbf{K}\left[r_t(\Omega),\psi(\Omega,\Omega'),\mathrm{R}\right]$ est la matrice des valeurs du noyau intégrale de Poisson multipliées par le facteur $\mathrm{R}/r_t(\Omega)/4\pi$ et par la taille élémentaire de la surface discrétisée, soit $\Delta\Omega=\Delta\lambda\,\Delta\phi\cos\phi$.

Nous utiliserons l'approche itérative de Jacobi (Ralston, 1965) pour estimer la solution du système d'équations linéaires, en exprimant la matrice $\mathbf{K}\left[r_t(\Omega),\psi(\Omega,\Omega'),\mathrm{R}\right]$ par

$$\mathbf{K}\left[r_t(\Omega),\psi(\Omega,\Omega'),\mathrm{R}\right]=\mathbf{E}-\mathbf{B}\left[r_t(\Omega),\psi(\Omega,\Omega'),\mathrm{R}\right], \tag{4.56}$$

où $\mathbf{E}$ est la matrice unité.

Introduisant (4.56) dans (4.55), on obtient le système d'équations linéaires suivant (Martinec, 1996)

$$\boldsymbol{\Delta}\mathbf{g}^h\left(\mathrm{R},\Omega'\right)=\boldsymbol{\Delta}\mathbf{g}^h\left(r_t(\Omega)\right)+\mathbf{B}\left[r_t(\Omega),\psi(\Omega,\Omega'),\mathrm{R}\right]\ \boldsymbol{\Delta}\mathbf{g}^h\left(\mathrm{R},\Omega'\right) \tag{4.57}$$

Ce système est résolu d'une manière itérative en partant de $\boldsymbol{\Delta}\mathbf{g}^{FA}\left(r_t(\Omega)\right)$ comme solution initiale sur le géoïde, soit

$$\boldsymbol{\Delta}\mathbf{g}^h\left(\mathrm{R},\Omega'\right)\Big|_0=\boldsymbol{\Delta}\mathbf{g}^{FA}(\mathrm{r_t}(\Omega)) \tag{4.58}$$

A l'itération k, $\boldsymbol{\Delta}\mathbf{g}^h\left(\mathrm{R},\Omega'\right)\Big|_k$ est obtenu par l'équation

$$\boldsymbol{\Delta}\mathbf{g}^h\left(\mathrm{R},\Omega'\right)\Big|_k=\mathbf{B}\left[r_t(\Omega),\psi(\Omega,\Omega'),\mathrm{R}\right]\ \boldsymbol{\Delta}\mathbf{g}^h\left(\mathrm{R},\Omega'\right)\Big|_{k-1} \tag{4.59}$$

Lorsque la différence de deux solutions successives $\left|\boldsymbol{\Delta}\mathbf{g}^h\left(\mathrm{R},\Omega'\right)\Big|_k-\boldsymbol{\Delta}\mathbf{g}^h\left(\mathrm{R},\Omega'\right)\Big|_{k-1}\right|$ est plus petite que le seuil de tolérance ε, le processus itératif est arrêté. La solution résultante est alors donnée par

$$\boldsymbol{\Delta}\mathbf{g}^h\left(\mathrm{R},\Omega'\right)=\boldsymbol{\Delta}\mathbf{g}^h\left(r_t(\Omega)\right)+\sum_{k=1}^{\bar{k}}\boldsymbol{\Delta}\mathbf{g}^h\left(\mathrm{R},\Omega'\right)\Big|_k, \tag{4.60}$$

avec $\bar{k}$ le nombre final d'itération.

Le prolongement vers le bas est réputé pour être une opération instable. Ainsi les erreurs sur $\boldsymbol{\Delta}\mathbf{g}^h\left(r_t(\Omega)\right)$ peuvent être amplifiées dans la solution. Le filtrage ou lissage initial des données permet de s'affranchir du bruit "haute fréquence" si nuisible dans le prolongement vers le bas.

1.5. Les corrections ellipsoïdales

Suivant les travaux de Wong (2001), on peut ajouter la correction ellipsoïdale au niveau du géoïde.

Dans ce paragraphe nous nous proposons d'évaluer les anomalies "ellipsoïdales" à partir des anomalies de type sphérique références au niveau du géoïde. Pour cela, on utilise l'expression suivante

$$\begin{aligned} -\frac{\partial T^h(R,\Omega)}{\partial r} - \frac{2}{R}T^h(R,\Omega) &= \Delta g^h(R,\Omega) + \varepsilon_n(R,\Omega) - \varepsilon_{\delta g}(R,\Omega) = \\ &= \Delta g^h(R,\Omega) - \frac{e^2}{R}(3\cos^2\theta - 2)T^h(R,\Omega) + \frac{e^2}{R}\cos\theta\sin\theta\frac{\partial T^h(R,\Omega)}{\partial\theta} \end{aligned} \tag{4.61}$$

où θ est la co-latitude géocentrique et e^2 est l'excentricité de l'ellipsoïde de référence. Le 2ème terme représente la correction ellipsoïdale sur la perturbation de gravité et le dernier terme est la correction ellipsoïdale pour l'approximation sphérique.

Dans l'equation (4.61) le potentiel de perturbation $T\left[r_t(\Omega)\right]$ de Helmert à l'extérieur des masses peut être estimé par un modèle géopotentiels en harmonique sphérique.

$$T^H\left[r_t(\Omega)\right] = \frac{\mathrm{GM}}{r_t(\Omega)}\sum_{n=2}^{\infty}\left[\frac{\mathrm{a}}{r_t(\Omega)}\right]^n\sum_{m=0}^{n}\left[\mathrm{C}^{\mathrm{T}}_{\mathrm{n,m}}\cos m\lambda + \mathrm{S}^{\mathrm{T}}_{\mathrm{n,m}}\sin m\lambda\right]\mathrm{P}_{\mathrm{n,m}}(\sin\phi) \tag{4.62}$$

Il en va de même pour sa dérivée première en introduisant les dérivées des fonctions de Legendre, soit

$$\frac{\partial T^H\left[R,(\Omega)\right]}{\partial\phi} = \frac{\mathrm{GM}}{R(\Omega)}\sum_{n=2}^{\infty}\left[\frac{\mathrm{a}}{R(\Omega)}\right]^n\sum_{m=0}^{n}\left[\mathrm{C}^{\mathrm{T}}_{\mathrm{n,m}}\cos m\lambda + \mathrm{S}^{\mathrm{T}}_{\mathrm{n,m}}\sin m\lambda\right]\frac{\partial\,\mathrm{P}_{\mathrm{n,m}}(\sin\phi)}{\partial\phi} \tag{4.63}$$

Le potentiel de perturbation de Helmert prend en compte la topographie dont la hauteur peut, elle aussi, être décomposée en harmonique.

1.6. Modèles géopotentiels, sphéroïde dans l'espace de Helmert

La résolution du problème de Stokes aux valeurs limites nécessite de connaître les anomalies de gravité sur toute la surface terrestre. Pour limiter les erreurs de troncature dans l'intégration inhérentes aux effets lointains, Les parties hautes et basses fréquences de l'anomalie de Helmert sur la zone d'étude doivent être connues.

Nous considérons que le champ de gravité de degré $\bar{n}$ peut être calculé à partir d'un potentiel de référence $W_{\mathrm{ref}}(r,\Omega)$ défini par

$$\forall\, \Omega \in \Omega_{\mathrm{O}},\, r \geq r_t(\Omega): \qquad W_{\mathrm{ref}}(r,\Omega) = \frac{\mathrm{GM}}{r} - \sum_{n=2}^{\bar{n}} \left(\frac{\mathrm{a_o}}{r}\right)^{n+1} \sum_{m=-n}^{n} \mathrm{W_{n,m}}(\Omega)\, \mathrm{Y_{n,m}}(\Omega), \tag{4.64}$$

où les $\mathrm{W_{n,m}}(\Omega)$ représentent les coefficients géopotentiels du développement harmonique du champ de gravité terrestre , $\mathrm{Y_{n,m}}(\Omega)$ sont les fonctions harmoniques normalisées de degré n et d'ordre m; $\mathrm{a_o}$ est un paramètre arbitraire de longueur (habituellement le grand axe de l'ellipsoïde de référence), et $\bar{n}$ est le degré maximum retenu dans le développement.

Dans l'espace de Helmert, le potentiel de gravité de référence $W^{\mathrm{H}}_{\mathrm{ref}}(r,\Omega)$ s'exprime par

$$\forall\, \Omega \in \Omega_{\mathrm{O}},\, r \in \Re^{+}: \qquad W^{\mathrm{H}}_{\mathrm{ref}}(r,\Omega) = W_{\mathrm{ref}}(r,\Omega) - \delta V^{t}_{\mathrm{ref}}(r,\Omega) - \delta V^{a}_{\mathrm{ref}}(r,\Omega), \tag{4.65}$$

Avec $\delta V^{t}_{\mathrm{ref}}(r,\Omega)$ le potentiel résiduel de gravité des masses topographiques, et $\delta V^{a}_{\mathrm{ref}}(r,\Omega)$ le potentiel résiduel de gravité des masses atmosphériques.

1.6.1 Le potentiel résiduel de gravité de référence pour les masses topographiques

Nous définissons le potentiel résiduel des masses topographiques $\delta V^{t}_{\mathrm{ref}}(r,\Omega)$ comme la différence entre le potentiel de référence des masses topographiques

$$V^{t}_{\mathrm{ref}}(r,\Omega) \approx \mathrm{G}\rho_{\mathrm{o}} \iint_{\Omega' \in \Omega_{\mathrm{O}}} \int_{H'=0}^{H^{\mathrm{O}}(\Omega')} \frac{1}{r} \sum_{n=0}^{\bar{n}} \left(\frac{\mathrm{R}+H'}{r}\right)^{n} \mathrm{P_n}\left(\cos\psi(\Omega,\Omega')\right)(\mathrm{R}+H')^{2}\, \mathrm{d}H'\, \mathrm{d}\Omega', \tag{4.66}$$

et le potentiel de référence des masses condensées $V^{ct}_{\mathrm{ref}}(r,\Omega)$

$$\forall\, \Omega \in \Omega_{\mathrm{O}}, r > \mathrm{R}: \qquad V^{ct}_{\mathrm{ref}}(r,\Omega) \approx \mathrm{G\,R} \iint_{\Omega' \in \Omega_{\mathrm{O}}} \sigma(\Omega') \sum_{n=0}^{\bar{n}} \left(\frac{\mathrm{R}}{r}\right)^{n+1} \mathrm{P_n}\left(\cos\psi(\Omega,\Omega')\right) \mathrm{d}\Omega'. \tag{4.67}$$

dans l'espace tel que $\forall\, \Omega \in \Omega_{\mathrm{O}} : r > \mathrm{R} + \mathrm{H_{lim}}$ à l'extérieur de la sphère de Brillouin (la sphère géocentrique "minimale" contenant toutes les masses terrestres. $V^{t}_{\mathrm{ref}}(r,\Omega)$ peut être exprimée par (Vaníček et al., 1995)

$\forall\, \Omega \in \Omega_{\mathrm{O}}, r > \mathrm{R} + \mathrm{H_{lim}}$:

$$V_{\mathrm{ref}}^{t}(r,\Omega)=\mathrm{G}\rho_{\mathrm{o}}\,\mathrm{R}^{2}\sum_{n=0}^{\bar{n}}\left(\frac{\mathrm{R}}{r}\right)^{n+1}\frac{1}{n+3}\sum_{k=1}^{n+3}\binom{n+3}{k}\iint_{\Omega'\in\Omega_{\mathrm{O}}}\left[\frac{H^{\mathrm{O}}(\Omega')}{\mathrm{R}}\right]^{k}\mathrm{P}_{\mathrm{n}}\left(\cos\psi(\Omega,\Omega')\right)\mathrm{d}\Omega'. \tag{4.68}$$

Ainsi, le potentiel résiduel $\delta V_{\mathrm{ref}}^{t}(r,\Omega)$ des masses topographiques devient (Novák, 2000)

$\forall\,\Omega\in\Omega_{\mathrm{O}}, r>\mathrm{R}+\mathrm{H}_{\mathrm{lim}}$:

$$\delta V_{\mathrm{ref}}^{t}(r,\Omega)\cong\mathrm{G}\,\rho_{\mathrm{o}}\mathrm{R}^{2}\sum_{n=0}^{\bar{n}}\left(\frac{\mathrm{R}}{r}\right)^{n+1}\left\{\frac{1}{n+3}\sum_{k=1}^{n+3}\binom{n+3}{k}\iint_{\Omega'\in\Omega_{\mathrm{O}}}\left[\frac{H^{\mathrm{O}}(\Omega')}{\mathrm{R}}\right]^{k}\mathrm{P}_{\mathrm{n}}\left(\cos\psi(\Omega,\Omega')\right)\mathrm{d}\Omega'\right.$$

$$\left.-\iint_{\Omega'\in\Omega_{\mathrm{O}}}\frac{H^{\mathrm{O}}(\Omega')}{\mathrm{R}}\left[1+\frac{H^{\mathrm{O}}(\Omega')}{\mathrm{R}}+\frac{1}{3}\left(\frac{H^{\mathrm{O}}(\Omega')}{\mathrm{R}}\right)^{2}\right]\mathrm{P}_{\mathrm{n}}\left(\cos\psi(\Omega,\Omega')\right)\mathrm{d}\Omega'\right\}. \tag{4.69}$$

Dans notre cas $H^{\mathrm{O}}(\Omega')<<\mathrm{R}$ et la sommation sur k converge rapidement (Vaníček et al., 1995). Alors, l'équation (4.69) est réécrite sous la forme (Novák, 2000)

$\forall\,\Omega\in\Omega_{\mathrm{O}}, r>\mathrm{R}+\mathrm{H}_{\mathrm{lim}}$:

$$\delta V_{\mathrm{ref}}^{t}(r,\Omega)\cong\mathrm{G}\rho_{\mathrm{o}}\,\mathrm{R}^{2}\sum_{n=1}^{\bar{n}}\frac{n}{2}\left(\frac{\mathrm{R}}{r}\right)^{n+1}\left\{\iint_{\Omega'\in\Omega_{\mathrm{O}}}\frac{\left[H^{\mathrm{O}}(\Omega')\right]^{2}}{\mathrm{R}^{2}}\mathrm{P}_{\mathrm{n}}\left(\cos\psi(\Omega,\Omega')\right)\mathrm{d}\Omega'\right.$$

$$\left.+\frac{n+3}{3}\iint_{\Omega'\in\Omega_{\mathrm{O}}}\frac{\left[H^{\mathrm{O}}(\Omega')\right]^{3}}{\mathrm{R}^{3}}\mathrm{P}_{\mathrm{n}}\left(\cos\psi(\Omega,\Omega')\right)\mathrm{d}\Omega'\right\}. \tag{4.70}$$

En développant la hauteur orthométrique en harmoniques sphériques

$$\sum_{n=0}^{\infty}\iint_{\Omega'\in\Omega_{\mathrm{O}}}H^{\mathrm{O}}(\Omega')\,\mathrm{P}_{\mathrm{n}}\left(\cos\psi(\Omega,\Omega')\right)\mathrm{d}\Omega'=\sum_{n=0}^{\infty}\frac{4\pi}{2n+1}\sum_{m=-n}^{n}\mathrm{H}_{\mathrm{n,m}}(\Omega)\,\mathrm{Y}_{\mathrm{n,m}}(\Omega), \tag{4.71}$$

Le potentiel résiduel $\delta V_{\mathrm{ref}}^{t}(r,\Omega)$ devient (Novák, 2000)

$\forall\,\Omega\in\Omega_{\mathrm{O}}, r>\mathrm{R}+\mathrm{H}_{\mathrm{lim}}$:

$$\delta V_{\mathrm{ref}}^{t}(\Omega)\cong 2\pi\,\mathrm{G}\,\rho_{\mathrm{o}}\sum_{n=1}^{\bar{n}}\frac{n}{2n+1}\left(\frac{\mathrm{R}}{r}\right)^{n+1}\sum_{m=-n}^{n}\mathrm{H}_{\mathrm{n,m}}^{2}(\Omega)\,\mathrm{Y}_{\mathrm{n,m}}(\Omega)$$

$$+\frac{2\pi}{3\mathrm{R}}\mathrm{G}\,\rho_{\mathrm{o}}\sum_{n=1}^{\bar{n}}\frac{n(n+3)}{2n+1}\left(\frac{\mathrm{R}}{r}\right)^{n+1}\sum_{m=-n}^{n}\mathrm{H}_{\mathrm{n,m}}^{3}(\Omega)\,\mathrm{Y}_{\mathrm{n,m}}(\Omega). \tag{4.72}$$

1.6.2 Potentiel résiduel de référence des masses atmosphériques

Nous définissons dans un premier temps le potentiel de référence des masses atmosphériques $V_{\mathrm{ref}}^{a}(r,\Omega)$ sur la base des polynômes de Legendre (Novák, 2000)

$$\forall\, \Omega \in \Omega_{\mathrm{O}},\, r > \mathrm{r_{lim}} : V^{a}_{\mathrm{ref}}(r,\Omega) = \mathrm{G}\sum_{n=0}^{\bar{n}} \frac{1}{r^{n+1}} \iint_{\Omega' \in \Omega_{\mathrm{O}}} \mathrm{P_n}\left(\cos\psi(\Omega,\Omega')\right) \int_{r'=\mathrm{R}+H^{\mathrm{O}}(\Omega')}^{r_{\mathrm{lim}}} \rho(r') r'^{n+2}\, \mathrm{d}r'\, \mathrm{d}\Omega' . \tag{4.73}$$

La densité de l'atmosphère est modélisée par la fonction $\rho^{a}(r)$ (Sjöberg, 1998; Novák, 2000)

$$\forall\, \Omega \in \Omega_{\mathrm{O}}, r \in \left\langle \mathrm{R} + H^{\mathrm{O}}(\Omega),\, \mathrm{r_{lim}} \right\rangle, \nu > 2 \wedge \nu \in \Im^{+} : \quad \rho^{a}(r) = \rho^{\mathrm{a}}_{\mathrm{o}} \left[\frac{\mathrm{R}}{\mathrm{R} + H^{\mathrm{O}}(\Omega)} \right]^{\nu}, \tag{4.74}$$

où $\rho^{\mathrm{a}}_{\mathrm{o}}$ est la densité au niveau de la mer, et $\nu \in \Im^{+}$ ($\Im^{+} = 1, 2, \ldots$) caractérise la distribution radiale.

Sachant que

$$\forall\, \Omega \in \Omega_{\mathrm{O}}, \nu > 2 \wedge \nu \in \Im^{+}, n = 0,2,\ldots,\bar{n} : \int_{r=\mathrm{R}+H^{\mathrm{O}}(\Omega)}^{\mathrm{r_{lim}}} \rho^{a}(r) r^{n+2}\, \mathrm{d}r = \rho^{\mathrm{a}}_{\mathrm{o}} \int_{r=\mathrm{R}+H^{\mathrm{O}}(\Omega)}^{\mathrm{r_{lim}}} \left(\frac{\mathrm{R}}{r}\right)^{\nu} r^{n+2}\, \mathrm{d}r , \tag{4.75}$$

Après introduction de l'équation (4.74) dans (4.73) $V^{a}_{\mathrm{ref}}(r,\Omega)$ s'écrit

$\forall\, \Omega \in \Omega_{\mathrm{O}}, r > \mathrm{r_{lim}}, \nu > 2 \wedge \nu \in \Im^{+}$:

$$V^{a}_{\mathrm{ref}}(r,\Omega) \cong \mathrm{G}\,\mathrm{R}^{\nu}\,\rho^{\mathrm{a}}_{\mathrm{o}} \sum_{n=0}^{\bar{n}} \frac{1}{r^{n+1}} \iint_{\Omega' \in \Omega_{\mathrm{O}}} \left| \frac{r'^{n-\nu+3}}{n-\nu+3} \right|_{r'=\mathrm{R}+H^{\mathrm{O}}(\Omega')}^{\mathrm{r_{lim}}} \mathrm{P_n}\left(\cos\psi(\Omega,\Omega')\right) \mathrm{d}\Omega'$$

$$\cong \mathrm{G}\,\mathrm{R}^{\nu}\,\rho^{\mathrm{a}}_{\mathrm{o}} \sum_{n=0}^{\bar{n}} \frac{1}{r^{n+1}} \iint_{\Omega' \in \Omega_{\mathrm{O}}} \frac{\mathrm{R}^{n-\nu+3}}{n-\nu+3} \sum_{k=1}^{n-\nu+3} \binom{n-\nu+3}{k} \frac{(r_{\mathrm{lim}} - \mathrm{R})^{k} - \left[H^{\mathrm{O}}(\Omega')\right]^{k}}{\mathrm{R}^{k}} \mathrm{P_n}\left(\cos\psi(\Omega,\Omega')\right) \mathrm{d}\Omega' . \tag{4.76}$$

Appliquant le théorème binomial à l'évaluation de la densité surfacique $\sigma^{a}(\Omega)$, soit

$$\forall\, \Omega \in \Omega_{\mathrm{O}}, \nu > 2 \wedge \nu \in \Im^{+} : \qquad \sigma^{a}(\Omega) = \frac{\rho^{\mathrm{a}}_{\mathrm{o}}}{\mathrm{R}^{2}} \int_{r=\mathrm{R}+H^{\mathrm{O}}(\Omega)}^{\mathrm{r_{lim}}} \left(\frac{\mathrm{R}}{r}\right)^{\nu} r^{2}\, \mathrm{d}r$$

$$= \rho^{\mathrm{a}}_{\mathrm{o}} \frac{\mathrm{R}^{3-\nu}}{3-\nu} \sum_{k=1}^{3-\nu} \binom{3-\nu}{k} \frac{(r_{\mathrm{lim}} - \mathrm{R})^{k} - \left[H^{\mathrm{O}}(\Omega)\right]^{k}}{\mathrm{R}^{k}}, \tag{4.77}$$

Le potentiel de référence des masses atmosphériques condensées $V^{ca}_{\mathrm{ref}}(r,\Omega)$ s'écrit

$\forall\, \Omega \in \Omega_{\mathrm{O}}, r > \mathrm{r_{lim}}, \nu > 2 \wedge \nu \in \Im^{+}$:

$$V^{ca}_{\mathrm{ref}}(r,\Omega) \cong \frac{\mathrm{G}\,\rho^{\mathrm{a}}_{\mathrm{o}}}{\mathrm{R}^{1-\nu}} \sum_{n=0}^{\bar{n}} \left(\frac{\mathrm{R}}{r}\right)^{n+1} \iint_{\Omega' \in \Omega_{\mathrm{O}}} \left| \frac{r'^{3-\nu}}{3-\nu} \right|_{r'=\mathrm{R}+H^{\mathrm{O}}(\Omega')}^{\mathrm{r_{lim}}} \mathrm{P_n}\left(\cos\psi(\Omega,\Omega')\right) \mathrm{d}\Omega'$$

$$= \frac{\mathrm{G}\,\rho^{\mathrm{a}}_{\mathrm{o}}}{\mathrm{R}^{1-\nu}} \sum_{n=0}^{\bar{n}} \left(\frac{\mathrm{R}}{r}\right)^{n+1} \iint_{\Omega' \in \Omega_{\mathrm{O}}} \frac{\mathrm{R}^{3-\nu}}{3-\nu} \sum_{k=1}^{3-\nu} \binom{3-\nu}{k} \frac{(\mathrm{r_{lim}} - \mathrm{R})^{k} - \left[H^{\mathrm{O}}(\Omega')\right]^{k}}{\mathrm{R}^{k}} \mathrm{P_n}\left(\cos\psi(\Omega,\Omega')\right) \mathrm{d}\Omega' \tag{4.78}$$

D'où l'expression finale du potentiel résiduel $\delta V^{a}_{\mathrm{ref}}(r,\Omega)$

$\forall\, \Omega \in \Omega_{\mathrm{O}}, r > \mathrm{r_{lim}}, \nu > 2 \wedge \nu \in \Im^{+}$:

$$\delta V^{a}_{\mathrm{ref}}(r,\Omega) \cong -2\pi \mathrm{G}\,\rho^{\mathrm{a}}_{\mathrm{o}} \sum_{n=1}^{\bar{n}} \frac{n}{2n+1}\left(\frac{\mathrm{R}}{r}\right)^{n+1} \sum_{m=-n}^{n} \mathrm{H}^{2}_{\mathrm{n,m}}(\Omega)\,\mathrm{Y}_{\mathrm{n,m}}(\Omega)$$

$$-2\pi \mathrm{G}\frac{\rho^{\mathrm{a}}_{\mathrm{o}}}{3\mathrm{R}} \sum_{n=1}^{\bar{n}} \frac{n(n-2\nu+3)}{2n+1}\left(\frac{\mathrm{R}}{r}\right)^{n+1} \sum_{m=-n}^{n} \mathrm{H}^{3}_{\mathrm{n,m}}(\Omega)\,\mathrm{Y}_{\mathrm{n,m}}(\Omega) \qquad (4.79)$$

1.6.3 Le potentiel global de référence dans l'espace de Helmert

Rappelons que le potentiel de référence global $W^{\mathrm{H}}_{\mathrm{ref}}(r,\Omega)$ dans l'espace de Helmert est donné par l'équation (4.65). Il peut être exprimé par la formule suivante

$$\forall\, \Omega \in \Omega_{\mathrm{O}},\, r > \mathrm{R}: \qquad W^{\mathrm{H}}_{\mathrm{ref}}(r,\Omega) = \frac{\mathrm{GM}}{r} - \sum_{n=2}^{\bar{n}} \left(\frac{\mathrm{a_o}}{r}\right)^{n+1} \sum_{m=-n}^{n} \mathrm{W}^{\mathrm{H}}_{\mathrm{n,m}}\ \mathrm{Y}_{\mathrm{n,m}}(\Omega). \qquad (4.80)$$

Le potentiel de Helmert $W^{\mathrm{H}}_{\mathrm{ref}}(r,\Omega)$ est exprimé par une sommation de termes en nombre fini, expression qui peut être utilisée à la surface du géoïde pour évaluer le champ de gravité de référence dans l'espace de Helmert. Si cette surface est inconnue, on la surface du géoïde est approximée par la surface de l'ellipsoïde de référence ($\forall\, \Omega \in \Omega_{\mathrm{O}}:\ r_g(\Omega) \approx r_o(\phi)$)

$$\forall\, \Omega \in \Omega_{\mathrm{O}}: \qquad r_g(\Omega) \approx r_o(\phi) \cong \mathrm{a}\left(1 - \mathrm{f}\sin^2\varphi\right) \qquad (4.81)$$

Ainsi, dans l'équation (4.80)

$$\forall\ \ \Omega \in \Omega_{\mathrm{O}},\, n = 1, 2, ..., \bar{n}: \qquad \left[\frac{\mathrm{a_o}}{r_g(\Omega)}\right]^{n+1} = 1 + (n+1)\mathrm{f}\sin^2\varphi\,, \qquad (4.82)$$

et le potentiel de référence dans l'espace de Helmert prend la forme

$$\forall\, \Omega \in \Omega_{\mathrm{O}},\, r > \mathrm{R}: \qquad W^{\mathrm{H}}_{\mathrm{ref}}\left(r_g(\Omega)\right) \approx \frac{\mathrm{GM}}{r_o(\Omega)} - \sum_{n=2}^{\bar{n}} \left[1 + (n+1)\mathrm{f}\sin^2\varphi\right] \sum_{m=-n}^{n} \mathrm{W}^{\mathrm{H}}_{\mathrm{n,m}}(\Omega)\,\mathrm{Y}_{\mathrm{n,m}}(\Omega). \qquad (4.83)$$

1.6.4 Comparaison des paramètres des systèmes GRS (Geodetic Reference Sytem) et GGM (Global Gravity Model)

Un des problèmes soulevés par ce formalisme réside dans la prise en compte de modèles de pesanteur globaux de type EGM et d'un modèle de référence ellipsoïdal dont les paramètres ne sont pas forcément identiques.

Nous utilisons l'indice "G" pour designer les valeurs des modèles globaux EGM et "E" pour les quantités relatives aux paramètres de l'ellipsoïde.

Le potentiel de gravité W_G est calculé à l'aide de l'expression suivante

$$W_G(r,\theta,\lambda)=\frac{GM_G}{r}\left(1+\sum_{n=2}^{n_{\max}}\sum_{m=0}^{n}\left(\frac{a_G}{r}\right)^n\{\bar{C}_{nm}^G\cos m\lambda+\bar{S}_{nm}^G\sin m\lambda\}\bar{P}_{nm}(\cos\theta)\right) \tag{4.84}$$

De même, le potentiel normal U_E de l'ellipsoïde de référence peut être représenté en série harmonique, tel que

$$U_E=\frac{GM_E}{r}\left(1+\sum_{n=2}^{10}\left(\frac{a_E}{r}\right)^n\bar{C}_{n0}^E\bar{P}_{n0}(\cos\theta)\right), \tag{4.85}$$

Soit T_G la différence de ces 2 potentiels au même point sur le géoïde, tel

$$T_G=\frac{GM_G-GM_E}{r}+\frac{GM_G}{r}\sum_{n=2}^{n_{\max}}\sum_{m=0}^{n}\left(\frac{a_G}{r}\right)^n\{\Delta\bar{C}_{nm}\cos m\lambda+\bar{S}_{nm}^G\sin m\lambda\}\bar{P}_{nm}(\cos\theta) \tag{4.86}$$

où $$\Delta\bar{C}_{n0}=\bar{C}_{n0}^G-\frac{GM_E}{GM_G}\left(\frac{a_E}{a_G}\right)^n\bar{C}_{n0}^E \tag{4.87}$$

L'ondulation du géoïde de degré zéro est alors

$$N_0=\frac{GM_G-GM_E}{r\gamma}-\frac{W_0-U}{\gamma}=\delta(GM)-\delta W \tag{4.88}$$

Le modèle géopotentiel EGM96 donné par la NASA GSFC et la NIMA, complet jusqu'au degré et ordre 360 (*Lemoine et al. 1998*) est souvent utilisé comme modèle global. Par ailleurs, l'ellipsoïde GRS-80 est conventionnellement utilise pour le calcul du Géoïde. Les paramètres *rayon équatorial* et *GM* de ces deux modèles sont donnés par le tableau 1.

Tableau 3.1 Paramètres des modèles EGM96 et GRS-80

Paramètre	**EGM96**	**GRS-80**
Rayon équatorial	*6378136.3 m*	6378137 m
GM	*398600.4415* km^3/s^2	*398600.5* km^3/s^2

Choisissant les valeurs du tableau 1 et les valeurs *R*=6371 *km* et $\gamma = 981$ *Gal*, le terme de degré zéro vaut

$$N_0 = \frac{GM_G - GM_E}{r\gamma} = -0.936\text{m} \tag{4.89}$$

1.6.5 Anomalie de référence global et sphéroïde de référence dans l'espace de Helmert

Suivant la condition aux limites (Heiskanen et Moritz, 1967), l'anomalie de référence de Helmert $\Delta g^{\mathrm{H}}_{\mathrm{ref}}\left(r_g(\Omega)\right)$ s'écrit

$$\forall\, \Omega \in \Omega_{\mathrm{O}}: \qquad \Delta g^{\mathrm{H}}_{\mathrm{ref}}\left(r_g(\Omega)\right) \approx -\left.\frac{\partial T^{\mathrm{H}}_{\mathrm{ref}}(r,\Omega)}{\partial r}\right|_{r=r_g(\Omega)} + \frac{2}{\mathrm{R}} T^{\mathrm{H}}_{\mathrm{ref}}\left(r_g(\Omega)\right), \tag{4.90}$$

où $T^{\mathrm{H}}_{\mathrm{ref}}\left(r_g(\Omega)\right) = W^{\mathrm{H}}_{\mathrm{ref}}\left(r_g(\Omega)\right) - U\left(r_g(\Omega)\right)$ est la perturbation du potentiel de référence dans l'espace de Helmert. Appliquant la formule de Bruns (Bruns, 1978), il est alors possible de calculer le sphéroïde de référence, assimilé ici aux hauteurs co-géoïdales $N^{\mathrm{H}}_{\mathrm{ref}}(\Omega)$ soit

$$\forall\, \Omega \in \Omega_{\mathrm{O}}: \qquad N^{\mathrm{H}}_{\mathrm{ref}}(\Omega) = \frac{T^{\mathrm{H}}_{\mathrm{ref}}\left(r_g(\Omega)\right)}{\gamma_o(\phi)}. \tag{4.91}$$

1.7. Résolution de l'intégrale de Stokes dans l'espace de Helmert

$N^{\mathrm{H}}(\Omega)$, définie comme la surface limite équipotentielle dans l'espace de Helmert, peut être évaluée à partir des anomalies de gravité $\Delta g^{\mathrm{H}}(\mathrm{R},\Omega)$ dans l'espace de Helmert, en référence à une sphère de rayon R en appliquant la formule de l'intégrale de Stokes (Stokes, 1849) et la formule de Bruns (Bruns, 1878), soit (Heiskanen et Moritz, 1967)

$$\forall\, \Omega \in \Omega_O : \qquad N^H(\Omega) = \frac{R}{4\pi\gamma_o(\phi)} \iint_{\Omega' \in \Omega_O} \Delta g^H(R,\Omega')\, S(\psi(\Omega,\Omega'))\, d\Omega' . \tag{4.92}$$

La fonction de Stokes sphérique $S(\psi(\Omega,\Omega'))$ est donnée par (Heiskanen et Moritz, 1967)

$$\forall\, \Omega,\Omega' \in \Omega_O : \quad S(\psi(\Omega,\Omega')) = \sum_{n=2}^{\infty} \frac{2n+1}{n-1} P_n(\cos\psi(\Omega,\Omega')) = 1 + \operatorname{cosec}\frac{\psi(\Omega,\Omega')}{2} - 6\sin\frac{\psi(\Omega,\Omega')}{2}$$

$$- 5\cos\psi(\Omega,\Omega') - 3\cos\psi(\Omega,\Omega')\ln\left(\sin\frac{\psi(\Omega,\Omega')}{2} + \sin^2\frac{\psi(\Omega,\Omega')}{2}\right) \tag{4.93}$$

L'évaluation de la hauteur co-géoïdale $N^H(\Omega)$ nécessite la connaissance de l'anomalie de gravité sur la surface entière de la terre.

1.7.1 La fonction de Stokes sphérique

En pratique, l'anomalie de gravité étant connue « en détail » que sur une surface limitée, Vaníček et Kleusberg (1987) ont émis l'idée de séparer la sommation sur *n* dans (4.93) en une partie de bas degré et une autre partie de haut degré.

$$\forall\, \Omega,\Omega' \in \Omega_O : \; S(\psi(\Omega,\Omega')) = \sum_{n=2}^{\bar{n}} \frac{2n+1}{n-1} P_n(\cos\psi(\Omega,\Omega')) + \sum_{n=\bar{n}+1}^{\infty} \frac{2n+1}{n-1} P_n(\cos\psi(\Omega,\Omega')) . \tag{4.94}$$

Le second terme du membre de droite de (4.94) représente la fonction de Stokes sphérique $S_{n>\bar{n}}(\psi(\Omega,\Omega'))$ (voir Vaníček et Kleusberg, 1987); Vaníček et Featherstone, 1998),

$$\forall\, \Omega,\Omega' \in \Omega_O : \qquad S_{n>\bar{n}}(\psi(\Omega,\Omega')) = \sum_{n=\bar{n}+1}^{\infty} \frac{2n+1}{n-1} P_n(\cos\psi(\Omega,\Omega')) . \tag{4.95}$$

Compte tenu de (4.94), (4.92) devient (Martinec, 1993)

$$\forall\, \Omega \in \Omega_O : \qquad N^H(\Omega) = N^H_{ref}(\Omega) + N^H_{n>\bar{n}}(\Omega) = \frac{R}{4\pi\gamma_o(\phi)} \iint_{\Omega' \in \Omega_O} \Delta g^H(R,\Omega') \sum_{n=2}^{\bar{n}} \frac{2n+1}{n-1} P_n(\cos\psi(\Omega,\Omega'))\, d\Omega'$$

$$+ \frac{R}{4\pi\gamma_o(\phi)} \iint_{\Omega' \in \Omega_O} \Delta g^H(R,\Omega') \sum_{n=\bar{n}+1}^{\infty} \frac{2n+1}{n-1} P_n(\cos\psi(\Omega,\Omega'))\, d\Omega' . \tag{4.96}$$

Le co-géoïde de référence (ou sphéroïde) de degré $\bar{n}$ est donné par les hauteurs co-géoïdales $N^H_{ref}(\Omega)$. $N^H_{n>\bar{n}}(\Omega)$ représente le co-géoïde résiduel (Novák et al., 2001). Ainsi, le sphéroïde de référence sera donné par les modèles globaux incluant en particulier les données satellitaires, tandis que l'intégration de la formule

de Stokes sera employée pour calculer la partie « haute fréquence » du co-géoïde à partir des données de pesanteur terrestres.

1.7.2 La fonction de Stokes sphérique modifiée

Le domaine d'intégration Ω_{O} de la formule de Stokes peut être divisé en un sous domaine proche Ω_{ψ_o}, défini sur l'intervalle $\psi \in \langle 0, \psi_o \rangle$ et la zone d'intégration lointaine correspondant au sous domaine $\Omega_{\mathrm{O}} - \Omega_{\psi_o}$, soit $\psi \in \langle \psi_o, \pi \rangle$.

La contribution respective de la zone proche sur la hauteur co-géoïdale « haute fréquence » $N^{\mathrm{H}}_{n>\bar{n},\Omega'_{\psi_o}}(\Omega)$ s'exprime alors par

$$\forall\, \Omega \in \Omega_{\mathrm{O}}: \qquad N^{\mathrm{H}}_{n>\bar{n},\Omega'_{\psi_o}}(\Omega) = \frac{\mathrm{R}}{4\pi\gamma_{\mathrm{o}}(\phi)} \iint_{\Omega' \in \Omega_{\psi_o}} \Delta g^{\mathrm{H}}(\mathrm{R},\Omega')\, \mathrm{S}_{\mathrm{n}>\bar{\mathrm{n}}}(\psi(\Omega,\Omega'))\, \mathrm{d}\Omega', \tag{4.97}$$

Tandis que la contribution "lointaine" et "haute fréquence"sur le co-géoïde $N^{\mathrm{H}}_{n>\bar{n},\Omega'_{\mathrm{O}}-\Omega'_{\psi_o}}(\Omega)$ est donnée par

$$\forall\, \Omega \in \Omega_{\mathrm{O}}: \qquad N^{\mathrm{H}}_{n>\bar{n},\Omega'_{\mathrm{O}}-\Omega'_{\psi_o}}(\Omega) = \frac{\mathrm{R}}{4\pi\gamma_{\mathrm{o}}(\phi)} \iint_{\Omega' \in \Omega_{\mathrm{O}}-\Omega_{\psi_o}} \Delta g^{\mathrm{H}}(\mathrm{R},\Omega')\, \mathrm{S}_{\mathrm{n}>\bar{\mathrm{n}}}(\psi(\Omega,\Omega'))\, \mathrm{d}\Omega'. \tag{4.98}$$

Sur la base des travaux de Molodensky et al. (1960), Vaníček et Kleusberg (1987) ont proposé de modifier la fonction de Stokes sphérique $\mathrm{S}_{\mathrm{n}>\bar{\mathrm{n}}}(\psi(\Omega,\Omega'))$ de telle façon que la contribution de la zone lointaine (erreur de troncature) $N^{\mathrm{H}}_{n>\bar{n},\Omega'_{\mathrm{O}}-\Omega'_{\psi_o}}(\Omega)$ soit minimum au sens des moindres carrés. La fonction de Stokes modifiée $\mathrm{S}_{\mathrm{n}>\bar{\mathrm{n}}}(\psi_o, \psi(\Omega,\Omega'))$ est alors définie selon ces auteurs par

$$\mathrm{S}_{\mathrm{n}>\bar{\mathrm{n}}}(\psi_o, \psi(\Omega,\Omega')) = \begin{cases} 0, & \psi \in \langle 0, \psi_o \rangle, \\ \mathrm{S}_{\mathrm{n}>\bar{\mathrm{n}}}(\psi(\Omega,\Omega')), & \psi \in (\psi_o, \pi\rangle, \end{cases} \tag{4.99}$$

et étendue en série sur la base des polynômes de Legendre, soit

$$\forall\, \psi \in \langle 0, \pi \rangle: \qquad \mathrm{S}_{\mathrm{n}>\bar{\mathrm{n}}}(\psi_o, \psi(\Omega,\Omega')) = \sum_{n=\bar{n}+1}^{\infty} \frac{2n+1}{2} \mathrm{Q}_{\mathrm{n}}(\psi_o, \psi(\Omega,\Omega'))\, \mathrm{P}_{\mathrm{n}}(\cos\psi(\Omega,\Omega')), \tag{4.100}$$

où $\mathrm{Q}_{\mathrm{n}}(\psi_o, \psi(\Omega,\Omega'))$ sont les coefficients de troncature pour la fonction de Stokes sphérique modifiée $\mathrm{S}_{\mathrm{n}>\bar{\mathrm{n}}}(\psi_o, \psi(\Omega,\Omega'))$, (voir Molodensky et al., 1960).

En multipliant l'équation. (4.100) par les polynômes de Legendre $\mathrm{P}_{\mathrm{m}}(\cos\psi(\Omega,\Omega'))$,

$\forall\, \psi \in \langle 0, \pi \rangle$:

$$S_{n>\bar{n}}(\psi_o, \psi(\Omega,\Omega')) P_m(\cos\psi(\Omega,\Omega')) = \sum_{n=\bar{n}+1}^{\infty} \frac{2n+1}{2} Q_n(\psi_o, \psi(\Omega,\Omega')) P_n(\cos\psi(\Omega,\Omega')) P_m(\cos\psi(\Omega,\Omega')) \tag{4.101}$$

Et intégrant le résultat sur l'intervalle $\psi \in \langle 0, \pi \rangle$, on obtient

$$\int_{\psi=0}^{\pi} S_{n>\bar{n}}(\psi_o, \psi(\Omega,\Omega')) P_m(\cos\psi(\Omega,\Omega')) \sin\psi(\Omega,\Omega')\, d\psi$$

$$= \sum_{n=\bar{n}+1}^{\infty} \frac{2n+1}{2} Q_n(\psi_o, \psi(\Omega,\Omega')) \int_{\psi=0}^{\pi} P_n(\cos\psi(\Omega,\Omega')) P_m(\cos\psi(\Omega,\Omega')) \sin\psi(\Omega,\Omega')\, d\psi \,. \tag{4.102}$$

Les propriétés d'orthogonalité des polynômes de Legendre entraînent les relations suivantes

$$\forall\, \psi \in \langle 0, \pi \rangle,\ n \neq m: \qquad \int_{\psi=0}^{\pi} P_n(\cos\psi(\Omega,\Omega')) P_m(\cos\psi(\Omega,\Omega')) \sin\psi(\Omega,\Omega')\, d\psi = 0 \,, \tag{4.103}$$

$$\forall\, \psi \in \langle 0, \pi \rangle,\ n = m: \qquad \int_{\psi=0}^{\pi} [P_n(\cos\psi(\Omega,\Omega'))]^2 \sin\psi(\Omega,\Omega')\, d\psi = \frac{2}{2n+1} \,, \tag{4.104}$$

Partant des équations (4.99), (4.100), les coefficients de troncature $Q_n(\psi_o, \psi(\Omega,\Omega'))$ deviennent

$$\forall\, \Omega \in \Omega_O: \qquad Q_n(\psi_o, \psi(\Omega,\Omega')) = \int_{\psi=0}^{\pi} S_{n>\bar{n}}(\psi_o, \psi(\Omega,\Omega')) P_n(\cos\psi(\Omega,\Omega')) \sin\psi(\Omega,\Omega')\, d\psi \,. \tag{4.105}$$

7.3 La contribution de la zone proche au co-géoïde « haute fréquence »

Nous avons vu que l'anomalie de gravité de Helmert référée à la surface du géoïde peut être scindée en une composante « basse fréquence » (modèle global donné par l'équation (4.84)), soit $\Delta g^{H}_{n<\bar{n}}(R,\Omega) \equiv \Delta g^{H}_{ref}(R,\Omega)$ et une composante haute fréquence (anomalie résiduelle obtenue en ôtant l'anomalie de référence globale $\Delta g^{H}_{ref}(R,\Omega)$ à l'anomalie de Helmert (équation (4.61)), soit $\Delta g^{H}_{n>\bar{n}}(R,\Omega)$.

Ainsi, la contribution de la gravité "haute fréquence" sur la zone proche sur la hauteur co-géoïde $N^{H}_{n>\bar{n},\Omega'_o}(\Omega)$ est exprimée par

$$\forall\, \Omega \in \Omega_O: \qquad N^{H}_{n>\bar{n},\Omega'_{\psi_o}}(\Omega) = \frac{R}{4\pi\gamma_o(\phi)} \iint_{\Omega' \in \Omega_{\psi_o}} \Delta g^{H}_{n>\bar{n}}(R,\Omega') S_{n>\bar{n}}(\psi_o, \psi(\Omega,\Omega'))\, d\Omega' \,. \tag{4.106}$$

L'intégrale de Stokes est singulière pour $\psi = 0$. On résout cette singularité en ajoutant et retirant la valeur de l'anomalie au point singulier (voir Martinec, 1993),

$$\forall\, \Omega \in \Omega_O: \qquad N^{H}_{n>\bar{n},\Omega'_{\psi_o}}(\Omega) = \frac{R}{4\pi\gamma_o(\phi)} \iint_{\Omega' \in \Omega_{\psi_o}} \left[\Delta g^{H}_{n>\bar{n}}(R,\Omega') - \Delta g^{H}_{n>\bar{n}}(R,\Omega) \right] S_{n>\bar{n}}(\psi_o, \psi(\Omega,\Omega'))\, d\Omega'$$

$$+\frac{\mathrm{R}}{4\pi\gamma_{\mathrm{o}}(\phi)}\Delta g^{\mathrm{H}}_{n>\bar{n}}(\mathrm{R},\Omega)\iint_{\Omega'\in\Omega_{\psi_{\mathrm{o}}}}\mathrm{S}_{\mathrm{n}>\bar{\mathrm{n}}}(\psi_o,\psi(\Omega,\Omega'))\,\mathrm{d}\Omega'. \qquad (4.107)$$

1.7.4 Contribution lointaine sur le co-géoïde "haute fréquence"

Cette contribution $N^{\mathrm{H}}_{n>\bar{n},\Omega_{\mathrm{O}}-\Omega'_{\psi_{\mathrm{o}}}}(\Omega)$se réfère à l'anomalie de gravité "haute fréquence" de Helmert $\Delta g^{\mathrm{H}}_{n>\bar{n}}(\mathrm{R},\Omega)$ de la zone lointaine et s'écrit

$$\forall\,\Omega\in\Omega_{\mathrm{O}}:\qquad N^{\mathrm{H}}_{n>\bar{n},\Omega_{\mathrm{O}}-\Omega'_{\psi_{\mathrm{o}}}}(\Omega)=\frac{\mathrm{R}}{4\pi\gamma_{\mathrm{o}}(\phi)}\iint_{\Omega'\in\Omega_{\mathrm{O}}-\Omega_{\psi_{\mathrm{o}}}}\Delta g^{\mathrm{H}}_{n>\bar{n}}(\mathrm{R},\Omega')\,\mathrm{S}_{\mathrm{n}>\bar{\mathrm{n}}}(\psi_o,\psi(\Omega,\Omega'))\,\mathrm{d}\Omega'. \qquad (4.108)$$

Si on ne dispose pas des anomalies de gravité sur la surface totale de la terre, le calcul numerique peux étre fait par l'équation suivante (Novak, 2000)

$$\forall\,\Omega\in\Omega_{\mathrm{O}}:\qquad N^{\mathrm{H}}_{n>\bar{n},\Omega_{\mathrm{O}}-\Omega'_{\psi_{\mathrm{o}}}}(\Omega)=\frac{\mathrm{R}}{2}\sum_{n=\bar{n}+1,\ldots}\mathrm{Q}_{\mathrm{n}}(\psi_o,\psi(\Omega,\Omega'))\sum_{m=-n}^{n}\mathrm{T}^{\mathrm{H}}_{\mathrm{n,m}}\,\mathrm{Y}_{\mathrm{n,m}}(\Omega). \qquad (4.109)$$

1.8. Evaluation des effets topographiques et atmosphériques indirects sur le géoïde

Ayant évaluer l'intégrale de Stokes, c'est à dire calculer le co-géoïde dans l'espace de Helmert, il est nécessaire d'accéder au géoïde dans l'espace réel en calculant la contribution indirecte des effets topographiques et atmosphériques sur la hauteur du géoïde

On rappelle que la perturbation de potentiel de Helmert sur le géoïde s'exprime par

$$\forall\,\Omega\in\Omega_{\mathrm{O}}:\qquad T^{\mathrm{H}}(\mathrm{R},\Omega)=T(\mathrm{R},\Omega)-\delta V^{t}(\mathrm{R},\Omega)-\delta V^{a}(\mathrm{R},\Omega), \qquad (4.110)$$

Avec $\delta V^{t}(\mathrm{R},\Omega)$ le potentiel résiduel des masses topographiques, et $\delta V^{a}(\mathrm{R},\Omega)$ le potentiel résiduel des masses atmosphériques.

Appliquant la formule de Bruns (1878) aux perturbations de potentiel $T(\mathrm{R},\Omega)$ et $T^{\mathrm{H}}(\mathrm{R},\Omega)$,

$$\forall\,\Omega\in\Omega_{\mathrm{O}}:\qquad N(\Omega)=\frac{T(\mathrm{R},\Omega)}{\gamma_o(\phi)}, \qquad (4.111)$$

$$\forall\, \Omega \in \Omega_O : \qquad N^H(\Omega) = \frac{T^H(R,\Omega)}{\gamma_o(\phi)} = \frac{T(R,\Omega) - \delta V^t(R,\Omega) - \delta V^a(R,\Omega)}{\gamma_o(\phi)}, \tag{4.112}$$

On obtient alors la relation entre la hauteur de géoïde $N(\Omega)$ et la hauteur du co-géoïde $N^H(\Omega)$, soit,

$$\forall\, \Omega \in \Omega_O : \qquad \delta N(\Omega) = N(\Omega) - N^H(\Omega) = \frac{T(R,\Omega)}{\gamma_o(\phi)} - \frac{T^H(R,\Omega)}{\gamma_o(\phi)} = \frac{\delta V^t(R,\Omega)}{\gamma_o(\phi)} + \frac{\delta V^a(R,\Omega)}{\gamma_o(\phi)}. \tag{4.113}$$

Faisant apparaître dans le membre de droite de l'équation (4.113), les effets indirects, respectivement topographique et atmosphérique, sur la hauteur du géoïde.

1.8.1 Estimation des effets indirects topographique et atmosphérique

Dans le §1.3.1, les équations du potentiel de gravité pour les masses topographiques et leur forme condensée, respectivement soit $V^t(R,\Omega)$ et $V^{ct}(R,\Omega)$, ont été explicitées sur le géoïde. La différence de ces deux équations permet de calculer $\frac{\delta V^t(R,\Omega)}{\gamma_o(\phi)}$. De même le potentiel de gravité des masses atmosphériques $V^a(R,\Omega)$ et de leur forme condensée $V^{ca}(R,\Omega)$ ont été formalisés dans le §1.3. Par différence de ces 2 expressions, on peut alors calculer $\frac{\delta V^a(R,\Omega)}{\gamma_o(\phi)}$.

1.9. Effet de la condensation de Helmert sur le terme de degré 1 du potentiel de pesanteur terrestre

Par convention, le centre de masse terrestre est confondu avec l'origine du système de coordonnées. La condensation de Helmert est souvent réalisée en supposant la masse topographique invariante. Le schéma de Stokes-Helmert utilisé pour le calcul du géoïde terrestre, conduit à modifier la position du centre de masse du "corps" de Helmert. Cette translation, exprimée en coordonnées cartésiennes dans le repère géocentrique, est donnée par

$[\delta X, \delta Y, \delta Z] = [-0.006 ; -0.015 ; +0.002]$ (m) (Martinec, 1998)

En d'autres termes, le décalage maximum de 16 mm du corps de Helmert se situe aux coordonnées géodésiques Longitude ~ 248° et lat+itude +7°. En ce lieu, il est nécessaire d'introduire une correction sur les hauteurs de géoïde de Helmert de -16 mm. A l'opposé (Longitude = -7° et Latitude =68°) la correction est de 16 mm.

2. Estimation du géoïde par les mesures GPS sur les points nivelés

La mesure GPS sur un point nivelé présente de déterminer ponctuelment la hauteur du géoïde. On définit trois paramètres:

Cote géopotentielle C , pour un point appartenant à la surface topographique, considérée comme la différence de potentiel entre la surface équipotentielle au point considéré et de potentiel du géoïde.

L'altitude orthométrique H^O , la distance curviligne le long de la ligne de force du champ de pesanteur entre le géoïde est le point appartenant à la surface topographique.

L'hauteur ellipsoïdale h^{elli} , la distance entre la surface référentielle ellipsoïdale et le point dans la direction normale ellipsoïdale. L'altitude orthométrique est défini par (Fig. 4.1) :

$$H^O = \frac{C}{\overline{g}} \qquad (4.114)$$

Où $\overline{g}$ est la valeur moyenne de g entre géoïde et surface topographique.

Ainsi, la hauteur du géoïde est obtenue par la différence suivante :

$$N = h^{elli} - H^O \qquad (4.115)$$

Le géoïde gravimétrique calculé par la méthode de l'intégral de Stokes et la procédure de retrait-restoration possède une grande résolution et généralement une bonne précision relative. L'inconvénient est que sa précision absolue est généralement faible (voir l'exemple du géoïde en France, Jiang, 1996) en raison des erreurs liées aux grandes longueurs d'onde des modèles géoptentiels utilisés (Rapp, 1992 ; Li et Sideris, 1994). Par contre, un réseau GPS nivelé n'a pas une bonne résolution, mais sa précision absolue est très grande. L'objectif ultime dans ce calcul du géoïde local est de trouver un compromis entre ces deux types d'estimations qui concilie les qualités intrinsèques du géoïde gravimétriques et du géoïde sur points GPS/ nivelé.

5. Détermination du géoïde sur l'Iran

1. Problème posé - Motivation

Etant donné poser le formalisme de Stokes-Helmert permettant de déterminer le géoïde dans le chapitre 4, il s'agit maintenant de mettre en œuvre une méthode numérique efficace (temps de calcul et précision) pour estimer le géoïde et de discuter si le calcul complet inhérent à cette méthode ne peut pas être simplifié. La détermination d'un géoïde gravimétrique nécessite d'évaluer trois intégrales correspondant respectivement aux corrections (effets direct et indirect) de pesanteur et de potentiel associés au modèle de terrain, et à l'intégrale de Stokes sur les anomalies résiduelles de pesanteur. Forsberg (1984) et Sideris (1985; 1990) ont aborder ces intégrations par la technique dite de « Fast Fourier Transform (FFT) ». Cependant, cette technique fait appel à l'hypothèse de l'approximation plane des trois intégrales. Haagmans et al (1993) ont introduit une technique 1-D FFT pour calculer l'intégrale de Stokes en approximation sphérique. Dans ce chapitre, nous utilisons cette méthode de calcul réputée rapide pour des régions aussi vastes que l'Iran (Forberg et al, 2002). La stratégie dite de « retrait-restoration » (Forsberg et Tscherning, 2008) complète la démarche de calcul, permettant de transformer les anomalies à l'air libre en anomalies de géoïde, après avoir corrigé les effets de gravité connus « hautes et basses fréquences » qui sont ensuite restitués en anomalie de géoïde dans le modèle final. L'intérêt de cette technique est de filtrer et d'atténuer la une grande partie du spectre des anomalies à l'air libre afin d'interpoler « correctement » cette fonction résiduelle sur une grille régulière. C'est à cette condition que l'estimation du géoïde par la méthode de Stokes-Helmert et retrait-restoration en région montagneuse peut-être opérée avec efficacité (voir *fig. 5.1*).

La stratégie de Stokes-Helmert a été légèrement simplifiée en négligeant l'effet de prolongement vers le bas de l'anomalie de pesanteur résiduelle sur le géoïde explicité dans le § 1.4 du chapitre 4. Compte tenu de la distribution des points gravimétriques, en particulier dans les régions montagneuses, la résolution de ce problème inverse à partir de points irrégulièrement espacés aurait probablement créé des instabilités dans le champ prolongé exprimé sur une grille à une haute résolution (ici 3'x3', voir le § suivant). Ardalan et al. (2001) ont montré que cet effet peut avoir une contribution moyenne de l'ordre de quelques centimètres sur l'Iran. Cette simplification a aussi été opérée par Corchete (2009) pour la détermination du géoïde

gravimétrique en Italie. Les principaux enjeux dans le calcul du géoïde sur l'Iran résident dans le choix du modèle géopotentiel global permettant de simuler correctement les grandes longueurs d'onde. Par ailleurs, le Modèle Numérique de Terrain (MNT) SRTM a été utilisé pour les corrections de terrain, en ayant au préalable tester sa qualité par comparaison à quelques modèles locaux iraniens. Nous avons considéré dans nos calculs que la densité du relief était constante (2670kg/m^3). Nous sommes conscients que sa variabilité conduit à des variations du géoïde du second ordre, mais qui ne doivent pas être négligés dans le futur pour aboutir à une precision meilleure que le décimètre. En effet, Kiamehr (2006) et Cheraghi et al. (2009) ont montré que cet effet du second ordre calculé à partir des densités des formations géologiques affleurantes pouvait atteindre plusieurs centimètres. Enfin, nous avons choisi le logiciel GRAVSOFT pour calculer le nouveau géoïde gravimétrique sur l'Iran (Forsberg et Tscherning, 2008). Dans une dernière partie, nous définissons la surface de référence des altitudes en Iran en ajustant le géoïde gravimétrique au géoïde estimé sur les points GPS nivelés.

L'ensemble de ce travail est présenté sous la forme d'un article à soumettre au J. of Geodesy.

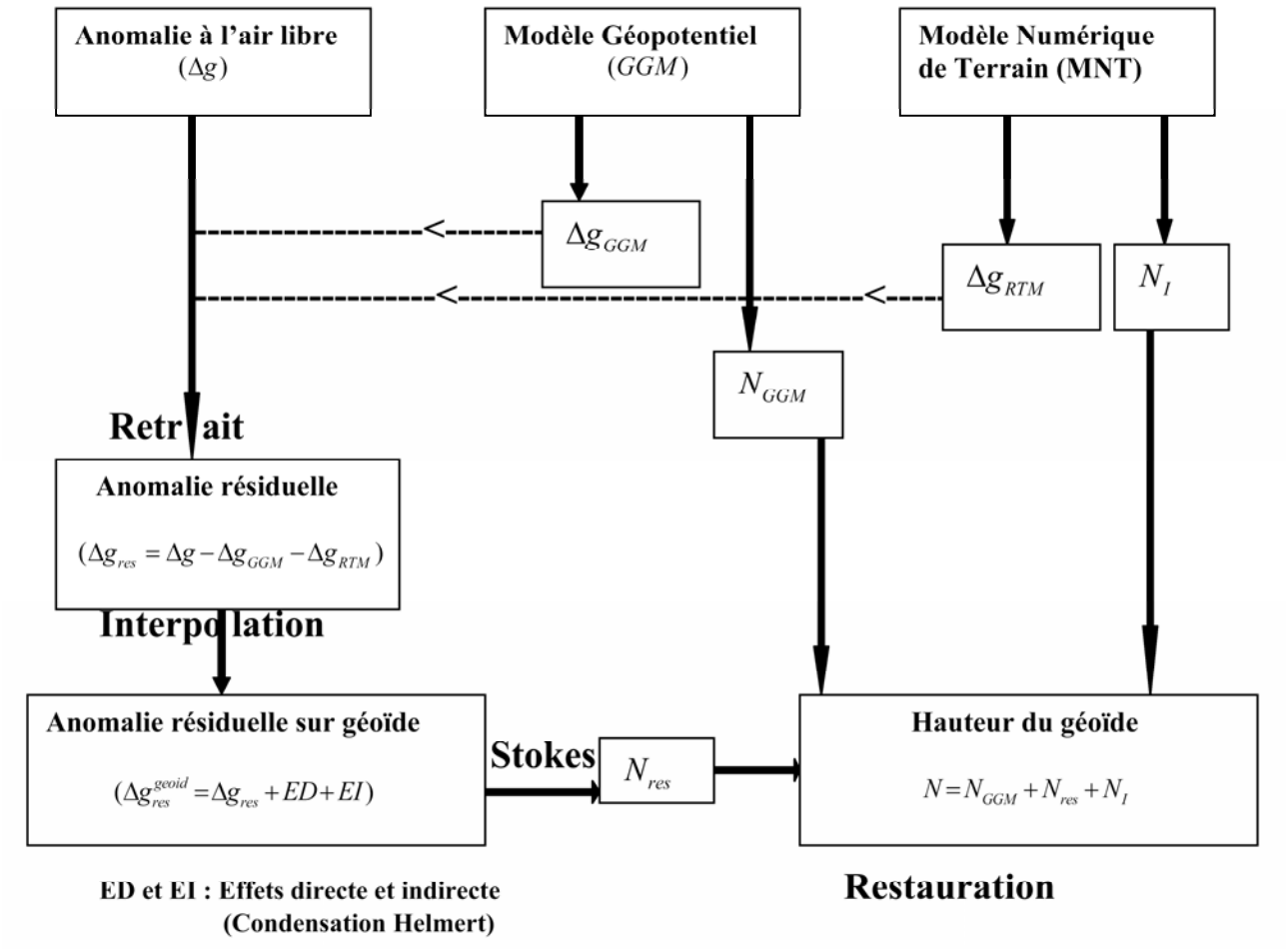

Figure 5.1. *Calcul du géoïde gravimétrique par retrait - restauration et condensation d'Helmert.*

2 The high resolution gravimetric geoid of Iran (IRGeoid10)

Y. Hatam(1,2), R. Bayer(1), P. Vanicek(3), Y. Djamour (4)

To be submitted to Journal of Geodesy

(1) Geosciences Montpellier cc60,Universite Montpellier 2–CNRS, Pl. E. Bataillon, 34095 Montpellier Cedex05, France. Email: yaghoub.hatam@gm.univ-montp2.fr , roger.bayer@gm.univ-montp2.fr

(2,4) [(2) Physical Geodesy Department, Geodesy and Land Surveying Management + (4)Geomatics College], National Cartographic Centre (NCC), PO Box 13185-1684, Meraj Ave, Tehran, Iran. Email: yaghoubhatam@yahoo.com, djamour@ncc.org.ir

(3) University of New Brunswick, Fredericton, Canada. Email: vanicek@unb.ca

Abstract

For many scientific and industrial purposes it is necessary to use the high precision orthometric heights. The classical method to determine the orthometric heights by levelling and gravimetry is slow and expensive. An alternative modern method to overcome the mentioned problems of the classical method is to sum the ellipsoidal heights with the geoid heights at the same interesting points. The ellipsoidal heights can be determined easily and with a high precision by global positioning system (GPS). Thus, it remains to determine a high precision geoid model. The computation of a geoid model for Iran has been the goal of several experiences in last two decades. To compute a geoid model by applying the gravimetric method, the main necessary data are local gravities, global geopotential models and elevation data. The precision of the geoid is directly determined by the amount and the quality of the mentioned different kinds of data. In recent years, different modified global geopotential models, e.g. EGM08 and GOCO01S, were released (in 2007 and 2010 respectively). A high resolution digital terrain model, $3'' \times 3''$ SRTM data (obtained from the Shuttle Radar Topography Mission), was also released. On the other hand, there is an augmentation in local geodetic data over Iran, containing the precise co-locallized gravity, GPS and levelling data. A new geoid model is computed for Iran territory ($25^\circ \le \varphi \le 40^\circ, 44^\circ \le \lambda \le 64^\circ$) by applying the Stokes integral in convolution form, with a mesh size of $3' \times 3'$ in the GRS80 reference system. The new geoid model and the previous ones are compared versus 819 GPS/levelling points, and an augmentation for the precision of the new geoid model is obtained. An adjustment of the new gravimetric geoid model at the GPS/levelling points is made by using a four-parameter model to obtain a reference height (zero) surface.

Keywords: Geoid, Gravity, GPS/levelling, GOCE, GRACE, DTM, SRTM, RTM

1. Introduction

A precise geoid model is needed to compute the orthometric heights, necessary for many works in Geosciences, from the ellipsoidal heights which usually determined by global positioning system (GPS). Since 1986, a number of efforts have been done to compute different gravimetric geoid models for whole or a part of Iran (Weber and Zomrrodian, 1988; Ardalan et al, 2001; Nahavandchi and Soltanpour, 2005; Safari et al, 2005; Kiamehr, 2006; Hatam et al, 2006; Safari et al, 2008). A brief explanation for these different geoids, determined for whole of Iran, are as follows:

The first geoid computation was done by improvement of the regional geopotential model of tailored GPM2 (Wenzel, 1985) up to degree and order 180, and an accuracy of ± 1.4 m is computed by comparison with Doppler and levelling data (Weber and Zomorrodian, 1988). As the next modifying step to the mentioned work, a $1_{km} \times 1_{km}$ DTM extracted from the 1/250,000 maps together with the OSU89B (Rapp and Pavlis 1990) and old terrestrial gravity data supplied by Bureau Gravimetrique International (BGI) were used by applying remove-restore technique (Hamesh and Zomorrodian, 1992).

Another research was done by using a new method (Ardalan, 1999) based on the ellipsoidal Bruns formula without the application of Stokes's formula. The old gravity data supplied by BGI together with NCC gravity data at first-order levelling network bench marks, the GLOBE (Hastings, 1996) $1_{km} \times 1_{km}$ DTM data, and the EGM96 (Lemoine et al, 1998) global geopotential model were used in this job (Ardalan et al., 2001). A total number of 258 GPS/levelling points were used to compare with the computed gravimetric geoid and un uncertainty with a root mean square (RMS) of ± 1.26 m is presented.

The next research has been done by developing a new gravimetric, satellite altimetry, astronomical ellipsoidal boundary value problem for geoid computations and using old terrestrial gravity data supplied by BGI, 10 points of first-order astronomical coordinates, satellite altimetry data, the GLOBE (Hastings, 1996) $1_{km} \times 1_{km}$ DTM data, and a reference gravitational field of the ellipsoidal harmonic expansion complete up to degree and order 360. A total number of 51 GPS/levelling points were used to compare with the computed gravimetric geoid and a standard deviation of ± 1.068 m is proposed (Safari et al, 2005).

Another work has been followed by applying the gravimetric method (Vanicek and Kleusberg, 1987) and using the old gravity data supplied by BGI together with NCC gravity data at first-order levelling network bench marks, the GLOBE (Hastings, 1996) $1_{km} \times 1_{km}$ DTM data, and the GGM02S (Tapely et al., 2005)

GRACE based global geopotential model. A total number of 200 GPS/levelling points were used to compare with the computed gravimetric geoid and a standard deviation of ± 0.672 m is presented (Nahavandch and Soltanpour, 2005).

Last research has been done by applying the least-squares modification of Stokes's formula, and using the old gravity data supplied by BGI together with NCC gravity data at first-order levelling network bench marks and satellite altimetry derived gravity anomalies at seas (Sandwell, 1997), the mean $15" \times 15"$ DEM based on the Shuttle Radar Topography Mission (SRTM) 100 m high-resolution data, and the GGM02S (Tapely et al., 2005) GRACE based global geopotential model. A total number of 260 GPS/levelling points were used to compare with the computed gravimetric geoid and a RMS of ± 0.58 m is presented (Kiamehr, 2006).

Since the last mentioned geoid computation, several new GRACE and GOCE based global geopotential models, e.g. EGM08 (Pavlis et al, 2008) and GOCO01S (GOCO consortium, 2010), are released with the accuracy improvements in comparison to the already published ones. A multi-purpose network with co-localized measurements of gravity, GPS and precise levelling and with a mesh size of $55^{km} \times 55^{km}$ is established over Iran (the levelling measurements are not completed yet) (Hatam et al., 2008). The establishment of Absolute Gravity Network of Iran (Hatam et al., to be submitted; Sec. 3.2) and National Gravity Calibration Line of Iran (Hatam et al., to be submitted; Sec. 3.3) were the efficient tools in precisely establishing the gravity part of the mentioned 55 km multi-purpose network.

The geoid computation in the present job is realized by applying the Stokes integral and the Helmert's second condensation method, with the one dimensional FFT technique (Haagmans et al., 1993). There are several techniques to compute numerically a gravimetric geoid, i.e. ring integration (Kearsley, 1985), 1-D FFT (Haagmans et al., 1993), 2-D FFT on a plane (Schwarz et al., 1990), 2-D FFT on a sphere (Strang van Hees, 1990), least-squares collocation (Tscherning, 1985). The FFT solutions are obtained much more quickly than the numerical integration solutions without the loss of accuracy (Schwarz et al., 1990; Corchete et al, 2005).

In this paper, gravimetric geoid of Iran computed with different global and local geoid models are compared to available GPS/Levelling points, leading to a more precise gravimetric geoid and zero order levelling reference surfaces.

2. Data

Basically, computing a local geoid need to collect different kinds of data with enough accuracy and resolution to compute a precise gravimetric geoid, i.e. terrestrial free-air gravity anomalies, satellite altimetry based gravity anomalies, digital terrain model (DTM) to compute the terrain correction and indirect effect, global geopotential model (GGM) to compute the long wavelengths contributions of geoid and gravity anomaly, co-locallized GPS and levelling data to validate the computed gravimetric geoid.

2.1 Gravity anomalies

A total number of 22320 terrestrial gravity data (**Table 5.1 and Fig. 5.2**) are used in this work. The old data set was supplied by the Bureau Gravimetrique International (BGI) and the new data set by the National Cartographic Centre of Iran (NCC). The accuracy of barometrically determined elevations of old gravity data is presented as ± 5 - ± 10 m (Weber and Zomorrodian, 1988), and for the elevations of recent gravity data determined by levelling is estimated to be ± 0.1 - ± 0.3 m. All the data are in GRS80 reference system. The atmospheric correction has been taken into account for the gravity data. The gap areas, at seas and on land, out of boundaries, are filled by the 1' V18.1 satellite altimetry based gravity anomalies (Sandwell et al., 2009) and by the EGM08 model (Pavlis et al, 2008) respectively on a large band of 3 degrees around the Iranian territory. An overall precision between ± 0.1 - ± 0.3 mGal is estimated for the terrestrial gravity data. The accuracy of the V18.1 gravity anomalies is presented between ± 2 and ± 4 mGals (ibid). the free-air gravity anomaly map is presented on figure 5.the mean value of the anomaly is closed to zero, and high amplitude – short wave length anomalies is often associated with high topographic roughness.

2.2 Global Geopotential Models

Computing a precise geoid, needs to select an efficient global geopotential with simulated gravity anomalies by the mentioned global model and using the local gravity data for short wave lengths. Many global geopotential models are analysed to select a reasonable one. Here 5 models are analysed. The models are EGM96 (Lemoine et al, 1998), EGM08 (Pavlis, et al, 2008), EIGEN-51C (Bruinsma et al, 2010), GOCO01S (GOCO consortium, 2010) and GO_CONS_GCF_2_DIR (Bruinsma et al, 2010).In order to compare all the models up to degree and order 360/360, the EGM08 is used to supply the incomplete models. The recent publications (See special issue of Newton's Bulletin, 2009) have shown that the accuracy of EGM08 is better than the before global geopotential models. Here we anticipate the results of the 819 GPS/levelling points

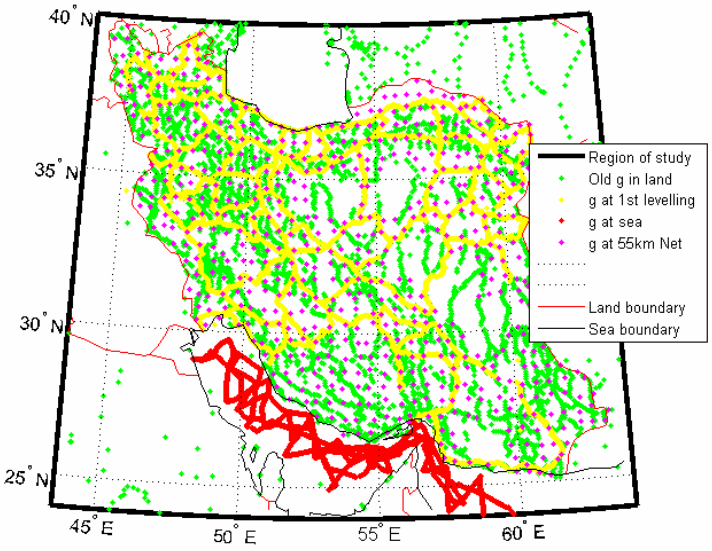

Fig. 5.2. *Distribution of gravity data over Iran*

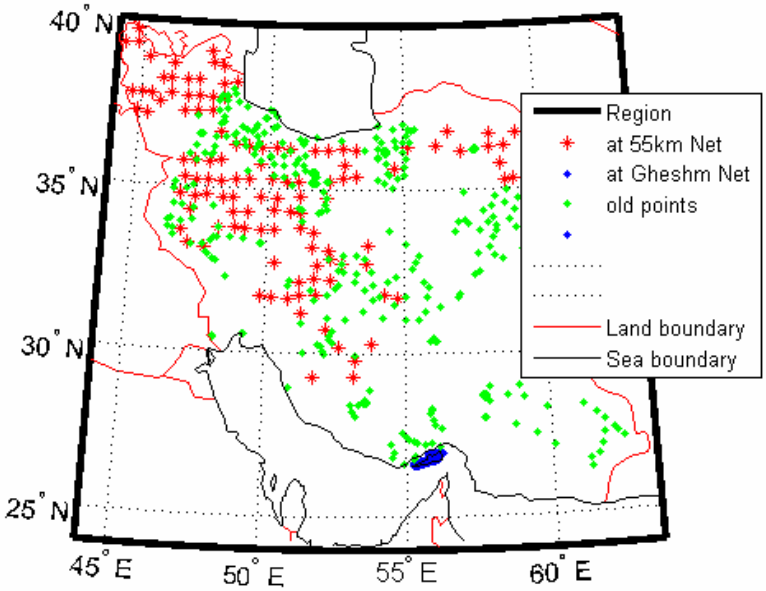

Fig. 5.3. *Distribution of GPS/levelling points over Iran*

[**Fig. 5.3**] by comparing the geoid heights given by the 5 global geopotential models to the GPS/levelling heights. We show that the model GOCO01S coupled by EGM08 up to degree and order 360/360 gives the best fit [mean=0.03 m, SD=$\pm$0.42 m, see **table 5.2**]. In the paper, this model is called later GOCO01SEGM08(360). Note that the standard deviations for all the models are roughly equivalent, ~0.44 m, whereas there is a decrease of the mean from EGM96 to GOCO01S. The high value of the standard deviation may be explained by the limited order and degree of the models, which do not explain the local deformation of the geoid. The reducing of mean value from EGM96 to GOCO01S reflects the decrease of long wavelengths errors of the recent global models. The combined GOCO01SEGM08(360) will be used to compute the long wavelengths components of the geoid [**Fig. 5.10** and **Fig. 5.11]**.

2.3 SRTM DTM data

To compute a gravimetric geoid with Stokes's integral, it is necessary to reduce the gravity anomalies to the geoid surface by using generally the Helmert's second condensation technique (see Sec. 4.2). For this purpose, it is necessary to compute the terrain correction and the indirect effect on geoid surface by applying a digital terrain model (DTM). Such a DTM is also necessary to compute the residual terrain model (RTM) effect in the remove-restore approach.

The mean elevation data is computed on a grid with a mesh size of $18''\times18''$ (**Table. 5.1** and **Fig. 5.4**) from the $3''\times3''$ SRTM data produced by the Shuttle Radar Topography Mission. Moreover, a mean elevation reference surface with a mesh size of $30'\times30'$ is computed (**Table. 5.1** and **Fig. 5.5**) from $18''\times18''$ SRTM data. This mean elevation reference surface corresponds to the topographical component included in the global geopotential model 360x360 in our computations. The $18''\times18''$ gridded mean elevation data are subtracted from the $30'\times30'$ gridded mean elevation reference surface to produce a residual terrain model (RTM).

The precision of the SRTM elevation is analysed by extracting heights from NCC DTM data (Hashemian, 2005) over 9 regions and comparing NCC DTM and SRTM heights. The selected heights consist in 3600 regularly spaced points where precise heights are produced by photogrametric precise triangulation technique. The difference between the 2 sets of data is characterized by a standard deviation of $\pm$15 m (Hashemian, 2005).

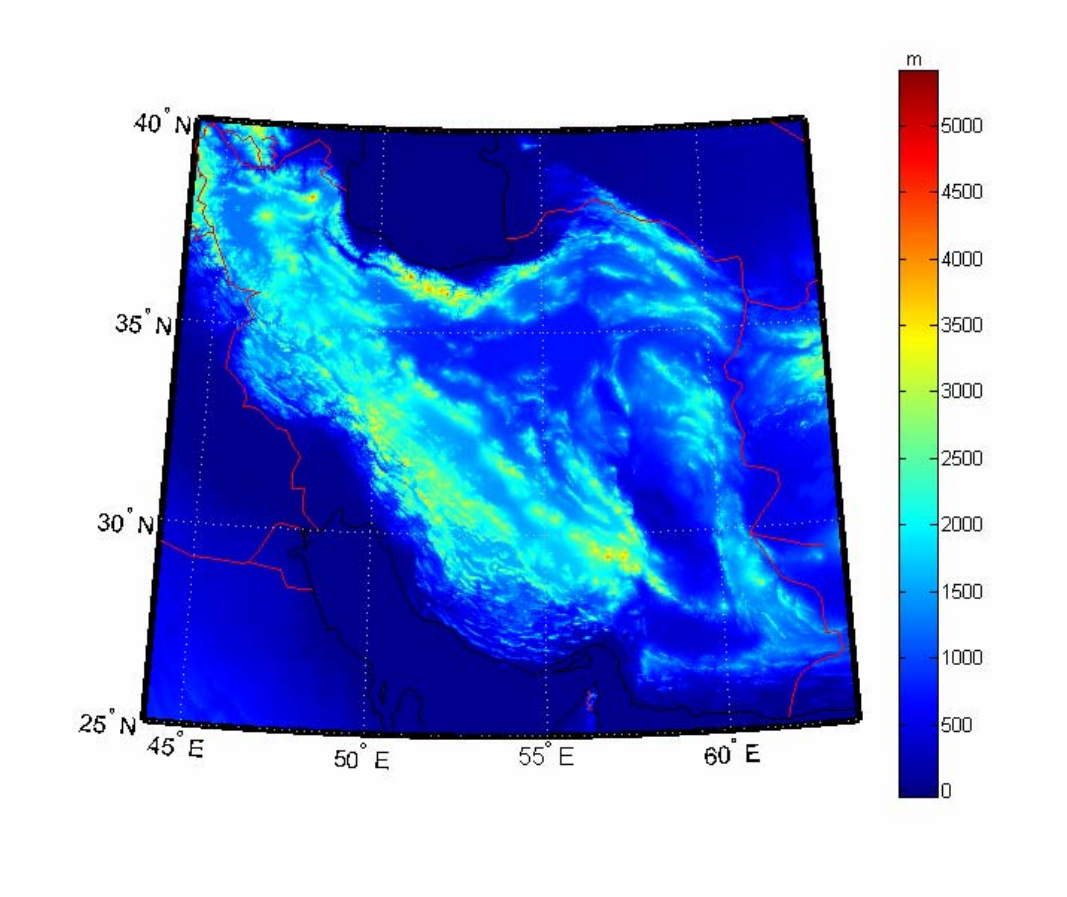

Fig. 5.4. *Mean 18'' by 18'' SRTM DTM of Iran*

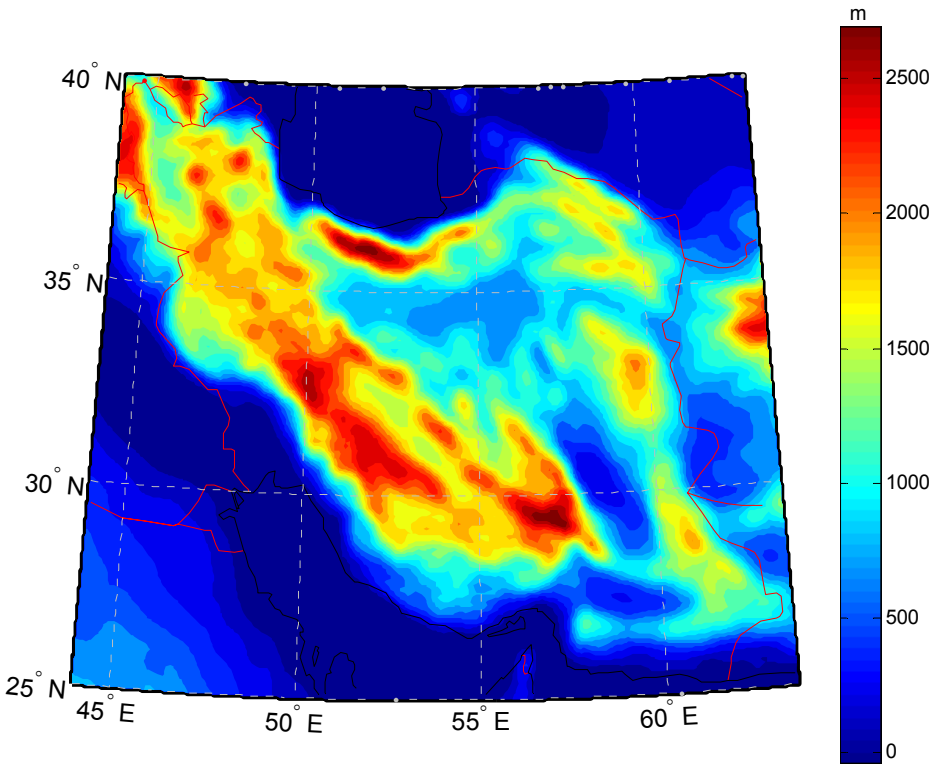

Fig. 5.5. *Mean 30' by 30' SRTM DTM of Iran as mean elevation surface for RTM effect computation*

			Mean	SD	Min	Max
Δg_{FA}^{pts}	(22300 points)	(mGal)	4.291	± 11.411	-151.088	198.786
SRTM DTM	18"×18"	(m)	821.6	± 149.8	-38	5416
SRTM DTM	30'×30'	(m)	817.1	± 144.9	-37	2833
$N_{GPS/Levelling}$	(819 points)	(m)	-14.27	± 16.25	-32.40	22.64

Table 5.1. *Statistics for different used data*

Difference: $N_{GPS/Levelling}$ - N_{GGM}	**Mean (m)**	**SD (m)**	**Min (m)**	**Max (m)**
EGM96 (360)	0.14	± 0.51	-1.29	2.72
EGM08 (360)	0.12	± 0.44	-1.46	1.34
EIGEN-51C_EGM08(360)	0.09	± 0.43	-1.54	1.51
GOCO01S EGM08(360)	**0.03**	**± 0.42**	**-1.67**	**1.54**
GO_CONS_GCF_2_DIR_EGM08(360)	0.050	± 0.43	-151	1.34

Table 5.2. *Statistics for comparison of different geoids obtained by global geopotential models versus 819 GPS/Levelling points*

		Mean (mGal)	SD (mGal)	Min (mGal)	Max (mGal)
c	3'×3'	1.607	± 1.121	-0.396	37.881
$2\pi k\rho(h-h_{ref})$	3'×3'	-3.024	± 3.342	-123.648	182.756
Δg_{red}	3'×3'	1.250	± 2.991	-104.328	113.101
Δg_{free}	3'×3'	-3.382	± 5.326	-221.479	257.596
δg	3'×3'	0.022	± 0.008	-0.000	0.343
Δg	3'×3'	-1.752	± 5.356	-195.565	278.498

Table 5.3. *Statistics for different components in eq. 2 and eq.9: terrain correction (c), principal RTM term ($2\pi k\rho(h-h_{ref})$), residual gravity anomaly (Δg_{red}), free-air gravity anomaly with respect to global geopotential model (Δg_{free}), indirect effect (δg), and fully reducied gravity anomaly on the geoid surface according to Helmert's second condensation method (Δg)*

2.4 GPS/Levelling data

A total number of 819 GPS/levelling points spread over Iran (**Table 5.1** and **Fig. 5.3**), supplied by NCC of Iran, in 3 different types: 1- old GPS/levelling data (382 points) which are measured for different purposes since 1988, mostly for requirements of producing the coverage maps of 1:25,000 scales, 2- GPS/levelling data at multi-purpose network with a mesh size of $15\,km \times 15\,km$ (118 points), 3- GPS/levelling data of the multi-purpose network over Gheshm island (319 points). The standard deviations for first-order levelling lines and loops over Iran are estimated as $\pm 1.43\,mm\sqrt{km}$ and $\pm 3.26\,mm\sqrt{km}$ respectively (Memarzadeh, 1998). The accuracy of GPS ellipsoidal heights for the above mentioned first data set is estimated as ± 0.25 m (Nilforoushan, 1995) and for the second and third data sets is ± 1 - ± 3 cm (Hatam et al. 2006, Hatam et al., 2008). An overall estimation of the accuracy for the mentioned GPS/levelling based geometrical geoid heights is from ± 0.03 m to ± 0.3 m.

3. Gravity data processing

Computation of the geoid by FFT technique needs to interpolate F.A. gravity anomaly on a regular grid by applying a suitable interpolation technique. The interpolation procedure consist in smoothing the point gravity anomaly data by removing the short wavelength effect of the roughness of topography with respect to a mean elevation reference surface. The smoothing procedure is completed by removing the long wavelength effect of gravity anomaly by applying the already introduced global geopotential model GOCO01SEGM08(360). The resulted reduced point gravity anomalies are therefore obtained by the following equation:

$$\Delta g_{red}^{pts} = \Delta g_{free}^{pts} - 2\pi k \rho (h - h_{ref})^{pts} + c^{pts} - \Delta g_{GGM}^{pts}, \qquad (1)$$

where 'pts' denotes point data, Δg_{free} is free-air gravity anomaly, k is Newton's gravitational constant, ρ is the density of the topography with the mean global value of $2.67\,g\,cm^{-3}$, h is the elevation, h_{ref} is the elevation of the mean elevation reference surface, c is the terrain correction, and Δg_{GGM} is given by the mentioned global geopotential model. The eq. (1) can be used precisely if the mean elevation surface corresponding to h_{ref} is an enough long-wave surface, usually with a resolution between 50 km and 100 km. The RTM effect is computed in relation with the resolution of global geopotential model up to degree and

order 360/360: the mean elevation reference surface with a resolution of 30' (approximately 55 km) is constructed by using a 2-D low pass filter and moving average window on the $18'' \times 18''$ resolution SRTM elevation data (**Fig. 5.4**), and the obtained results is presented in **Table 5.1** and **Fig. 5.5**. The terrain correction is computed, taking into account by the relief inside a circle of radius 1°

To interpolate the values of Δg_{red}^{pts} on a regular grid, the least squares collocation technique embedded in GRAVSOFT (Forsberg and Tscherning, 2008) is used to interpolate the smoothed values Δg_{red}^{pts} . The reduced free-air gravity anomalies are produced over Iran on a regular grid of $3' \times 3'$ and **Fig. 5.6**. The free-air gravity anomalies are reduced with the same resolution by adding to the global geopotential model, the residual terrain model effect with by the following equation:

$$\Delta g_{free}^{grid} = \Delta g_{red}^{grid} + 2\pi k \rho (h - h_{ref})^{grid} - c^{grid}, \quad (2)$$

where 'grid' means the corresponding value on the grid, Δg_{free} is free-air gravity anomaly with respect to the global geopotential model, Δg_{red} is the reduced free-air gravity anomaly according to eq. (1) and gridded by least squares collocation technique. The free-air gravity anomalies are presented in **figure 5.7**. The principal term of RTM effect, i.e. $2\pi k \rho (h - h_{ref})$, and the terrain correction c are computed over the $3' \times 3'$ grid (**Table 5.3**, **Fig. 5.8** and **Fig. 5.9**) using the same collocation method from data of the gravity field..

4. Geoid computation procedure

The classical remove-restore technique with the Helmert's second condensation method is chozen to compute the new gravimetric geoid model over Iran. According to this technique, the geoid model is calculated by computing and then summing three different terms:

$$N = N_1 + N_2 + N_3, \quad (3)$$

where N_1 is the long-wavelengths contribution computed from a global geopotential model, N_2 is the indirect effect computed by using elevation data, N_3 is the short wavelengths contribution computed from the gravity anomalies reduced to the geoid surface by the Helmert's second condensation method.

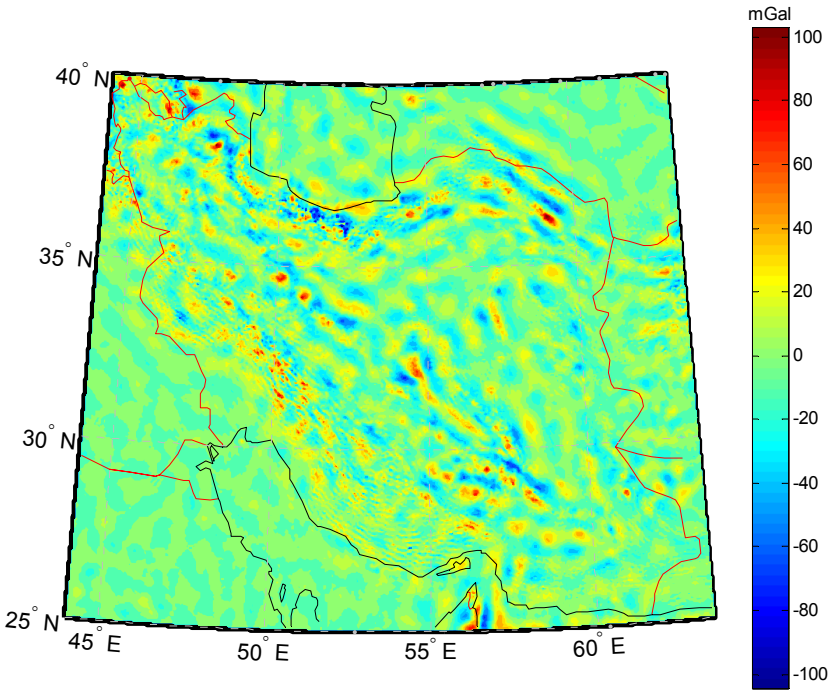

Fig. 5.6 *Residual free-air gravity anomaly over Iran with* 3'× 3' *mesh size*

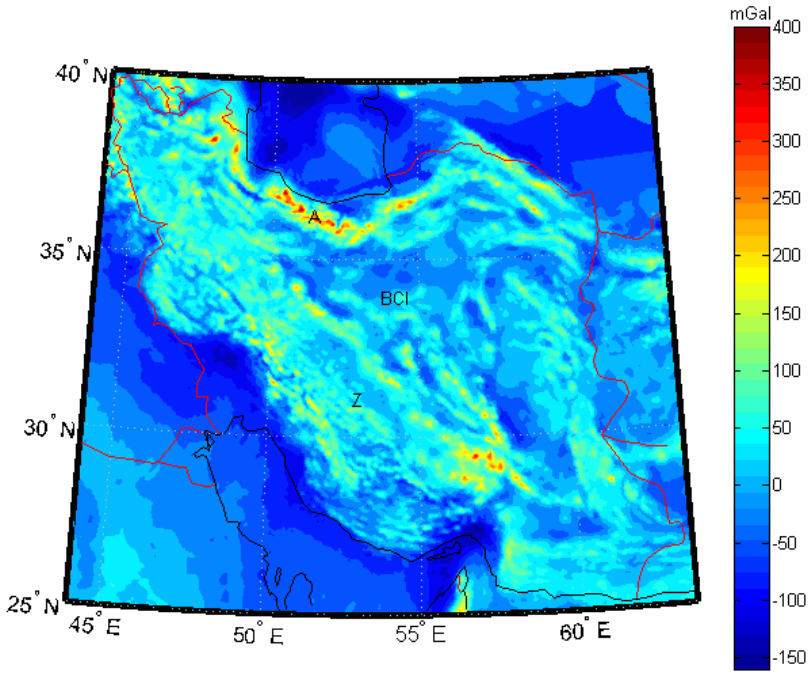

Fig. 5.7. *Free-air gravity anomaly over Iran with* 3'× 3' *mesh size*

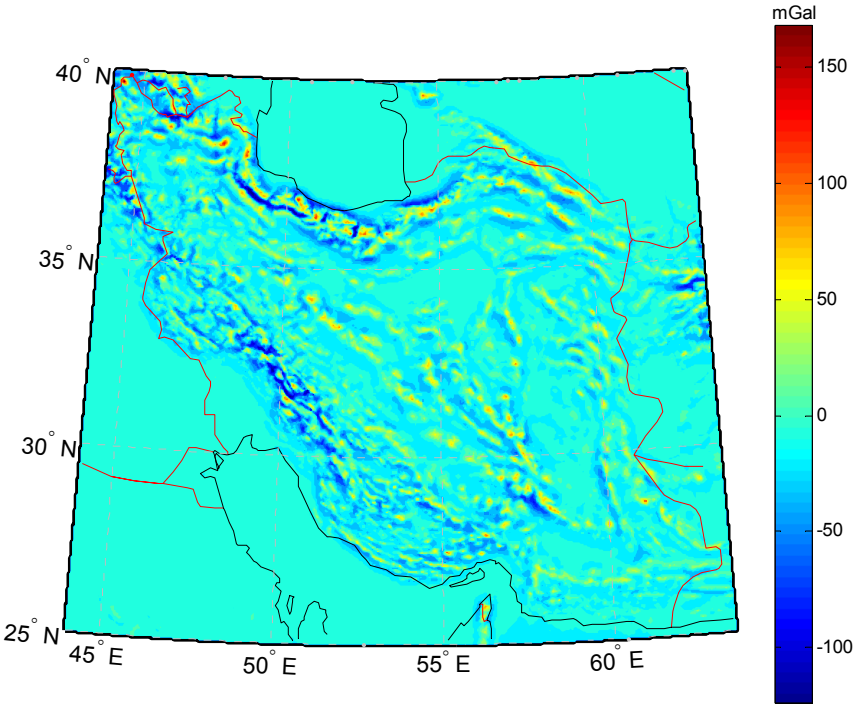

Fig. 5.8. *RTM principal term* $2\pi k\rho(h-h_{ref})$ *computed by the DTM model presented in* ***Fig. 5.4*** *with respect to the mean elevartion reference surface presented in* ***Fig. 5.5.***

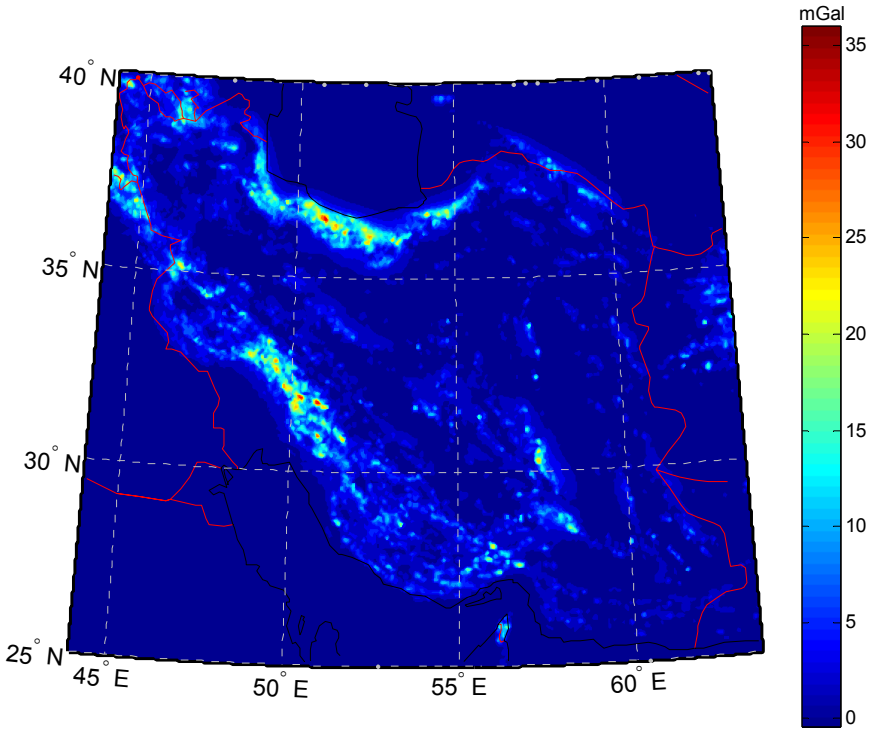

Fig. *5.9.* *The terrain correction over Iran computed from the DTM model presented in* ***Fig. 5.4***

4.1 Contribution of Global Geopotential Model

The long-wavelengths part of the geoid can be computed with the spherical harmonic coefficients of the global geopotential model by applying the following equation (Heiskanen and Moritz, 1987):

$$N_1 = \frac{kM}{r\gamma}\sum_{n=2}^{n_{\max}}\left(\frac{a}{r}\right)^n \sum_{m=0}^{n} P_{nm}(\sin\varphi)(\delta J_{nm}\cos m\lambda + \delta K_{nm}\sin m\lambda) + N_0, \quad (4)$$

where δJ_{nm} and δK_{nm} are fully normalized geopotential coefficients of the anomalous potential, kM is the earth's geocentric gravitational constant, a is semi major axis of the reference ellipsoid, P_{nm} are the fully normalized Legendre functions, the coordinates r, φ, λ define the geocentric location of the points on the geoid surface, γ is the normal gravity at reference ellipsoid, $n_{\max}$ is the maximum degree of the geopotential model used in computation, and N_0 is the zero degree term.

The long wavelengths part of the geoid is calculated on a grid of $3' \times 3'$ over Iran from eq. 4, considering the radius r as the geocentric position of a point P on the geoid surface instead of on the earth surface. Thus, the geoid heights (**Fig. 5.10**) are computed directly instead of height anomalies. We recall that the reduced gravity anomalies are estimated from eq. 1 after removing the long wavelengths part of the gravity anomaly from global geopotential model is computed by the following equation (Heiskanen and Moritz, 1987):

$$\Delta g_{GGM} = \frac{kM}{r^2}\sum_{n=2}^{n_{\max}}(n-1)\left(\frac{a}{r}\right)^n \sum_{m=0}^{n} P_{nm}(\sin\varphi)(\delta J_{nm}\cos m\lambda + \delta K_{nm}\sin m\lambda) + \Delta g_0, \quad (5)$$

where Δg_0 is the zero degree term. The geocentric radius r is considered as the sum of the geocentric radius r_E over the reference ellipsoid and the geoid height obtained by eq. 4. The **figure 5.11** shows the long wavelengths free air anomalies of the global model with amplitude ranging from -150 to 150 mGal.

4.2 contribution of indirect effect

In plane approximation, we recall that our formalism must be taken into account the condensation of the topography on the geoid. The indirect effect of Helmert's second condensation method on the geoid is computed from the following equation (Sideris 1990):

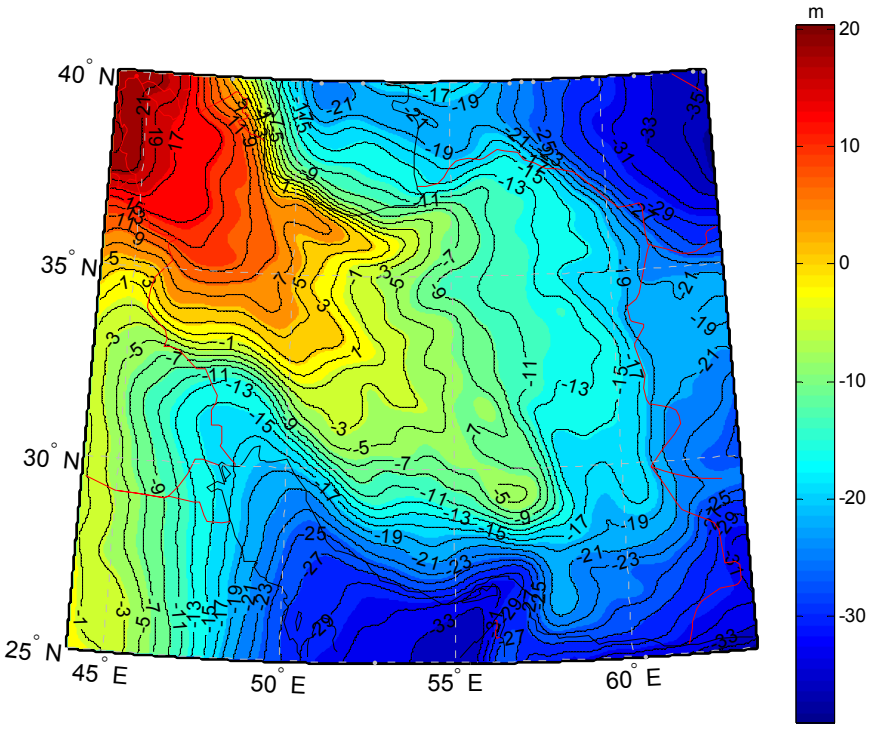

Fig. 5.10. *Geoid undulation, N_1 (eq. 4), based on the GOCO01SEGM08(360) model*

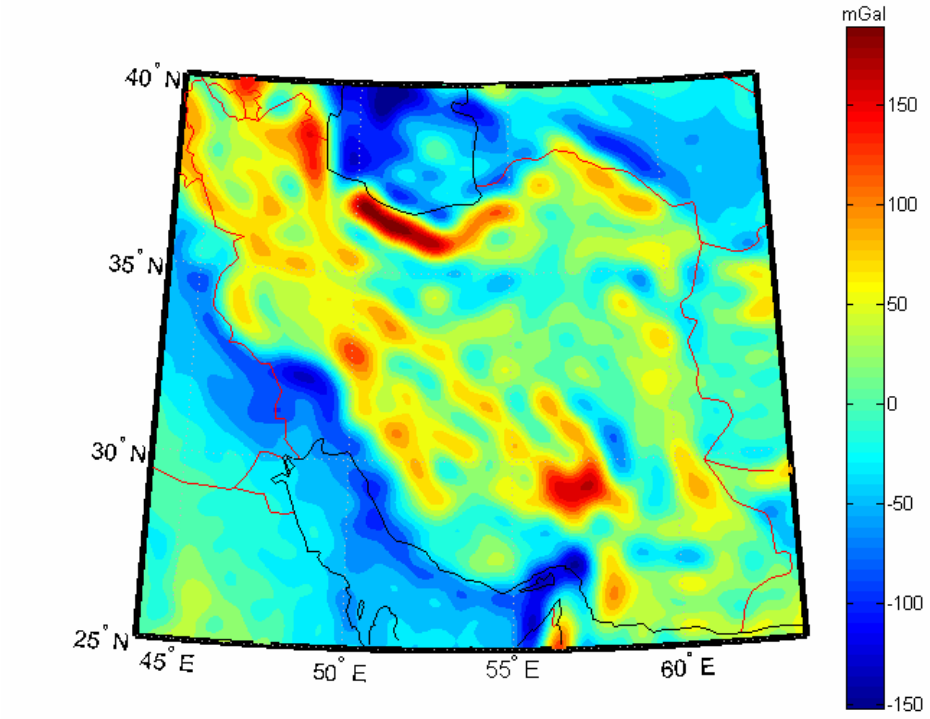

Fig. 5.11. *Free-air gravity anomalies over Iran based on the GOCO01SEGM08(360) model, necessary to reduce the observed point gravity anomalies to grid them (eq. 1)*

$$N_2 = -\frac{\pi k\rho}{\gamma} h^2(x_p, y_p) - \frac{k\rho}{6\gamma} \iint_A \frac{h^3(x,y) - h^3(x_p, y_p)}{[(x_p - x)^2 + (y_p - y)^2]^{3/2}}, \quad (6)$$

where k is Newton's gravitational constant, ρ is the density of the topography with a mean global constant value of $2.67\, g\, cm^{-3}$, (x_p, y_p) are the coordinates of the computation point, (x, y) are the coordinates of the integration points, γ is the normal gravity at reference ellipsoid, A is the computation region with elevation data, $h(x, y)$ are the elevation data (**Fig. 5.4**). The eq. 6 can be presented in convolution form as following (Schwarz et al. 1990):

$$N_2 = -\frac{\pi k\rho}{\gamma} h^2 - \frac{k\rho}{6\gamma} f * h^3 + \frac{k\rho}{6\gamma} g h^3, \quad (7)$$

where $f(x,y) = \frac{1}{(x^2 + y^2)^{3/2}}$, $\quad g = \iint_A f(x,y)\, dx\, dy$.

The indirect effect of Helmert's second condensation method, N_2, is computed by using eq. 7 (**Fig. 5.12**). This effect is mostly less than 0.1 m, augmented in mountainous areas (example: Zagros and Alborz mountains) where it can be higher than 0.5 m [**Fig. 5.12**].

4.3 Contribution of residual gravity

The residual gravity contribution, N_3, is computed by the following equation (Heiskanen and Moritz, 1987):

$$N_3 = \frac{R}{4\pi\gamma} \iint_\sigma \Delta g(\psi, \alpha) S(\psi)\, d\sigma, \quad (8)$$

where γ is the normal gravity at reference ellipsoid, R is the mean earth radius, $S(\psi)$ is the Stokes function, σ is the unit sphere of integration, and Δg are the fully reduced anomalies according to Helmert's second condensation method as follows (Heiskanen and Moritz 1987; Sideris, 1990; Ellmann and Vanicek 2007):

$$\Delta g = \Delta g_{free} + c + \delta g, \quad (9)$$

where Δg_{free} is the free-air gravity anomalies according to eq. 2, c is the terrain correction, and δg is the secondary indirect effect on gravity. The term δg is computed from the knowledge of primary indirect effect on geoid, N_2, and by using the following equation (Hiskanen and Moritz, 1987):

$$\delta g = 0.3086\, N_2, \quad (10)$$

The variation of δg shown in figure 11 ranges from 0 to 0.3 mGal as a consequence of N_2 term in the studied area [**Fig. 5.13**].

The reduced anomaly Δg is presented in **figure 5.14**. the observed large amplitudes are mostly augmented from the principal term of RTM effect (see eq. 2).

The N_3 term may be written in convolution in 1-D FFT domain (Haagmans et al. 1993) by:

$$N_3 = \frac{R\,\Delta\phi\,\Delta\lambda}{4\pi\gamma} F_1^{-1}\left[\sum_{\phi'=\phi_1}^{\phi_n} F_1(\Delta g\cos) F_1(S)\right], \qquad (11)$$

where S is the stokes function, F_1 is the discrete periodic Fourier transform and F_1^{-1} is its inverse. The main problem regarding the approximation of the continuous with discrete Fourier transform is the periodicity effect of the signal. Such an effect avoided by using zero padding, i.e by replacing for the outside of computation region with zero values (see Forsberg and Tcsherning, 2008). The computed residual geoid, N_3, is presented in **Table 5.5** and **Fig. 5.15**.

The new gravimetric geoid of Iran, called IRGeoid10, is computed by summing the N_1, N_2, and N_3 terms and presented in **Table 5.5** and F**ig. 5.16**. The geoid heights vary from 23 m to -30, from NW to SN of Iran respectively.

5 Comparison and adjustment of a gravimetric geoid model at GPS/Levelling points

The adjustment of a gravimetric geoid at the GPS/levelling points takes into account the relative and absolute precisions on the geoid. The advantage of a gravimetric geoid model computed by the remove-retore technique is its high resolution and its high relative precision. The estimated absolute and relative accuracies of the IRGeoid gravimetric geoid, by comparing it at 819 GPS/levelling points, are 0.26 m and 0.28 ppm respectively (Featherstone, 2001). The disadvantage comes from its low absolute presicion (Jiang, 1996; Doerflinger et al., 1997), due to errors on the long wavelengths components global geopotential models (Rapp, 1992; Li and Sideris, 1994). In contrary, a geometrical geoid model based on GPS/levelling points has a low resolution and high absolute precision. In many scientific and industrial applications, a geoid model with high relative and absolute precision is needed.Comparing a gravimetric geoid model at the GPS/levelling points permit to evaluate its absolute precision. Then, a combined adjustment of the two geoids is realized.

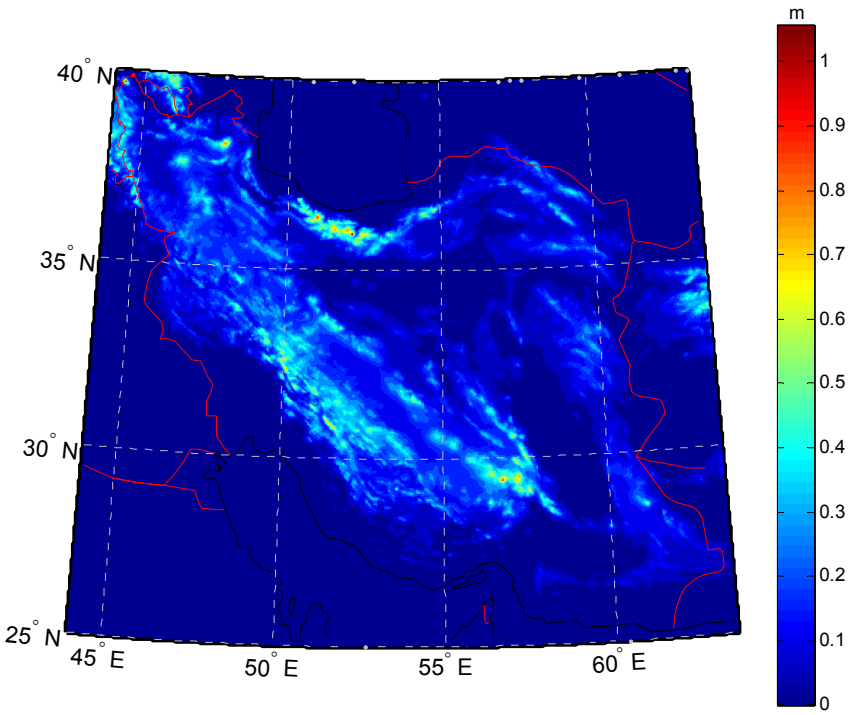

Fig. 5.12. *The indirect effect on the geoid height computed from the DTM model presented in* ***Fig. 5.4***

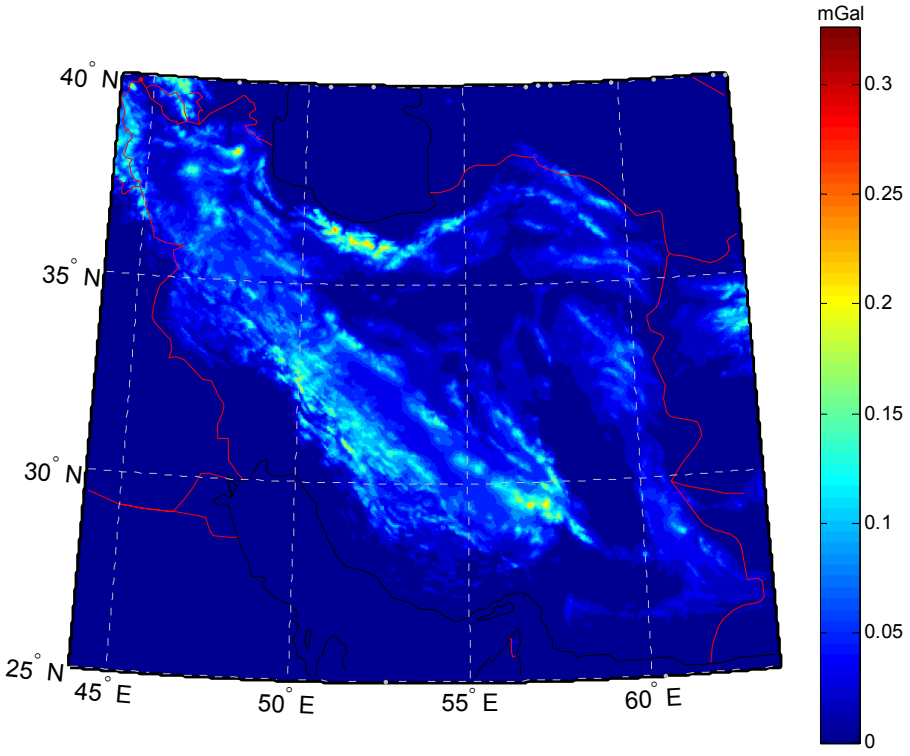

Fig. 5.13. *The indirect effect on the gravity computed from the DTM model presented in* ***Fig. 5.4***

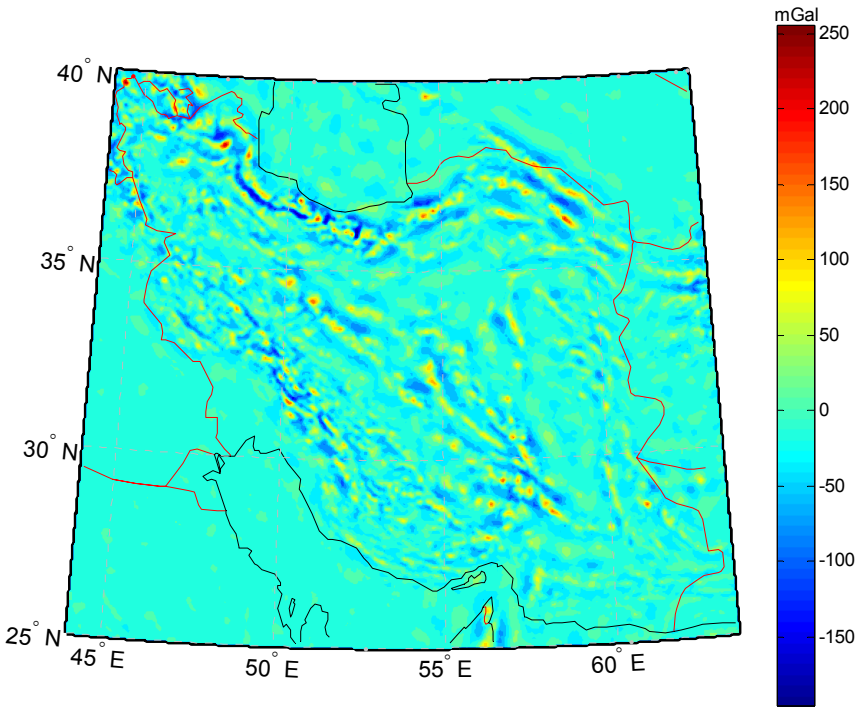

Fig. 5.14. *Residual gravity anomaly on the geoid surface over Iran with* $3' \times 3'$ *mesh size,* ***(eq. 9)***

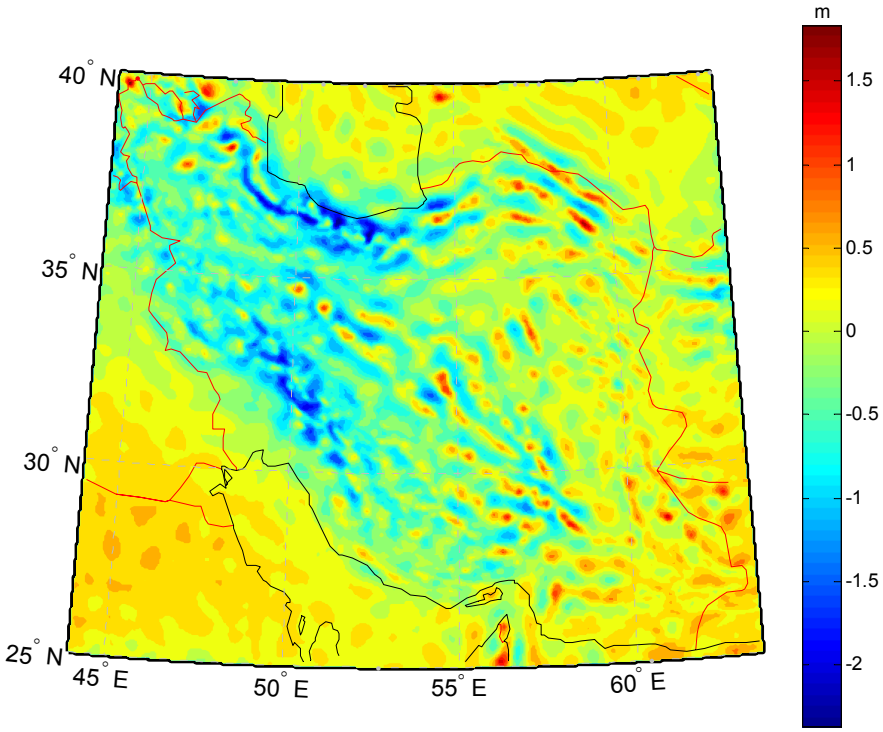

Fig. 5.15. *Residual geoid undulation computed by eq. 10*

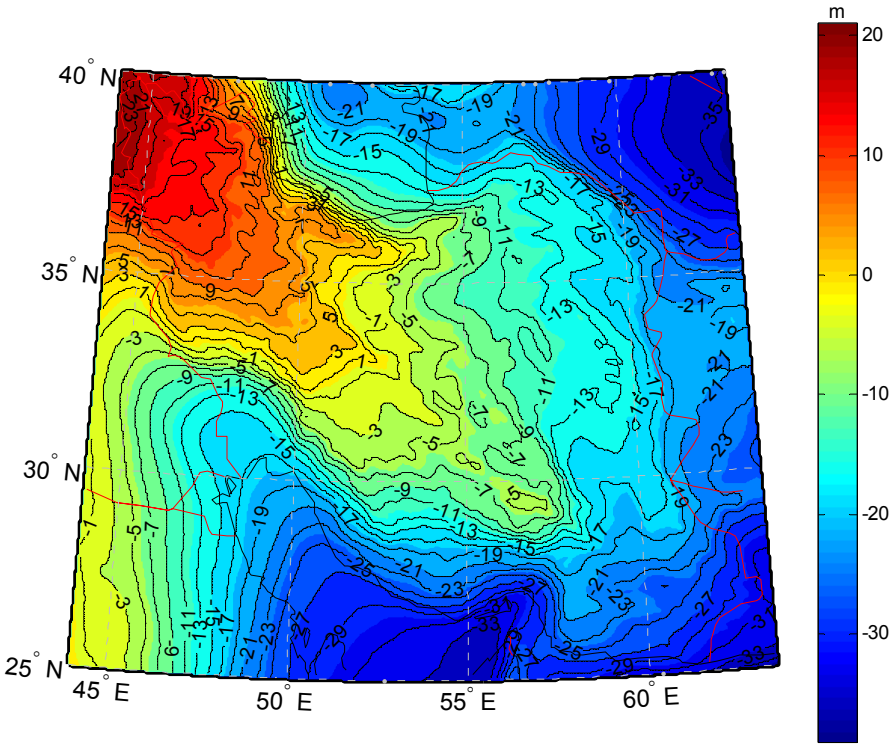

Fig. 5.16. *Gravimetric geoid of Iran (IRGeoid10)*

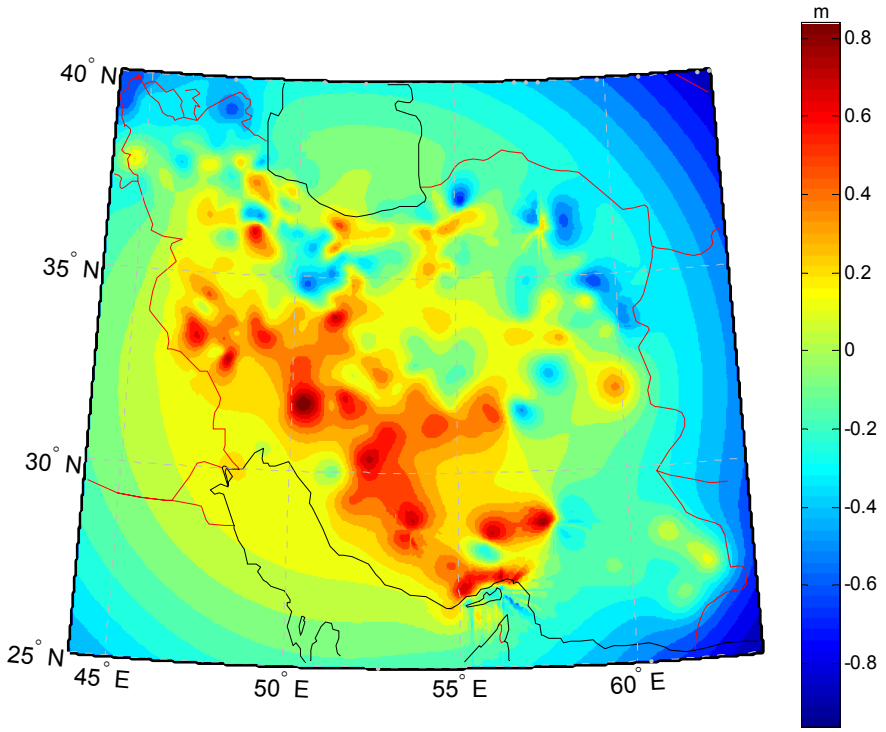

Fig. 5.17. *Difference between Gravimetric geoid and GPS/Levelling points*

The four-parametric model is the most commonly used to fit the gravimetric geoid at GPS/Levelling points. The respected mathematical model is given by the following formula (Hiskanen and Moritz, 1987):

$$N^{GPS} - N_i = \cos\varphi_i \cos\lambda_i \, a_1 + \cos\varphi_i \sin\lambda_i \, a_2 + \sin\varphi_i \, a_3 + a_4 + v_i \qquad (5)$$

Where N^{GPS}, N_i are geoidal heights by GPS/Levelling and gravimetric methods respectively; φ_i, λ_i are the horizontal geodetic coordinate of point i; v_i is the residual at point i; a_1, a_2, a_3 and a_4 are trend and shift, parameters, calculated by least squares method.

First we interpolate the gravimetric geoid heights at the GPS/levelling points. The difference is presented in figure 15. The interpolation of the differences is made on a grid $3' \times 3'$. The observed differences between the 2 geoids at these points are used for the combined adjustment (**Fig. 5.17**). Because the precise levelling networks have in general larger errors in montaineous regions, it is possible the large difference (red colour) at this figure in Zagros and Alborz regions has the origin partly in the levelling network. After least squares adjustment, the gravimetric geoid is corrected from four-parametric model in the initial $3' \times 3'$ grid and the final adjusted gravimetric geoid is shown on **figure 5.18**.

The IRGeoid10 model and the previous ones already published are compared to the geoid heights at the available GPS/levelling points (**table 5.4)**. The good quality of the IRGeoid10 is attested by 0.26 m of the standard deviation, which has been divided by a factor 2 with respect to IRGeoid5b and IRGeoid06 (**Table 5.5**).

6. Conclusions

A new gravimetric geoid model, IRGeoid10, is computed for Iran territory ($25^\circ \le \varphi \le 40^\circ, 44^\circ \le \lambda \le 64^\circ$) on a grid of $3' \times 3'$ by using the remove-restore technique and Helmert's second condensation method. The external estimated accuracy for it versus 819 GPS/levelling points, ± 0.26 m, is highest in comparison with all before computed geoids. The quality of the new computed geoid is also higher in comparison to many global geopotential models (**Table 2),** thanks to the recent GRACE and GOCE based global gravity model, high resolution and precision of SRTM elevation model, and augmented local gravity and GPS/levelling data**.** The new computed gravimetric geoid is adjusted at the 819 GPS/levelling points, by applying a four-parameter model, and a new combined geoid model is obtained which is suitable to determine orthometric

height by GPS. The new geoid model will complement other geoids computed in the region in Asia. It can be also used for geophysical applications, as a constraint for the density distribution and the thermal state. In fact there are some elementary relations between mass distribution inside the earth and geoid (Strang Van Hess, 2000). In plate tectonics studies (Wessel, et al, 1996; Kiamehr, et al, 2006), geoid exhibit linear anomalies trending in the direction of the absolute plate motion.

The scarcity of the gravity data in high roughness mountains of Alborz and Zagross, and in Kavir and Lout deserts is a severe problem to ameliorate the accuracy of the geoid. Applying the airborne gravimetry technique is an efficient solution to densify the gravity data satisfactorily for the mentioned laborious regions.

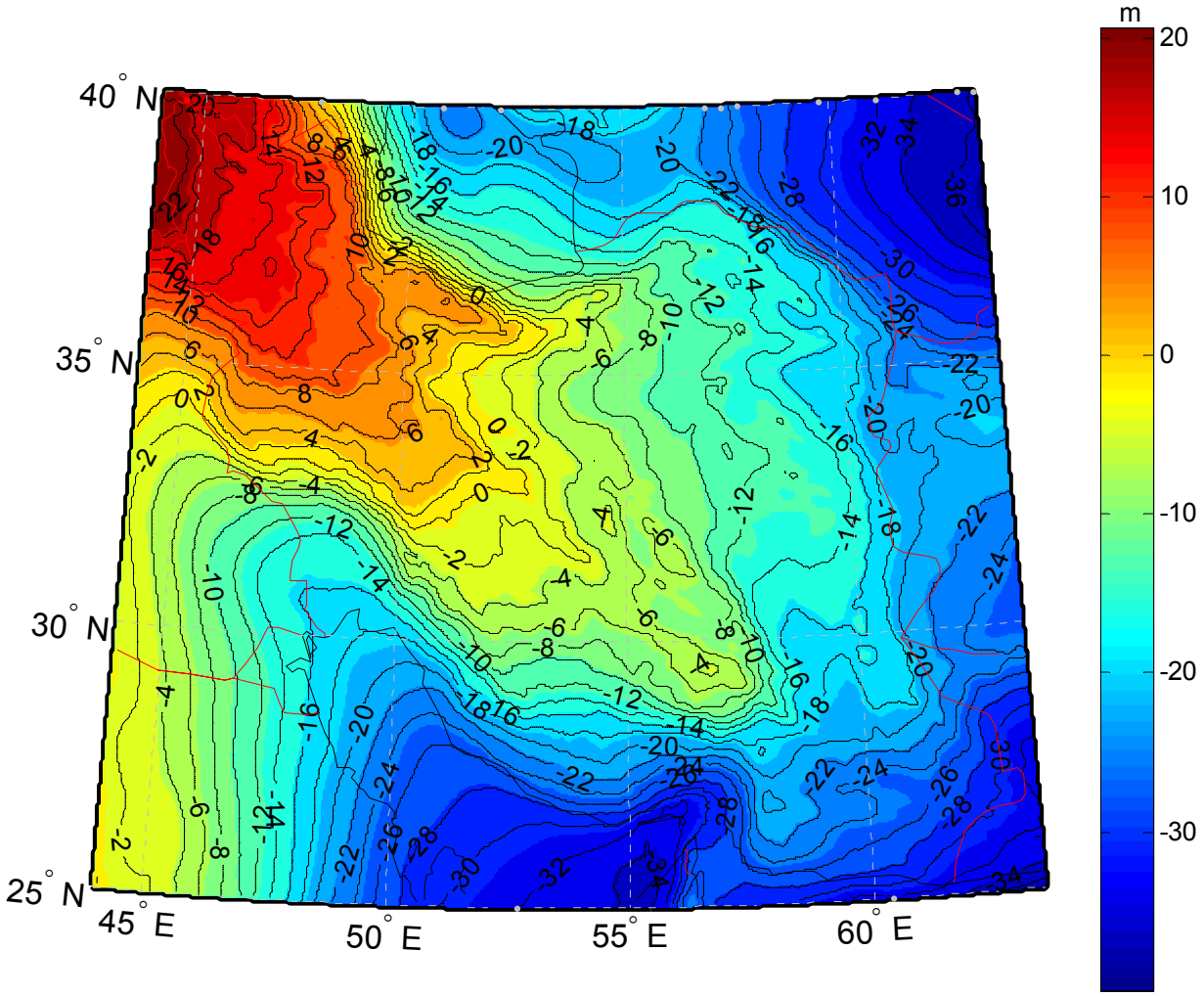

Fig. 5.18. *Adjusted gravimetric geoid at GPS/Levelling points*

Geoid and its components		Mean (m)	SD (m)	Min (m)	Max (m)
N_1	3'×3'	-12.85	±2.85	-39.00	23.41
N_2	3'×3'	0.07	±0.03	-0.00	1.11
N_3	3'×3'	0.024	±0.10	-2.37	2.05
N	3'×3'	-12.84	±2.79	-38.99	23.98
$N_{combined}$	3'×3'	-12.88	±2.75	-39.95	23.69

Table 5.4. *Statistics for the computed gravimetric geoid by Helmert's second condensation method and its components (eq. 3), and adjusting it versus GPS/Levelling points*

Gravimetric Geoid Models of Iran	SD or RMS (m)	Number of GPS/Levelling points used
IRGeoid88 (Weber and Zomorrodian, 1988)	±1.40 (RMS)	----
IRGeoid01 (Ardalan et al, 2001)	±1.26 (RMS)	258
IRGeoid05a (Safari et al,)	±1.068 (SD)	51
IRGeoid05b (Nahavandchi et Soltanpour, 2005)	±0.672 (SD)	200
IRGeoid06 (Kiamehr, 2006)	±0.58 (RMS)	260
IRGeoid10 (Hatam et al, 2010)	±0.26 (SD)	819

Table 5.5. *Accuracy of different gravimetric Geoid model for Iran by comparison versus GPS/levelling points (in terms of Standard Deviation (SD) or Root Mean Squares (RMS))*

7. References

Ardalan, A.A., 1999. high resolution regional geoid computation in the World Geodetic Datum 2000 based upon collocation of linearized observational functionals of the type gravity potential and gravity intensity. Phd dissertation, Stuttgart university. 250 pp.

Ardalan, A.A., Hatam, Y., Sharifi, M.A., Safari, A., Ghazavi, K., Motagh, M., 2001. High resolution geoid of Iran. Technical report, NCC, Iran, 155 pp.

Bruinsma, S.L., Marty, J.C., Balmino, G., Biancale, R., Foerste, C., Abrikosov, O., Neumayer, H., 2010. GOCE Gravity Field Recovery by Means of the Direct Numerical Method.Presented at the ESA Living Planet Symposium 2010, Bergen, June 27 - July 2 2010, Bergen, Norway.
http://icgem.gfz-potsdam.de/ICGEM/modelstab.html

Doerflinger, E., 1997. Utilisation de la méthode de positionnement satellitaire GPS pour la détermination précise des altitudes relatives et absolues. Thése de Doctorat, Université Montpellier II, Montpellier, France. 279 pp.

Doerflinger, E., Jiang, Z., Duquenne, H., Bayer, R., 1997. International Association of Geodesy Symposia, Vol. 177: Segawa et al (eds.), Gravity, Geoid and Marine Geodesy, Springer-Verlag Berlin Heidelberg.

Ellmann, A., Vanicek, P., 2007. UNB application of Stokes-Helmert's approach to geoid computation. J Geody 43(2): 200-213.

Forsberg, R., 1984. A study of terrain reductions, density anomalies and geophysical inversion methods in gravity field modelling. Scientific report No. 5, Ohio State University. 129 pp.

Forsberg, R., Tcsherning, C.C., 2008. An overview manual for the GRAVSOFT.

GOCO consortium, 2010. http://portal.tugraz.at/portal/page/portal/TU_Graz/Einrichtungen/Institute/Homepages/i5080/forschung/GOCO/

Haagmans, R., de Min, E., von Gelderen, M., 1993.Fast evaluation of convolution integralson the sphere using 1D FFT, and a comparison with existing methods for Stokes's integral. Manuscr Geod 18: 227-241.

Hamesh, M., Zomorrodian, H., 1992.Iranian gravimetric geoid determination, second step. NCC J Surveying 6: 17-24, 52-63.

Hashemian, M.S., 2005. Evaluation of the accuracy of SRTM elevation data over Iran. NCC Journal, No. 69: 6-9.

Hastings, DA., 1996.The global land 1-km base elevation (GLOBE) project.Boulder, Colorado National Geophysical Data Center.

Hatam, Y., Vanicek, P., Najafi Alamdari, M., Abolghasem, A.M., Soltanpour, A., Rafiey, S., Sedighi, M., Saadat, R., Gharakhani, J., 2006. Local geoid computation for Gheshm island. Technical report, NCC, Iran, pp. 84.

Hatam, Y., Djamour, Y., Vanicek, P., Bayer, R., Abolghasem, A.M., Hinderer, J., Mohammad Karim, M., Najafi Alamdari, M., Cheraghi, H., Saadat, R., Soltanpour, A., Sedighi, M., Nankali, H., Arabi, S., Azizian, N., Rafiey, S., 2008. The established Multi-purpose physical geodesy and geodynamics network of Iran (MPGGNI) for modelling the earth gravity field and its variations. Paper presented in annual Surveying and Geomatics Conference of NCC, Iran.
(http://www.ncc.org.ir/HomePage.aspx?TabID=4522&Site=NccPortal&Lang=fa-IR)

Hatam, Y., Bayer, R., Hinderer, J., Djamour, Y., Ghazavi, K., Sedighi, M., Luck, B., Le Moigne, N., Vanicek, P., Cheraghi, H., Saadat, R., Bahrampour, A., Asghari, H., Vanicek, P., Mohammad Karim, M., Le Moigne, N., Luck, B., Karpychev, M., Azizian, N., Cheraghi, H., Saadat, R., Bahrampour, A., Asghari, H.,

Meygooni, H, Rafiey, S., Tavakoli, F., Soltanpour, A., Azizian, N., Hossainali, M.M., Boy, J.P. Establishment of National Absolute Gravity Network of Iran: An opportunity to detect long-term and seasonal gravity changes, and their relation to crustal deformation and hydrology. To be submitted to Newton's Bulletin.

Hatam, Y., Bayer, R., Djamour, Y., Hinderer, J., Vanicek, P., Mohammad Karim, M., Le Moigne, N., Luck, B., Karpychev, M., Azizian, N., Cheraghi, H., Saadat, R., Bahrampour, A., Asghari, H., Meygooni, H. Establishment of National (Tele Cabin/ Land) Gravity Calibration Line of Iran (NGCLI10), and calibrating six Scintrex relative micro-gravimeters. To be submitted to Newton's Bulletin.

Heiskanen, W.A., Moritz, H., 1987. *Physical Geodesy*. Institute of Physical Geodesy, Technical University, Graz, Austria.

Jiang, Z., Duquenne, H., 1996. On combined adjustment of a gravimetrically determined geoid and the GPS levelling points, J Geod, No. 5.

Kearsley, A.H.W, 1985. Towards the optimum evaluation of the inner-zone contribution to geoidal heights, Aust. J. Geod., Photogramm. Surv., 42, 75-98.

Kiamehr, R., 2006. A strategy for determining the regional geoid by combining limited ground data with satellite-based global geopotential and topographical models: a case study of Iran. J Geoid 79: 602-612.

Lemoine, F. G., S.C. Kenyon, J.K. Factor, R.G. Trimmer, N.K. Pavlis, C.M.Cox, S.M. Klosko, S.B. Luthcke, M.H. Torrence, Y.M.Wang, R.G. Williamson, E.C. Pavlis, R.H. Rapp, and T.R. Olson, 1998.The Development of the Joint NASA GSFC and the National Imagery and Mapping Agency (NIMA) Geopotential Model EGM96. NASA/TP-1998-206861.

Li, Y.C., Sideris, M.G., 1994. Minimization and estimation of the geoid undulation errors. Bullletin Géodésique, Vol. 68, pp. 201-209.

Memarzadeh, Y., 1998. Refraction effect and statistical analysis of the Iranian first-order precise levelling data. Ms.c thesis, Dep. of Surveying Engineering, K. N. Toosi University, Tehran, Iran.

Nahavandchi, H., Soltanpour, A., 2005. High resolution geoid determination, Iranian Gravimetric geoid 2005 (IRGG05). Technical report, NCC, Iran, 121 pp.

Newton's Bulletin, 2009. External quality evaluation reports of EGM08. Issue No. 4, 334 pp.

Nilforoushan, F., 1995. Adjustment of Iranian GPS network. MSc thesis, Faculty of Civil Engineering, K.N. Toosi university of technology, Tehran, Iran.

Pavlis, N.A., H olmes, SA, Kenyon, SC, Factor, JK, 2008. An Earth Gravitational Model to degree 2160: EGM2008.Presented at the EGU General Assembly, Vienna, Austria, April, 13-18, 2008. Also, http://earth-info.nga.mil/GandG/wgs84/gravitymod/egm2008/

Rapp, R., Pavlis, N., 1990.The development and analysis of geopotential coefficient models to spherical harmonic degree 360. JGR 95(B13): 0148-022

Rapp, R.H., 1992. Computation and accuracy of global undulation models, Proc.Of the 6th International Geodetic Symposium on Satellite Positioning, pp. 865-871.

Safari, A., Ardalan, A. A., Grafarend, 2005. A new ellipsoidal gravimetric, satellite altimetry and astronomic boundary value problem, a case study: The geoid of Iran. J. Geodyn., 39: 545-568.

Safari, A., Hatam, Y., Shahaidari, M, 2008. Fixed gravimetric-altimetry boundary value problem for geoid determination on islands, case study: Geshm island. J. Physics of Earth and Space, 344: 81-104.

Sandwell, D. T., Smith, W. H. F., 1997.Marine gravity anomaly from Geosat and ERS-1 satellite altimetry: Ridge segmentation versus spreading rate. J. Geophys. Res., 102, B5: 10039-10054

Sandwell, D. T., Smith, W. H. F., 2009.Global marine gravity from retracked Geosat and ERS-1 satellite altimetry: Ridge segmentation versus spreading rate. J. Geophys. Res., 114, B01411, doi: 10.1029/2008JB006008.

Schwarz, K.P., Sideris, M.G., Forsberg, R., 1990. The use of FFT in physical geodesy. Geophys. J. Int., 100, 485-514.

Sharifi, M.A., Hatam, Y., Djamour, Y., Saadat, A., 2008. Determination of the earth's gravity field temporal variations using the GRACE satellites' monthly solutions and Its comparison with hydrology data in Iran. Technical report, NCC, Iran, 86 pp.

Sideris, M.G., 1990. Rigorous gravimetric terrain modelling using Molodensky's operator. Manuscr. Geod., 15, 97-106.

Strang van Hees, G., 1990. Stokes formula using fast Fourier techniques, Manuscr. Geod., 15, 235-139.

Strang van Hees, G., 2000. Some elementary relations between mass distributions inside the earth and the geoid and gravity field. J Geody 29, 111-123.

Tapely, B., Ries, J., Bettadpur, S., Chambers, D., Cheng M., Condi, F., Gunter, B., Kang, Z., Nagel, P., Pastor, R., Pekker, T., Poole, S., Wang, F., 2005. GGM02 – An improved Earth gravity field model from GRACE, J Geod, DOI 10.1007/s00190-005-0480-z.

Tscherning, C.C., 1985. Geoid modelling using collocation in Scandinavia and Greenland, Manuscr. Geod., 10, 136-149.

Vanicek, P., Kleusberg, A., 1987. The Canadian geoid-Stokesian approach. Manuscr Geod 12(2): 86-98.

Weber, G., Zomorrodian, H., 1988.Regional geopotential model improvement for the Iranian geoid determination. Bull. Géod., 62: 125-141.

Wenzel, H.G., 1985. Hochauflösende Kugelfunktionsmodelle für das Gravitationspotential der Erde. Wissenschaftliche Arbetien der Fachrichtung Vermessungswesen der Universität Hannover, Nr.137, Hannover, 1985.

Wessel, P., Kroneke, L.W., Bercovici, D., 1996. Pacific plate motion and undulations in geoid and bathymetry. Earth and Planetary Science Lettres 140, 53-66.

6. Conclusion et perspectives

Dans cette thèse, nous avons établi un nouveau modèle de géoïde gravimétrique qui, ajusté aux observations GPS/ nivellement du réseau national, a permis d'augmenter de manière significatives la précision de la surface de référence des altitudes sur l'Iran. Cependant, l'établissement d'un géoïde centimétrique reste un objective majeur à la fois sur le plan de la géodésie fondamentale et aussi pour répondre aux enjeux économiques. Pour cela, il est nécessaire dans le futur de densifier la couverture gravimétrique sur le territoire iranien en envisagent un ensemble des réseaux $1^{ére}$, $2^{éme}$ et $3^{éme}$ ordres aboutissent à une maille finale de ~3km pour une précision de l'ordre 0.01 à 1 mGal sur l'anomalie de pesanteur (Sideris, 1993 ; Vanicek and Martinec, 1994). Le calcul d'un géoïde de grande précision exige une transformation des anomalies de pesanteur dans un système de référence unique afin d'éviter les biais sur la surface de référence. En effet, un biais de 1 mGal sur l'ensemble des observations peut introduire une erreur de plusieurs mètres. Cette préoccupation nous a conduit à l'établissement d'un réseau gravimétrique absolu (NAGNI09) dont la maille est en moyenne de 300 km avec une précision meilleure que 5 μGal. Nous avons démontré sur deux exemples qu'il était indispensable de conserver une telle précision en évaluant la variation séculaire par réitération du réseau tout les 5 ans. Il s'agit là d'un enjeu important si nous souhaitons respecter l'hypothèse d'homogénéité des observations gravimétriques lors de l'établissement des réseaux MPGGNI10 ($1^{ére}$), $2^{éme}$ et $3^{éme}$ ordres. Nous avons montré aussi que les séries temporelles absolues en Iran pourraient contribuer à une meilleure connaissance des stokes d'eau et de la déformation tectonique actuelle en Iran. Par ailleurs, le couplage des mesures absolues de pesanteur aux mesures GPS aux marégraphes, en particulier sur le rivage de la mer Caspienne devrait permettre de différencier la déformation tectonique verticale de l'évolution du niveau moyen des mers bordant l'Iran. Il a été montré que l'établissement des réseuax gravimétriques sur le territoire aussi étendu que l'Iran nécessitait la connaissance précise des coefficients d'étalonnage des gravimètres relatifs, et leur évolution inter- annuelles. La ligne d'étalonnage NGCLI10 établie dans ce travail répond à ces préoccupations.

L'Iran dispose maintenant d'un réseau multi- observations géodésiques et gravimétriques, le MPGGNI10, de maille 55 km et aux nœuds duquel la pesanteur, la hauteur GPS et la hauteur de nivellement ont été mesurés respectivement avec une précision de 10-20 μGal, 1-3 cm, et 3mm$\sqrt{km}$. Les observations gravimétriques

ont été accordées au réseau absolu NAGNI09, tandis que les points GPS ont été positionnés dans l'IRTF. Les points nivelés ont été rattachés au système de référence des altitudes en Iran (Meamarzadeh, 1998).

Le calcul du géoïde gravimétrique a été opéré par la méthode classique de retrait – restoration couplée à la méthode de condensation de Helmert. Cette méthode classique s'est appuyée d'un point de vue calculassions sur le logiciel GRAVSOFT [Forsberg et Tcsherning, 2008] avec utilisation de la technique 1D FFT exposé par Haagmans et al, 1993. Le géoïde Iranien IRGeoid10 présenté a été confronté à plusieurs centaines des sités GPS/ nivelés permettant de le qualifier une moyenne de 0.02 m et une précision absolue de 0.26 m sur les différences. Le modèle amélioré de manière significative la précision des précédents modèles dont la précision n'était pas meilleure que 0.58 m. Nous avons mis en évidence la contribution importante des nouveaux modèles globaux issues des observations satellitaires GRACE et GOCE, à la bonne qualité de ce nouveau géoïde. Enfin, nous proposons une nouvelle surface de référence d'altitude qui sera d'une grande utilité pour la détermination des altitudes orthometriques à partir du positionnement GPS sur le territoire Iranien.

Comme nous l'avons déjà signalé, l'amélioration de la qualité du géoïde en Iran passera par la densification des mesures de pesanteur. Les travaux au sol pourraient être couplés par des levés gravimétriques aéroportés, sur les zones désertiques iraniennes difficiles d'accès, les chaînes de montagnes de l'Alborz et du Zagros et enfin sur les zones côtières afin d'assurer la continuité des observations gravimétriques au sol et altimétrique en mer.

7. Références

Afshar, H.K., Zomorrodian, H., 1970. The measurement and adjustment of the first order gravity network of Iran. Pub No 48, Institute of Geophysics, Tehran University, Tehran, Iran.

Allen, M.B., Jones, S., Ismail-Zadeh, A., Simmons, M., and Anderson, L., 2002, Onset of subduction as the cause of rapid Pliocene-Quaternary subsidence in the South Caspian basin: Geology, v. 30, p. 775–778, doi: 10.1130/ 0091-7613(2002)030<0775:OOSATC>2.0.CO;2.

Altamimi Z., P. Sillard, and C. Boucher, 2002, ITRF2000: A new release of the International Terrestrial Reference Frame for earth sciences applications, *J. Geophys. Res.*, *107* (B10), NIL_119-NIL_137.

Andersen, O.B., Hinderer, J., 2005. Global inter-annual gravity changes from GRACE: early results, Geophysical Research Letters 32 (1), 4.

Antoine, P., Bahain, J.-J., Berillon, G., Asgari Khaneghah, A., 2006. Tuf calcaire et se'quence alluvial en contexte tectonique actif : La formation de Baliran(province du Mazandaran,Iran), Quaternaire, 17 (4), 321-331.

Ardalan, A.A., 1999. high resolution regional geoid computation in the World Geodetic Datum 2000 based upon collocation of linearized observational functionals of the type gravity potential and gravity intensity. Phd dissertation, Stuttgart university. 250 pp.

Ardalan, A.A., Hatam, Y., Sharifi, M.A., Safari, A., Ghazavi, K., Motagh, M., 2001. High resolution geoid of Iran. Technical report, NCC, Iran, 155 pp
Ardalan, A.A., Hatam, Y., Ghazavi, K., Ghavamian, S., 2004. Standard and specifications for gravimetry. NCC, Iran.

Berberian, M., 1983. Continental Deformation in the Iranian Plateau, *Report* 52, Geological Survey of Iran

Bock Y., S. A. Gourevitch, C. C. Counselman, R. W. King, and R. I, 1986. Abbot, Interferometric analysis of GPS phase observations, *Manuscripta Geodaetica*, *11*, 282-288

Bock Y., J. Behr, P. Fang, J. Dean, and R. Leigh, 1997. Scripps Orbit and Permanent Array Center (SOPAC) and Southern Californian Permanent GPS Geodetic Array (PGGA), in *The Global Positioning System for the Geosciences*, pp. 55-61, Nat. Acad. Press, Washington, D.C.

Bonvalot, S., Diament, M., Gabalda, G., 1998. Continuous gravity recording with Scintrex CG-3M meters: a promising tool for monitoring active zones. Geophys. J. Int., 135: 470-494.
Bruinsma, S.L., Marty, J.C., Balmino, G., Biancale, R., Foerste, C., Abrikosov, O., Neumayer, H., 2010. GOCE Gravity Field Recovery by Means of the Direct Numerical Method.Presented at the ESA Living Planet Symposium 2010, Bergen, June 27 - July 2 2010, Bergen, Norway.
http://icgem.gfz-potsdam.de/ICGEM/modelstab.html

Bruns H., 1878: Die Figur der Erde. Berlin, Publ. Preuss. Geod. Inst.

Bomford G., 1971: Geodesy. 3rd edition, Clarendon Press.

Budetta, G., Carbone, D., 1997. Potential of application of the Scintrex CG-3M gravimeter for monitoring volcanic activity: results of field trials on Mt. Etna, Sicily. J. Volcanol. Geotherm. Res., 76: 199-214.

Cheraghi, H., Hatam, Y., Vanicek, P., Najafi Alamdari, M., Gharakhani, J., Djamour, Y., Saadat, A.R., 2007. Effect of lateral topographical mass density variations on the geoid in Iran, NCC Surveying Journal, No. 18, 21-30.

Corchete, V., Chourak, M., Khattach, D., 2005. The high-resolution gravimetric geoid of Iberia: IGG2005, Geophys. J. Int., 162, 676-684.

Corchete, V., 2010. The high-resolution gravimetric geoid of Italy: ITG2009, J. African Earth Sciences, 58, 580-584.

Crossley, D., Hinderer, J., Boy, J.P., 2005.Time variation of the European gravity field from superconducting gravimeters. Geophys. J. Int., 161: 257-264.

De Saint-Jean, B., 2008. Etude et Développement d'un système de gravimétrie mobel. Thèse de doctorat, Observatoire de Paris.

Djamour, Y., Vernant, P., Bayer, R., Nankali, H. R., Ritz, J.-F., Hinderer, J., Hatam, Y., Luck, B., Le Moigne, N., Sedighi, M. and Khorrami, F., GPS and gravity constraints on continental deformation in the Alborz mountain range, Iran. Geophysical Journal International, no. doi: 10.1111/j.1365-246X.2010.04811.x

Djamour, Y., Nankali, H., 2009. Historical background of using Global Positioning System (GPS) in different national projects, Journal of Surveying, NCC, No. 105, 2009

Defense Mapping Agency, 1979. Gravity stations data in the area 25-40 degree north and 43-65 degree east [4], Aerospace center, St. Louis air force stations.

Dehghani, G. A., Makris, J., 1984.The gravity field and crustal structure of Iran. Neues Jahrbuch Fuer geologie und Palaeontologie, Abhandlungen 168, 215-229.

Dias, F.J.S.S., Escobar, I.P., 2001.A model for adjustment of differential gravity measurements with simultaneous gravimeter calibration. J Geod 75: 151-156.

Doerflinger, E., 1997. Utilisation de la méthode de positionnement satellitaire GPS pour la détermination précise des altitudes relatives et absolues. Thése de Doctorat, Université Montpellier II, Montpellier, France. 279 pp.

Doerflinger, E., Jiang, Z., Duquenne, H., Bayer, R., 1997. International Association of Geodesy Symposia, Vol. 177: Segawa et al (eds.), Gravity, Geoid and Marine Geodesy, Springer-Verlag Berlin Heidelberg.

Ellmann, A., Vanicek, P., 2007. UNB application of Stokes-Helmert's approach to geoid computation. J Geody 43(2): 200-213.

Engalenc, M., 1968. Contribution à la Géologie, Géomorphologie, Hydrogéologie de la région de Teheran (Iran), Ph.D. thesis, 365 pp., Univ. of Montpellier II, Montpellier, France.

Farrell, W.E., 1972. Deformations of the Earth by surface loads. Reviews of Geophysics and Space physics 10 (3), 761-797.

Feigl K. L., D. C. Agnew, Y. Bock, D. Dong, A. Donnellan, B. H. Hager, T. A. Herring, D. D. Jackson, T. H. Jordan, R. W. King, S. Larsen, K. M. Larson, M. H. Murray, Z. Shen, and F. H. Webb, 1993. Space geodetic measurement of crustal deformation in central and southern California, *J. Geophys. Res.*, *98*, 21677-21712

Forsberg, R., 1984. A study of terrain reductions, density anomalies and geophysical inversion methods in gravity field modelling. Scientific report No. 5, Ohio State University. 129 pp.

Forsberg, R., Tcsherning, C.C., 2008. An overview manual for the GRAVSOFT.

Francis, O., van Dam, T., Germak, A., et al., 2010. Results of the European Comparison of Absolute Gravimeters in Walferdange (Luxembourg) of November 2007, IAG International Symposium on Gravity, Geoid and Earth Observation 2008, Crete, June 2008 (in press).

Gauss C.F., 1828: Bestimmung des Breitenunterschiedes zwischen den Sternwarten von Göttingen und Altona durch Beobachtungen am Ramsdenschen Zenithsector. Vanderschoeck und Ruprecht, Göttingen.

Ghazavi, K., tavakoli, F., 2003.National Gravity Calibration Line of Iran. Technical report, NCC.
GOCO consortium, 2010. http://portal.tugraz.at/portal/page/portal/TU_Graz/Einrichtungen/ Institute/ Homepages/i5080/forschung/GOCO/

Gradshteyn I.S., Ryzhik I.M., 1980: Table of Integrals, Series and Products. Corrected and enlarged edition, Translated by A. Jeffrey, Academic Press, New York.

Haagmans, R., de Min, E., von Gelderen, M., 1993.Fast evaluation of convolution integralson the sphere using 1D FFT, and a comparison with existing methods for Stokes's integral. Manuscr Geod 18: 227-241.

Hamesh, M., Zomorrodian, H., 1992.Iranian gravimetric geoid determination, second step. NCC J Surveying 6: 17-24, 52-63.

Hashemian, M.S., 2005. Evaluation of the accuracy of SRTM elevation data over Iran. NCC Journal, No. 69: 6-9.

Hastings, DA., 1996.The global land 1-km base elevation (GLOBE) project.Boulder, Colorado National Geophysical Data Center.

Hatam, Y., Djamour, Y., 2004. Multi-purpose Physical Geodesy and Geodynamics Network of Iran. Technical report, NCC, Iran, 28 pp.

Hatam, Y., Vanicek, P., Najafi Alamdari, M., Abolghasem, A.M., Soltanpour, A., Rafiey, S., Sedighi, M., Saadat, R., Gharakhani, J., 2006. Local geoid computation for Gheshm island. Technical report, NCC, Iran, pp. 84.

Hatam, Y., Djamour, Y., Vanicek, P., Bayer, R., Abolghasem, A.M., Hinderer, J., Mohammad Karim, M., Najafi Alamdari, M., Cheraghi, H., Saadat, R., Soltanpour, A., Sedighi, M., Nankali, H., Arabi, S., Azizian, N., Rafiey, S., 2008. The established Multi-purpose physical geodesy and geodynamics network of Iran (MPGGNI) for modelling the earth gravity field and its variations. Paper presented in annual Surveying and Geomatics Conference of NCC, Iran.
(http://www.ncc.org.ir/HomePage.aspx?TabID=4522&Site=NccPortal&Lang=fa-IR)

Hatam, Y., Bayer, R., Djamour, Y., Hinderer, J., Vanicek, P., Mohammad Karim, M., Le Moigne, N., Luck, B., Karpychev, M., Azizian, N., Cheraghi, H., Saadat, R., Bahrampour, A., Asghari, H., Meygooni, H. Establishment of National Absolute Gravity Network of Iran: An opportunity to detect long-term and seasonal gravity changes, and their relation to crustal deformation and hydrology. To be submitted to Newton's Bulletin.

Hatam, Y., Bayer, R., Djamour, Y., Hinderer, J., Vanicek, P., Mohammad Karim, M., Le Moigne, N., Luck, B., Karpychev, M., Azizian, N., Cheraghi, H., Saadat, R., Bahrampour, A., Asghari, H., Meygooni, H. Establishment of National (Tele Cabin/ Land) Gravity Calibration Line of Iran (NGCLI10), and calibrating six Scintrex relative micro-gravimeters. To be submitted to Newton's Bulletin.

Heck B., 1993: A revision of Helmert's second method of condensation in the geoid and quasigeoid determination. Presented at 7th I.A.G. Symposium „Geodesy and Physics of the Earth", No. 112, Potsdam, October 1992.

Hein, G.W. (1995). Progress in airborne gravimetry: Solved, open and critical problems. In : proceedings of the IAG Symposium on Airborne Gravity Field Determination, IUGG XXI General Assembly, Boulder, Colorado, USA, 2-14 july 1995.

Heiskanen W. H., Moritz H., 1967: Physical geodesy. W.H. Freeman and Co., San Francisco.
Heiskanen, W.A., Moritz, H., 1987. *Physical Geodesy*. Institute of Physical Geodesy, Technical University, Graz, Austria.

Helmert F.R., 1884: Die mathematische und physikalische Theorien der höheren Geodäsie, vol.2, B.G. Teubner, Leipzig.

Helmert F.R., 1890: Die Schwerkraft im Hochgebirge, insbesondere in den Tyroler Alpen. Veröff. Königl. Preuss. Geod. Inst., No.1.

Herring T. A., 2002. *GLOBK: Global Kalman filter VLBI and GPS analysis program, version 10.0*, Mass. Inst. of Technol., Cambridge

Hobson E.W., 1931: The theory of spherical and ellipsoidal harmonics. Cambridge University Press. Cambridge.

Huang J., 2002: Computational Methods for the Discrete Downward Continuation of the Earth Gravity and Effect of Lateral Topographical Mass Density Variation on Gravity and the Geoid. Ph.D. Thesis. UNB, Fredericton.

Jackson J. A., K. Priestley, M. Allen, and M. Berberian, 2002. Active tectonics of the South Caspian Basin, *Geophys. J. Int.*, *148*, 214-245.

Jacob, T., Bayer, R., Chery, J, and Le Moigne, N., 2010. Time lapse microgravity surveys reveal water storage heterogeneity of a karst aquifer, J. Geophys. Res. , 115, B06402, doi:10.1029/2009JB006616.

Jackson, J., 1983. Strength of the continental lithosphere : time to abandon the jelly sanwich?, *GSA Today*, *12* (9), 4-9.

Jiang, Z., Duquenne, H., 1996. On combined adjustment of a gravimetrically determined geoid and the GPS levelling points, J Geod, No. 5.

Kaviani A., A. Paul, E. Bourova, D. Hatzfeld, H. Pedersen, M. Mokhtari, 2007, A strong seismic velocity contrast in the shallow mantle across the Zagros collision zone (Iran), *Geophy. J. Int.*, 171, 399-410, doi: 10.1111/j.1365-246X.2007.03535.x.

Kearsley, A.H.W, 1985. Towards the optimum evaluation of the inner-zone contribution to geoidal heights, Aust. J. Geod., Photogramm. Surv., 42, 75-98.

Kiamehr, R., 2006. A strategy for determining the regional geoid by combining limited ground data with satellite-based global geopotential and topographical models: a case study of Iran. J Geoid 79: 602-612.

Kreye, C. ,Niedermeier, H., Heyen, R., Stelkens-Kobsch, T., Boedecker, G., 2006. Galileo and the Erath gravity field using GNSS for airborne gravimetry- an overview. In InsideGNSS 1.8. pp 53-65.

Lemoine, F. G., S.C. Kenyon, J.K. Factor, R.G. Trimmer, N.K. Pavlis, C.M.Cox, S.M. Klosko, S.B. Luthcke,

Li, Y.C., Sideris, M.G., 1994. Minimization and estimation of the geoid undulation errors. Bullletin Géodésique, Vol. 68, pp. 201-209.

Longman, I. M., 1959. “Formulas for computing the tidal accelerations due to the Moon and the Sun,” J. Geophys. Res., 64, 2351-2356.

McClusky S., S. Balassanian, A. Barka, C. Demir, S. Ergintav, I. Georgiev, O. Gurkan, M. Hamburger, K. Hurst, H. Kahle, K. Kasten, G. Kekelidze, R. W. King, V. Kotzev, O. Lenk, S. Mahmoud, A. Mishin, M. Nadariya, A. Ouzoumis, D. Paradissis, Y. Peter, M. Prilepin, R. Reilinger, I. Sanli, H. Seeger, A. Tealeb, M. N. Toksöz, and G. Veis, 2000. GPS constraints on plate motions and deformations in eastern Mediterranean and Caucasus, *J. Geophys. Res.*, *105*, 5695-5719

M.H. Torrence, Y.M.Wang, R.G. Williamson, E.C. Pavlis, R.H. Rapp, and T.R. Olson, 1998.The Development of the Joint NASA GSFC and the National Imagery and Mapping Agency (NIMA) Geopotential Model EGM96. NASA/TP-1998-206861.

Kellogg O.D., 1929: Foundations of potential theory. Springer. Berlin.
Listing J.B., 1873: Über unsere jetzige Kenntniss der Gestalt und Grösse der Erde. Nachrichten von der Köning. Göttingen VLG der Dietrichschen Buchhandlung.

Llubes, M., Florsch, N., Hinderer, J., Longuevergne, L., Amalvict, M., 2004. Local hydrology, the Global Geodynamics Project and CHAMP/GRACE perspective: some case studies. J. Geodyn., 38 (58): 355-374.

Lyard F., Lefevre, F., Letellier, T., Francis, O., 2006. Modelling the global ocean tides: modern insights from FES2004. Ocean Dynamics, 56(5-6): 394-415.

Mac Millan W.D., 1930: The theory of the potential, Dover, New York.

Mäkinen, J., Stahlberg, B., 1998. Long- term frequency stability and temperature response of a polarization-stabilized He–Ne laser, Measurements, 24, pp. 179–185.

Martinec Z., 1993: Effect of lateral density variations of topographical masses in view of improving geoid model accuracy over Canada. Final report of the contract DSS No. 23244-2-4356. Geodetic Survey of Canada, Ottawa.

Martinec Z. and Vaníček P., 1994a: Direct topographical effect of Helmert's condensation for a spherical approximation of the geoid. Manuscripta Geodaetica, No.19. Springer.

Martinec Z. and Vaníček P., 1994b: Indirect effect of topography in the Stokes-Helmert technique for a spherical approximation of the geoid. Manuscripta Geodaetica, No.19, Springer.

Martinec Z., 1996: Stability investigations of a discrete downward continuation problem for geoid determination in the Canadian Rocky Mountains. Journal of Geodesy, Vol. 70. Springer.

Martinec Z., Vaníček P., Mainville A., Véronneau M., 1996: Evaluation of topographical effects in precise geoid computation from densely sampled heights. Journal of Geodesy, Vol. 70, Springer.
Martinec Z., 1998: Boundary value problems for gravimetric determination of a precise geoid. Lecture notes in earth sciences, Vol. 73, Springer.

Memarzadeh, Y., 1998. Refraction effect and statistical analysis of the Iranian first-order precise levelling data. Ms.c thesis, Dep. of Surveying Engineering, K. N. Toosi University, Tehran, Iran.
Microg, 2007. 'g' 7.00 absolute gravity data acquisition and processing. In: M.-g. Solutions (Editor). Micro-g Solutions, Lafayette, Colorado,USA.

Microg, 2007. 'g' 7.0 absolute gravity data acquisition and processing. In: M.-g. Solutions (Editor). Micro-g Solutions, Lafayette,Colorado,USA.

Molodensky M.S., 1945: Fundamental problems of Geodetic Gravimetry (in Russian). TRUDY Ts NIIGAIK 42, Geodezizdat, Moscow.

Molodensky M. S., Yeremeev V. F., Yurkina M. I, 1960: Methods for Study of the External Gravitational Field and Figure of the Earth. TRUDY Ts NIIGAiK, 131, Geodezizdat, Moscow. English translat.: Israel Program for Scientific Translation, pp 248, Jerusalem 1962.

Moritz H., 1980: Advanced Physical Geodesy, H. Wichmann, Karlsruhe.

Nadjafi, M., Mashhadi, M., Hatam, Y., Tavakoli, F., 1998. Design of a gravity base network for Iran, Technical report, NCC, Iran. 51 pp.

Nadjafi, M., Mashhadi, M., Hatam, Y., Tavakoli, F., 2006. Design of a gravity base network, Journal of Allgemeine Vermessungs – Nachrichten (AVN), 11-12, 374-382, http://imperia.mi-verlag.de/imperia/md/upload/article/374_382_alamdari.pdf

Nahavandchi, H., Soltanpour, A., 2005. High resolution geoid determination, Iranian Gravimetric geoid 2005 (IRGG05). Technical report, NCC, Iran. 121 pp.

Neumeyer, J., Barthelmes, F., Dierks, O., Flechtner, F., Harnisch, M., Harnisch, G., Hinderer, J., Imanishi, Y., Kroner, C., Meurers, B., Petrovic, S., Reigber, Ch., Schmidt, R., Schwintzer, P., Sun, H.-P., Virtanen, H., , 2006. Combination of temporal gravity variations resulting from Superconducting Gravimeter recordings, GRACE satellite observations and global hydrology models. J Geod 79(10-11): 573-585, doi: 10.1007/S00190-005-0014-8

Newton's Bulletin, 2009. External quality evaluation reports of EGM08. Issue No. 4, 334 pp.

Niebauer, T.M., Sasagawa, G.S., Faller, J.E., Hilt, R., Klopping, F., 1995. A new generation of absolute gravimeters. Metrologia, 32, 159-180.

Niebauer, T.M., 1989. The effective measurement height of free-fall absolute gravimeters. Metrologia, 26,: 115-118.

Nilforoushan, F., 1995. Adjustment of Iranian GPS network. MSc thesis, Faculty of Civil Engineering, K.N. Toosi university of technology, Tehran, Iran.

Novák P., 2000: Evaluation of gravity data for the Stokes-Helmert solution to the geodetic boundary-value problem. Technical report No.207, GGE UNB, Fredericton.

Novák P., Vaníček P., Martinec Z., Véronneau M., 2001: Effect of the spherical terrain on gravity and the geoid. Journal of Geodesy, Vol.75, Springer.

Novák P., 2000: Evaluation of gravity data for the Stokes-Helmert solution to the geodetic boundary-value problem. Technical report, No. 207, UNB, Fredericton.
Pavlis, N.A., H olmes, SA, Kenyon, SC, Factor, JK, 2008. An Earth Gravitational Model to degree 2160: EGM2008.Presented at the EGU General Assembly, Vienna, Austria, April, 13-18, 2008. Also, http://earth-info.nga.mil/GandG/wgs84/gravitymod/egm2008/

Oral B., 1994. Global Positioning System (GPS) measurements in Turkey (1988-1992): Kinematics of the Africa-Arabia-Eurasia Plate collision zone, Cambrige, 344 pp. p., thesis

Paul, A., Kaviani, A., Hatzfeld, D., Vergne, J. & Mokhtari, M., 2006. Seismological evidence for crustal-scale thrusting in the Zagros mountain belt (Iran), *Geophys. J. Int.,* **166,** 227–237.

Paul, A., Hatzfeld, D., Kaviani, A., Tatar, M., Péquegnat, C., 2010. Seismc imaging of the lithospheric structure of the Zagros mountain belt (Iran), Geol. Soc. London. Spec. Pub., Feb. 2010.

Poursharifi, A., Aghamohammadi, A., Hatam, Y., Djamour, Y., Sedighi, M., Kasser, M., Asgari, J., Mohammadkarim, M., Arabi, S., Bayat, K., 2008. Construction of a motorised precise levelling system with the aim of replacing it for the existed foot precise levelling, NCC technical report, 2008.

Ralston A., 1965: A First Course in Numerical Analysis. McGraw-Hill, New York.

Ramillien, G., Cazenave A., Brunau, O., 2004. Global time variations of hydrological signals from GRACE satellite gravimetry, Geophys. J. Int., 158, 3, 813-826.

Ramillien, G., Lombard, A., Cazenave, A., Ivins, E. R., Llubes, M., Remy, F. Biancale, R. 2006. Interannual variations of the mass balance of the Antarctica and Greenland ice sheets from GRACE. *Global and Planetary Change,* 53, 198-208.

Rapp, R., Pavlis, N., 1990.The development and analysis of geopotential coefficient models to spherical harmonic degree 360. JGR 95(B13): 0148-022

Rapp, R.H., 1992. Computation and accuracy of global undulation models, Proc.Of the 6th International Geodetic Symposium on Satellite Positioning, pp. 865-871.

Rodell, M., P. R. Houser, U. Jambor, J. Gottschalck, K. Mitchell, C.-J. Meng, K. Arsenault, B.Cosgrove, J. Radakovich, M. Bosilovich, J. K. Entin, J. P. Walker, D. Lohmann, and D. Toll, 2004. The Global Land Data Assimilation System, Bull. Amer. Meteor. Soc., 85 (3), 381–394.

Safari, A., Ardalan, A. A., Grafarend, 2005. A new ellipsoidal gravimetric, satellite altimetry and astronomic boundary value problem, a case study: The geoid of Iran. J. Geodyn., 39: 545-568.
Safari, A., Hatam, Y., Shahaidari, M, 2008. Fixed gravimetric-altimetry boundary value problem for geoid determination on islands, case study: Geshm island. J. Physics of Earth and Space, 344: 81-104.

Sandwell, D. T., Smith, W. H. F., 1997.Marine gravity anomaly from Geosat and ERS-1 satellite altimetry: Ridge segmentation versus spreading rate. J. Geophys. Res., 102, B5: 10039-10054
Sandwell, D. T., Smith, W. H. F., 2009.Global marine gravity from retracked Geosat and ERS-1 satellite altimetry: Ridge segmentation versus spreading rate. J. Geophys. Res., 114, B01411, doi: 10.1029/2008JB006008.

Schwarz, K.P., Sideris, M.G., Forsberg, R., 1990. The use of FFT in physical geodesy. Geophys. J. Int., 100, 485-514.
Schwiderski, E. W., 1980. Ocean tides, II: a hydrological interpolation model, Marine Geodesy 3, 219-255.

Scintrex limited, 2006.CG-5 Scintrex Autograv System Operation Manual. Scintrex Limited, Concord, Ontarion.

Seigel, H.O., (1995). A guide to high precision land gravimeter surveys. Scintrex L.T.D, Concord, Ontraio, Canada.

Sharifi, M.A., Hatam, Y., Djamour, Y., Saadat, A., 2008. Determination of the Earth's Gravity Field Temporal Variations Using The GRACE Satellites' Monthly Solutions and Its Comparison with Hydrology Data in Iran.

Sideris, M.G., 1990. Rigorous gravimetric terrain modelling using Molodensky's operator. Manuscr. Geod., 15, 97-106.

Sideris M., Vaníček P., Huang J., Tsiavos I.N., 1999: Comparison of downward continuation techniques of terrestrial gravity anomalies, IUGG General Assembly, Birmingham, July 18 – 30.
Sjöberg L.E., 1998: The atmospheric geoid and gravity corrections. Bolletino di Geodesia e Scienze Affini, 57.

Sjöberg L.E., 1999: The IAG approach to the atmospheric geoid correction in Stokes' formula and a new strategy. Journal of Geodesy, Vol.73, Springer.

Stokes G.G., 1849: On the variation of gravity on the surface of the Earth. Transactions of the Cambridge Philosophical Society, No. 8.

Strang van Hees, G., 1990. Stokes formula using fast Fourier techniques, Manuscr. Geod., 15, 235-139.

Strang van Hees, G., 2000. Some elementary relations between mass distributions inside the earth and the geoid and gravity field. J Geody 29, 111-123.

Sun W., Vaníček P., 1998: On some problems of the downward continuation of the 5'x 5' mean Helmert gravity disturbance. Journal of Geodesy, Vol. 72. Springer.

Tamura Y., 1987.A harmonic development of the tide-generating potential. Bull. d'Inf. Marées Terrestres, 99, 6813-6855.

Tapley, B.D., Bettadpur, S., Ries, J.C., Thompson, P.F., Watkins, M.M., 2004. GRACE Measurements of mass variability in the earth system. *Science* 23 July 2004, 305, 5683, 503-505.
Tapely, B., Ries, J., Bettadpur, S., Chambers, D., Cheng M., Condi, F., Gunter, B., Kang, Z., Nagel, P., Pastor, R., Pekker, T., Poole, S., Wang, F., 2005. GGM02 – An improved Earth gravity field model from GRACE, J Geod, DOI 10.1007/s00190-005-0480-z.

Tscherning, C.C., 1985. Geoid modelling using collocation in Scandinavia and Greenland, Manuscr. Geod., 10, 136-149.

Torge, G., 1989. Gravimetry, Walter de Gruyter & Co., Berlin, 465 pp.

Timmen, L., 2003. Precise definition of the effective height of free- fall absolute gravimeters. Metrologia, 40, 62, doi: 10.1088/0026-1394/40/2/310

Ukawa, M., Nozaki, K., Ueda, H., Fujita, E., 2010. Calibration shifts in Scintrex CG-3M gravimeters with an application to detection of microgravity changes at Iwo-tou caldera, Japan. Geophysical Prospecting, 47: 73-83

Van Camp, M., S. D. P. Williams, O. Francis (2005). Uncertainty of absolute gravity measurements, J. Geophys. Res., 110, B05406, doi: 10.1029/2004JB003497

Vaníček P., Krakiwsky E., 1986: Geodesy, The concepts (second edition), Elsevier Science B.V., Amsterdam.

Vanicek, P., Kleusberg, A., 1987. The Canadian geoid-Stokesian approach. Manuscr Geod 12(2): 86-98.

Vaníček P., Christou N., 1993: Geoid and its geophysical interpretations. CRC Press, Boca Raton, Fla., USA. 343 pp.

Vaníček P., Martinec Z., 1994: The Stokes-Helmert scheme for the evaluation of a precise geoid. Manuscripta Geodaetica, No.19., Springer.
Vaníček P., Najafi M., Martinec Z., Harrie L., Sjöberg L.E., 1995: Higher-degree reference field in the generalised Stokes-Helmert scheme for geoid computation. Journal of Geodesy, Vol. 70, Springer.

Vaníček P., Huang J., Novák P., Pagiatakis S.D., Véronneau M., Martinec Z., Featherstone W.E., 1999: Determination of the boundary values for the Stokes-Helmert problem, Journal of Geodesy, Vol.73, Springer.

Viterbo, P., Beljaars, A.C.M, 1995. An improved land surface parameterization scheme in the ECMWF model and its validation, J. Climate, 8, 2716-2748.

Wahr, J., Swenson, S., Zlotnicki V., Velicogna, I., 2004. Time-variable gravity from GRACE: first results, Geophys. Res. Lett., 31**,** L11501*,* doi:10.1029/2004GL019779.

Weber, G., Zomorrodian, H., 1988.Regional geopotential model improvement for the Iranian geoid determination. Bull. Géod., 62: 125-141.

Wenzel, H.G., 1985. Hochauflösende Kugelfunktionsmodelle für das Gravitationspotential der Erde. Wissenschaftliche Arbetien der Fachrichtung Vermessungswesen der Universität Hannover, Nr.137, Hannover, 1985.

Wenzel H.G., 1996. The Nanogal software: earth tide data processing package ETERNA 3.30. Bull. Inf. Marées Terrestres , 124, 9425-9439.

Wessel, P., Kroneke, L.W., Bercovici, D., 1996. Pacific plate motion and undulations in geoid and bathymetry. Earth and Planetary Science Lettres 140, 53-66.
Wichiencharoen C., 1982: The indirect effects on the computation of geoid undulations. Dept. of Geod. Sci. Report No.336, Ohio State University, Columbus.
Zomorrodian, H., 1971. The measurements and adjustments of the second order gravity network in Iran, Pub. No. 53, IGTU, Tehran.

Zomorrodian, H., 1985.The Iranian National Calibration Line 1985. Technical Report of the Institute of Geophysics, Tehran University

Zomorrodian, H., 1987.The establishment of the Iranian Gravity Datum, Bureau Gravimetrique International, Bul. Information, 60.

Zumberge, M. A., 1981.A portable apparatus for absolute measurement of the earth's gravity, PhD Thesis, University of Colorado at Boulder.

8. Annexes

1. Annexe 1: Autres articles publiés

Article1: GPS and gravity constraints on continental deformation in the Alborz mountain range, Iran

(Geophysical Journal International, 2010)

Article2: Fixed gravimetric-altimetry boundary value problem for geoid determination on islands, case study: Qeshm island

(Journal of the Earth and Space Physics, 2008, Vol. 34, No. 4, 81-104)

Article3: Design of a Gravity Base Network

(Journal of AVN - Allgemeine Vermessungs-Nachrichten, 2006, No. 11-12, 374-382)

Geophysical Journal International

Geophys. J. Int. (2010) doi: 10.1111/j.1365-246X.2010.04811.x

GPS and gravity constraints on continental deformation in the Alborz mountain range, Iran

Yahya Djamour,[1•*] Philippe Vernant,[1] Roger Bayer,[1] Hamid Reza Nankali,[2] Jean-François Ritz,[1] Jacques Hinderer,[3] Yaghoub Hatam,[1•2] Bernard Luck,[3] Nicolas Le Moigne,[1] Morteza Sedighi[2] and Fateme Khorrami[2]

[1]Lab. Geosiences Montpellier, University Montpellier 2 – CNRS, 34095 Montpellier, France. E-mail: pvernant@um2.fr
[2]National Cartographic Center (NCC), Meraj Av., Azadi square, P.O. Box 13185–1684, Tehran, Iran
[3]EOST/IPGS (UMR 7516) 5 rue Descartes, 67084 Strasbourg Cedex, France

Accepted 2010 September 13. Received 2010 September 13; in original form 2010 April 28

SUMMARY

A network of 54 survey GPS sites, 28 continuous GPS stations and three absolute gravity (AG) observation sites have been set up in the Alborz mountain range to quantify the present-day kinematics of the range. Our results allow us to accurately estimate the motion of the South Caspian block (SCB) for the first time, and indicate rotation of the SCB relative to Eurasia, accounting for the left lateral motion in the Alborz range. In light of these new results, it clearly appears that deformation rates vary along the range, the eastern part accommodating mainly left lateral strike slip (2 mm yr^{-1} south of the range and 5 mm yr^{-1} north of the range) with a very low range normal shortening rate on the Khazar thrust fault (• 2 mm yr^{-1}), and the western part accommodating range normal shortening (• 6 mm yr^{-1}) on the Khazar thrust fault with a left lateral component of • 2 mm yr^{-1} north of the range and 1 mm yr^{-1} south of the range. These present-day kinematics agree with geomorphologic estimated slip rates, but not the long-term deformation, corroborating the idea that the kinematics of the range have changed recently due to the change of SCB motion.

Modelling of the interseismic deformation suggests a deep locking depth on the central-western segment of the Khazar fault (• 30 km) in agreement with the Baladeh earthquake rupture and aftershock ranging between 10 and 30 km. Given this unusual deep locking depth and the 34° dip of the thrust, a large part of the Alborz range is located above the seismically coupled part of the fault. Based on our AG measurements this part of the range seems to uplift at a rate of 1–5 mm yr^{-1}, in agreement with terrace uplift.

Key words: Satellite geodesy; Gravity anomalies and Earth structure; Plate motions; Intraplate processes; Neotectonics.

1 INTRODUCTION

The Alborz mountain range encircles the South Caspian Basin from the Talesh to the Kopeh Dag mountains (Fig. 1). Numerous active faults strike mainly parallel to the belt and form a 'V' shaped pattern (Berberian 1983; Berberian & Yeats 2001; Allen et al. 2003b; Ritz et al. 2006), with WNW–ESE trending faults in Western Central Alborz passing abruptly to ENE–WSW trending faults in the Eastern Central Alborz (Fig. 1). Numerous strong historical earthquakes are reported in the Central Alborz (Tchalenko 1975; Ambraseys & Melville 1982; Berberian & Yeats 1999; Berberian & Yeats 2001) indicating rather high seismic activity, a result supported by the instrumental seismicity (Engdahl et al. 2006). The centroid moment tensors (CMT) of the Harvard Catalogue for earthquakes larger than M_w 5.0 (http://www.globalcmt.org) and complemented by the CMT solutions computed by Jackson et al. (2002) for events larger than M_w 5.4 (Fig. 1) show that the present-day deformation in Alborz is characterized by range-parallel left-lateral strike-slip and thrust faults. Located at the immediate southern foothills of the Central Alborz, historical sites in the Tehran region have been destroyed several times by earthquakes in the past (Ambraseys & Melville 1982; Berberian & Yeats 1999) and the present-day Tehran megapole (12 million people) is facing a critical seismic hazard. No large earthquake has occurred since 1830, but the recent M_w 6.2 Baladeh earthquake in 2004 (Tatar et al. 2007), though 70 km further north (Fig. 1), served as a reminder of the risk encountered if one of the closer faults break, which is likely to occur since most of the deformation is accommodated by seismic processes (Masson et al. 2005).

*Now at: Geomatics College, National Cartographic Center (NCC), Meraj Av., Azadi square, P.O. Box 13185-1684, Tehran, Iran.

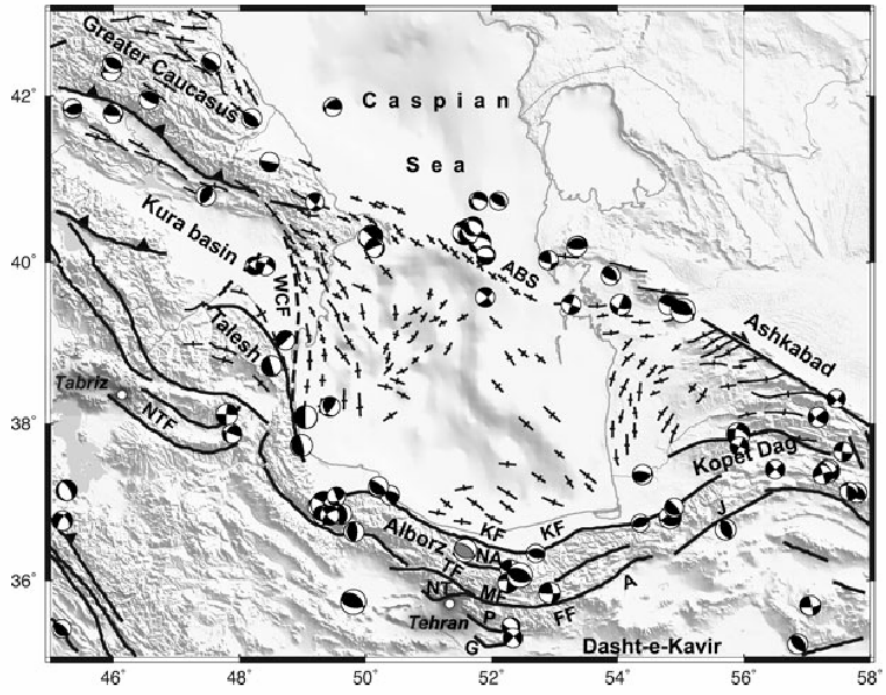

Figure 1. Summary structural map adapted from Jackson et al. (2002), the black focal mechanisms are from Jackson et al. (2002), the grey one (Baladeh earthquake) is from Tatar et al. (2007). A, Astaneh fault; ABS, Apsheron-Balkhan sill; FF, Firuzkuh fault; G, Garmsar fault; J, Jajarm fault, KF, Khazar fault; MF, Mosha fault; NA, North Alborz fault, NT, North Tehran fault; NTF, North Tabriz fault; P, Parchin fault; TF, Taleghan fault; WCF, West Caspian fault.

The main active thrust structures bound the range to the north (North Alborz and Khazar (hidden) south-dipping thrust faults, Fig. 1) and to the south (North Tehran, Garmsar and Parchin north-dipping thrust faults), while the left-lateral strike-slip deformation concentrates inside the mountain range, in its southern half, along the Taleghan, Mosha, Firuzkuh and As left-lateral strike slip faults. In terms of historical seismicity, three historical earthquakes with magnitudes greater than 6.5 occurred along the eastern part of the northern faults during the last two centuries, and active microseismicity is present in this area (Ashtari et al. 2005). On the southern side of the range, three historical earthquakes were reported in 958 AD (M_s • 7.7), 1665 AD (M_s • 6.5) and 1830 AD (M_s • 7.1) (Berberian & Yeats 1999). From morphotectonics and structural analyses, Allen et al. (2003a) and Bachmanov et al. (2004) deduced the left-lateral motion of the Mosha fault, to which the later authors identified an additional reverse component. Analyzing the morphology in detail with digital elevation models and palaeoseismology, Ritz et al. (2006) and Nazari et al. (2009) concluded that the left-lateral motion along the Taleghan–Mosha–Firuzkuh faults was associated with normal faulting, and that these transtensional kinematics are active since the Middle Pleistocene (• 1.5 Myr), implying a recent change in the tectonic regime as suggested also by Landgraf et al. (2009) and Solaymani et al. (2010). The present-day microseismicity south of the range is mainly concentrated near the eastern branch of the Mosha fault and the focal mechanism solutions are consistent with the left-lateral normal motion observed along a steep north-dipping fault Ashtari et al. (2005). The North Tehran and the Parchin thrust faults dip northward and limit the relief of the Central Alborz to the south and could have been the sources of historical earthquakes in 312–280 BC (M_s • 7.6), 743 (M_s • 7.2), 855 (M_s • 7.1), 1177 (M_s • 7.2) and 1384 AD (Ambraseys & Melville 1982; Berberian & Yeats 1999).

The recent geodynamic evolution of the Central Alborz has been attributed to strain partitioning of oblique shortening (Jackson et al. 2002; Allen et al. 2003b). This would be the result of a transpressive regime that started during the Pliocene (3–5 Ma) and would be associated with the southwestward displacement of the South Caspian Basin with respect to the Central Iran Block. Before this epoch and since the Miocene, NS shortening occurred in Alborz and was distributed on fan shaped thrusts dipping inwards from the limits of the belt, associated with right-lateral and left-lateral strike-slip movements within the western and eastern parts of the range, respectively (Allen et al. 2004). This tectonic setting resulted in an uplift of the central part of the belt between 6 and 4 Ma (Axen et al. 2001). On the base of estimates of slip rates and total displacements along left-lateral strike-slip faults (i.e. Astaneh, Jajarm faults, Fig. 1), Hollingsworth et al. (2008) proposed that the strain partionning in Alborz associated with the southwestward motion of the South Caspian Basin was two times older (i.e. 10 Ma).

On the other hand, Ritz et al. (2006) proposed that the motion of the South Caspian Basin (southwestward motion and clockwise rotation) was much younger. Their interpretation is based on the fact that the general left-lateral wrenching of the belt (which is related to the South Caspian Basin motion) shows a normal component due to the obliquity of some of the faults (e.g. Taleghan, Mosha) with respect to the general trend of the range, and that the cumulated topography associated with this normal component is small and has not yet reversed the relief. Ritz et al. (2006) point out that the kinematical change (from mainly reverse to left-lateral-normal) occurs contemporaneously with the Damavand volcanic activity.

The first estimation of the present-day kinematic of the central Alborz results from a survey mode GPS (SGPS) profile across the central Alborz (Vernant et al. 2004a). However, the SGPS sites were sparse and only the bulk N–S shortening (5 • 2 mm yr• 1) and a global left lateral motion (4 • 2 mm yr• 1) could be estimated. Since then, several more SGPS sites have been implemented as well as a continuous GPS (CGPS) network. Moreover, precise absolute gravity (AG) measurements have been repeated across the range in order to better constrain the uplifting rate.

In this paper, we present our latest GPS velocity field and we interpret the present-day kinematics of the Alborz mountain range using an elastic block model. We use the gravity measurements to estimate the rate of uplift of the range. Then, we combine these results to investigate the active tectonics and geodynamics of the region.

2 GPS OBSERVATIONS AND PROCESSING

Our network consists of 54 SGPS sites implemented in the Alborz in the framework of a cooperative program between the French Centre National de la Recherche Scientifique (CNRS) and the Iranian National Cartographic Center (NCC) and 28 CGPS sites implemented by the NCC. This network spreads from the Caspian Sea to the north to the Central Iranian desert to the south (Fig. 2). Average distance between two sites is 10 km around Tehran and 30–70 km elsewhere. Most of the sites are anchored in bedrock. The others consist of geodetic pillars or concrete blocks installed in consolidated sediments.

The SGPS sites were surveyed at least three times from 2000 to 2008. All SGPS sites were measured with Ashtech Z12 and Trimble 4000SSI receivers equipped with choke-ring antennas. The CGPS sites were installed since 2005, and all but FOIM have at least three years of continuous recording.

We use the GAMIT/GLOBK software package (Herring et al. 2009a,b,c) to compute the coordinates and velocities of the sites, using a three-step strategy (Feigl et al. 1993; Dong et al. 1998). GPS data of 14 IGS stations were introduced in the process to tie our local network to the ITRF reference frame. Our local quasi-observations were combined with the global quasi-observations provided by MIT (http://www-gpsg.mit.edu/simon/gtgk/index.htm) from 1996 to 2008 day of year 245. Following Reilinger et al. (2006), we account for the correlated errors in the time-series by calculating a unique noise model for each CGPS station. The algorithm used to model the data noise spectrum assumes that each time-series can be adequately modelled using a first-order Gauss Markov (FOGM) process noise (Gelb 1974). The FOGM is estimated from individual stations time-series by averaging the residuals over increasingly longer intervals that range from a minimum of 7 d to a maximum of 1/10th of the total time-series span. For each interval we compute the Chi-square per degree of freedom (d.o.f.). To the opposite of a white process noise, the Chi-square/d.o.f. values of non-white noise spectra increase with increasing averaging time. The

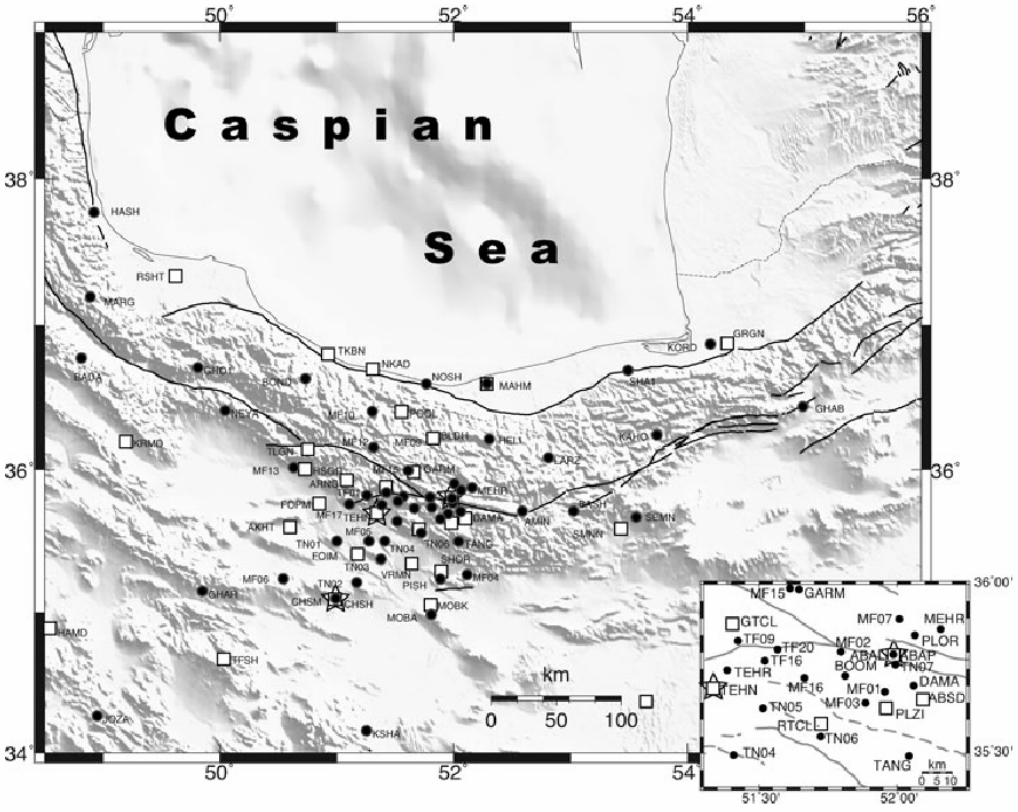

Figure 2. Location of the CGPS (squares), SGPS (circles) and gravity (stars) sites used in this study, the inset is for the eastern Tehran region.

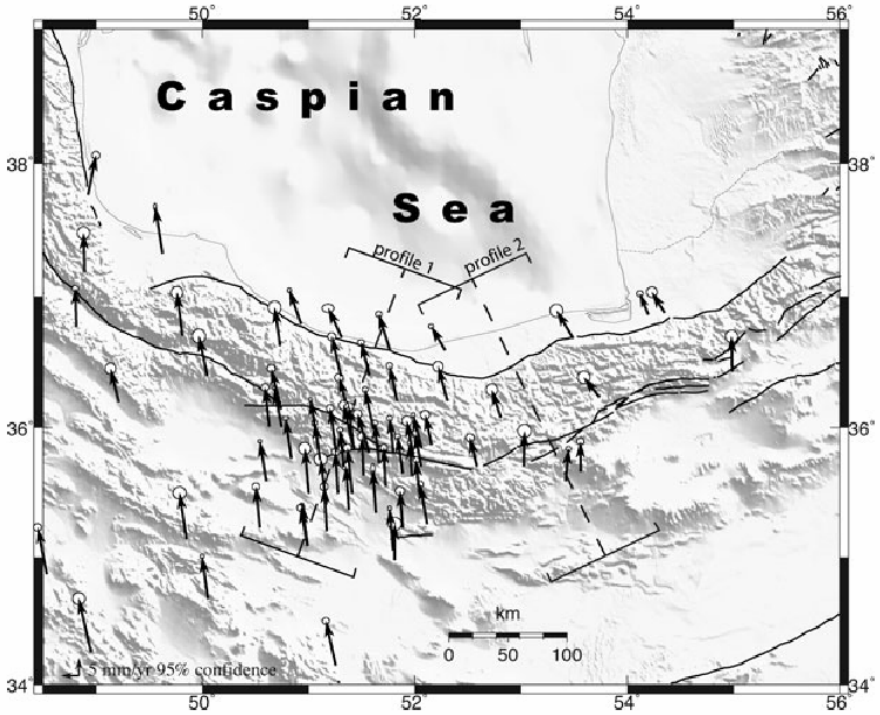

Figure 3. Map showing decimated GPS velocities and 95 per cent confidence ellipses relative to Eurasia determined in this study (all velocities are given in Table 1). The location and width of the two trans-Alborz velocity profiles plotted in Fig. 8 are also shown.

interval averaged Chi square/d.o.f. values are then fit to the FOGM model where a correlation time and long-term variance are estimated. This estimated FOGM model is then used to predict the site velocity uncertainty based on the time span of the time-series. The equivalent random-walk noise values obtained for the Alborz CGPS sites range from 0.25 to 1.2 mm $(\dot{\ }\ \bar{y}r)^{\cdot 1}$ in horizontal and 0.8–4.1 mm $(\dot{\ }\ \bar{y}r)^{\cdot 1}$ in vertical. The upper value of 1.2 mm $(\dot{\ }\ \bar{y}r)^{\cdot 1}$ in horizontal is for one station (VRMN), all the other being less or equal to 0.8 mm $(\dot{\ }\ \bar{y}r)^{\cdot 1}$, therefore we choose to use this value to estimate the SGPS horizontal uncertainties. For the vertical random walk noise value, 4.1 mm $(\dot{\ }\ \bar{y}r)^{\cdot 1}$ corresponds to the CGPS site PLOR, all the others are less or equal to 3 mm $(\dot{\ }\ \bar{y}r)^{\cdot 1}$, therefore we use 3 mm $(\dot{\ }\ \bar{y}r)^{\cdot 1}$. Finally, velocities and their 1• confidence uncertainties were estimated in ITRF2005 and then the Eurasian reference frame was defined by minimizing the horizontal velocities of 23 IGS stations located in Europe and Central Asia (ARTU, BOR1, BRUS, GRAS, GRAZ, IRKT, JOZE, KOSG, KSTU, MADR, METS, NYAL, ONSA, POTS, TIXI, TOUL, TROM, VILL, WTZR, YAKT, ZECK, ZIMM and ZWEN). The WRMS value for the velocity residuals of these 23 sites is 0.48 mm $yr^{\cdot 1}$. There is good agreement between the SGPS and CGPS velocities for nearby Iranian sites since the differences are lower than 1 mm $yr^{\cdot 1}$. The GPS velocities and their uncertainties are shown on Fig. 3 and given in Table 1 in a Eurasia-fixed reference frame.

3 GPS VELOCITY FIELD AND BLOCK MODEL

The most striking, and systematic aspect of the velocity map shown in Fig. 3 is the azimuth change of the vectors from almost due north for the sites south of the Alborz range to NNW for the sites along the south Caspian shore. This indicates that, as noted earlier (Jackson et al. 2002; Allen et al. 2003a; Bachmanov et al. 2004; Vernant et al. 2004b; Ritz et al. 2006), left lateral strike slip is occurring in the Alborz range. Another striking aspect is the rather abrupt change in velocity along the south Caspian shoreline. Indeed, velocities north of the western Alborz (RSHT, TKBN, NKAD and NOSH) are • 3 mm $yr^{\cdot 1}$ faster than the eastern sites (MAHM, SHA1, KORD and GRGN) in the Eurasia fixed reference frame. Furthermore, the site SHA1 shows a velocity that is in between the average velocities of the eastern and western sites. This suggests that the GPS sites northeast of Alborz are farther away from the main active thrust fault than the northwestern GPS sites, consistent with the mapped location of the Kahzar thrust fault except for the site RSHT. Another explanation could be that western and eastern Alborz have different kinematics.

To investigate further this issue and to estimate fault slip rates for the main active faults, we use a block model. Several authors (e.g. McCaffrey 2002; Meade et al. 2002; Meade & Hager 2005) have demonstrated that, to first order, elastic block models can be used to fit the interseismic velocity field. No significant earthquake has occurred during the time interval of the measurements and the time-series of the closest SGPS sites (MF09, MF10, MF12 and NOSH) and CGPS sites (POOL and BLDH) from the Baladeh earthquake (M_w 6.2, 2004) do not show any significant coseismic nor post-seismic deformation. Furthermore, the last large earthquake of the region occurred in 1935. Hence our GPS measurements depict the interseismic deformation of the Alborz mountain range. We use McCaffrey's code (McCaffrey 2002) to solve for relative block motions by minimizing the GPS residual motions within the blocks in a least-square sense. The elastic strain accumulation on block

Table 1. East and north GPS velocity components (E Vel., N Vel.) and 1σ uncertainties (σ E, σ N) in a Eurasia-fixed reference frame as determined in this study are given in mm yr^{-1}. The correlation between E and N velocities (σ EN), residual velocities (Res E, Res N) from our preferred block model, are also given. An '*' in the site column designates continuous GPS stations. Block abbreviations are EU, Eurasia; AL, Alborz; CIB, central Iranian block; KA, Dasht-e-Kavir region; SCB, South Caspian Block.

Lon. (°E)	Lat. (°N)	E Vel.	N Vel.	σ E	σ N	σ EN	Site	Block	Res. E	Res. N
51.986	35.793	1.17	9.96	0.52	0.51	0.014	ABAL	AL	0.84	0.63
51.987	35.793	1.84	9.58	0.58	0.58	−0.002	ABAP*	AL	0.17	0.25
52.586	35.701	2.01	8.2	0.47	0.46	0.01	AMIN	AL	−0.19	−0.87
51.829	36.208	2.02	9.36	0.49	0.31	0.001	BLDH*	AL	0.63	−0.75
50.732	36.623	1.52	10.85	0.74	0.76	0.004	BOND	AL	0.51	−0.2
51.646	35.985	2.18	10.41	0.2	0.36	0.002	GARM*	AL	0.19	0.56
49.812	36.699	1.53	12.29	0.68	0.71	−0.002	GHO1	AL	−0.13	−0.22
48.922	37.764	2.25	11.28	0.44	0.46	0.002	HASH	AL	2.17	−0.74
52.305	36.206	2.57	9.68	0.58	0.56	0.023	HELI	AL	0.65	0.6
53.739	36.236	4.38	5.56	0.71	0.72	0.003	KAHO	AL	−2.23	−2.1
52.811	36.078	2.57	7.87	0.68	0.69	0.001	LARZ	AL	0.63	−0.42
48.891	37.187	0.33	10.98	0.7	0.72	−0.011	MARG	AL	0.37	−2.63
52.157	35.868	1.79	8.52	0.52	0.52	0.009	MEHR	AL	0.53	−0.8
51.797	35.801	1.04	10	0.33	0.33	0.001	MF02	AL	0.89	0.42
52.008	35.897	0.48	8.37	0.33	0.34	0	MF07	AL	1.85	−1.17
51.833	36.205	2.15	9.87	0.36	0.36	0.004	MF09	AL	0.51	−0.23
51.304	36.394	2.62	11.08	0.46	0.47	−0.002	MF10	AL	0.12	0.55
51.315	36.15	1.23	11.63	0.54	0.54	0.006	MF12	AL	1.13	1.22
51.613	35.988	2.46	11.26	0.33	0.33	−0.005	MF15	AL	−0.1	1.4
51.768	36.586	3.22	10.37	0.37	0.34	0.005	NOSH	AL	0.06	1.33
52.064	35.85	2.39	9.12	0.23	0.29	−0.002	PLOR	AL	−0.16	−0.24
51.574	36.403	2.42	9.12	0.39	0.33	−0.001	POOL*	AL	0.5	−0.86
49.624	37.323	2.07	13.26	0.17	0.41	−0.002	RSHT*	AL	−0.85	0.75
53.492	36.679	4.71	7.93	0.74	0.76	0.006	SHA1	AL	−1	1.3
51.994	35.763	1.83	9.34	0.47	0.48	0.012	TN07	AL	0.08	0.03
54.353	36.876	3.63	5.83	0.61	0.61	0	GRGN*	SCB	−0.3	0.71
54.199	36.86	2.41	6	0.36	0.34	0.006	KORD	SCB	0.97	0.73
52.285	36.588	3.94	6.79	0.29	0.26	0.001	MAHM*	SCB	−0.3	−0.49
51.31	36.685	3.82	8.38	0.66	0.49	0	NKAD*	SCB	−0.48	−0.21
57.308	37.814	2.9	3.49	0.44	0.41	0.013	SHIR	SCB	−0.31	1.68
50.93	36.786	3.3	9.68	0.24	0.26	−0.001	TKBN*	SCB	−0.19	0.62
48.005	37.169	0.77	12.46	0.53	0.54	0.006	AGKA	CIB	0.97	0.31
53.822	32.313	1.14	13.47	0.33	0.32	−0.001	ARDA	CIB	−0.58	−0.5
48.814	36.764	0.34	11.07	0.35	0.35	0.001	BADA	CIB	1.48	−1.73
54.832	29.363	0.77	13.73	0.41	0.39	0.003	BES2	CIB	−1.16	−0.6
47.93	36.232	2.13	12.99	0.35	0.35	0.002	BIJA	CIB	−0.36	−0.21
48.183	36.607	0.34	11.52	0.66	0.69	−0.009	DAND	CIB	2.19	−1.48
56.504	28.529	4.64	13.95	1.04	0.95	−0.017	DENA	CIB	3.92	−0.04
49.851	35.14	1.97	13.08	0.74	0.72	0	GHAR	CIB	−0.65	−0.4
57.217	28.01	2.07	14.69	0.98	0.89	−0.005	GHOL	CIB	1.66	0.61
48.534	34.869	2.55	13.24	0.45	0.44	−0.002	HAMD*	CIB	−1.17	−0.2
54.608	30.079	0.69	13.3	0.41	0.38	−0.001	HARA	CIB	0.46	−1.12
48.952	34.256	3.47	15.25	0.73	0.7	0	JOZA	CIB	−2.26	1.74
57.119	30.277	0.45	15.63	0.53	0.45	0	KERM	CIB	1.26	2.5
54.126	29.923	1.29	14.25	0.41	0.39	0.006	KHO2	CIB	−1.48	−0.07
50.458	33.157	2.81	12.9	0.75	0.72	0.005	KHON	CIB	−1.98	−0.88
47.123	37.368	2.87	12.9	0.55	0.57	0.011	KHOR	CIB	−1.1	1.05
49.211	36.196	2.3	9.44	0.61	0.61	0	KRMD*	CIB	−0.51	−3.61
51.255	34.15	2.78	12.7	0.4	0.38	−0.002	KSHA	CIB	−1.43	−0.6
46.162	36.908	2.31	13.47	0.37	0.35	0.001	MIAN	CIB	−0.38	0.4
51.799	32.25	2.58	13.75	0.74	0.7	0.004	QOMS	CIB	−2.08	−0.28
45.887	38.228	1.43	11.93	0.37	0.37	0.006	SHAB	CIB	2.68	−3.37
50.748	32.367	2.34	12.51	0.4	0.37	−0.005	SHAH	CIB	−1.66	−1.25
49.668	33.073	0.75	13.5	0.74	0.71	0.001	SHOL	CIB	0.18	−0.05
46.343	38.056	0.74	13.51	0.52	0.53	0	TABZ*	CIB	0.1	−4.19
50.052	34.676	1.64	12	0.24	0.24	−0.003	TFSH*	CIB	−0.46	−1.6
52.091	35.661	2	7.95	0.14	0.19	−0.003	ABSD*	KA	−0.59	−2.22
50.601	35.588	1.77	11.31	0.24	0.18	−0.003	AKHT*	KA	−0.59	−0.72
51.075	35.928	1.69	10.61	0.23	0.21	−0.002	ARNG*	KA	−0.45	−0.51
53.025	35.705	0.27	9.96	0.76	0.78	0	BASH	KA	1.38	0.57
51.812	35.73	1.7	10.22	0.36	0.34	0	BOOM	KA	−0.25	−0.14

Table 1. (Continued.)

Lon. (° E)	Lat. (° N)	E Vel.	N Vel.	± E	± N	± EN	Site	Block	Res. E	Res. N
50.988	35•088	± 1•79	10•75	0•43	0•43	0•002	CHSH	KA	± 0•29	± 1•19
50.989	35•088	± 1•53	11•74	0•18	0•16	± 0•003	CHSM*	KA	± 0•03	± 0•2
52.059	35•701	± 1•7	9•26	0•38	0•38	0•006	DAMA	KA	± 0•18	± 0•88
51.166	35•409	± 1•6	12•82	0•73	0•74	0•001	FOIM*	KA	± 0•38	1•27
50.84	35•765	± 1•66	11•36	0•37	0•2	± 0•001	FOPM*	KA	± 0•55	± 0•19
54.989	36•43	± 0•17	9•79	0•71	0•72	0•009	GHAB	KA	0•42	2•26
51.41	35•882	± 2•43	10•76	0•55	0•55	0	GTCL*	KA	± 1•01	± 0•02
50.747	36•007	± 2•05	11•01	0•18	0•21	± 0•002	HSGD*	KA	± 0•85	± 0•32
58.464	35•293	± 0•08	5•31	0•34	0•33	± 0•002	KASH	KA	0•23	± 0•24
51.955	35•683	± 1•38	9•59	0•42	0•42	± 0•004	MF01	KA	0•04	± 0•7
51.885	35•649	± 1•48	10•5	0•32	0•32	± 0•001	MF03	KA	± 0•17	0•07
52.117	35•258	± 1•98	11•27	0•36	0•36	0•003	MF04	KA	± 0•79	0•56
51.277	35•493	± 0•74	11•78	0•44	0•43	± 0•002	MF05	KA	0•43	0•42
50.543	35•227	± 1•12	11•7	0•43	0•43	0•002	MF06	KA	0•47	± 0•69
50.632	36•009	± 1•21	11•12	0•44	0•44	0•002	MF13	KA	± 0•04	± 0•38
51.665	35•724	± 1•25	11•53	0•33	0•33	± 0•001	MF16	KA	0•08	0•93
51.108	35•753	± 1•51	10•47	0•32	0•33	± 0•001	MF17	KA	± 0•38	± 0•8
51.808	34•977	0•07	10•31	0•77	0•76	0•04	MOBA	KA	1•52	± 0•87
51.795	35•053	± 0•99	11•86	0•22	0•26	± 0•002	MOBK*	KA	0•4	0•71
50.045	36•401	± 2•35	10•96	0•76	0•8	± 0•003	NEYA	KA	± 1•21	± 1•1
51.885	35•224	± 0•79	10•58	0•52	0•51	0•014	PISH	KA	0•46	± 0•37
51.971	35•63	± 0•63	9•25	0•25	0•31	± 0•002	PLZI*	KA	0•67	± 1•12
56.07	33•369	0•68	10•04	0•42	0•39	0•002	ROBA	KA	3•36	2•28
51.711	35•574	± 1•28	10•51	0•3	0•19	± 0•001	RTCL*	KA	± 0•08	± 0•26
53.564	35•662	± 0•06	8•58	0•42	0•4	0•009	SEMN	KA	0•66	± 0•81
51.884	35•277	± 0•83	12•88	0•17	0•16	± 0•003	SHOR*	KA	0•39	1•97
53.421	35•588	0•82	9•24	0•3	0•28	± 0•001	SMNN*	KA	1•58	± 0•28
52.043	35•492	± 0•9	9•59	0•36	0•36	0•005	TANG	KA	0•26	± 0•93
51.334	35•697	± 1•15	10•52	0•31	0•3	0	TEHN*	KA	0•01	± 0•57
51.386	35•747	± 0•72	12•53	0•79	0•75	0•014	TEHR	KA	0•48	1•56
51.257	35•812	± 1•68	12•48	0•42	0•42	0•01	TF01	KA	± 0•48	1•43
51.425	35•833	± 1•33	12•16	0•5	0•5	0•009	TF09	KA	0	1•35
51.522	35•774	± 1•77	11•96	0•41	0•41	0•009	TF16	KA	± 0•46	1•2
51.568	35•808	± 3•27	11•04	0•51	0•52	0•013	TF20	KA	± 1•86	0•4
50.745	36•144	± 2•84	11•43	0•48	0•37	± 0•001	TLGN*	KA	± 1•43	0•23
51	35•493	± 1•1	12•79	0•7	0•7	0•022	TN01	KA	0•08	1•13
51.17	35•203	± 0•72	12•56	0•45	0•46	0•008	TN02	KA	0•64	0•88
51.379	35•366	± 0•83	12•43	0•48	0•49	0•011	TN03	KA	0•4	1•08
51.409	35•495	± 1•34	12•89	0•46	0•47	0•009	TN04	KA	± 0•17	1•68
51.515	35•633	± 0•38	11•01	0•49	0•5	0•01	TN05	KA	0•8	0•07
51.724	35•55	± 0•52	10•91	0•4	0•4	0•008	TN06	KA	0•67	0•13
51.632	35•344	± 0•82	12•32	0•25	0•63	± 0•001	VRMN*	KA	0•4	1•21
58.56	56•43	± 0•27	± 0•04	0•11	0•12	± 0•005	ARTU*	EU	± 0•04	0•11
17.073	52•277	± 0•07	0•18	0•13	0•1	± 0•004	BOR1*	EU	0•18	0•13
4.359	50•798	± 0•55	± 0•45	0•1	0•08	± 0•003	BRUS*	EU	± 0•45	0•1
6.921	43•755	0•11	0•41	0•1	0•11	± 0•004	GRAS*	EU	0•41	0•1
15.493	47•067	0•8	0•66	0•14	0•1	± 0•004	GRAZ*	EU	0•66	0•14
104.316	52•219	± 0•37	± 0•85	0•22	0•12	± 0•001	IRKT*	EU	± 0•85	0•22
21.032	52•097	± 0•03	0•32	0•09	0•08	± 0•009	JOZE*	EU	0•32	0•09
5.81	52•178	± 0•15	0•73	0•11	0•09	± 0•002	KOSG*	EU	0•73	0•11
92.794	55•993	± 1•05	± 1•54	0•23	0•22	0•002	KSTU*	EU	± 1•54	0•23
355.75	40•429	1•38	± 1•42	0•1	0•1	± 0•004	MADR*	EU	± 1•42	0•1
24.395	60•217	0•28	± 0•81	0•08	0•1	± 0•005	METS*	EU	± 0•81	0•08
11.865	78•93	± 0•06	± 1•02	0•08	0•1	0	NYAL*	EU	± 1•02	0•08
11.926	57•395	± 0•74	± 0•44	0•08	0•11	± 0•003	ONSA*	EU	± 0•44	0•08
13.066	52•379	± 0•35	0•18	0•23	0•23	± 0•002	POTS*	EU	0•18	0•23
128.866	71•634	± 0•13	0•06	0•14	0•15	0•005	TIXI*	EU	0•06	0•14
1.481	43•561	± 0•88	1•03	0•45	0•44	± 0•001	TOUL*	EU	1•03	0•45
18.938	69•663	± 0•58	0•92	0•08	0•08	± 0•005	TROM*	EU	0•92	0•08
356.048	40•444	± 0•28	0•42	0•13	0•08	± 0•001	VILL*	EU	0•42	0•13
12.879	49•144	± 0•04	0•32	0•08	0•08	± 0•005	WTZR*	EU	0•32	0•08
129.68	62•031	± 0•98	± 0•52	0•38	0•25	0•002	YAKT*	EU	± 0•52	0•38
41.565	43•788	± 0•54	0•66	0•11	0•08	± 0•007	ZECK*	EU	0•66	0•11
7.465	46•877	0•49	0•61	0•11	0•09	± 0•004	ZIMM*	EU	0•61	0•11
36.759	55•699	0•29	± 0•2	0•12	0•14	± 0•004	ZWEN*	EU	± 0•2	0•12

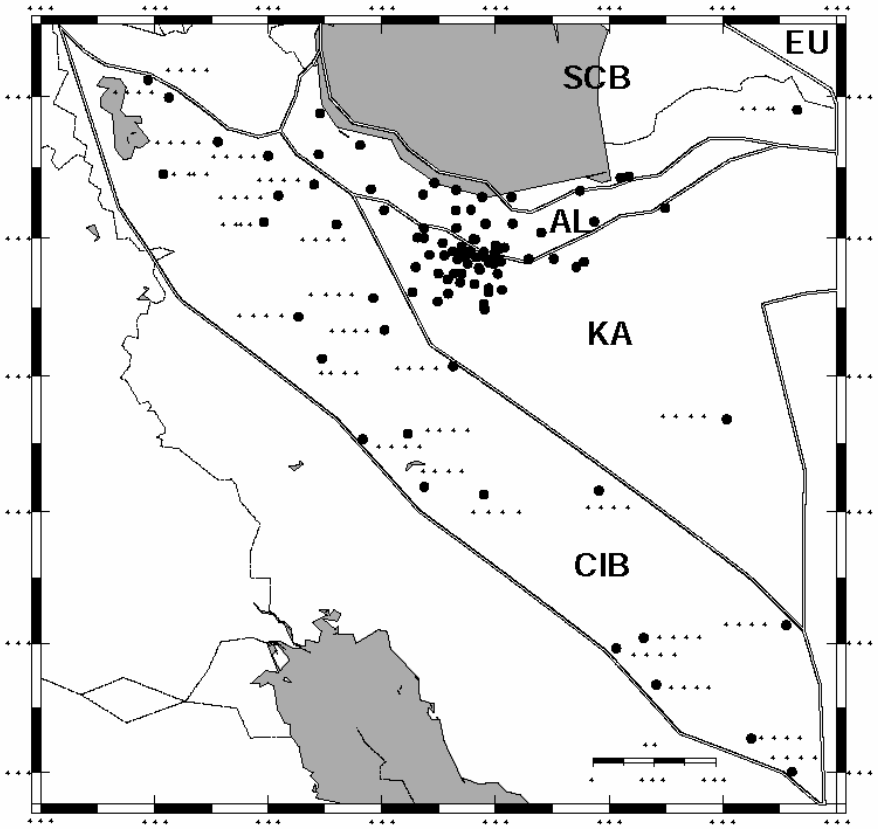

Figure 4. Map showing our preferred block model consisting of five plates/blocks. Abbreviations are Eurasian (EU), Alborz (AL), Central Iranian block (CIB), Dasht-e-Kavir (KA) and South Caspian (SCB).

bounding faults follows Okada's formulation (Okada 1985, 1992). The model allows no permanent deformation of the blocks or slip on unconnected faults, this implies that all the faults used must be on a block boundary.

25 GPS sites are located on the Alborz block (Fig. 4). North of Alborz, the motion of the South Caspian block (SCB) is constrained by six sites (GRGN, KORD, MAHM, NKAD, SHIR and TKBN). To the south, according to earlier studies (Vernant et al. 2004a, c), we use two blocks: the Central Iranian Block (CIB) and the Dasht-e-Kavir block. As the CIB and the Dasht-e-Kavir block encompass a region larger than our study we have also combined some of the data of (Walpersdorf et al. 2006; Masson et al. 2007) to have 25 sites on the CIB, 46 sites on the Dasht-e-Kavir and the site SHIR on the SCB (Fig. 4).

The block geometry is defined using the main active faults mapped in the region. The southern Alborz boundary corresponds to the main strike slip faults dipping steeply to the North (Taleghan, Mosha and Firuzku). According to Ashtari et al. (2005), the depth of microseismicity in the southern Alborz ranges from 0 to 16 km. Therefore, the modelled faults bounding the southern part of the Alborz block are assigned an 85° dip to the North and are locked from 0 to 16 km. The northwestern boundary of the Alborz block (heavy black line in Fig. 5) is rather poorly constrained by the geology and the geodesy, and no slip rates are estimated since we don't invert for the block motion west of these segments. The eastern boundary (longitudes greater than 55.5° E) is also poorly constrained by our GPS measurements, and several geometries could be used. The northern boundary of the Alborz block corresponds to the Khazar fault where the Baladeh earthquake involved slip at 10–30 km depth, with an average 34° south-dipping aftershock zone also restricted to the range 10–30 km (Tatar et al. 2007). In order to check if the GPS velocity field is consistent with a deeper than usual locking depth in this region and if aseismic slip could occur at shallow depth, we run several models where we vary the locking depth of the Khazar fault (black line, Fig. 6). The results suggest an optimum solution for a locking depth of 33 km. Although completely independent from the seismic study of Tatar et al. (2007), our results agree well with their findings. This deep locking depth is only possible for the central and western segments of the Khazar thrust fault since the residuals of the sites KAHO and GHAB are smaller with a shallower locking depth (10 km). We run a second set of experiments where we keep the depth of the locked Khazar fault equal to 33 km and we allow for an unlocked upper part of the fault (dashed line, Fig. 6). The results of this second set of experiments suggest that the upper part of the Khazar faults has to be locked to account for the geodetic observations.

Fig. 5 shows the residuals for each block (i.e. observed-modelled velocities) of our preferred model. The WRMS values for the Alborz, Caspian, CIB and Dasht-e-Kavir blocks are 0.85, 0.66, 1.45 and 0.80 mm yr^{-1}, respectively, with no significant systematic

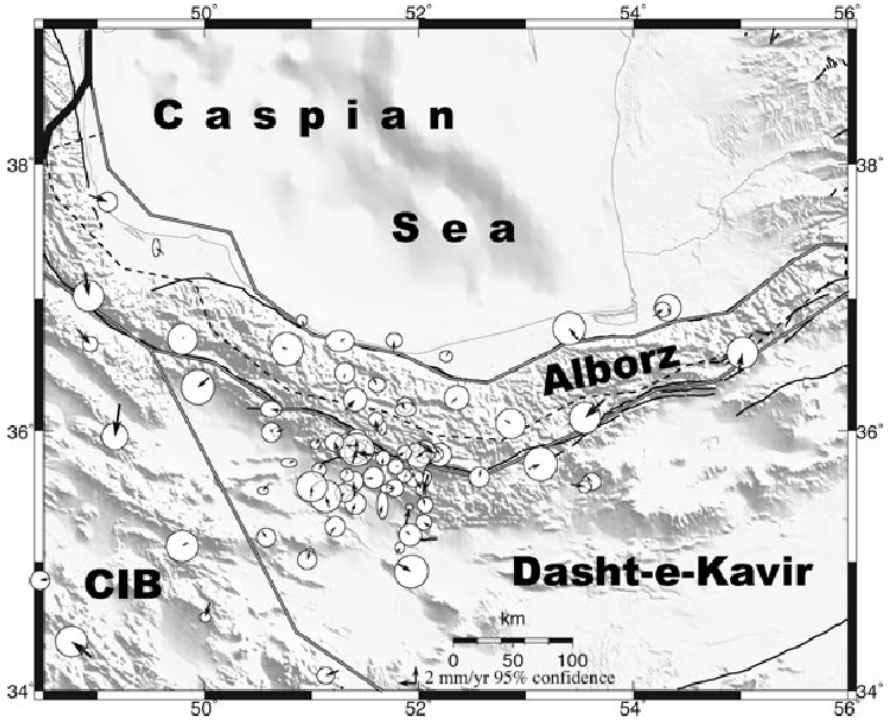

Figure 5. Map showing block model residual velocities (observed minus modelled) and 95 per cent confidence ellipses for the block model shown in Fig. 4 and described in the text. Light block boundaries show fault with estimated slip rate. Heavy black line in NW corner of the map shows block boundaries with no estimation of slip rate. The dashed line shows the estimated southern extent of the locked interface of the northern Alborz block boundary (Khazar fault).

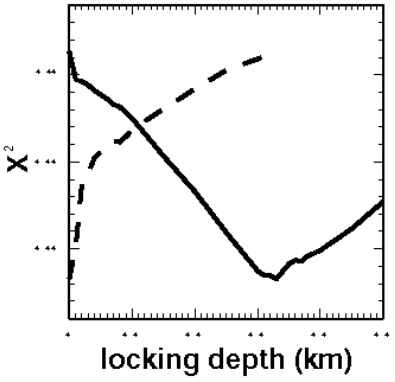

Figure 6. • ^{2} plotted versus locking depth for the Khazar thrust fault. Black curve indicate the value for a locked fault from the surface down to the locking depth. Dashed curve indicates the value for a locked fault from the locking depth value down to 33 km depth.

residuals (Fig. 7). This fairly good fit to the data suggests that deformation in the Alborz range is well explained by a simple model with faults bounding the range to the north and south, the northern fault having a deeper locking depth (• 33 km) in its western part. Slightly higher residuals are seen on the western extremity of the Alborz Mountains, but given the sparse GPS coverage and the lack of geological studies of the active faults of this region, the models are very poorly constrained. The interseismic modelled deformation along the two profiles shows that, due to the orientation of the faults, the dominant faulting is mainly left lateral strike slip to the east and left lateral and thrust faulting to the west (Fig. 8).

Although the SCB is only constrained by six GPS sites, the slip rates obtained for the faults bounding the SCB to the South (Fig. 9) and to the north along the Apsheron Balkan sill (• 6 mm yr^{-1} of fault normal compression and • 2 mm yr^{-1} of right lateral strike slip) and the Ashkhabad fault (• 1 mm yr^{-1} of fault normal compression and • 3 mm yr^{-1} of right lateral strike slip) are reasonable. Therefore, at the longitude of the Alborz range the deformation related to the Arabia–Eurasia collision is accommodated almost equally on three main structures: Zagros, Alborz and the Apsheron-Balkan sill. The fault slip rates obtained for the main Alborz fault zones are given in Fig. 9. These slip rates correspond to a case where no off-fault deformation occurs and only one fault accommodates the differential motion between two blocks. Therefore the uncertainties on the slip rates depend only on the uncertainties on the Euler vectors and are • 1 mm yr^{-1} along the southern Alborz region. The motion of the SCB is mainly based on GPS sites that are located very close to the southern boundary of the block, and therefore in the interseismic deformation zone along the faults. This implies that the slip rates estimated along the southern boundary of the SCB are maximum slip rates and their uncertainties are • 2 mm yr^{-1}.

4 GRAVITY OBSERVATIONS AND PROCESSING

Since 2000, the AG field was surveyed in and nearby the Alborz range on three sites (Fig. 2): one is located within the range near the Mosha fault at an elevation of 3200 m (ABAL); another is located

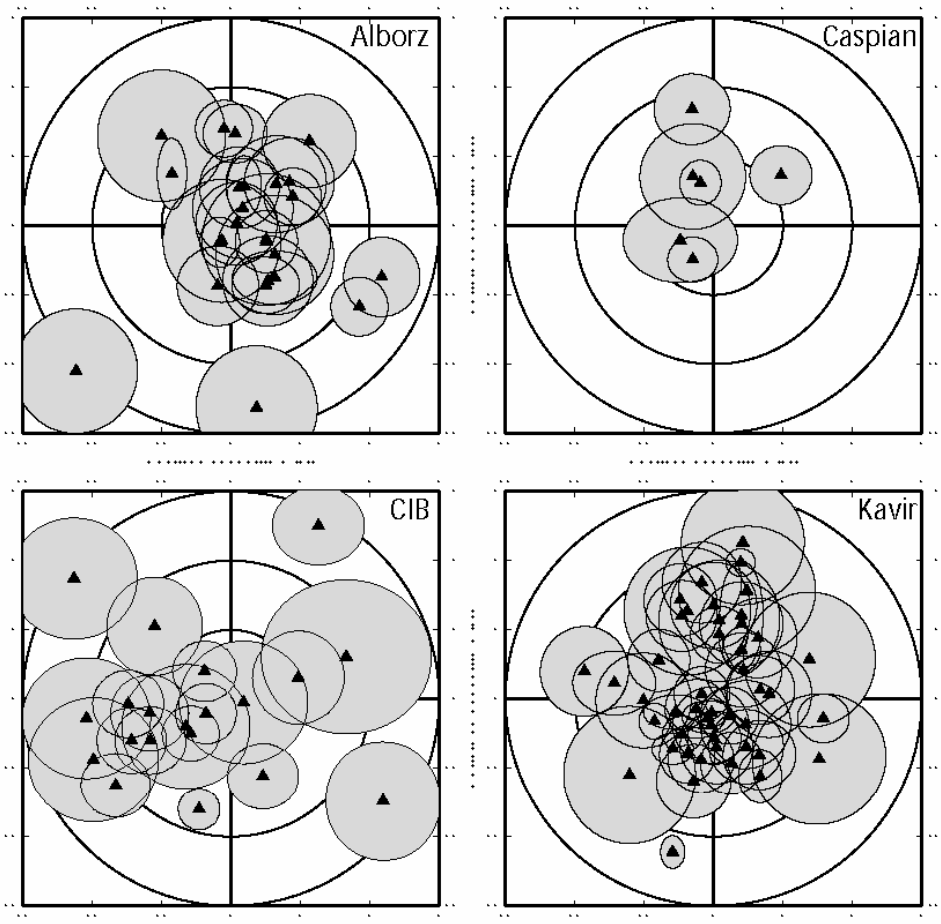

Figure 7. East and north component of the residuals of each block indicating no systematic misfit to the block model.

at the foothills of the range in Tehran city with an elevation of 1200 m (TEHN), and the last one is located in the desert zone 80 km south of Tehran where low seismic activity is reported (CHSH).

These sites where surveyed every year from 2000 to 2006. Each AG measurement took place in September–October, in order to minimize the variation of the seasonal component on the long-term fluctuations. The FG5#206 and FG5#228 absolute gravimeters belonging to the French national pool of gravimeters were used together with a Scintrex CG-3M microgravimeter to accurately estimate the AG value at each site.

The AG value g is estimated from the position of a dropping test mass as a function of time. The experimental protocol consists of estimating the mean value of g from 100 drops per hour. The 'drop to drop' precision on measurements at ABAL site was • 5 • Gal. Finally, the AG value was estimated by averaging the measurements over time periods greater than 12 hours. All the data sets were processed identically using the new processing software g-version 6.0 from Micro-g Solutions Inc. The geographical coordinates, the vertical gradient, and the nominal reference air pressure are fixed for each site. Models are applied to correct for the solid Earth tides (Wenzel 1994) and tidal ocean loading (FES2004, Lyard et al. 2006). Air pressure effects are corrected using the same barometric admittance and observed pressure data; finally, polar motion effects are subtracted using IERS observed pole coordinates.

With only one measurement per year, no coloured noise can be estimated from an analysis of our data set. The unknown coloured noise model for our data set should reflect hydrological and atmospheric effects in the Alborz. Indeed, the GRACE satellite experiments revealed seasonal (Wahr et al. 2004) and interannual variations (Andersen & Hinderer 2005) that can be fit with a global hydrological model (soil moisture). Using the European Centre for Medium-Range Weather Forecasts (ECMWF) and LadWorld global hydrological models to compute temporal variation of the terrestrial water storage and the associated gravity changes shows seasonal variations of 6–8 • Gal in the Tehran area during the 2000–2007 epoch. These global models suggest that repeating the AG campaigns at the same epoch introduces a weak variation of the coloured noise (• • Gal). Hence, the 'hydrological and atmospheric colored noise' is neglected and we only rely on a white noise model being the sum of the instrumental high frequency noise and the setup noise (• 1.6 • Gal). However, gravity effects deduced from long wavelength terrestrial soil moisture LadWorld and ECMWF models (• 100 km) do not account for local ground water induced gravity effects and their temporal variation due to water circulation. But this

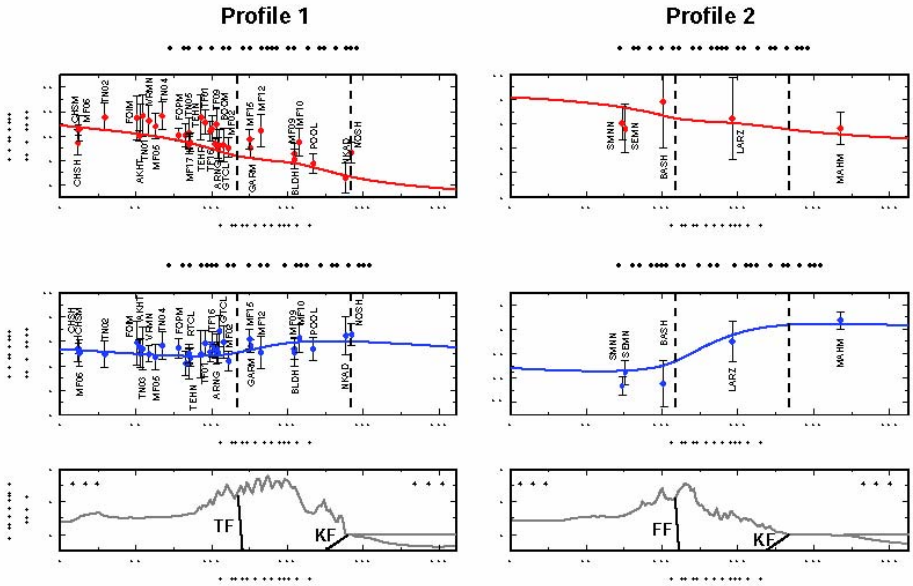

Figure 8. West (profile 1) and east (profile 2) Alborz velocity profile showing along profile, and profile normal velocities and 2• uncertainties relative to Eurasia (see Fig. 3 for profile location and width). The curve is the theoretical strain accumulation obtained with the block model described in the text. The topography along the profile is extracted from the SRTM30 Plus database. TF, Taleghan fault; KF, Khazar fault; FF, Firuzkuh fault.

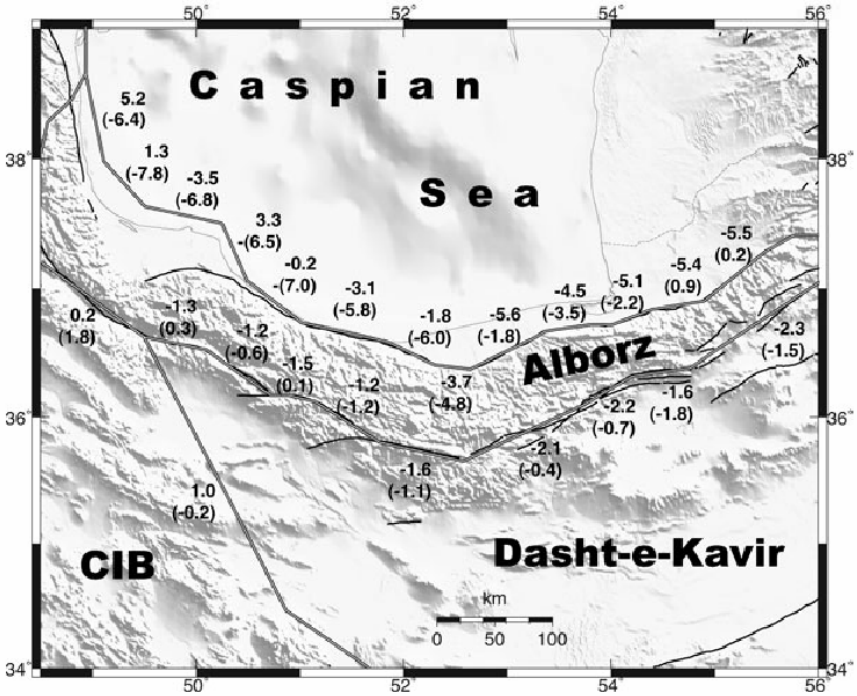

Figure 9. Map showing fault slip rates (mm yr• 1) deduced from the block model shown in Figs 4 and 5. Top numbers (no parentheses) are strike-slip rates, positive being right-lateral. Numbers in parentheses are fault-normal slip rates, negative being closing.

is the case for AG measurements at TEHN, since the temporal variations are mainly correlated with the depth of underground water tables beneath Tehran city. Therefore we do not report the AG values at TEHN. The temporal variations at Chesmeh-shour are lower than 2 • Gal during the 2001–2006 interval but we do not have enough measurements to estimate a rate.

The site ABAL is located at 3200 m on the summit of a steep mountain attenuating the local hydrological related gravity changes.

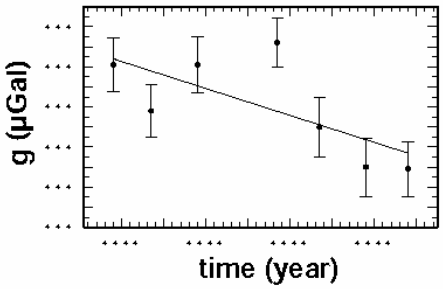

Figure 10. Time-series of the absolute gravity measurements at the site ABAL.

Estimating a rate of AG change for the ABAL station with either a white noise model or a statistical coloured noise model proposed by Van Camp et al. (2005) does not show significant differences, therefore we use the white noise model since we don't have enough data to constrain a coloured noise model. The rate inferred from AG time-series for the site ABAL is • 0.67 • 0.25 • Gal yr• 1 (1• level) suggesting a low uplift rate (Fig. 10). Using the free-air gravity gradient, the gravity change • g_z/•t due to the vertical displacement and erosion is given by

$$\bullet g_z \bullet\bullet t(\bullet \text{ Gal yr}^{\bullet 1}) \bullet \ \bullet\ 2g \bullet a \bullet_z \bullet \ \bullet\ 0{\cdot}3 \bullet_z (\text{mm yr}^{\bullet 1}) \qquad (1)$$

with g the gravitational acceleration, v_z the vertical rate and a the Earth's radius. Unfortunately, the AG values give the gravity variation •g that corresponds to the sum of the variation due to the mass distribution change (• g_m) and the vertical displacement (• g_z). Converting a rate of gravity change into a vertical velocity needs to account for lithospheric loading and mechanical response of the earth. In the case of postglacial rebound (PGR) and present-day ice sheet evolution, vertical uplift and gravity changes have been predicted for a large variety of mantle viscosities and elastic lithospheric thicknesses (Wahr et al. 1995; James & Ivins 1998). A factor of • 0.16 • Gal mm• 1 was found, in agreement with AG observations in the northern part of the North American Plate (Larson & van Dam 2000).

In the mountain building processes, the lithosphere is flexed in response to tectonic loads (relief, subsurface loads). Goetze & Evans (1979) have shown that loads are supported for long periods of geological time (• 10^5 yr) by a quasi-elastic layer that gives strength to the lithosphere. This elastic 'core' may be characterized by its flexural rigidity, or elastic thickness (Watts et al. 1980). The mechanical response of the lithosphere to topographic loads may be described in terms of an admittance function T, that is, free air anomaly/altitude ratio in the Fourier domain. Loads and isostatic deflection of the Moho are responsible for the free air gravity anomaly. In this study, the gravity change is associated with variation of the topographic load and correspond to the sum of the free air anomaly change and gravity perturbation due to vertical displacements. Using the relation (1), the rate of gravity change and the vertical rate are tied by the relation

$$T(k) \bullet \ \bullet G(k) \bullet\bullet Z(k) \bullet \ 2g \bullet a \qquad (2)$$

with k the wavenumber in the Fourier domain, •G(k) and •Z(k) the Fourier transforms of the free air anomaly change • g_z/•t and the vertical rate v_z. T(k) may be predicted for an infinite thin elastic plate overlying an inviscid fluid (Karner & Watts 1983). Fig. 11 shows the admittance as a function of wavenumber (or wavelength • of the relief change), for various elastic thicknesses ranging from 0 (local isostatic compensation) to 50 km (high rigidity). In the uncompensated waveband, • • 50 km, the ratio is • 0.19 • Gal mm• 1. In the compensated waveband for • • 50 km, the ratio depends on the elastic thickness of the lithosphere and varies from

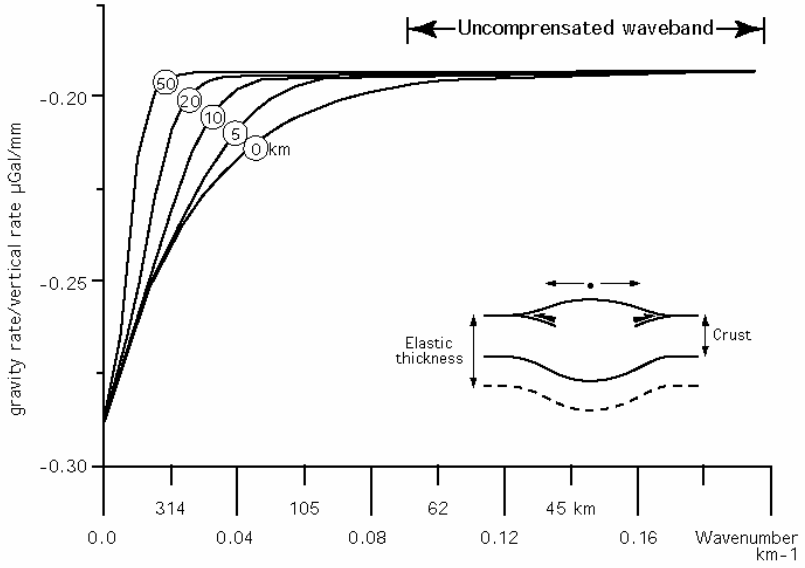

Figure 11. Admittance function versus wavenumber (gravity change/vertical change in Fourier domain). The continental lithosphere is considered as a homogeneous elastic plate overlying an inviscid fluid. The topography loads the lithosphere whose flexure depends on the wavelength of the relief and the elastic thickness of the plate. The temporal variation of the gravity field is the sum of the free-air anomaly change (relief and Moho effects) and the free-air variation due to vertical displacement. The admittance function is calculated for various elastic thicknesses from 0 to 50 km (crustal thickness: 30 km; crustal density: 2800 kg m• 3; density of the upper mantle 3300 kg m• 3). Note that the value of the admittance function within the 'uncompensated waveband' (• • 100 km) is • • 0.2 • Gal mm• 1.

Table 2. Euler vectors relative to Eurasia and 1• uncertainties for the block model determined in this and prior studies. The number of GPS sites and WRMS residuals for each block in our model are also given. Plate abbreviations are EU, Eurasia; AL, Alborz; CIB, Central Iranian block; KA, Dasht-e-Kavir region; SCB, South Caspian Block. References are ts, this study; jm, Jackson & McKenzie (1984); re, Reilinger et al. (2006); ve, Vernant et al. (2004c).

Plates	Longitude (°E)	•	Latitude (°N)	•	Rate (deg Myr• 1)	•	WRMS	Number of sites	References
AL-EU	59•4	0•7	36•6	0•2	• 0•969	0•072	0•85	25	ts
AL-EU	57•9	3•0	36•6	0•6	• 1•299	0•790	1•95	4	re
SCB-EU	59•1	0•8	40•4	0•3	• 0•622	0•055	0•66	6	ts
CIB-EU	• 13•6	4•2	13•4	2•6	0•149	0•007	1•45	25	ts
CIB-EU	4•2	0•1	18•9	4•9	0•207	0•020	1•93	19	re
CIB-EU	0•98	1•2	23•15	13•2	0•189	0•1		6	ve
CIB-EU	65•8		27•5		0•56				jm
KA-EU	64•3	0•1	35•3	0•6	• 0•61	0•024	0•80	47	ts
KA-EU	81•5	14•9	29•4	4•9	• 0•225	0•124	1•42	8	re

• 0.19 to • 0.3 • Gal mm• 1. This last value is close to the estimation of James and Ivins (1998) for an elastic spherical Earth (PREM model).

Therefore the absolute uplift rate at the site ABAL ranges between 3.5 and 2.2 • 1.5 mm yr• 1 with the admittance values of • 0.19 and • 0.3 • Gal mm• 1, respectively. Vertical strain induced by tectonic loading for a site close to an active fault in a narrow mountain range such as Alborz is related to the interseismic deformation. The main strain accumulations near active faults occur over a width of usually less than 60 km on both sides of the active faults (Savage & Burford 1973). Therefore, from a spectral point of view, tectonic loading acts on the lithosphere in the uncompensated waveband domain and the admittance value may be close to the • 0.2 • Gal mm• 1 value used by Meurers et al. (2007) in northwest Europe (Ardennes and Roer Graben). Hence the absolute uplift rate is more likely to be in the upper range of these estimates (• 3 mm yr• 1).

5 DISCUSSION

This study allows us to greatly improve the uncertainties of the estimation of Euler vectors obtained for the Alborz, Kavir and CIBs with respect to previous geodetic results (Vernant et al. 2004b; Reilinger et al. 2006). Moreover, we are able for the first time to estimate the SCB Euler vector from direct measurements (Table 2). The location of the SCB-Eurasia Euler vector explain why most of the deformation along the Ashkhabad fault is accommodated by right lateral strike slip (• 3 mm yr• 1) that evolves into a thrust fault north of the SCB (• 6 mm yr• 1 of fault normal shortening). Given the position of the SCB-Eurasia pole of rotation close to the SCB, the motion of this block is more complicated than the 300° Azimuth vector suggested by Jackson et al. (2002) and Allen et al. (2003b) for the entire block. Indeed the velocity vector in a Eurasia reference frame for the SCB will change from 315°, south of the SCB to 000°, north of the SCB (Fig. 12).

Being able to estimate the motion of the SCB for the first time allows us to better determine the strike-slip and dip-slip on the faults bounding the Alborz range to the north (Fig. 9). South of the range along the Taleghan, Mosha, Firuzkuh and Astaneh faults, the fault normal component is not significant, indicating the mainly left lateral, strike slip character of these faults with a slip rate decreasing from • 2 mm yr• 1 in the eastern Alborz to • 1 mm yr• 1 in the western part of the range, which is consistent with morphotectonic studies (Ritz et al. 2006; Nazari et al. 2009). The lack of significant shortening (or extension) along these faults show that most of the shortening in Alborz occurs north of the range. However, several

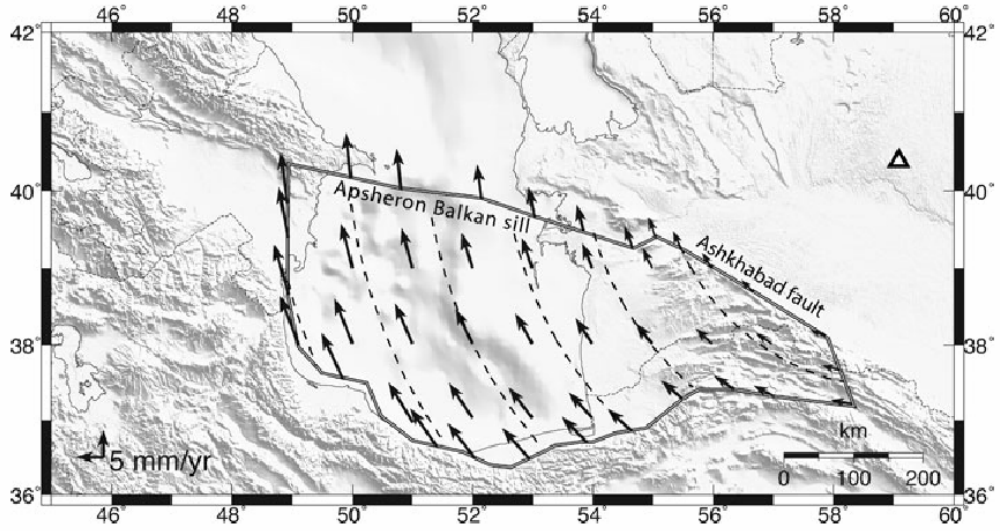

Figure 12. Location of the South Caspian/Eurasia Euler pole (triangle), predicted block motion direction (dashed lines and vectors) without taking into account the interseismic elastic strain along the block boundaries.

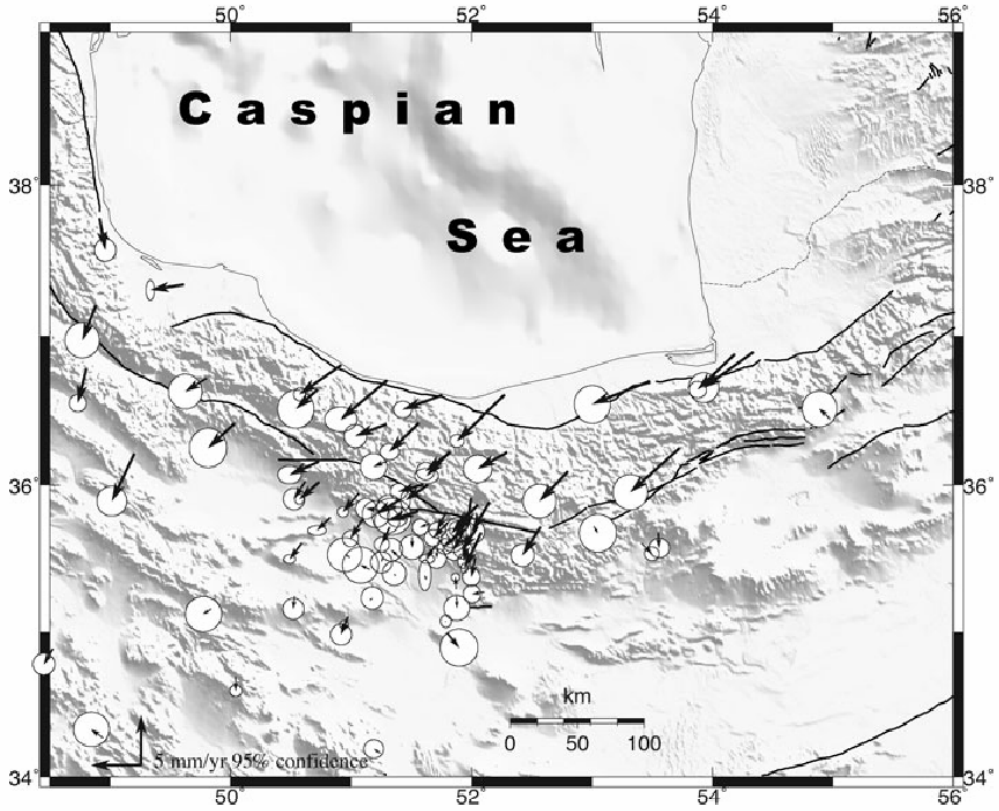

Figure 13. Map showing GPS velocities and 95 per cent confidence ellipses relative to the Dasht-e-Kavir region determined in this study.

thrust faults are reported along the southern foothills of the range such as the North Tehran thrust fault or the Parchin thrust fault (e.g. Berberian 1981; Landgraf et al. 2009), but the residuals within the Kavir block are lower than 1 mm yr^{-1} and for most of them not significant. This is consistent with results estimated from palaeoseismological studies and show that the slip rates of these reported active thrust faults are very low (• 1 mm yr^{-1}).

Looking at the fault kinematics along the Khazar thrust north of the range suggest that it can be divided into two segments; the western segment that is mainly a thrust fault (• 6 mm yr^{-1}) with a slight left lateral strike slip component (2–3 mm yr^{-1}), and the eastern segment that has a thrust component (2–3 mm yr^{-1}) with a high left-lateral strike-slip rate (• 5 mm yr^{-1}). It seems clear also that the eastern and western segment behave differently since the locking depths obtained are significantly different (• 33 km to the west and 10 km to the east). The shallower locking depth for the eastern segment could indicate the dip of the fault is steeper, but we have no constraint on the dip of this segment. It must be pointed out also that the Alborz range was modelled here as one block. We have chosen to do so because the GPS coverage in eastern Alborz is less dense than the western part of the range. A denser network to the east could reveal low deformation within the Alborz range, but this wouldn't significantly modify our conclusions on the present-day kinematic of the range.

Looking at the velocity field in a Dasht-e-Kavir fixed reference frame is very instructive for deciphering the present-day kinematic of the range (Fig. 13). Indeed, for the western Alborz, it is clear that the motion of the SCB relative to the Kavir induces a collision with an obliquity of about 25°. This obliquity has already been reported by several authors (Jackson et al. 2002; Allen et al. 2003b; Ritz et al. 2006) who suggest that strain partitioning occurs in the Alborz range. Our results agree in part with partitioning in the range since the fault slip rates estimated on the southwest boundary of the Alborz show only left-lateral strike slip (Fig. 9). However, even though all the compression seems to occur on the northern Khazar thrust, a left-lateral component also occurs on this fault. Therefore, as suggested by the modelling of the Zagros range (Vernant & Chery 2006), a full strain partitioning (i.e. one pure thrust fault and one pure strike slip fault) seems almost impossible in continental collisions, and the Alborz is another example to support this conclusion. The most interesting feature of the Dasht-e-Kavir fixed reference frame is the very high obliquity of the convergence direction (• 70°) between the SCB and the Dasht-e-Kavir in the eastern part of the Alborz range. The velocities of the sites GRGN, KORD and SHA1 together with the slip rates estimated by the block model show that the shortening in eastern Alborz is very low. This present-day kinematic of eastern Alborz is not consistent with the topography of the range, and suggests that the kinematic of the SCB has changed recently as suggested by Ritz et al. (2006), Nazari et al. (2009), Landgraf et al. (2009) and Ritz (2009). This is further corroborated by the estimate of shortening across the range based on the balanced cross section of Guest et al. (2006). The authors suggest that shortening across the range over the past 12 Myr has been higher for the Central Alborz (50–56 km) than for western Alborz (15–18 km).

Our results show that overall present-day shortening rates across central and western Alborz are similar, suggesting that shortening estimated over 12 Myr is not consistent with the one estimated either from GPS observations or geomorphologic studies (Ritz et al. 2006; Ritz 2009). Therefore, even though the rate of shortening between Arabia and Eurasia has not significantly changed over the last 10–20 Myr (McQuarrie et al. 2003; Vernant et al. 2004c; Reilinger et al. 2006), the kinematics of the Alborz range has evolved during this time period.

Gravity measurements nearby the GPS site of ABAL suggest that the uplift rate of the range is about 2 to 3.3 • 1.5 mm yr• 1 depending on the admittance used to convert the gravity rate of change into an absolute uplift rate. This result is consistent with the uplift rate of • 2 mm yr• 1 that can be deduced from the drainage incision in northern Alborz, south of the Khazar thrust fault (Antoine et al. 2006). This rate is also consistent with 5 mm yr• 1 of shortening on a thrust fault dipping at 34• to the south, but suggests that either the river does not incise as fast as the topography grows, or that some kind of isostatic compensation of the range occurs in this region. Given that this study and the study of the Baladeh Earthquake (Tatar et al. 2007) suggest that the Khazar thrust fault behaves seismically down to • 30 km depth, and that the Alborz is a narrow range and the seismic part of the fault encompasses most of the range (Fig. 5), further suggesting that the whole range could uplift with a constant rate of about 2–3 mm yr• 1. Unfortunately the CGPS data span is not long enough to accurately evaluate the uplift rates, and the hydrological effects of water pumping complicate using the gravity measurements south of the Taleghan, Mosha and Firuzkuh faults. Ritz et al. (2006) suggest that these faults have a very low normal faulting component, hence the region south of these faults should uplift at a very slightly higher rate that the northern region. The location of this fault system seems to limit the overriding part of the range that is seismically coupled to the south Caspian oceanic basement from the southern foothills of the range. Based on receiver functions cross section (Paul et al. 2010), it seems that the deepest part of the root is located below the southern part of the range. Therefore the uplifting processes, although probably linked, could be different south and north of the Taleghan, Mosha and Firuzkuh fault system.

6 CONCLUSION

We have been able to estimate the motion of the SCB accurately for the first time. Our results suggest an important rotation of the SCB relative to Eurasia, which explains the left lateral motion in the Alborz range. The motion of the SCB relative to the Dasht-e-Kavir allows estimating the upper bound of the deformation accommodated by the Alborz range. The slip rates vary along the range, the thrusting component on the Khazar fault changes from 2 mm yr• 1 to the east to 6 mm yr• 1 to the west and the left lateral strike-slip rate from 2 to 1 mm yr• 1 along the Astaneh, Firuzkuh, Mosha and Taleghan faults, and from 5 to 2 mm yr• 1 along the Khazar fault from east to west. Hence, some partitioning occurs, but not complete partitioning. Given the motion of SCB and Alborz blocks and the V shaped structure of the Alborz range, the deformation cannot be summarized by only two slip rate values as it has been proposed earlier by Vernant et al. (2004a), and one needs to take into account along-range slip rate variations. Our results suggest that the eastern Alborz mainly accommodates strike slip deformation, and that the western Alborz accommodates thrusting. These present-day kinematics agree with the results from geomorphologic studies (Ritz et al. 2006; Landgraf et al. 2009), but not the long-term deformation (see Guest et al. 2006; Hollingsworth et al. 2008; Ritz 2009). This supports the idea that the kinematics of the range have changed recently due to the change of SCB motion.

The interseismic deformation suggests a deep locking depth on the central-western segment of the Khazar fault (• 30 km) in agreement with the Baladeh earthquake rupture and aftershocks (Tatar et al. 2007). Furthermore, our AG observations suggest that the part of the range seismically coupled on the Khazar thrust fault uplifts with a rate of 1–5 mm yr• 1, in agreement with the terrace uplift reported north of the range (Antoine et al. 2006).

ACKNOWLEDGMENTS

This work was realized in the frame of a co-operative research agreement between INSU-CNRS (DYETI, RNCC), MAE (French Foreign Office Ministry) and National Cartographic Center (NCC, Tehran). We thank all the teams who went out in the field to collect the data. We are grateful to R. Reilinger and an anonymous reviewer for their constructive comments on this manuscript and their tremendous help to improve our English. We are also thankful to Jean Paul Boy (EOST, Louis Pasteur University, Strasbourg, France) for providing the 2000–2007 hydrological gravity affect from the ECMWF and LadWorld global hydrological models.

REFERENCES

Allen, M., Ghassemi, M.R., Sharabi, M. & Qorashi, M., 2003a. Accomodation of late Cenozoic oblique shortening in the Alborz range, Iran, J. Struct. Geol., **25,** 659–672.

Allen, M.B., Vincent, S.J., Alsop, I., Ismail-zadeh, A. & Flecker, R., 2003b. Late Cenozoic deformation in the South Caspian region: effects of a rigid basement block within a collision zone, Tectonophysics, **366,** 223–239.

Allen, M.B. et al., 2004. Late Cenozoic reorganization of the Arabia-Eurasia collision and the comparison of short-term and long-term deformation rates, Tectonics, **23,** TC2008, doi:10.1029/2003TC001530.

Ambraseys, N.N. & Melville, C.P., 1982. A History of Persian Earthquakes, Cambridge University Press, New York.

Andersen, O.B. & Hinderer, J., 2005. Global inter-annual gravity changes from GRACE: early results, Geophys. Res. Lett., **32,** L01402, doi:10.1029/2004GL020948.

Antoine, P., Bahain, J.J., Berillon, G. & Asgari-Khaneghah, A., 2006. Tuf calcaire et séquence alluviale en contexte tectonique actif: la formation de Baliran (province du Mazandaran, Iran), Quaternaire, **17,** 321–331.

Ashtari, M., Hatzfeld, D. & Kamalian, N., 2005. Microseismicity in the region of Tehran, Tectonophysics, **395,** 193–208.

Axen, G.J., Lam, P.S., Grove, M. & Stockli, D.F., 2001. Exhumation of the west-central Alborz mountains, Iran, Caspian subsidence, and collision-related tectonics, Geology, **6,** 559–562.

Bachmanov, D.M., Trifonov, V.G., Hessami, K.T., Kozhurin, A.I., Ivanova, T.P., Rogozhin, E.A., Hademi, M.C. & Jamali, F.H., 2004. Active faults in the Zagros and central Iran, Tectonophysics, **380,** 221–241.

Berberian, M., 1981. Active Faulting and Tectonics of Iran, in Zagros-Hindu Kush-Himalaya Geodynamic Evolution, pp. 33–69, AGU, Geodyn. Ser.

Berberian, M., 1983. The southern Caspian: a compressional depression floored by a trapped, modified oceanic crust, Can. J. Earth Sci., **20**(2), 163–183.

Berberian, M. & Yeats, R. S., 1999. Patterns of historical earthquake rupture in the Iranian Plateau, Bull. seism. Soc. Am., **89,** 120–139.

Berberian, M. & Yeats, R. S., 2001. Contribution of archaeological data to studies of earthquakes history in the Iranian plateau, J. Struct. Geol., **23,** 563–584.

Dong, D., Herring, T.A. & King, R.W., 1998. Estimating regional deformation from a combination of space and terrestrial geodetic data, J. Geodyn., **72,** 200–211.

Engdahl, E.R., Jackson, J.A., Myers, S.C., Bergman, E.A. & Priestley, K., 2006. Relocation and assessment of seismicity in the Iran region, Geophys. J. Int., **167,** 761–778.

Feigl, K.L. et al., 1993. Space geodetic measurement of crustal deformation in central and southern California, J. Geophys. Res., **98,** 21 677–21 712.

Gelb, A., 1974. Applied Optimal Estimation, MIT Press, Cambridge, MA.

Goetze, C. & Evans, B., 1979. Stress and temperature in the bending lithosphere as constrained by experimental rock mechanics, Geophys. J. R. astr. Soc., **59,** 463–478.

Guest, B., Axen, G.J., Lam, P.S. & Hassanzadeh, J., 2006. Late Cenozoic shortening in the west-central Alborz Mountains, northern Iran, by combined conjugate strike-slip and thin-skinned deformation, Geosphere, **2,** 35–52.

Herring, T.A., King, R.W. & McClusky, S.C., 2009a. GAMIT reference manual, Release 10.3, Massachussets Institute of Technology, Cambridge, MA.

Herring, T.A., King, R.W. & McClusky, S.C., 2009b. GLOBK reference manual, Release 10.3, Massachussets Institute of Technology, Cambridge, MA.

Herring, T.A., King, R.W. & McClusky, S.C., 2009c. Introduction to GAMIT/GLOBK, Release 10.35, Massachussetts Institute of Technology, Cambridge, MA.

Hollingsworth, J., Jackson, J., Walker, R. & Nazari, H., 2008. Extrusion tectonics and subduction in the eastern South Caspian region since 10 Ma, Geology, **36,** 763–766, doi:10.1130/G25008A.1.

Jackson, J.A. & McKenzie, D.P., 1984. Active tectonics of the Alpine-Himalayan Belt between western Turkey and Pakistan, Geophys. J. R. astr. Soc., **77,** 185–246.

Jackson, J.A., Priestley, K., Allen, M. & Berberian, M., 2002. Active tectonics of the South Caspian Basin, Geophys. J. Int., **148,** 214–245.

James, T.S. & Ivins, E.R., 1998. Predictions of Antarctic crustal motions driven by present-day ice sheet evolution and by isostatic memory of the Last Glacial Maximum, J. geophys. Res., **103,** 4993–5017.

Karner, G.D. & Watts, A.B., 1983. Gravity-anomalies and flexure of the lithosphere at mountain ranges, J. geophys. Res., **88,** 449–477.

Landgraf, A., Ballato, P., Strecker, M.R., Friedrich, A., Tabatabaei, S.H. & Shahpasandzadeh, M., 2009. Fault-kinematic and geomorphic observations along the North Tehran Thrust and Mosha Fasham Fault, Alborz mountains Iran: implications for fault-system evolution and interaction in a changing tectonic regime, Geophys. J. Int., **177,** 676–690.

Larson, K.M. & van Dam, T., 2000. Measuring postglacial rebound with GPS and absolute gravity, Geophys. Res. Lett., **27,** 3925–3928.

Lyard, F., Lefevre, F., Letellier, T. & Francis, O., 2006. Modelling the global ocean tides: modern insights from FES2004, Ocean Dyn., **56,** 394–415.

Masson, F., Chery, J., Hatzfeld, D., Martinod, J., Vernant, P., Tavakoli, F. & Ghafory-Ashtiani, M., 2005. Seismic versus aseismic deformation in Iran inferred from earthquakes and geodetic data, Geophys. J. Int., **160,** 217–226.

Masson, F., Anvari, M., Djamour, Y., Walpersdorf, A., Tavakoli, F., Daignieres, M., Nankali, H. & Van Gorp, S., 2007. Large-scale velocity field and strain tensor in Iran inferred from GPS measurements: new insight for the present-day deformation pattern within NE Iran, Geophys. J. Int., **170,** 436–440.

McCaffrey, R., 2002. Crustal block rotations and plate coupling. in Plate Boundary Zones, pp. 101–122, eds Stein, S. & Freymueller, J. T., AGU Geodynamics Series.

McQuarrie, N., Stock, J.M., Verdel, C. & Wernicke, B.P., 2003. Cenozoic evolution of Neotethys and implications for the causes of plate motions, Geophys. Res. Lett., **30,** doi:10.1029/2003GL017992.

Meade, B.J. & Hager, B.H., 2005. Block models of crustal motion in southern California constrained by GPS measurements, J. geophys. Res., **110,** B04402, doi:10.1029/2004JB003331.

Meade, B.J., Hager, B.H., McClusky, S., Reilinger, R., Ergintav, S., Lenk, O., Barka, A. & Ozener, H., 2002. Estimates of seismic potential in the Marmara Sea regions from block models of secular deformation constrained by Global Positioning System Measurements, Bull. seism. Soc. Am., **92,** 208–215.

Meurers, B., Van Camp, M. & Petermans, T., 2007. Correcting superconducting gravity time-series using rainfall modelling at the Vienna and Membach stations and application to Earth tide analysis, J. Geodyn., **81,** 703–712.

Nazari H., Ritz, J.-F., Shafei, A., Ghassemi, A., Salamati, R., Michelot, J.-L. & Massault, M., 2009. Morphological and paleoseismological analyses of the Taleghan fault, Alborz, Iran, Geophys. J. Int, **178,** 1028–1041, doi:10.1111/j.1365-246X.2009.04173.x.

Nazari, H., Ritz, J.-F., Salamati, R., Shahidi, A., Habibi, H., Ghorashi & Karimi Bavandpur, A., 2010. Distinguishing between fault scarps and shore lines: the question of the nature of the Rey and Kahrizak features in Tehran region, Terra Nova, **22**, 227–237, doi:10.1111/j.1365-3121.2010.00938.x.

Okada, Y., 1985. Surface deformation due to shear and tensile faults in a half-space, Bull. seism. Soc. Am., **75,** 1135–1154.

Okada, Y., 1992. Internal deformation due to shear and tensile faults in a half-space, Bull. seism. Soc. Am., **82,** 1018–1040.

Paul, A., Hatzfeld, D., Kaviani, A., Tatar, M. & Péquegnat, C., 2010. Seismic imaging of the lithospheric structure of the Zagros mountain belt (Iran), Tectonic and Stratigraphic Evolution of Zagros and Makran during the Meso-Cenozoic, eds, Leturmy, P. & Robin, C., Geol. Soc. London, Spec. Pub., in press.

Reilinger, R. et al., 2006. GPS constraints on continental deformation in the Africa-Arabia-Eurasia continental collision zone and implications for the dynamics of plate interactions, J. geophys. Res., **111,** B05411, doi:10.1029/2005JB004051.

Ritz, J.-F., 2009. Extrusion tectonics and subduction in the eastern South Caspian region since 10 Ma: COMMENT, Geology, **37,** e191, doi:10.1130/G25627C.1.

Ritz, J.-F., Nazari, H., Ghassemi, A., Salamati, R., Shafei, A., Solaymani, S. & Vernant, P., 2006. Active transtension inside central Alborz: a new insight into northern Iran-southern Caspian geodynamics, Geology, **34,** 477–480.

Savage, J. & Burford, R., 1973. Geodetic determination of relative plate motion in Central California, J. geophys. Res., **95,** 4873–4879.

Solaymani, S., Ritz, J-F. & Abbassi, M., 2010. Analysing the junction between the Mosha and the North Tehran active faults, Tectonophysics, in press.

Tatar, M., Jackson, J., Hatzfeld, D. & Bergman, E., 2007. The 2004 May 28 Baladeh earthquake (M-w 6.2) in the Alborz, Iran: overthrusting the South Caspian Basin margin, partitioning of oblique convergence and the seismic hazard of Tehran, Geophys. J Int., **170,** 249–261.

Tchalenko, J.S., 1975. Seismotectonic framework of north tehran fault, Tectonophysics, **29,** 411–420.

Van Camp, M., Williams, S.D.P. & Francis, O., 2005. Uncertainty of absolute gravity measurements, J. geophys. Res., **110,** B05406, doi:10.1029/2004JB003497.

Vernant, P. & Chery, J., 2006. Mechanical modelling of oblique convergence in the Zagros, Iran, Geophys. J Int., **165,** 991–1002.

Vernant, P. et al., 2004a. Deciphering oblique shortening of central Alborz in Iran using geodetic data, Earth planet. Sci. Lett., **223,** 177–185.

Vernant, P. et al., 2004b. Deciphering oblique shortening of central Alborz in Iran using geodetic data, Earth planet. Sci. Lett., **223,** 177–185.

Vernant, P. et al., 2004c. Present-day crustal deformation and plate kinematics in the Middle East constrained by GPS measurements in Iran and northern Oman, Geophys. J. Int., **157,** 381–398.

Wahr, J., Dazhong, H. & Trupin, A., 1995. Predictions of vertical uplift caused by changing polar ice volumes on a viscoelastic earth, Geophys. Res. Lett., **22,** 977–980.

Wahr, J., Swenson, S., Zlotnicki, V. & Velicogna, I., 2004. Time-variable gravity from GRACE: first results, Geophys. Res. Lett., **31,** L11501, doi:10.1029/2004GL019779.

Walpersdorf, A. et al., 2006. Difference in the GPS deformation pattern of north and central zagros (Iran), Geophys. J. Int., **167,** 1077–1088.

Watts, A.B., Bodine, J.H. & Steckler, M.S., 1980. Observations of flexure and the state of stress in the oceanic lithosphere, J. geophys. Res., **85,** 6369–6376.

Wenzel, H.-G., 1994. Earth tide analysis package ETERNA 3.0, Bulletin d'Informations des Marées Terrestres, **118,** 8719–8721.

Article2: Fixed gravimetric-altimetry boundary value problem for geoid determination on islands, case study: Qeshm island

(Journal of the Earth and Space Physics, 2008, Vol. 34, No. 4, 81-104)

Journal of the Earth and Space Physics, 2008, Vol. 34, No. 4, 81-104

Fixed garvimetric-altimetry boundary value problem for geoid determination on islands
Case study: Qeshm island

Safari, A[1]., Hatam, Y[2]. and Sha Haidary, M[3].

[1]*Assistant Professor, Department of Surveying and Geomatics Engineering, Faculty of Engineering, University of Tehran, Iran*

[2]*Research Assistant, National Cartography Center, Tehran, Iran*

[3]*M.Sc. student of Geodesy, Department of Surveying and Geomatics Engineering, Faculty of Engineering, University of Tehran, Iran*

(Received: 27 Oct 2007 , Accepted: 23 Jun 2008)

Abstract

Precise geoid determination on islands suffers from the lack of accurate gravity data on the open seas. Nowadays, sub-microgal accuracy for the land gravity observations is obtainable. But the sea gravity data which are collected via shipborne techniques, due to the measuring environment at sea area, are usually highly noisy and are contaminated with various systematic errors.

On the other hand, satellite altimetry has provided a new source of information for geoid determination at sea area. It should be noted that satellite altimetry has accuracy at centimeter level which reaches decimeters at coastal. Such accuracy in geometric space is equivalent to microgal in gravity space. Therefore, one can see the altimetry data as a relatively accurate source of information for gravity applications.

With satellite altimetry observations at the sea area and accurate gravity data on the islands, we can define a gravimetric-altimery boundary value problem. Geometry of the oceanic part of the Earth'surface is given by the altimetric data. Ergo the problem at the oceanic part is a fixed boundary value problem. At the continental part, now, GPS is operable. The availability of the GPS coordinates means the geometry of the continental part can be considered as known. Ergo, we deal with a fixed gravimetric-altimetry boundary value problem.

By applying variational techniques to the fixed gravimetric-altimetry boundary value problem the existence and uniqueness of its weak solution can be proved (Keller, 1996).

In this paper, using satellite altimetry observations on the open sea and gravity from gravimetry on the island, a fixed gravimetric-altimetry boundary value problem for geoid computations at islands has been developed. The problem is defined as follows:

$$
\begin{cases}
1.\,div\,grad\,w(x)=2\omega^2 & \forall x\in\Re^3/D\bigcup\partial\mathrm{G}_e^+ \\
(outside\,the\,Earth's\,masses) & \\
2.\,div\,grad\,w(x)=-4\pi G\sigma+2\omega^2 & \forall x\in D\bigcup\partial\mathrm{G}_e^- \\
(\mathrm{int}\,egral\,space\,plus\,boundary\,of\,the\,planet\,of\,the\,Earth & \\
3.\,E\left\{\left\|gradw\right\|\right\}=\gamma\left(x\right) & \forall x\in\partial\mathrm{G}_e=M_h^2 \\
(boundary\,value\,data\,of\,type\,\mathrm{mod}\,ulus\,of\,gravity & \\
4.\,E\left\{h\right\}=h_{Satellite\,Altimetry} & \forall x\in\partial\mathrm{G}_e=M_s^2 \\
(boundary\,value\,data\,of\,type\,satellite\,altimetry & \\
5.\,w(x)=w_0 & \forall x\in\partial\mathrm{G}_e=M_g^2 \\
(equipotential\,value\,at\,the\,level\,of\,the\,geoid\,close\,to\,mean\,sea\,level) & \\
6.\,w(x)=\frac{1}{2}\omega^2\left\|x-\langle x|e_\omega\rangle e_\omega\right\|_2^2+\frac{gm}{\left\|x\right\|_2}+O_w(\frac{1}{\left\|x\right\|_2^3}) & \left\|x\right\|_2\to\infty \\
(regularity\,condition\,at\,\mathrm{inf}\,inity &
\end{cases}
$$

where w is the gravity potential of the Earth, γ the norm of the gravity vector on the island, $h_{Satellite\ Altimetry}$ geoid from satellite altimetry observations, σ mass density, ω the angular velocity and w_0 geoid potential. The first step towards the solution of the proposed fixed-free two-boundary value problem is the linearization of the problem. After linearization we obtained an oblique boundary condition on the island and a Dirichlet condition on the sea area.

The algorithmic steps of the solution of the fixed garvimetric-altimetry boundary value problem for geoid computations at islands are as follows:

- Application of the ellipsoidal harmonic expansion complete up to degree and order 360 and of the ellipsoidal centrifugal field for removal of the effect of the global gravity from gravity intensity at the surface of the island.
- The removal from the gravity intensity at the surface of the Earth the effect of residual masses at the radius of up to 55 km from the computational point.
- Derivation marine geoid from satellite altimetry data.
- Application of the ellipsoidal harmonic expansion complete up to degree and order 360 and of ellipsoidal centrifugal field for removal of from the geoidal undulations derived from satellite altimetry the effect of the global gravity.
- The removal from geoidal undulations derived from satellite altimetry of the effect of water masses at the radius of up to 55 km from the computational point.
- Application of Koch and Kusche algorithm (Koch and Kusche, 2002) for derivation of disturbing gravity potential at the surface of the reference ellipsoid from residual gravity intensity and residual gravity potential of satellite altimetry data.
- Restoration of the removed effects on the surface of the reference ellipsoid.
- Application of ellipsoidal Bruns formula in order to compute geoid undulations.
- Computation of the geoid of Qeshm Island of Iran has successfully tested this methodology.

Key words: Satellite altimetry, Geoid computations on islands, GPS/leveling, Gravity, Variational methods

Article3: Design of a Gravity Base Network

(Journal of AVN - Allgemeine Vermessungs-Nachrichten, 2006, No. 11-12, 374-382)

M. Najafi-Alamdari,
M. Mashhadi Hossainali,
Y. Hatam Chavari,
F. Tavakoli

Design of a Gravity Base Network

Es wird ein Basis-Schwerenetz für den Iran vorgestellt. Die 19 Schwerestationen liegen an nationalen Flugplätzen. An neun Stationen sollen absolute Schweremessungen durchgeführt werden und sechs Stationen bilden eine Eichstrecke vom Nordwesten zum Südosten des Landes.

1 Introduction

Following the request of the National Cartographic Center (NCC) of Iran and in a joint project between the NCC and the K.N. Toosi University of Technology, a gravity base network was designed and proposed for Iran. This paper reviews the design process of the network. The network when it is measured will consist of stations with known absolute gravity to serve as a base for future densification networks needed in the country. It is supposed to meet the international gravity standards required also by the international gravity network called the International Gravity Standardization Network of 1971 (IGSN71), Morelli et al. (1971).

1.1 A gravity base network

A gravity base network is supposed to be a set of benchmarks uniformly distributed across the country and the absolute gravity values at the benchmarks are known to the best accessible accuracy. The gravity at the benchmark stations are either measured directly with absolute devices or transferred by gravity difference measurements by gravimeters from known stations. To decrease the accumulation of random measuring errors arising from these transfers, the number of base stations distributed across the country should be as small as possible. This is feasible if the stations are selected in the national airports long distances apart but faster accessible and measurable by a gravimeter carried in an airplane between the stations. The gravimeter used for the gravity difference measurement should be accurate to a few micro Gal, e.g., CG-3/3M, Scintrex L.T.D. (1995), to result in the gravity base stations of required accuracies fulfilling various engineering applications of gravity. To realize the importance of such a network, various applications of a gravity base network are firstly reviewed.

1.2 Applications of a gravity base network

A gravity base network is the required reference frame for establishing 1st, 2nd, 3rd order gravity networks. As stated in Torge (1989) a gravity network is used for:

a. Mapping of the structure of upper crust in geology maps. The required accuracy for the measured gravity values is about 0.2 to 0.4 mGal.
b. Oil and mineral explorations. The required accuracy for the measured gravity values is about 5 μGal.
c. Geotechnical studies in mining areas for exploring the underground cavities as well as archeological studies. The required accuracy is about 5 μGal and better.
d. Subsurface water resource explorations and mapping crustal layers which absorb it. An accuracy of the same level of previous applications is required here too.
e. Studying the tectonics of the Earth's crust. Repeated precise gravity measurements at the gravity network stations can assist us in identifying systematic height changes. The accuracy of the order of 5 μGal and more is required.
f. Studying volcanoes and their evolution. Repeated precise gravity measurements at the gravity network stations can provide valuable information on the gradual upward movement of lava.
g. Producing precise mean gravity anomaly for precise geoid determination. Replacing precise spirit leveling by the GPS leveling using precise geoid model is one of the forth coming application of the precise geoid.

1.3 History of the gravimetric surveys in Iran

According to Afshar and Zomorrodian (1970), a preliminary First Order Gravity Network (FOGN) in Iran was established using bench marks and points marked on buildings. The instrument used for the measurements was Askania Graf Instrument providing accuracies of $\pm$ 0.01 mGal or better. For the fact that the bench marks were demolished or transferred and also for the rather low accuracy of the net, a new FOGN was established in 1970 in the country. The new network consisted of 23 stations 14 of which were selected in airports for the best accessibility by the air transportation. The other 9 points were located in the railway stations. These 9 stations were selected to accomplish a uniform network. The Mehrabad airport station in Tehran with known absolute gravity was the only reference station defining the datum of network. This station is a component of IGSN71 network measured partly by the US Air Force using La coste & Romberg gravimeter. The over all accuracy of the network was estimated to be $\pm$ 0.004 mGal/km. Fig. 1 illustrates the distribution of the new FOGN network in Iran. In this figure, green stations showing the airports and blue ones are the rest.
In 1970, the Institute of Geophysics of Tehran University (IGTU) established a national calibration line for Iran. The line extended from Shiraz in the south to Chalus in the north of the country. The line covered latitudes

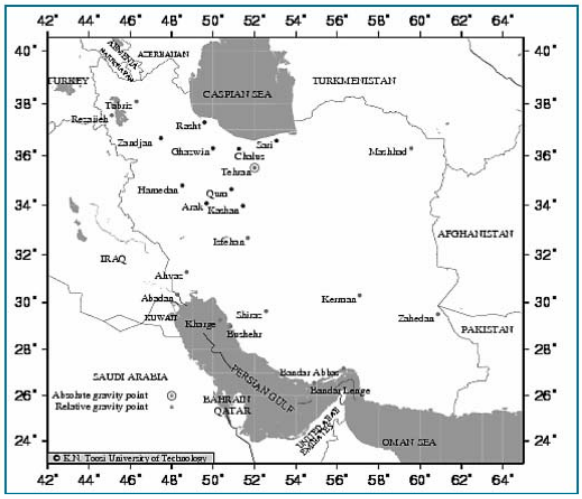

Fig. 1: The first order gravity network of Iran, Afshar and Zomorrodian (1970)

range from 29.55° to 36.4∅°, ZOMORRODIAN (1972). It was later extended in the south and north directions in a joint project between the National Cartographic Center (NCC) and IGTU, ZOMORRODIAN (1985). In 1987 IGTU established a new gravity datum in IGTU building in Tehran, ZOMORRODIAN (1987).

In 1980, NCC also take hold of gravity measurements in the country. The primary goal was to investigate the systematic effect of gravity field in the leveling network, VANICEK and KRAKIWSKY (1986), in order to correct the orthometric heights in the country. In 1996 NCC bought two sets of CG-3M micro gravimeters. In June 1997 a technical committee was organized in the department of Land Surveying and Geodesy of NCC to promote academic studies on gravity. This committee decided to firstly establish a new gravity base network as a foundation supporting the modern demands:

i. High accuracy inquiry by the modern gravity projects
ii. Maintaining high reliability required by integral gravimetric activites
iii. Inquiry for high resolution and accurate gravity anomaly data needed for a precise geoid.
iv. Evolution of micro gravimetric networks.

2 Computation of a gravity base network

In a gravity network, the absolute gravity values at the stations are sought. Aiming at obtaining absolute gravity with a pre-determined accuracy, a measurement program has to be pre-analyzed. For the gravity difference measurements to result in the absolute gravity values at stations, at least one station is required to be known in its absolute gravity. It is called the reference station. Existence of more than one reference station with known accuracy would help the better adjustment of the network. Assuming gravity differences $\delta\mathbf{g}$ (vector of observations) measured between the reference stations with known gravity values $\mathbf{g}^{(0)}$ (vector of initial known values) and the stations with unknown gravity values $\mathbf{g}$ (vector of unknowns) in the network, two mathematical models one is called the observation equations as the main mathematical model, Eq. (1), describing the relations between the gravity difference measurements and the unknowns, and other as the constraint model, Eq. (2), formulating the known absolute gravity values:

$$\delta_{\mathbf{g}} = \mathbf{A}\mathbf{g};\ \mathbf{C}_{\delta\mathbf{g}} \tag{1}$$

$$\mathbf{g}^{(0)} = \mathbf{H}\mathbf{g};\ \mathbf{C}_{\mathbf{g}^{(0)}} \tag{2}$$

are performed where $\mathbf{A}$ and $\mathbf{H}$ are the corresponding design matrices. Two typical equations making up the main and the constraint models read

$$\delta g_{ij} = g_j - g_i + \Delta t_{ij} d, \tag{3}$$

$$g_k - g_k^{(0)} = 0 \tag{4}$$

respectively, where g_i and g_j are the sought absolute gravity values at stations number i and j, d is the unknown drift of a particular gravimeter, Δt_{ij} is the travel time spent for the measurement, g_k is the assumed unknown absolute gravity of the k-th reference station while $g_k^{(0)}$ is the initially known absolute gravity at the same station. The statistical models $\mathbf{C}_{\delta\mathbf{g}}$ and $\mathbf{C}_{\mathbf{g}^{(0)}}$ introduced in Eqs. (1) and (2) are the variance and covariance matrices describing accuracies of the gravity difference observations and the known initial absolute gravity values. The matrix $\mathbf{C}_{\delta\mathbf{g}}$ is fully populated embedding the variances as well as the covariances between gravity difference measurements obtained from gravimeter readings. The matrix is obtained using the covariance propagation law from the variances of gravimeter readings stored in the diagonal matrix $\mathbf{C}_R$:

$$\mathbf{C}_{\delta\mathbf{g}} = \mathbf{B}\mathbf{C}_{\mathrm{R}}\mathbf{B}^{\mathrm{T}} \tag{5}$$

where $\mathbf{B}$ is the matrix defining the relation between gravimeter readings and the gravity difference measurements. Using weight matrices as the inverse of covariance matrices:

$$\mathbf{P}_{\delta\mathbf{g}} = \mathbf{C}_{\delta\mathbf{g}}^{\ 1},\quad \mathbf{P}_{\mathbf{g}^{(0)}} = \mathbf{C}_{\mathbf{g}^{(0)}}^{\ 1} \tag{6}$$

the least-squares solution to the system of Eqs. (1) and (2) is

$$\hat{\mathbf{g}} = \mathbf{N}^{\ 1}\mathbf{u},\quad \mathbf{C}_{\hat{\mathbf{g}}} = \mathbf{N}^{\ 1} \tag{7}$$

$$\hat{\mathbf{r}}_{\delta\mathbf{g}} = -\delta\mathbf{g} + \mathbf{A}\mathbf{C}_{\hat{\mathbf{g}}}\mathbf{A}^{\mathrm{T}}\mathbf{C}_{\delta\mathbf{g}}^{\ 1}\delta\mathbf{g} + \mathbf{A}\mathbf{C}_{\hat{\mathbf{g}}}\mathbf{H}^{T}\mathbf{C}_{\mathbf{g}^{(0)}}^{\ 1}\mathbf{g}^{(0)} \tag{8}$$

$$\hat{\mathbf{r}}_{\mathbf{g}^{(0)}} = -\mathbf{g}^{(0)} + \mathbf{H}\mathbf{C}_{\hat{\mathbf{g}}}\mathbf{H}^{\mathrm{T}}\mathbf{C}_{\mathbf{g}^{(0)}}^{\ 1}\mathbf{g}^{(0)} + \mathbf{H}\mathbf{C}_{\hat{\mathbf{g}}}\mathbf{A}^{T}\mathbf{C}_{\delta\mathbf{g}}^{\ 1}\delta\mathbf{g} \tag{9}$$

$$\hat{\sigma}_0^2 = \frac{1}{\mathrm{df}}\left(\hat{\mathbf{r}}_{\delta\mathbf{g}}^{\mathrm{T}}\mathbf{P}_{\delta\mathbf{g}}\hat{\mathbf{r}}_{\delta\mathbf{g}} + \hat{\mathbf{r}}_{\mathbf{g}^{(0)}}^{\mathrm{T}}\mathbf{P}_{\mathbf{g}^{(0)}}\hat{\mathbf{r}}_{\mathbf{g}^{(0)}}\right) \tag{10}$$

in which

$$\mathbf{N} = \mathbf{A}^{\mathrm{T}}\mathbf{P}_{\delta\mathbf{g}}\mathbf{A} + \mathbf{H}^{\mathrm{T}}\mathbf{P}_{\mathbf{g}^{(0)}}\mathbf{H} \tag{11}$$

$$\mathbf{u} = \mathbf{A}^{\mathrm{T}}\mathbf{P}_{\delta\mathbf{g}}\delta\mathbf{g} + \mathbf{H}^{\mathrm{T}}\mathbf{P}_{\mathbf{g}^{(0)}}\mathbf{g}^{(0)} \tag{12}$$

The vector $\hat{\mathbf{g}}$ is the least-squares estimate of unknown absolute gravity values including the new values for the reference stations, while $\mathbf{C}_{\hat{\mathbf{g}}}$ is the corresponding variance-

covariance matrix. $\mathbf{r}_{\delta \mathbf{g}}$ and $\mathbf{r}_{\mathbf{g}^{(0)}}$ are the vectors of the estimated residuals to correct the observations and the initial absolute gravity values. $\hat{\sigma}_0^2$ is the a-posteriori estimate of the variance factor or the variance of unit weight with df being the degree of freedom in the mathematical model. A statistical test of quadratic forms of the residuals (8) and (9) is carried out to test for the compatibility of the a-posteriori value with its a-priori value. The test is passed if the scale of the covariance matrix $\mathbf{C}_{\delta \mathbf{g}}$ is correct. Rejection of the test may be caused by the

a. incorrect scale of the covariance matrix,
b. systematic and/or outlying observations,
c. inconsistency of the mathematical model and the observations.

It should be reminded that in the method of least-squares, systematic and gross errors may distort the estimate of unknowns. Therefore, controlling the quality of observations both before and after adjustment for the detection of any systematic error and outlier should be necessarily carried out. Nevertheless, depending on the reliability and robustness of a network, outliers that are smaller than a certain limit can cause distortions in the network, i.e., the deformation or distortion of the network is unavoidable. The analysis of these distortions and their quantification is of special interest in the quality control and design of a gravity network, a subject to be followed in this paper.

3 Relative gravimeter CG-3M

The relative gravimeter CG-3M is a production of the Canadian company Scintrex, Scintrex L.T.D. (1995). Using an internal microprocessor, the instrument operates automatically. The instrument is capable of measuring gravity variation in the range of 7000 mGal without changing the zero of its counter, from pole to the equator, Fig. 2. Starting measurement, the instrument automatically records the gravity every second. Outlying records are eliminated and replaced by new ones through statistical assessment of the sample of measurements.

Measurements and corrections are stored in the memory of instrument and can be transferred to a computer or printer if inquired. The resolution of the instrument is 1 μGal and its sample standard deviation is normally 5 μGal. The measurements and other relevant information are displayed in the instrument during the measurement. Following table compares the instrument to the CG-3 model and to other types of L&R (LaCoste Rhomberg) gravimeters:

Tab. 1: Accuracy comparison of different gravimeters

Model	Resolution (mGal)	Range (mGal)	Accuracy (mGal)
L&R-G	0.01	7000	0.015
L&R-D	0.001	200	0.005
CG-3	0.005	7000	0.010
CG-3M	0.001	7000	0.005

The accuracy in the table refers to the mean standard deviation of one observation by the instrument inferred from the sample of observation. For further details, the interested reader is referred to the manual of the instrument (Scintrex L.T.D., 1995, Siegel, 1995).

4 Specifications of a gravity base network

Based on the specifications mentioned above for the CG-3M gravimeter, and to fulfill the requirements of section 1.2 for obtaining an accuracy of better than 5 μGal in the absolute gravity across the network, the geometry of the network, the number of known reference stations, and the number of gravity difference measurement ties should be designed. The number of measurements should be as large as to make the network reliable to detect gross errors in the measurements. Secondly, a robustness analysis is required to design a strong enough network to resist undetectable gross errors, so that the inevitable distortions on the estimated absolute gravity values remain below the desired accuracy. On the other hand, the physical durability of the station benchmarks should be enough to maintain the accuracy of the determined absolute gravity values. To maintain the accuracy of 5 μGal, vertical stability of 2 centimeters in the vertical direction for the benchmarks is required in the life-time of the network. Considering the small horizontal gradient of gravity, the horizontal stability of the stations is easily maintained. Nevertheless, with all pre-cautions spent in construction of the benchmarks, the physical stability of stations is subject to the tectonic movement in the region.

A network of 19 stations to be built in the national airports of Iran is assumed. Airports are usually built in geologically stable places and they are also suitable places for the gravity stations in long distances apart since they are quickly accessible by airplanes. Figure 3 shows a network of totally 19 stations assumed in the airports of Yazd, Tehran, Tabriz, Rasht, Kermanshah, Isfehan, Ahvaz, Abadan, Shiraz, Lar, BandarAbbas, Chabahar, Iranshahr, Kerman, Zabol, Birjand, Mashhad, Kolaleh, and Tabas in Iran. The average spacing between the stations is 460 km, while the minimum distance is 100 km and the maximum distance

Fig. 2: Scintrex gravimeter at a gravity base station in Tehran

is 800 km. Among the 19 stations, 9 stations Yazd, Tehran, Tabriz, Ahvaz, Abadan, Chabahar, Iranshahr, Kerman, and Mashhad are considered as known reference stations, so that the absolute gravity is supposed to be measured at these stations. The station Abadan is located in Arabian plate, Berberian and Berberian (1981). The gravity at this station may have a different behavior in comparison to the other stations of the network. For this reason and despite of the small distance between this and the station Ahvaz, absolute gravity is required to be measured at this station too. The study of the gravity change between these stations can provide valuable information in the tectonics of this area. Today, absolute gravity can be measured to an accuracy of 3 μGal by FG5, SASAGAWA et al. (1995).

5 Design of measurement of the gravity base network

Taking the 9 stations mentioned above as the reference stations, absolute gravity at which are supposed to be measured to the accuracy of 3 μGal using modern absolute devices, NIEBAUER 1995, SEIGEL (1995), and assuming that the gravity difference measurements are to be done with CG-3M gravimeter whose nominal accuracy is 5 μGal, different designs of gravity difference measurements between the known and unknown stations have been analyzed. The mathematical tool for the analysis is the relation between the measurement accuracies, the accuracy of the known stations, and the accuracy of unknowns, deduced from Eqs. (5), (7), and (11) as

$$\mathbf{C}_{\hat{\mathbf{g}}} = \left(\mathbf{A}^{\mathrm{T}}(\mathbf{B}\mathbf{C}_{\mathrm{R}}\mathbf{B}^{\mathrm{T}})^{-1}\mathbf{A} + \mathbf{H}^{\mathrm{T}}\mathbf{C}_{\mathbf{g}_{(0)}}^{-1}\mathbf{H}\right)^{-1}. \tag{13}$$

The matrices **A**, **B**, and **H** are defining the geometry of the proposed gravity difference measurements and the known stations. The matrices $\mathbf{C}_{\mathbf{g}_{(0)}}$ and $\mathbf{C}_R$ are built up in accordance with the proposed scheme of the measurement and the nominal accuracies of the absolute and relative instruments. To assess the contribution of an observation in the adjustment of the measurements, its redundancy number (VANICEK et al. 1990) among other observations

$$d_i = 1 - \frac{\sigma^2_{\delta\hat{g}_i}}{\sigma^2_{\delta g_i}}, \tag{14}$$

has to be investigated. The number can also be visualized as the corresponding diagonal element of the matrix:

$$\mathbf{I} - \mathbf{A}\mathbf{C}_{\hat{\mathbf{g}}}\mathbf{A}^{\mathrm{T}}(\mathbf{B}\mathbf{C}_{\mathrm{R}}\mathbf{B}^{\mathrm{T}})^{-1}. \tag{15}$$

For the weighted parameters or the initial absolute gravity values too, the redundancy numbers are seen as the diagonal elements of the matrix:

$$\mathbf{I} - \mathbf{H}\mathbf{C}_{\hat{\mathbf{g}}}\mathbf{H}^{\mathrm{T}}\mathbf{C}_{\mathbf{g}_{(0)}}^{-1}. \tag{16}$$

Five different sets of gravity difference observations were proposed for the network measurement. At each set, a nuisance unknown parameter of the gravimeter called drift is also considered. To solve for the daily drift rate, multiple forward and backward running of gravimeter measurements are required. Each set of observations was analyzed

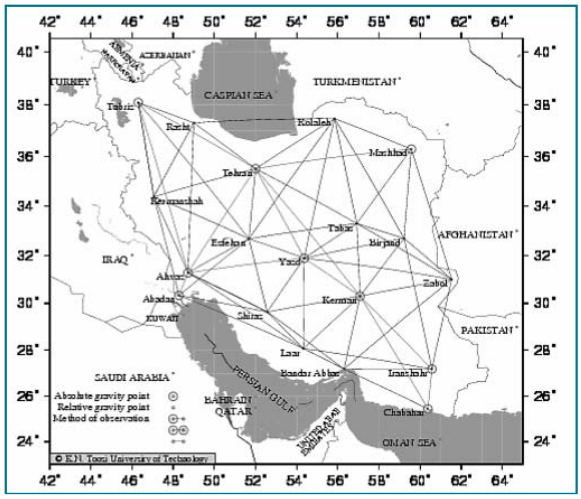

Fig. 3: The proposed gravity base network of Iran with gravity difference measurements ties

for the internal and external reliability assigns to the network in accordance with the reliability theory of BAARDA (1976). In his reliability theory, BAARDA (1976) uses the concept of alternative hypothesis test, WONNACOTT and WONNACOTT (1977), to determine how a network is reliable in detecting a blunder(s) among its observations. BAARDA measures the reliability in terms of the power of alternative test $1-\beta$, β being the probability of type II error, conducted on each observation in the network. That is, a network is $(1-\beta)\%$ reliable to detect a blunder equal to or larger than a certain size Δ_i in an observation. This means that, the blunders or gross errors smaller than Δ_i may remain undetectable in the network. This threshold gross error is shown to be a function of measured accuracy, redundancy number of the observation, and is proportional to the non-centrality parameter δ of the alternative hypothesis test as well. The parameter itself is a function of the significance level α, i.e., complementary to the confidence level of the null hypothesis test, and the β. Opting for $\alpha = 0.05$, $\beta = 0.10$, and for the statistic being the normal standard, the non-centrality parameter δ would be equal to 3.24. The threshold gross error is then given by

$$\Delta_i = \frac{3.24\sigma_i}{\sqrt{d_i}} \tag{17}$$

where σ_i is the standard deviation of the observation number i, and d_i is the redundancy number. According to the equation, an observation with smaller standard deviation and larger redundancy number leaves smaller gross error undetected in the network. To keep all undetected gross errors smaller so that the caused gravity distortions in the network drop under a desired value, the stations are required to be evenly distributed across the network in a way to keep the travel times between stations almost the same, and the observations are repeated as frequently as possible, BECKER (1995). The largest value of Δ_i computed across is known as the internal reliability of the network at the 90 % confidence level. Observational errors smaller than this value are assumed to remain undetected.

Hence, they may cause virtual as such unwanted distortions in the network. The amount of distortions at the network stations are computed by the following equation

$$\Delta\hat{\mathbf{g}} = \mathbf{N}^{-1}\Delta\mathbf{u} = \mathbf{N}^{-1}\left(\mathbf{A}^{\mathrm{T}}\mathbf{P}_{\delta\mathbf{g}}\Delta_{\delta\mathbf{g}} + \mathbf{H}^{\mathrm{T}}\mathbf{P}_{\mathbf{g}^{(0)}}\Delta_{\mathbf{g}^{(0)}}\right). \quad (18)$$

This is known as the external reliability of the network. This equation gives the change or distortion in the gravity value of the stations. Using Eq. (18), distortions in the network initiated from each of the five proposed set of observations are computed. The optimum set of observations is the one causing distortions under 5 μGal.

6 Configuration of the optimum set of observations

One of the five proposed sets of observations satisfies as the optimal design of the network measurement due to its small total flight distances, its high accuracy in estimating the unknowns, uniformly distribution of the absolute gravity accuracy across the network, and the minimal unavoidable distortions caused in the network. In this design, gravity difference measurements are to be done using relative gravimeter CG-3M in the forward and backward mode. The gravimeter is to be carried by an airplane between the stations. Each forward and backward measurement adds a new unknown parameter the instrumental drift rate to the number of unknowns. It is assumed that the measurement accuracy depends on the travel time for gravity difference measurements. There are totally 66 forth and back flights in this design. The longest flight line is 800 km and the smallest one is 100 km. Measurements of long distances such as Tehran to Tabriz, Mashhad, Isfehan, Shiraz, Yazd, Kerman, Bandar Abbas, Ahvaz and Kermanshah are proposed to be done in a shorter time interval using the Iran-Air commercial flights, while short distances are supposed to be done using the NCC charter planes usually used for the photogrammetry flights. To improve the accuracy of drift estimates, gravity is to be measured after arrival and before departure in every station. This will result in one degree of freedom for each drift. The gravity difference measurements of the selected design are classified in three distinct groups:

a. Gravity difference measurements between the reference stations: there are totally 12 back and forth gravity difference measurements between the known reference stations. Using these measurements, the scale factor of the instrument is determined. In addition, a test on the instrument can also be conducted to see if the accuracy of the gravity difference measurement depends at least partially on the travel time of measurement by the gravimeter. For this, a model of variance accommodating for a linear dependency on the time of measurement was assumed as

$$\sigma^2_{\delta g} = 50 + a\Delta t, \quad (19)$$

where 50 micro Gal squared is the two times of the variance of one gravimetry record, a is the coefficient to be determined, and Δt is the measurement time.

b. Gravity difference measurements between the known and unknown stations: gravity difference measurements connecting each unknown station to at least three known stations were considered.
c. Gravity difference measurements between all unknown stations: there are totally 15 measurements between unknown stations.

Table 2 summarizes the pre-analysis results of the measurement design.

7 Conclusions and discussions

The gravity base network proposed for Iran consisting of 19 stations uniformly covers the country. With the geometry of proposed observations considered, the maximum virtual distortion anticipated in the absolute gravity values at the network stations is less than 5 μGal. Measurement errors larger than 25 μGal are designed to be detected when entering the network, while the distortions caused by undetected errors (less than 25 μGal) at the stations will remain smaller than 5 μGal. However, it is probable (10 %) that some of the network stations may be deteriorated in accuracy by distortions larger than 5 μGal. To avoid such circumstances, safety measures are to be taken, e.g., gravimeter should be carried very carefully between stations, absolute and gravity difference measurements should be carried out in appropriate weather conditions. Magnitudes of the distortions estimated by Eq. (18) are surely datum dependent, i.e., they depend on the position(s) of reference station(s) relative to the other stations. Any change in the position of a reference station would affect the magnitudes. Since in the proposed design, the gravity datum is introduced by a set of 9 reference stations that uniformly cover the network and each unknown station is connected by at least 3 gravity difference measurements to 3 of the reference stations, the influence of the gravity datum (reference stations distribution) has been minimized.

Contrary to the 2-D horizontal geodetic networks in which the horizontal angels and distances are the measurable quantities, it is gravity that has to be measured in a gravity network. In a geodetic network, designing equal angles (60°) and equal distances may bring about a uniform distribution of stations and as such a strong network resisting the horizontal angles and distances errors. Designing a strong gravity network to resist the gravity measurement errors, i.e., a network not allowing measurement errors to evolve into the gravity distortions at the stations, however, requires stations in equal time (travel time) distances a part and the gravity differences of adjacent stations not abruptly varying in the neighborhood. This resembles a geodetic horizontal network of evenly distributed stations across. For this, at least the elevation differences (creating gravity differences) between the stations are reduced by avoiding the rough topography to be selected as a station location. Airports located in flat areas, escaping high lands, are suitable places in this respect. Also selecting airports as the stations would bring shorter and almost uniform travel time distances among the stations.

Tab. 2: Accuracy analysis of the network design

From	To	d_i	Internal reliability (μGal)	gravity distortion at station #																		
				1	2	3	4	5	6	7	8	9	10	11	12	13	14	15	16	17	18	19
3	5	0.78	18.34	1	0	−3	0	1	0	1	0	0	0	0	0	0	1	1	0	−1	1	0
3	6	0.71	19.23	0	1	−5	0	0	1	1	1	0	1	1	0	1	0	1	1	−1	1	0
17	6	0.87	17.37	0	1	−3	0	0	1	0	0	0	1	1	0	1	−1	0	1	−2	1	0
1	11	0.81	18.00	−1	1	−2	1	0	0	−1	−1	0	1	2	0	1	−1	1	0	−1	0	0
1	2	0.81	18.00	−2	2	−1	1	0	0	−1	−1	0	0	1	0	1	1	1	0	0	0	0
1	14	0.72	19.09	−2	1	0	1	1	−1	−1	−1	0	1	0	1	1	4	1	0	1	0	0
3	5	0.78	18.34	1	0	−3	0	1	0	1	0	0	0	0	0	0	1	1	0	−1	1	0
3	6	0.71	19.23	0	1	−5	0	0	1	1	1	0	1	1	0	1	0	1	1	−1	1	0
17	6	0.87	17.37	0	1	−3	0	0	1	0	0	0	1	1	0	1	−1	0	1	−2	1	0
1	11	0.81	18.00	−1	1	−2	1	0	0	−1	−1	0	1	2	0	1	−1	1	0	−1	0	0
1	2	0.81	18.00	−2	2	−1	1	0	0	−1	−1	0	0	1	0	1	1	1	0	0	0	0
1	14	0.72	19.09	−2	1	0	1	1	−1	−1	−1	0	1	0	1	1	4	1	0	1	0	0
1	15	0.83	17.78	−2	1	0	1	0	0	−1	−1	0	1	1	1	1	2	1	0	1	0	0
1	10	0.85	17.57	−2	0	1	0	0	0	0	0	1	1	1	1	0	1	1	0	1	0	0
1	12	0.84	17.68	−2	0	1	0	0	0	1	1	1	0	0	1	0	0	0	0	0	1	1
1	8	0.75	18.71	2	1	1	1	0	0	3	3	1	0	0	0	1	1	0	1	0	1	1
1	7	0.70	19.36	−1	−1	0	−2	0	1	4	3	0	0	0	0	−1	−1	0	1	0	1	1
2	15	0.92	16.89	0	−1	0	−2	1	0	3	2	0	0	0	0	−1	0	1	0	0	1	0
3	2	0.94	16.71	0	0	−1	−3	1	0	2	1	0	0	0	0	0	−1	0	0	0	1	0
4	3	0.72	19.09	0	0	1	−4	1	0	1	0	0	0	0	0	0	−1	0	−1	−1	0	0
4	2	0.72	19.09	0	1	0	−5	1	0	0	0	0	0	0	0	0	−1	0	−1	−1	0	0
4	5	0.73	18.96	0	0	0	−5	0	0	0	0	0	0	0	0	0	1	0	−1	−1	0	0
4	6	0.77	18.46	0	0	0	−4	−1	0	0	0	0	0	0	0	0	1	0	−1	−1	0	0
4	6	0.77	18.46	0	0	0	−4	−1	0	0	0	0	0	0	0	0	1	0	−1	−1	0	0
5	2	0.81	18.00	0	1	0	−2	−3	0	−1	0	0	0	0	0	0	1	0	−1	0	0	0
5	14	0.69	19.50	1	0	−1	−1	−3	0	0	0	0	0	0	1	1	3	1	−1	0	0	0
5	15	0.75	18.71	1	0	−1	−1	−4	0	0	0	0	0	1	1	0	1	1	−1	0	0	0
5	1	0.78	18.34	0	0	−1	0	−4	−1	1	0	0	0	1	0	0	0	0	−1	0	1	0
5	7	0.73	18.96	0	1	−1	0	−3	−1	2	0	0	0	1	0	1	−1	0	0	0	1	0
6	2	0.77	18.46	0	2	−1	0	−1	−2	1	−1	0	0	1	1	1	0	1	0	0	1	0
6	5	0.82	17.89	1	1	−1	0	0	−3	1	0	0	1	1	1	1	1	1	0	0	1	0
6	1	0.80	18.11	1	1	−1	0	1	−3	1	1	1	1	1	1	1	1	1	0	0	1	1
6	7	0.80	18.11	1	0	−1	0	1	−2	1	2	0	1	1	0	1	1	0	0	0	1	1
6	8	0.72	19.09	0	0	−1	0	0	−2	−1	3	1	1	1	0	0	0	0	0	−1	1	1
7	10	0.75	18.71	0	0	−1	0	−1	−1	−4	3	0	1	1	0	0	0	0	0	−1	1	0
7	8	0.62	20.57	0	0	0	0	−1	−1	−4	4	−1	1	0	0	0	0	0	0	0	0	0
9	8	0.68	19.65	1	0	0	0	0	0	−1	4	−3	0	0	1	0	0	0	1	0	0	−1
9	12	0.72	19.09	1	1	1	1	1	1	0	2	−3	0	2	2	1	1	1	1	1	0	−1
9	11	0.70	19.36	1	0	1	1	1	0	0	0	−3	−1	3	3	1	1	1	1	1	0	−1
10	12	0.74	18.83	1	0	1	0	1	0	0	0	−1	−2	3	3	1	1	1	1	1	0	−1
10	11	0.73	18.96	0	0	0	0	0	0	0	1	1	−2	3	2	1	0	1	0	1	1	−1
10	9	0.75	18.71	0	0	0	0	0	0	0	1	1	−2	3	2	1	0	1	0	1	1	−1

Tab. 2: (Continue)

From	To	d_i	Internal reliability (μGal)	gravity distortion at station #																	
				1	2	3	4	5	6	7	8	9	10	11	12	13	14	15	16	17	18	19
10	8	0.70	19.36	0	1	0	1	0	1	1	3	1	−3	0	−1	0	1	−1	1	1	1	−1
10	2	0.80	18.11	0	1	0	1	0	0	0	2	0	−2	0	−2	1	2	−1	1	1	0	−1
12	14	0.64	20.25	0	0	1	1	1	0	1	2	−1	−1	0	−4	1	4	−1	1	1	0	−1
12	13	0.73	18.96	0	0	1	0	0	0	1	1	−1	0	2	−5	1	1	−1	0	1	0	0
12	11	0.59	21.09	0	0	1	0	0	0	1	1	0	1	4	−4	−1	−1	0	0	0	1	0
13	11	0.67	19.79	0	0	1	0	0	0	1	0	0	1	4	−2	−3	0	1	0	0	1	0
13	15	0.75	18.71	1	0	1	1	1	1	1	0	0	1	2	−1	−4	1	1	0	1	1	0
13	14	0.63	20.41	1	1	1	1	1	1	1	1	0	0	0	0	−4	3	0	1	1	0	0
13	2	0.68	19.65	0	2	0	1	0	1	0	0	0	0	−1	0	−4	0	−1	1	1	0	0
14	2	0.76	18.58	−1	3	0	1	0	0	0	0	0	0	0	−1	−3	−2	−2	0	1	0	0
15	14	0.70	19.36	0	1	0	0	0	0	1	1	0	0	−1	0	−2	2	−4	1	1	0	0
15	10	0.74	18.83	0	0	0	0	−1	0	1	1	0	1	0	0	−1	1	−4	0	0	1	0
15	12	0.75	18.71	0	0	0	−1	−1	0	1	0	1	1	1	1	−1	1	−4	0	0	1	0
15	11	0.72	19.09	0	0	0	−1	−1	0	1	0	1	1	2	1	0	0	−3	−2	0	1	1
16	6	0.83	17.78	0	0	0	0	0	0	0	0	1	1	1	1	0	0	−1	−3	1	0	0
16	4	0.77	18.46	0	1	0	1	0	0	0	0	0	1	1	1	1	1	0	3	1	0	0
16	5	0.76	18.58	1	1	0	1	1	0	1	0	0	0	0	1	0	1	1	−4	1	0	0
16	8	0.77	18.46	1	0	0	0	1	1	1	2	0	0	0	0	0	0	1	−3	0	1	0
16	7	0.78	18.34	0	0	1	1	0	1	2	1	0	0	0	0	0	0	0	−2	−2	1	0
17	4	0.77	18.46	0	0	1	0	0	0	1	1	0	0	−1	0	0	−1	0	−1	−4	1	0
17	3	0.65	20.09	0	0	2	0	0	0	0	0	0	0	0	0	0	−1	0	0	−5	0	0
17	2	0.74	18.83	0	0	1	0	0	0	−1	0	0	0	0	0	0	0	0	0	−5	−1	0
17	14	0.68	19.65	0	−1	0	0	1	0	−1	−1	0	0	0	1	0	3	0	0	−4	−2	0
18	11	0.77	18.46	0	0	0	0	0	−1	−1	−1	0	0	1	1	0	1	0	0	−2	−3	0
18	9	0.74	18.83	0	0	0	0	0	0	−1	0	1	0	0	0	0	0	0	0	−1	−4	0
18	8	0.73	18.96	0	0	0	0	0	0	0	1	0	0	−1	0	0	0	0	0	0	−4	−1
18	7	0.71	19.23	0	0	0	1	0	1	2	1	−1	0	0	0	0	0	0	1	1	−4	−2
18	10	0.83	17.78	0	0	0	1	0	0	1	1	0	1	0	0	0	0	0	0	1	−2	−3
19	9	0.69	19.50	1	0	0	1	0	1	1	1	1	1	1	1	0	0	1	1	1	0	−5
19	18	0.70	19.36	1	0	0	1	1	1	1	1	1	1	1	1	1	1	1	1	0	1	−5
19	10	0.80	18.11	0	0	0	0	0	0	0	0	0	1	1	0	0	0	0	0	0	1	−3
1	1	0.83	10.67	2	1	1	1	2	1	2	1	1	1	1	2	1	2	2	1	1	1	1
2	2	0.68	11.79	1	4	1	2	2	1	1	0	0	1	0	1	2	0	2	1	2	0	1
3	3	0.60	12.55	1	1	5	1	1	1	1	1	1	1	1	1	1	1	1	1	2	1	1
6	6	0.81	10.80	1	1	1	1	1	2	2	2	1	1	1	1	1	1	1	1	1	1	1
9	9	0.64	12.15	1	1	1	1	1	1	0	2	4	1	2	2	1	1	1	1	1	2	2
10	10	0.82	10.73	1	1	1	1	1	1	1	1	1	2	2	1	1	1	1	1	1	1	1
13	13	0.76	11.15	1	2	1	1	1	1	1	0	1	1	2	1	3	2	1	1	2	1	1
16	16	0.78	11.01	1	1	1	1	1	1	2	2	1	1	1	1	1	1	1	2	1	2	1
19	19	0.67	11.87	1	1	1	1	1	1	1	1	2	1	1	1	1	1	1	1	1	1	4

Tab. 2: (Continue)

Standard deviations of gravity stations			
Standard deviation	Station Number	Standard deviation	Station Number
1.24	1	1.92	11
1.70	2	1.71	12
1.91	3	1.47	13
1.46	4	2.77	14
1.59	5	1.58	15
1.31	6	1.42	16
2.15	7	1.67	17
1.83	8	1.59	18
1.79	9	1.74	19
1.26	10		

A linear drift model was assumed for the CG-3M gravimeter in the observation equation (3). This would require the measurements to be carried out as fast as possible between the stations. For this, it is proposed that the long distances to be measured using national flights. Short connections can be measured using the charters of the National Cartographic Center (NCC). Finally, it can be said that the designed observations for the gravity base network will bring about accuracies of better than 5 μGal. The parallel use of second gravimeter side by side of the first gravimeter in the network measurement would bring about more redundancy of the observations even if one more scale factor and some drift rates are added to the number of nuisance parameters to be solved for in the network.

References

[1] Afshar, H. K.; Zomorrodian, H. (1970): The Measurement and Adjustment of the First Order Gravity Network of Iran, Institute of Geophysics, Tehran University

[2] Baarda, W. (1976): Reliability and precision of Networks. Delft Geodetic Institute, Publications of the Computing Center, Delft, Netherlands

[3] Becker, M. (1995): „Techniques of Precise Gravimetry. Report of the chairman of SSG 3.133." XXIth General Assembly of the International Association of Geodesy, Boulder, Colorado, USA, July 3–14, 1995

[4] Berberian, F.; Berberian, M. (1981): Tectono-Plutonic Episodes in Iran, Paper submitted in the Book, Zagros, Hindu Kush, Himalaya Geodynamic Evolution

[5] Morelli, C.; Gantar, C.; Honkaslo, T.; McConnell, R. K.; Tanner, T. G.; Szabo, B.; Uotila, U.; Whalen, C. T. (1971): „The International Gravity Standardization Network 1971 (IGSN71), Special Publication 4 of Bulletin Geodesique." International Association of Geodesy

[6] Niebauer, T.; Sasagawa, G.; Faller, J.; Hilt, R.; Klopping, F. (1995): A new generation of absolute gravimeters, Metrologia, 32, 159–180

[7] Sasagawa, G.; Klopping, F.; Niebauer, T.; Faller, J.; Hilt, R. (1995): Inter-comparison tests of the FG5 absolute gravity meter, Geophys. Res. Lett., 22, 461–464

[8] Scintrex User's Guide, (1995): CG-3/3M gravity meter. Scintrex Ltd., Concord, Ontario

[9] Seigel, H. O. (1995): „High Precision Gravity Guide, Scintrex L.T.D."

[10] Torge, W. (1989): Gravimetry, Walter de Gruyter, Berlin and New York, 1989, 465 pp., 253 figs. and 35 tables, DM 178, $94.95, ISBN: 3-11-010702-3

[11] Vanicek, P.; Krakiwsky, E. J. (1986): Geodesy: The Concepts, Elsevier Science Publishing Company, Inc., Second Edition, Netherlands, ISBN: 0-4444-87775-4

[12] Vanicek, P.; Krakiwsky, E. J.; Craymer, M. R.; Gao, Y.; Ong, P. S. (1990): Robustness Analysis. Final contract report, Department of Surveying Engineering echnical Report No. 156, university of New Brunswick, Fredericton, New Brunswick, Canada

[13] Wonnacott, H.; Wonnacott, T. and R. J. (1977): Introductory Statistics, John Wiley and Sons, Inc.

[14] Zomorrodian, H. (1972): The Establishment of the Iranian National Gravity Calibration Line. Technical Report of the Institute of Geophysics, Tehran University

[15] Zomorrodian H. (1985): The Iranian National Calibration Line 1985. Technical Report of the Institute of Geophysics, Tehran University

[16] Zomorrodian H. (1987): The establishment of the Iranian Gravity Datum, Bureau Gravimetrique International, Bul. D Information, No 60, June 1987

M. Najafi-Alamdari, K.N. Toosi, University of Technology, Faculty of Geodesy and Geomatics Engineering, 1346 Valiasr Street, Mirdaamaad intersection, Tehran, Iran, Tel: +98 21 88 78 62 12, Fax: +98 21 88 78 62 13. mnajalm@yahoo.com

M. Mashadi Hossainali, K.N. Toosi, University of Technology, Faculty of Geodesy and Geomatics Engineering, 1346 Valiasr Street, Mirdaamaad intersection, Tehran, Iran, Tel: +98 21 88 78 62 12, Fax: +98 21 88 78 62 13. hossainali@kntu.ac.ir

Y. Hatam Chavari, National Cartographic Center, Mearaj Street, Azadi Square, Tehran, Iran, Tel: +98 21 66 00 10 90, Fax: +98 21 66 00 19 72. yaghoubhatam@yahoo.com

F. Tavakoli, LGIT, Geosciences-UJF, BP 53, 38041, Grenoble, Cedex 9, France, Tel: ++33-4 76-82 80 74, Fax: ++33-4 76-82 81 04. farokh.tavakoli@obs.ujf-grenoble.fr

Abstract

A gravity base network including 19 stations is proposed for Iran. For the fast accessibility by a gravimeter, the stations are assumed in the national airports. Nine of the stations are selected as the reference stations at which absolute gravity values are to be measured. Six of them make a calibration line extending from the extreme North-West to the extreme South-East end of the country. The remaining stations, uniformly distributed throughout, are connected to at least 3 reference stations by precise gravity difference measurements. Based on the 5 μGal accuracy of the CG-3M gravimeter and the assumed 3 μGal accuracy of FG5 absolute gravimeter, pre-analysis of five different designs of the network observations was carried out. The reference stations were considered initially known at absolute gravity values with observational weights inversely proportional to the variance of absolute measurements. The drift of gravimeter was assumed linear in time within an interval of 8 hours. Individual gravimeter readings were assumed uncorrelated, while mathematical correlations among reading differences (gravity difference measurements) were assessed. Gravity difference measurement accuracies were taken to be partly proportional to the spent time of measurements with the constant of proportionality to be determined in the computation. Redundancy numbers and internal reliabilities at 90 % confidence level were evaluated to study the robustness of the network against gross errors. Individual undetectable gross errors were then applied to show the corresponding distortions in the network. In the optimal design, the redundancy numbers, all larger than 0.5, are uniformly distributed throughout the network and the achievable accuracy is the best. Even for the optimal design, gross errors up to 25 μGal may survive the statistical test, but the distortion caused by these errors would remain under the sought accuracy of 5 μGal.

Keywords
Gravity Base network, gravimeter, gravimetry, network design, internal reliability.

Iran covers a large area limited in longitude by the meridians 44°E and 64°E and in latitude by the parallels 25°N and 40°N. Mapping a new gravity field over Iran is the first important data for geodetic, geophysical and geodynamical considerations. In this thesis, the gravity measurements are used to determine the gravimetric geoid over Iran. This geoid is coupled with the GPS height and altitude (levelling) to realize an operational vertical surface at the territory of Iran. The contribution of the principal geodetic and gravimetric works realized in recent years are the establishment of: 1) the national absolute gravity network of Iran (NAGNI09), 2) the national gravity calibration line of Iran (NGCLI10) and 3) the multi-observations geodetic and gravimetric network of Iran (MPGGNI10).

The absolute gravity network consists in 24 stations where the gravity measurement has been realized with the help of gravimeters FG5, with a precision better than 5μGal. The repetition of the observations at two stations between 2000 and 2007 makes obvious the inter-annual variations of gravity in relation of the amount of underground water changes and (or) tectonic deformation.

The absolute gravity network has served the base stations for the realization of the MPGGNI10 geodetic and gravimetric network with a mesh of 55 km, at which the gravity is measured with the help of relative gravimeters CG-5 and CG-3/M, the GPS height and the altitude with a precision of 0.010 mGal, 0.03 m, and 3mmkmrespectively. The remove-restore technique coupled with the Helmert's condensation method is chousen to compute a new gravimetric geoid model, IRGeoid10, with a absolute and relative precision of the order of 0.26 m and 2.8 ppm respectively. The gravimetric geoid is adjusted at the GPS/levelling points to define new vertical reference surface over Iran.

Géosciences Montpellier

UM2, Place E.Bataillon - cc 60 - 34095 Montpellier cedex 5

http://www.gm.univ-montp2.fr